SYNTHETIC STUDIES TOWARD THE TOTAL SYNTHESIS OF ENTEROCIN

Thesis by

Yujia Tao

In Partial Fulfillment of the Requirements

for the Degree of

Doctor of Philosophy

CALIFORNIA INSTITUTE OF TECHNOLOGY

Pasadena, California

2023

(Defended May 5th, 2023)

Yujia Tao

ORCID: 0000-0003-4615-6409

I would like to express my sincere gratitude to my advisor, Dr. Sarah Reisman, for her guidance and support throughout my research. Her expertise and patience were invaluable. I would also like to extend my heartfelt appreciation to my mentors, team members, and lab mates for their invaluable guidance, support, and camaraderie. Their dedication and commitment to excellence have inspired me to push the boundaries of my research. Finally, I would like to thank my family and friends for their unwavering support and encouragement.

ABSTRACT

As part of a broader program aimed at the synthesis of complex and highly oxygenated natural products, we initiated a chemical synthesis of the natural polyketide enterocin. This dissertation will disclose our efforts to bridge that gap through the development of synthetic strategies for the total synthesis of the enterocin. The studies herein will address three unique strategies to access the tactical difficulties in the rich oxygenation patterns and caged core structure of enterocin. The program was first inspired by a SeO_2 multioxidation reaction, and the methodology has been successfully applied to install bridgehead oxygenation patterns in enterocin. A strategy featuring a radical-polar crossover reaction as an annulation step to quickly construct the [3.2.1] bicyclic core of enterocin is detailed. Initial studies have successfully achieved the radical-polar crossover annulation reaction to forge [3.2.1]bicycles with bridgehead hydroxyl groups, and will guide the future development toward the total synthesis of enterocin. An intermolecular aldol approach will be discussed to address the challenge on pyrone installation and core structure synthesis. In summary, the development of an efficient and general approach will allow the development of novel reactions and a comprehensive evaluation of the potential of caged polyketides to serve as medicinally interesting molecules.

.

PUBLISHED CONTENT AND CONTRIBUTIONS

Portions of the work described herein were disclosed in the following communications:

Han, A.; Tao, Y.; Reisman, S. E. *Nature* **2019**, *573*, 563;

This article is available online at: https://www.nature.com/articles/s41586-019-1580-x

Mendoza, S. D.; Rombola, M.; Tao, Y.; Zuend, S. J.; Götz, R.; McLaughlin, M. J.;

Reisman, S. E. *Org. Lett.* **2022**, *24* (21), 3802–3806.

This article is available online at:

https://pubs.acs.org/doi/full/10.1021/acs.orglett.2c01343

Y.T. contributed to the development of the synthetic strategy, conducted the experiments described herein, prepared the supporting data, and participated in writing the manuscript.

TABLE OF CONTENTS

LIST OF ABBREVIATIONS

$[\alpha]_D$	angle of optical rotation of plane-polarized light
Å	angstrom(s)
ABNO	9-azabicyclo[3.3.1]nonane *N*-oxyl
Ac	acetyl
acac	acetylacetonate
AIBN	azobisisobutyronitrile
Anth	anthracene
APCI	atmospheric-pressure chemical ionization
aq	aqueous
atm	atmosphere(s)
bipy	2,2'-bipyridine
BMEA	bis(2-methoxyethyl)amine
Bn	benzyl
Boc	*tert*-butoxycarbonyl
BOM	benzyloxymethyl
bp	boiling point
br	broad
Bu	butyl
i-Bu	*iso*-butyl
n-Bu	butyl or *norm*-butyl
t-Bu	*tert*-butyl
c	concentration of sample for measurement of optical rotation

^{13}C	carbon-13 isotope
/C	supported on activated carbon charcoal
°C	degrees Celcius
calc'd	calculated
CAN	ceric ammonium nitrate
Cbz	benzyloxycarbonyl
cf.	consult or compare to (Latin: *confer*)
cis	on the same side
cm^{-1}	wavenumber(s)
CO	carbon monoxide
conv.	Conversion
COSY	homonuclear correlation spectroscopy
CSA	camphor sulfonic acid
Δ	heat or difference
δ	chemical shift in ppm
d	doublet
d	deutero or dextrorotatory
D	deuterium
DBB	4,4'-di-*tert*-butylbiphenyl
DBU	1,8-diazabicyclo[5.4.0]undec-7-ene
DBN	1,5-diazabicyclo[4.3.0]non-5-ene
DBNap	2,6-di-*tert*-butylnaphthalene
DCB	dichlorobenzene

DCC	*N,N'*-dicyclohexylcarbodiimide
DCE	1,2-dichloroethane
DDQ	2,3-dichloro-5,6-dicyano-1,4-benzoquinone
de novo	starting from the beginning; anew
DIBAL	diisobutylaluminum hydride
DMA	*N,N*-dimethylacetamide
DMAP	4-(dimethylamino)pyridine
DMDO	dimethyldioxirane
DME	1,2-dimethoxyethane
DMF	*N,N*-dimethylformamide
DMPU	1,3-dimethyl-3,4,5,6-tetrahydro-2(1H)-pyrimidinone
DMSO	dimethylsulfoxide
dppf	1,1'-bis(diphenylphosphino)ferrocene
dr	diastereomeric ratio
ee	enantiomeric excess
E^+	electrophile
E	*trans* (entgegen) olefin geometry
EDCI	*N*-(3-dimethylaminopropyl)-*N'*-ethylcarbodiimide hydrochloride
e.g.	for example (Latin: *exempli gratia*)
EI	electron impact
ent	enantiomer of
epi	epimeric
equiv	equivalent(s)

ESI	electrospray ionization
Et	ethyl
et al.	and others (Latin: *et alii*)
FAB	fast atom bombardment
FTIR	fourier transform infrared spectroscopy
Fur	furyl
g	gram(s)
h	hour(s)
^{1}H	proton
[H]	reduction
HFIP	hexafluoroisopropanol
HG-II	Hoveyda–Grubbs' catalyst™ 2nd generation
HMBC	heteronuclear multiple-bond correlation spectroscopy
HMDS	hexamethyldisilazide
HMPA	hexamethylphosphoramide
$h\upsilon$	irradiation with light
HPLC	high performance liquid chromatography
HRMS	high resolution mass spectrometry
HSQC	heteronuclear single quantum coherence spectroscopy
Hz	hertz
i.e.	that is (Latin: *id est*)
iso	isomeric
in situ	in the reaction mixture

J	coupling constant in Hz
k	rate constant
kcal	kilocalorie(s)
kg	kilogram(s)
L	liter
l	levorotatory
LCMS	liquid chromatography–mass spectrometry
LDA	lithium diisopropylamide
m	multiplet or meter(s)
M	molar or molecular ion
m	*meta*
μ	micro
m-CPBA	*meta*-chloroperbenzoic acid
Me	methyl
MeOH	methanol
MeCN	acetonitrile
mg	milligram(s)
MHz	megahertz
min	minute(s)
mL	milliliter(s)
MM	mixed method
mol	mole(s)
MOM	methoxymethyl

Ms	methanesulfonyl (mesyl)
MS	molecular sieves
m/z	mass-to-charge ratio
Nap	naphthalene
NBS	*N*-bromosuccinimide
NCS	*N*-chlorosuccinimide
ND	not determined
Nf	nonafluorobutanesulfonyl
nm	nanometer(s)
nM	nanomolar
NMI	1-methylimidazole
NMO	*N*-methylmorpholine *N*-oxide
NMR	nuclear magnetic resonance
nOe	nuclear Overhauser effect
NOESY	nuclear Overhauser enhancement spectroscopy
Nu^-	nucleophile
o	*ortho*
[O]	oxidation
n-Oct	octyl or *norm*-octyl
p	*para*
PCC	pyridinium chlorochromate
Ph	phenyl
pH	hydrogen ion concentration in aqueous solution

PhH	benzene
PhMe	toluene
PIDA	[bis(acetoxy)iodo]benzene
PIFA	[bis(trifluoroacetoxy)iodo]benzene
Pin	pinacol
pK_a	acid dissociation constant
pm	picometer(s)
PMB	*para*-methoxybenzyl
PNap	2-phenylnaphthalene
ppm	parts per million
PPTS	pyridinium *para*-toluenesulfonate
Pr	propyl
i-Pr	isopropyl
n-Pr	propyl or *norm*-propyl
psi	pounds per square inch
Pyr	pyridine
q	quartet
quant.	quantitative
R	generic (alkyl) group
R_L	large group
R	rectus
RCM	ring-closing metathesis
recry.	recrystallization

ref	reference
R_f	retention factor
rgt.	Reagent
rr	regioisomeric ratio
rt	room temperature
RyR	ryanodine receptor
s	singlet or seconds
S	sinister
SAR	structure-activity relationship
sat.	saturated
SFC	supercritical fluid chromatography
t	triplet
TAS-F	tris(dimethylamino)sulfonium difluorotrimethylsilicate
TBABr	tetra-*n*-butylammonium bromide
TBACl	tetra-*n*-butylammonium chloride
TBAF	tetra-*n*-butylammonium fluoride
TBAI	tetra-*n*-butylammonium iodide
TBDPS	*tert*-butyldiphenylsilyl
TBHP	*tert*-butyl hydroperoxide
TBP	4,4'-thiobis(6-*tert*-butyl-3-methylphenol)
TBS	*tert*-butyldimethylsilyl
temp	temperature
TEACl	tetraethylammonium chloride

TEMPO	2,2,6,6-tetramethylpiperidine 1-oxyl
Tf	trifluoromethanesulfonyl
TFA	trifluoroacetic acid
THF	tetrahydrofuran
TLC	thin layer chromatography
TMEDA	*N,N,N′,N′*-tetramethylethylenediamine
TMS	trimethylsilyl
TMP	2,2,6,6-tetramethylpiperidine
TOF	time-of-flight
Tol	tolyl
trans	on the opposite side
Ts	*para*-toluenesulfonyl (tosyl)
UV	ultraviolet
vide infra	see below
w/v	weight per volume
X	anionic ligand or halide
xs	excess
Z	*cis* (zusammen) olefin geometry

Chapter 1

Development of a Pd-catalyzed Carbopalladation/Carbonylation Cascade for the Total Synthesis of (+)-Perseanol[†]

1.1. Background and Significance

(+)-Perseanol **(4)** is an isoryanodane diterpene, isolated from *Persea indica*.[1] It has potent insecticidal and antifeedant properties.[1] (+)-Perseanol **(4)** (Figure 1) bears an isomeric carbon framework to (+)-ryanodine (**1**), an active modulator of the ryanodine receptors (RyR) - intracellular calcium ion channels present in skeletal and cardiac muscle.[2-3] In addition, **4** lacks the pyrrole-2-carboxylate ester at C3, which is critical for **1**'s binding to the mammalian RyR. Indeed,

[†]Portions of this chapter have been reproduced from: Han, A.; Tao, Y.; Reisman, S. E. *Nature* **2019**, *573*, 563. The research discussed was completed in collaboration with Dr. Arthur Han in our laboratory.

4 and **5** already show selectivity for lepidopteran pests with minimal toxicity to mammals in preliminary assays, but the study was not comprehensive enough to confirm the mode of action of the isomeric framework.[4] Towards this end, we envisioned a concise and modular synthesis of (+)-perseanol that would provide a versatile platform for the elucidation of its mode of action and development of new insect antifeedants.

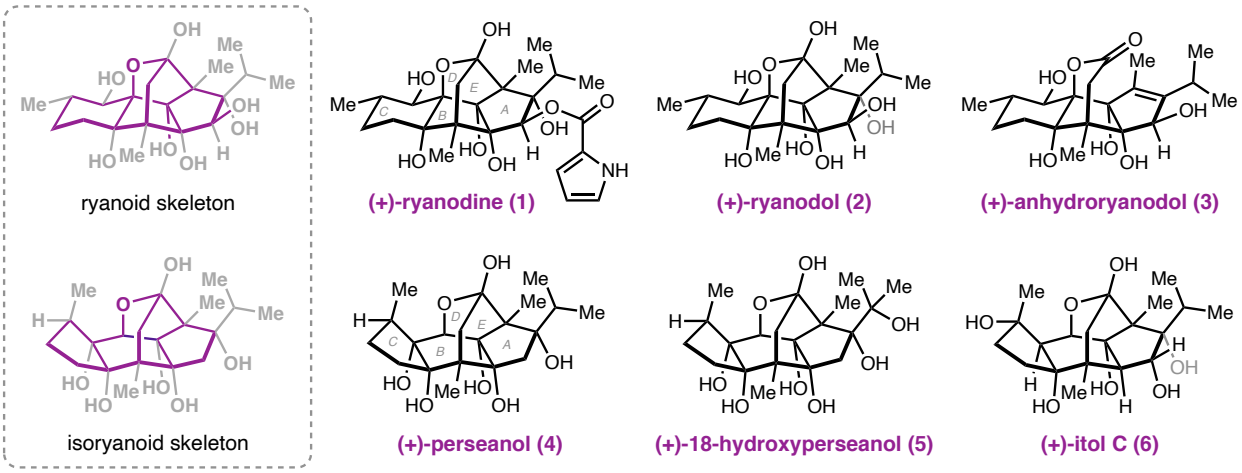

Figure 1. *Structures of ryanodine and isoryanodane diterpenes.*

Aiming for a modular route to access isoryanodane family of natural products, we conceived a convergent fragment coupling approach that possesses potential for fragment derivatization (Figure 2). In analogy to the key reductive cyclization step previously used in our lab in the total synthesis of ryanodol[2], perseanol (**4**) was simplified to anhydroperseanol (**7**). It was thought that the AB ring junction diol be brought in as the masked olefin, leading back to **8** strategic intermediate. It was hypothesized that the tetracyclic lactone in **8** could be built in one-step via a Pd-catalyzed carbopalladation/carbonylation cascade from vinyl bromide **9**, which could be synthesized from a 1,2 addition of **10** to aldehyde **11**.

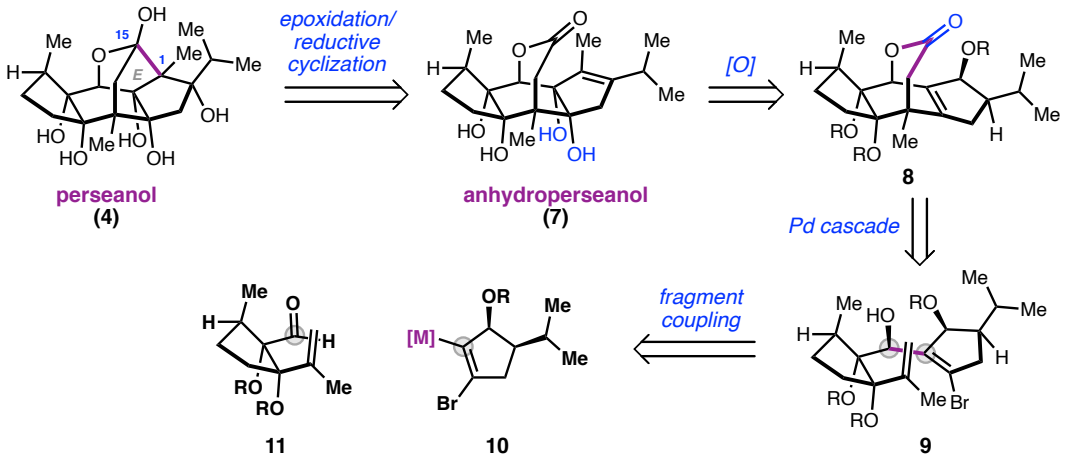

Figure 2. *Retrosynthetic analysis of perseanol.*

Taking a closer look at the proposed key Pd cascade step (Figure 3), it was thought that the treatment of vinyl bromide **12** with a palladium catalyst could induce oxidative addition to the C-Br bond. A 6-*exo*-trig migratory insertion into the 1,1-disubstituted alkene was expected to take place and provide alkylpalladium **15**, which would be incapable of β-hydride elimination due to the adjacent newly formed quaternary center. **16** would form after CO insertion, and capture by the C11 alcohol would yield **17** as the desired product. In an alternative 3-step route to construct tetracycle **17** from **12** developed by Dr. Arthur Han, the feasibility of such a 6-*exo*-trig migratory insertion was demonstrated in a Pd-catalyzed Heck/Stille cascade to access **13**. Compared to the older 3-step sequence, this one-step Pd-catalyzed carbopalladation/ carbonylation cascade could afford a higher overall yield and step efficiency and make the synthesis more concise.

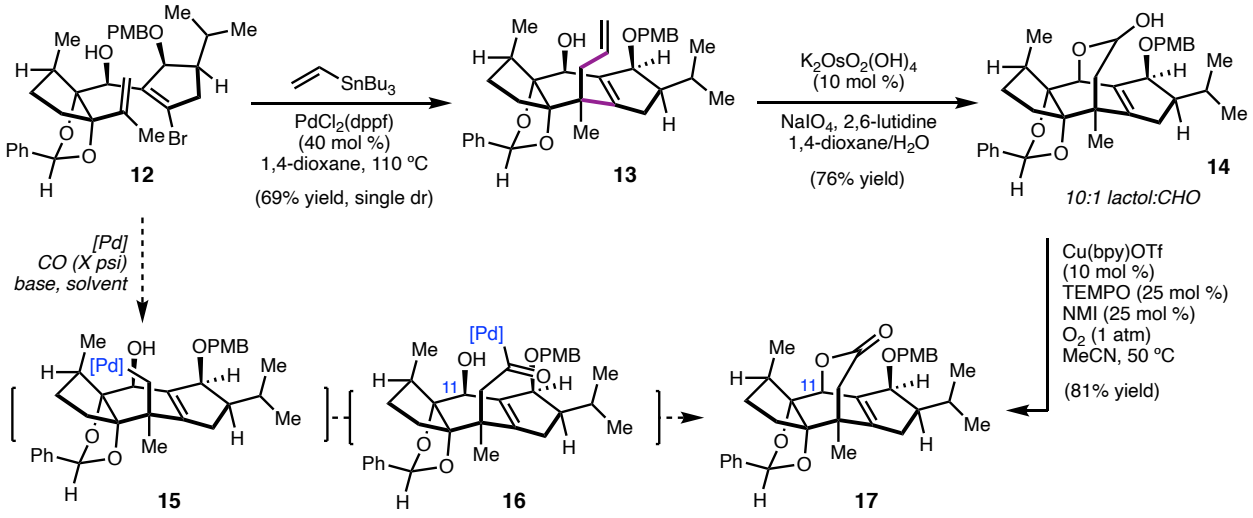

Figure 3. *Pd-catalyzed cascade and alternative three-step sequence.*

While there were related carbopalladation/carbonylation cascade examples reported[5-8], there were potential challenges in realizing the proposed reaction (Figure 4). One major concern was that the rate of the desired 6-*exo*-trig migratory insertion could be slow, considering that the palladium needs to migrate into a sterically congested space. As a result, premature carbonylation product **20** could be observed. Other concerns included the possibility that the vinyl-palladium species **18** could engage in an undesired 7-*endo*-trig migratory insertion to afford **21,** or that primary alkyl-Pd **19** could perform a second insertion into the A-ring alkene to afford **22**.

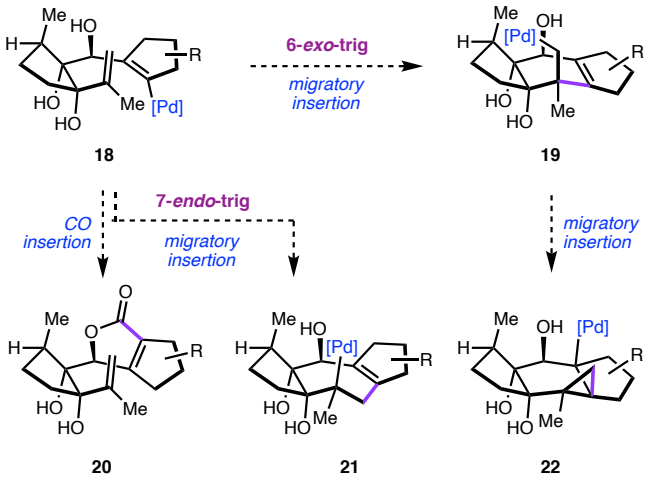

Figure 4. *Potential side reaction pathways.*

1.2. Results and Discussion

Investigations commenced with screening conditions reported in literature[5-8] on model system **23** to perform a Heck/carbonylation cascade to afford **24** (Table 1). Under most conditions, no reaction took place, and starting material was cleanly recovered. Notably, TlOAc, which was reported to facilitate oxidative addition[9], had no helpful reactivity but resulted in TES deprotection (entry 3). $PdCl_2$(dppf), which was found to be the optimal catalyst for the previously discussed Heck/Stille cascade (Figure 3), also gave no reaction (entry 4). It was hypothesized that the tin reagent used for the Heck/Stille cascade might be critical for activating the Pd catalyst in addition to acting as a cross-coupling partner[10]. Therefore, Bu_3SnH was added to the Heck/carbonylation cascade (entry 5), but still no reaction was observed. Lastly, running the reaction under higher CO pressures (entries 6, 7) was also fruitless.

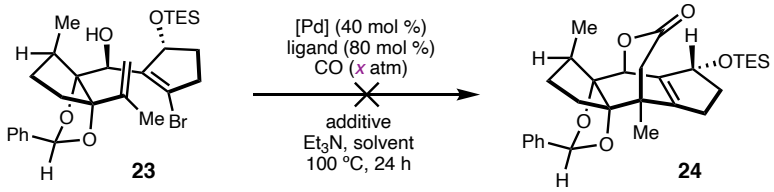

entry	[Pd]	ligand	CO Pressure	additive	solvent	result
1	$Pd(OAc)_2$	P(*o*-Tol)$_3$	1 atm	–	MeCN	Recovered SM
2	$Pd(OAc)_2$	P(*o*-Tol)$_3$	1 atm	–	DMF	Recovered SM
3	$Pd(OAc)_2$	P(*o*-Tol)$_3$	1 atm	TlOAc	DMF	TES deprotection
4	$PdCl_2$(dppf)	–	1 atm	–	Dioxane	Recovered SM
5	$PdCl_2$(dppf)	–	1 atm	Bu_3SnH	Dioxane	Recovered SM
6	$Pd(OAc)_2$	P(2-furyl)$_3$	3 atm	–	Dioxane	Recovered SM
7	$PdCl_2$(dppf)	–	10 atm	–	Dioxane	Recovered SM

Table 1. *Preliminary studies on a model system.*

Failure of these preliminary screens prompted us to question which step in the desired catalytic cycle was being impeded. Since no reactivity was found across any of the preliminary screens, the initial hypothesis was that the first step in the catalytic cycle, oxidative addition of palladium to the alkenyl bromide, might be the problem. This hypothesis was further supported by

the fact that no proto-debromination was observed in entry 5 in Table 1. It was thought that if oxidative addition took place with Bu_3SnH in the reaction, a Stille reaction might be a side pathway to deliver **26** and/or **27** as products (Figure 5).

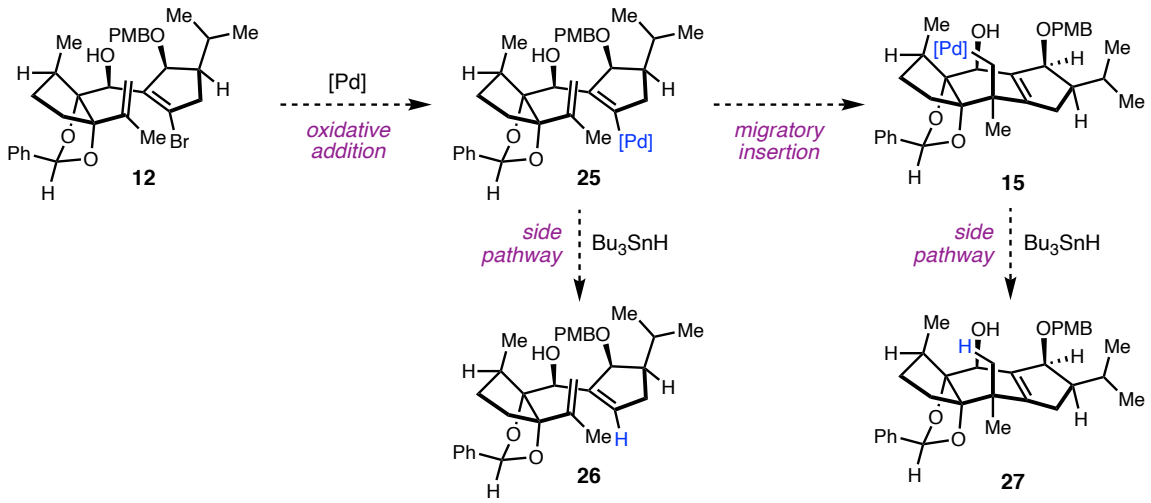

Figure 5. *Potential side Stille pathway*.

With this hypothesis in mind, control experiments were conducted to determine under what conditions oxidative addition could be induced (Figure 6). Using $Pd(P(t\text{-}Bu)_3)_2$ and $P(p\text{-}F\text{-}Ph)_3$ as the catalyst system, it was found that the longer substrate **12** was heated in the presence of the Pd catalyst under N_2 before the introduction of CO, the higher the conversion of **12**. These results confirmed that oxidative addition to the alkenyl bromide was possible in the absence of CO. Therefore, it was proposed that perhaps the catalyst deactivation by CO impedes the oxidative addition and prevent the reaction from proceeding as desired.

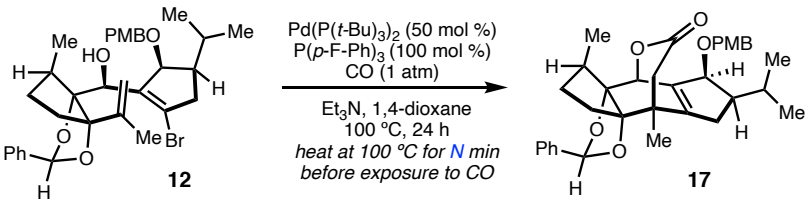

N min	Conversion	Yield
0	8 %	1 %
8	20 %	11 %
30	40 %	22 %
60	56 %	34 %

Figure 6. *Investigation on the feasibility of oxidative addition in the absence of CO.*

To overcome the slow oxidative addition of the palladium catalyst to the alkenyl bromide in the presence of 1 atm CO, a stoichiometric quantity of the Pd catalyst in the absence of CO was used to drive all of the starting material to undergo oxidative addition and migratory insertion to arrive at alkyl-Pd **15**. Then, CO could be introduced to afford desired tetracycle **17**. Indeed, after extensive investigation (Table 2), several conditions (entry 1, 18, 35) were found that provided **17** at around 50 % isolated yield. Despite thorough screening of a variety of different Pd sources, ligands, bases, solvents and additives, no conditions were found that afforded the desired product in yields greater than 57% (entry 1).

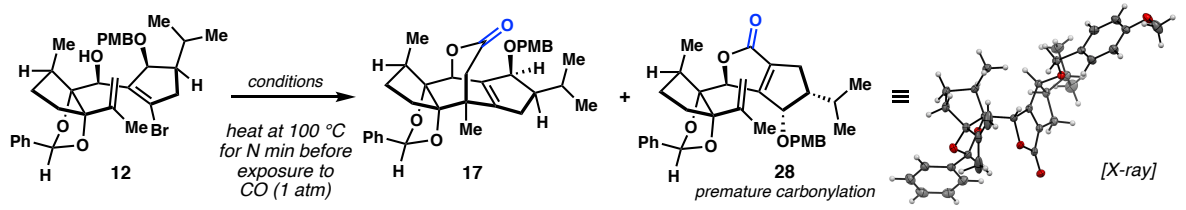

entry	[M]	mol %	[L]	mol %	base	solvent	additive	*N* (min)	12[b] (%)	17[b] (%)	28[b] (%)
1	$Pd(P(t\text{-}Bu)_3)_2$	120	$P(p\text{-}F\text{-}Ph)_3$	240	Et_3N	1,4 dioxane	–	80	–	57	6
2	$Pd(OAc)_2$	50	$P(2\text{-furyl})_3$	100	Et_3N	1,4 dioxane	–	80	97	0	–
3	$Pd(OAc)_2$	120	$P(p\text{-}F\text{-}Ph)_3$	240	Et_3N	1,4 dioxane	–	80	32	0	–
4	$PdCl_2(dppf)$	50	–	–	Et_3N	1,4 dioxane	–	80	96	0	–
5	Pd_2dba_3	25	Xantphos	100	Et_3N	1,4 dioxane	–	80	94	1	3
6	Pd_2dba_3	60	$P(p\text{-}F\text{-}Ph)_3$	240	Et_3N	1,4 dioxane	–	80	62	23	9
7	$Pd(P(t\text{-}Bu)_3)_2$	120	–	–	Et_3N	DMF	–	80	35	28	20
8	$Pd(P(t\text{-}Bu)_3)_2$	120	–	–	Et_3N	PhMe	–	80	–	0	–
9	$Pd(P(t\text{-}Bu)_3)_2$	120	–	–	Et_3N	1,4 dioxane	–	80	–	0	–
10	$Pd(P(t\text{-}Bu)_3)_2$	120	–	–	Et_3N	1,4 dioxane	–	70	–	0	–
11	$Pd(P(t\text{-}Bu)_3)_2$	120	–	–	Et_3N	1,4 dioxane	–	60	–	0	–
12	$Pd(P(t\text{-}Bu)_3)_2$	120	–	–	Et_3N	1,4 dioxane	–	40	6	0	–
13	$Pd(P(t\text{-}Bu)_3)_2$	120	$P(t\text{-}Bu)_3$	240	Et_3N	1,4 dioxane	–	60	28	11	–
14	$Pd(P(o\text{-}Tol)_3)_2$	120	–	–	DIPEA	1,4 dioxane	–	80	–	51	–
15	$Pd(P(o\text{-}Tol)_3)_2$	120	–	–	DBU	1,4 dioxane	–	80	–	6	–
16	$Pd(P(o\text{-}Tol)_3)_2$	120	–	–	Cs_2CO_3	1,4 dioxane	–	80	–	0	–
17	$Pd(P(o\text{-}Tol)_3)_2$	120	–	–	DMAP	1,4 dioxane	–	80	–	0	–
18	$Pd(P(o\text{-}Tol)_3)_2$	120	–	–	Et_3N	1,4 dioxane	–	80	–	52	–
19[c]	$Pd(P(o\text{-}Tol)_3)_2$	120	–	–	Et_3N	1,4 dioxane	–	80	–	53	–
20	$Pd(P(o\text{-}Tol)_3)_2$	120	$P(p\text{-}F\text{-}Ph)_3$	240	Et_3N	1,4 dioxane	–	80	7	42	7
21	$Pd(P(o\text{-}Tol)_3)_2$	120	*rac*-BINAP	240	Et_3N	1,4 dioxane	–	80	–	41	29
22	$Pd(P(o\text{-}Tol)_3)_2$	120	PEt_3	240	Et_3N	1,4 dioxane	–	80	–	0	75
23	$Pd(P(o\text{-}Tol)_3)_2$	120	SPhos	240	Et_3N	1,4 dioxane	–	80	–	51	–
24	$Pd(P(o\text{-}Tol)_3)_2$	120	dtbpf	240	Et_3N	1,4 dioxane	–	80	18	7	22
25	$Pd(P(o\text{-}Tol)_3)_2$	120	dppf	240	Et_3N	1,4 dioxane	–	80	9	13	48
26	$Pd(P(o\text{-}Tol)_3)_2$	120	dppb	240	Et_3N	1,4 dioxane	–	80	6	18	19
27	$Pd(P(o\text{-}Tol)_3)_2$	120	dppp	240	Et_3N	1,4 dioxane	–	80	6	21	31
28	$Pd(P(o\text{-}Tol)_3)_2$	120	dppe	240	Et_3N	1,4 dioxane	–	80	17	17	17
29	$Pd(P(o\text{-}Tol)_3)_2$	120	dppm	240	Et_3N	1,4 dioxane	–	80	80	0	12
30	$Pd(P(o\text{-}Tol)_3)_2$	120	–	–	Et_3N	1,4 dioxane	MeOH	80	6	18	14
31	$Pd(P(o\text{-}Tol)_3)_2$	120	–	–	Et_3N	1,4 dioxane	*t*-BuOH	80	–	31	6
32	$Pd(PPh_3)_4$	50	–	–	Et_3N	DMF	–	90	35	27	12
33	$Pd(PPh_3)_4$	50	–	–	Et_3N	PhMe	–	90	35	5	–
34	$Pd(PPh_3)_4$	50	–	–	Et_3N	1,4 dioxane	–	90	34	31	9
35	$Pd(PPh_3)_4$	120	–	–	Et_3N	1,4 dioxane	–	90	23	48	13
36	$Pd(PPh_3)_4$	120	–	–	Et_3N	1,4 dioxane	TBAI	90	3	5	1
37	$Pd(PPh_3)_4$	120	–	–	Et_3N	1,4 dioxane	TBABr	90	20	15	20
38	$Pd(PPh_3)_4$	120	–	–	Et_3N	1,4 dioxane	TBACl	90	22	12	22
39	$Ni(COD)_2$	50	–	–	Et_3N	1,4 dioxane	–	30	35	0	–
40	$NiCl_2(PPh_3)_2$	50	–	–	Et_3N	1,4 dioxane	–	30	28	0	–

[a]Reactions were run on 0.01 mmol scale of **128** at 100 °C. [b]Yields determined by ^1H NMR of the crude product using pyrazine as the internal standard. [c]10 atm instead of 1 atm of CO pressure

Table 2. *Investigation of the carbopalladation/carbonylation cascade.*

Having validated the ability of the carbopalladation/carbonylation cascade to afford the desired product in 50 % yield with stoichiometric Pd catalyst, we sought to further optimize the reaction by reducing the Pd loading. Since 1 atm CO resulted in oversaturation that prevented oxidative addition, a lower CO pressure might enable the reaction to proceed with a catalytic amount of Pd. Since *ex situ* CO generation protocols are usually set-up dependent[11], *in situ* CO generation conditions were investigated (Table 3). Little to no desired reactivity was observed

when $Mo(CO)_6$ (**29**),[12] *t*-BuNC (**30**),[13] or phenyl formate (**31**)[14] were used as CO surrogates (entries 1–6). However, a 31 % yield was obtained when using *N*-formyl saccharin (**32**)[15] as the CO source with 50 mol % of $Pd(PPh_3)_4$ (entry 7). Furthermore, the addition of excess KF facilitated the release of CO from N-formyl saccharin, increasing the yield to 57 % (entry 8).

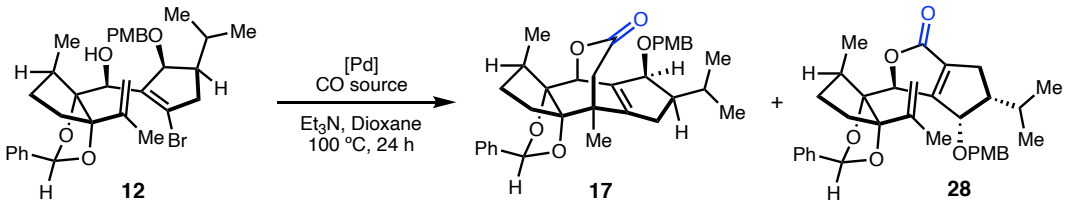

entry	[M]	mol %	CO source	additive	12 (%)	17 (%)	18 (%)
1	$Pd(PPh_3)_4$	50	**29**	DBU	85	0	8
2	$Pd(P(o\text{-}Tol)_3)_2$	50	**29**	DBU	75	0	14
3	$Pd(PPh_3)_4$	50	**30**	–	90	0	0
4	$Pd(P(o\text{-}Tol)_3)_2$	50	**30**	–	93	0	0
5	$Pd(PPh_3)_4$	50	**31**	–	14	7	4
6	$Pd(P(t\text{-}Bu)_3)_2$	50	**31**	–	4	1	0
7	$Pd(PPh_3)_4$	50	**32**	–	22	31	10
8	$Pd(PPh_3)_4$	50	**32**	KF	1	57	14

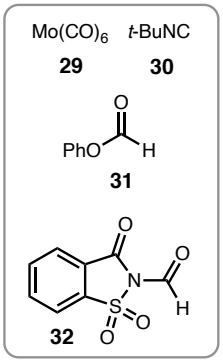

Table 3. *Investigation of various CO surrogates.*

With this new result in hand, further investigations were carried out using *N*-formyl saccharin as the CO surrogate (Table 4). In contrast to the original literature[15], bisphosphine-ligated palladium catalysts such as $PdCl_2$(dppf) and $PdCl_2$(Xantphos) performed poorly in this system. Interestingly, $PdCl_2(PPh_3)_2$ only gave 7 % yield, while $Pd(PPh_3)_4$ gave 57 % yield. Varying the Pd catalyst loading revealed that lowering the loading below 50 mol% resulted in a decrease in yield. However, using a higher Pd catalyst loading did not improve the reaction (entries 8, 9). Other fluoride bases (LiF, NaF, CsF) performed poorly, despite Manade's[15] previous report that CsF was comparale to KF (entries 10-12). Therefore, a combination of 50 mol% $Pd(PPh_3)_4$ with 1.2 equiv *N*-formylsaccharin and 2.5 equiv KF as the CO source (entry 1) was found to be the optimal conditions, and the reaction was successfully scaled up to 400 mg with no change in yield.

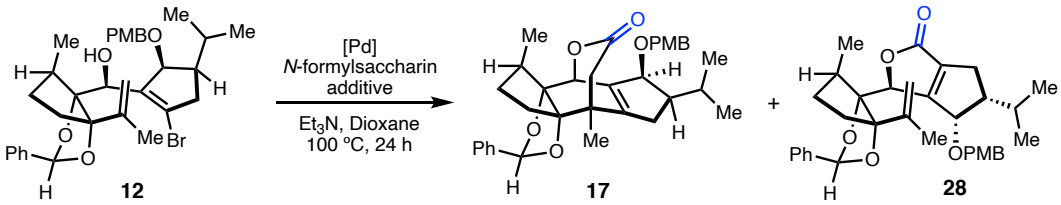

entry	[M]	mol %	additive	12 (%)	17 (%)	28 (%)
1	$Pd(PPh_3)_4$	50	KF	1	57	14
2	$Pd(P(o\text{-}Tol)_3)_2$	50	KF	60	0	0
3	$PdCl_2$(dppf)	50	KF	80	1	4
4	$PdCl_2$(Xantphos)	50	KF	55	4	11
5	$PdCl_2(PPh_3)_2$	50	KF	14	7	4
6	$Pd(PPh_3)_4$	30	KF	14	32	14
7	$Pd(PPh_3)_4$	40	KF	13	44	12
8	$Pd(PPh_3)_4$	60	KF	0	52	0
9	$Pd(PPh_3)_4$	120	KF	0	59	0
10	$Pd(PPh_3)_4$	50	LiF	19	30	10
11	$Pd(PPh_3)_4$	50	NaF	13	28	9
12	$Pd(PPh_3)_4$	50	CsF	0	16	13

Table 4. *Final optimization of the N-formylsaccharin conditions.*

1.3. Conclusion and future directions

A thorough investigation of a Pd-catalyzed carbopalladation/carbonylation cascade for the total synthesis of (+)-perseanol has been detailed. A major challenge in the reaction was coordination of CO to the palladium catalyst inhibiting the rate of oxidative addition. Two solutions were examined: using a stoichiometric amount of palladium catalyst or adopting an *in situ* CO generation protocol. Eventually, the combination of N-formylsaccharin, KF, and 50 mol % $Pd(PPh_3)_4$ with Et_3N and 1,4-dioxane was found to be the optimal conditions, providing the desired product in 57 % yield on a 400 mg scale. Future work involves applying this carbopalladation/ carbonylation reaction to synthesize other isoryanodane natural products, which will allow further studies of their mode of action.

1.4. References

1. González-Coloma, A., Terrero, D., Perales, A., Escoubas, P. & Fraga, B. M. *J. Agric. Food Chem*. **1996**, *44*, 296–300.
2. Sutko, J. L.; Thompson, L. J.; Schlatterer, R. G.; Lattanzio, F. A.; Fairhurst, A. S.; Campbell, C.; Martin, S. F.; Deslongchamps, P.; Ruest, L.; Taylor, D. R. *J. Labelled Compd. Radiopharm.* **1986**, *23*, 215.
3. Sutko, J. L.; Airey, J. A.; Welch, W.; Ruest, L. *Pharmacol. Rev.* **1997**, *49*, 53.
4. Gonzalez-Coloma, A.; Reina, M.; Gutierrez, C.; Fraga, B. M. *Studies in Natural Products Chemistry*, 2002; Vol. 26, pp 849.
5. Artman, G. D.; Weinreb, S. M. *Org. Lett.* **2003**, *5*, 1523.
6. Aggarwal, V. K.; Davies, P. W.; Schmidt, A. T. *Chem. Commun.* **2004**, 1232.
7. Bai, Y.; Shen, X. Y.; Li, Y.; Dai, M. J. *J. Am. Chem. Soc.* **2016**, *138*, 10838.
8. Bai, Y.; Davis, D. C.; Dai, M. J. *J. Org. Chem.* **2017**, *82*, 2319.
9. Cabri, W.; Candiani, I.; Bedeschi, A.; Santi, R. *Tetrahedron Lett.* **1991**, *32*, 1753-1756.
10. Holt, M. S.; Wilson, W. L.; Nelson, J. H. *Chem. Rev.* **1989**, *89*, 1, 11.
11. Hermange, P.; Lindhardt, A. T.; Taaning, R. H.; Bjerglund, K.; Lupp, D.; Skrydstrup, T. *J. Am. Chem. Soc.* **2011**, *133*, 15, 6061-6071.
12. Odell, L. R.; Russo, F.; Larhed, M. *Synlett* **2012**, *5*, 685–698.
13. Jiang, X.; Wang, J.; Zhang, Y.; Chen, Z.; Zhu, Y.; Ji, S. *Org. Lett*. **2014**, *16*, 3492–3495.
14. Ueda, T.; Konishi, H.; Manabe, K. *Org. Lett*. **2012**, *14*, 3100–3103.
15. Ueda, T.; Konishi, H.; Manabe, K. *Org. Lett*. **2013**, *15*, 5370–5373.
16. (1)

1.5. Appendix

The following article was copied from published manuscript: Han, A.; Tao, Y.; Reisman, S. E. *Nature* **2019**, *573*, 563.

A 16-Step Synthesis of the Isoryanodane Diterpene (+)-Perseanol

Arthur Han, Yujia Tao, Sarah E. Reisman*

Affiliations:

Division of Chemistry and Chemical Engineering, California Institute of Technology, Pasadena, CA 91125, USA.

*To whom correspondence should be addressed: reisman@caltech.edu

(+)-Perseanol is an isoryanodane diterpene with potent antifeedant and insecticidal properties isolated from the tropical shrub *Persea indica*.[1] It is structurally related to (+)-ryanodine, a high affinity ligand and modulator of ryanodine receptors (RyRs)—ligand-gated ion channels critical for intracellular Ca^{2+} signaling in vertebrates and invertebrates.[2] Whereas ryanodine modulates RyR-dependent Ca^{2+} release across many organisms, including mammals, preliminary data indicate that ryanodane and isoryanodane congeners that lack the pyrrole-2-carboxylate ester, such as perseanol, may have selective activity in insects.[3] Here we report the first chemical synthesis of (+)-perseanol, which proceeds in 16 steps from commercially available (*R*)-pulegone. The synthesis features a two-step annulation process that rapidly assembles the tetracyclic core from readily accessible cyclopentyl building blocks. This work demonstrates how convergent fragment coupling, when combined with strategic oxidation tactics, can enable the concise synthesis of complex and highly oxidized diterpene natural products.

The ryanodane and isoryanodane natural products are oxidized diterpenes with antifeedant and insecticidal activities against insects of the Hemiptera and Lepidoptera orders. Ryanodine (**1**, Figure 1a), isolated from *Ryania speciosa* Vahl, was the first of these natural products to be characterized, and powdered *R. speciosa* wood was marketed as a botanical insecticide with peak annual production reaching 200 metric tons.[4] The insecticidal properties of **1** result from its

modulation of Ca^{2+} release by RyR.[2] In the early 2000s, renewed interest in the insect RyR as a biological target for pest control agents resulted in the discovery and development of the phthalic acid diamide and anthranilic diamide insecticides—which bind at an allosteric site in the transmembrane domain of the insect RyR—with sales of these products exceeding 1 billion USD.[5-6]

Decades after the discovery of **1**, Fraga and coworkers isolated the natural product (+)-perseanol (**3**, Figure 1b) and related congeners from the shrub *Persea indica* found in the Canarian Archipelago. Perseanol (**3**) features an isomeric carbon framework to **1** but bears a similar oxidation pattern and likely results from a shared biosynthetic pathway.[1] A key difference between the structures of **3** and **1**, in addition to their carbon skeletons, is that **3** lacks the pyrrole-2-carboxylate ester at C3, a functional group that is required for high affinity binding of **1** to mammalian isoforms of the RyR.[2] Indeed, in preliminary assays, **3**, **4**, and related metabolites[7-9] were found to exhibit potent antifeedant activity for lepidopteran pests with low toxicity toward mammalian cell lines (in contrast to **1**), although the mode-of-action of **3** was not confirmed to be modulation of the insect RyR.[10] Synthetic access to **3** could enable the elucidation of its mode-of-action and aid the identification of new approaches to target insect RyRs that have evolved resistance to the phthalic acid diamide and anthranilic diamide pesticides.[11] Although Inoue and coworkers have reported an approach to the pentacyclic core of the isoryanodanes, there are no prior completed syntheses of this complex diterpene.[12] Here we report the first chemical synthesis of (+)-perseanol (**3**), which proceeds in 16 steps from commercially available (*R*)-pulegone. The concise synthesis is enabled by a convergent fragment coupling approach that rapidly builds the anhydroperseanol tetracycle and uses strategic C–O bond constructions to minimize unnecessary functional group interconversions.

The structure of perseanol presents several synthetic challenges, including the central bridging 7-membered lactol and the two *syn*-diol motifs at the A–B and B–C ring fusions (Figure 1b). A critical aspect of our synthetic design was the strategic introduction of the six hydroxyl groups in order to minimize extraneous protecting group and oxidation state manipulations. With this in mind, we envisioned initially targeting the synthesis of anhydroperseanol (**5**), in which the C6–C10 diol would be introduced early in the synthetic sequence and the C4–C12 diol would be installed at a late stage (Figure 1c). Although the conversion of anhydroperseanol to perseanol had

not previously been validated experimentally, this disconnection was guided by Deslongchamps' synthesis of (+)-ryanodol (**2**),[13] as well as our own synthesis of (+)-ryanodine.[14-15] Having simplified our target to **5**, we sought to identify a convergent fragment coupling that would rapidly assemble the tetracyclic lactone from two building blocks of similar size and complexity. Ultimately, lactone **6** was recognized as a strategic intermediate that could be accessed from simple cyclopentyl fragments by an annulation process involving two C–C bond forming steps: 1) the 1,2-addition of an organometallic species, such as **9**, to aldehyde **10** to initially join the A and C rings, and 2) an intramolecular carbopalladation/carbonylation cascade reaction of **8** to close the B and D rings. In the key Pd-catalyzed cascade, it was envisioned that oxidative addition of alkenyl halide **8** to Pd^0 followed by 6-*exo*-trig migratory insertion of the pendant 1,1-disubstituted alkene would give rise to σ-alkylpalladium species **7**, which would be incapable of β-hydride elimination. Subsequent CO insertion of **7** and intramolecular capture by the C11 secondary alcohol would deliver **6**, bearing the tetracyclic ring system of anhydroperseanol. In practice, this would require a bifunctional cyclopentene, **9**, which we anticipated accessing via the selective lithiation of the corresponding iodide following precedent established by Vidari and coworkers.[16] The second fragment, aldehyde **10**, would be prepared from commercially available (*R*)-pulegone via the methyl pulegenate.[17] The successful realization of this fragment coupling strategy would provide a modular route to **3** that we anticipated could ultimately give rise to additional designed and natural isoryanodanes.

Our investigations began with the preparation of C-ring aldehyde **10**. Starting with (*R*)-(+)-pulegone (**11**), a known one-step oxidative ring contraction was performed to give methyl pulegenate (**12**) as an inconsequential mixture of diastereomers (Figure 2).[18] Enolization of methyl ester **12** with KHMDS followed by exposure to O_2 then $P(OMe)_3$ resulted in diastereoconvergent α-hydroxylation to furnish α-hydroxyester **13** (9:1 dr). Hydroxyl-directed epoxidation with *m*-CPBA provided epoxide **14** as a single diastereomer, and subsequent treatment of **14** with $Et_2Al(TMP)$[19] induced epoxide isomerization to reveal *syn*-diol **15**, bearing the requisite oxidation at C6 and C10 for elaboration to **3**. Protection of the diol as the benzylidene acetal (**16**) followed by *in situ* DIBAL reduction of the ester provided alcohol **17** as a single diastereomer in 87% yield. Alcohol **17** was oxidized to aldehyde **18** via Stahl's Cu-catalyzed aerobic conditions.[20] This 6-step sequence provided gram scale access to a fully-elaborated C-ring precursor of (+)-perseanol (**3**).

Preparation of the A-ring fragment commenced with commercially available vinylogous ester **19** (Figure 2). Due to concerns about potential racemization under the conditions required to install the vicinal dihalide, we elected to prepare **24** first as a racemate, and then resolve the enantiomers in a subsequent asymmetric reduction step. To this end, the zinc enolate of 3-ethoxy-2-cyclopentenone (**19**) was alkylated under conditions reported by Overman and coworkers[21] to generate *rac*-**21**. Iodination of the vinylogous ester with I_2 and ammonium cerium(IV) nitrate (CAN) afforded iodide **22**, which was hydrolyzed with aqueous sodium hydroxide. Diketone **23** was converted to *rac*-bromoiodocyclopentenone **24** upon treatment with a mixture of oxalyl bromide and DMF.[22] The reaction proceeds with 5:1 regioselectivity, favoring bromination of the enol tautomer distal to the *i*-propyl group. Corey-Bakshi-Shibata (CBS) reduction of *rac*-**24** using catalyst (*R*)-**25**[23] resulted in a kinetic resolution to deliver alcohol (–)-(1*S*, 5*R*)-**27** in 44% yield and 91% ee ($S = 44$, see Supplemental Information for details). The kinetic resolution is consistent with the stereochemical model developed by Corey (see **26**),[24] wherein the *i*-propyl substituent of (*R*)-**24** projects away from the coordinated borane, resulting in reduction of (*R*)-**24** at a faster rate than (*S*)-**24**. Unreacted enone (*S*)-**24** could be recovered in 56% yield and 68% ee; resubjection of (*R*)-**24** to (*R*)-**25** allows it to be further enriched to 95% ee (79% recovery). Protection of alcohol **27** using Dudley's conditions[25] provided the C-ring fragment, PMB ether **29**.

With the requisite fragments in hand, a two-step annulation to forge the anhydroperseanol tetracyclic ring system was investigated (Figure 3). First, the A and C ring fragments were joined by addition of aldehyde **18** to the alkenyllithium generated by selective lithium–iodide exchange of **29**, which provided secondary alcohol **30** in 75% yield (3.2:1 dr, major diastereomer drawn). However, preliminary attempts to induce the subsequent carbopalladation/carbonylation cascade under canonical conditions, which involved exposure of the substrate to a Pd catalyst and base under a CO atmosphere, resulted in the clean recovery of alkenyl bromide **30** (Table 1, entry 1). A control experiment demonstrated that bromide **30** can undergo oxidative addition to $Pd(P(o\text{-}Tol)_3)_2$ in the absence of CO, which led to the hypothesis that coordination of CO to Pd was inhibiting the rate of oxidative addition.[26] To investigate the feasibility of the carbonylation step, bromide **30** was heated with stoichiometric $Pd(P(o\text{-}Tol)_3)_2$ to induce oxidative addition and alkene insertion, and upon consumption of starting material, CO was introduced. Gratifyingly, the desired tetracyclic lactone **31** was isolated in 52% yield under these stoichiometric conditions (entry 3).

An extensive investigation of different Pd sources and ligands did not improve the yield further (entries 4 and 5, see Supplementary Information for further details). The major side product observed under these conditions was direct carbonylation of the bromide of **30** to give butyrolactone **32**. Having validated that the cascade could be effected under stoichiometric conditions, we reasoned that *in situ* generation of CO, to maintain low concentrations of CO in solution,[27-30] might enable the reaction to proceed with catalytic Pd. Ultimately, it was determined that the combination of 1.2 equiv *N*-formylsaccharin (**36**) and KF, in the presence of 50 mol % $Pd(PPh_3)_4$ and Et_3N provided the tetracyclic lactone **31** in 57% yield, as a single diastereomer at the newly formed quaternary carbon (entry 10). In contrast to the Manabe's original report[29] of Pd-catalyzed carbonylation with *N*-formylsaccharin, bisphosphine-ligated Pd complexes performed poorly (entries 12 and 13). This key transformation forges two C–C bonds, with perfect control over the C5 quaternary center, while forming the central 7-membered lactone of anhydroperseanol.

With the tetracyclic framework of anhydroperseanol (**5**) in place, our focus transitioned to the final adjustments of the A-ring oxidation pattern (Figure 3). To this end, PMB ether **31** was first subjected to DDQ to reveal C1 secondary alcohol **37**, which was oxidized with DMDO to the corresponding enone. In the presence of excess DMDO, the benzylidene acetal was unexpectedly oxidized to deliver hydroxybenzoate **38** (3:1 rr, major isomer drawn). Treatment of **38** with MeMgCl in the presence of $CeCl_3$•2LiCl[31] effected 1,2-addition to generate diol **39** (55% isolated yield of a single isomer, over two steps), an intermediate that now harbors all of the carbons present in the isoryanodane framework. Serendipitously, it was discovered that exposure of allylic alcohol **39** to TFA at 0 °C gives rise to orthobenzoate **41** in excellent yield. This 1,3-allylic transposition presumably proceeded by solvolysis under anchimeric assistance to generate dioxolenium ion **40**, which is followed by intramolecular trapping with the C10 alcohol. Thus, over the course of these four steps, the benzylidene acetal protecting group was transiently repurposed as a directing group to guide the installation of the C4 tertiary alcohol and then reinstated as an orthobenzoate protecting group to mask the resulting triol for the rest of the synthesis.

With this fortuitous discovery, we were left to reconsider the final sequence of steps to prepare perseanol. Although we had initially targeted the preparation of anhydroperseanol (see Figure 1),

the ability to prepare **41** led us to consider whether epoxide **43**—potentially accessible from **41** by allylic C–H oxidation and hydroxyl-directed epoxidation—could undergo reductive cyclization. It was recognized that this cyclization might be challenging, given that formation of the C1–C15 bond via epoxylactone isomer **43** would require a Baldwin disfavored[32] 5-*endo*-tet epoxide ring opening, when viewed from the formation of the THF ring. Successful *endo*-ring openings of epoxides have been reported in the literature, but they generally rely on directing groups to stabilize the epoxonium intermediate under Brønsted or Lewis acidic conditions; the related *endo*-cyclizations of epoxides under neutral or basic conditions are less common. Nevertheless, given the strategic advantage of this approach, we elected to investigate it.

To this end, exposure of **41** to SeO_2 in 1,4-dioxane at 100 °C resulted in site-selective and stereospecific oxidation at C2 to give tertiary allylic alcohol **42** in 78% yield (Figure 3). Vanadium-mediated hydroxyl-directed epoxidation of **42** then provided epoxyalcohol **43** as a single diastereomer. The use of $VO(O\textit{n}\text{-}Pr)_3$ proved essential to obtain full conversion of alkene **42**; the more routinely used $VO(acac)_2$ gave only 5–10% conversion under otherwise identical conditions. Treatment of epoxylactone **43** with LiDBB, the optimal conditions from our (+)-ryanodine synthesis,[15] did produce small quantities of the desired pentacycle **46**; however, significant decomposition was observed. Analysis of the side products revealed that reduction of the orthobenzoate was a competing process, prompting a screen of different reductants in order to prevent this undesired reactivity. Use of lithium naphthalenide (LiNap) provided the desired pentacycle in 17% isolated yield. Weaker reductants, like lithium anthracenide (LiAnth), gave rise to epoxide isomerization products instead of reductive cyclization. A further screen of modified naphthalenes revealed that use of lithium 2-phenylnaphthalenide (LiPhNap) effects cyclization to give the desired pentacycle **46** in 25% yield (43% yield based on recovered starting material). The use of PhH as a co-solvent, which had previously been reported by Carreira and coworkers to improve ketyl anion chemistry, was critical for the improved yield.[33] We note that a similar substrate, lacking the C2 *i*-propyl substituent, undergoes the reductive cyclization mediated by LiDBB in 50% yield, demonstrating that the position of the epoxide itself is not chiefly responsible for the reduced efficiency in the cyclization. Deprotection of **46** with $Pd(OH)_2/C$ under an atmosphere of H_2 afforded (+)-perseanol (**3**) in 90% yield. This approach provides (+)-perseanol (**3**) in 16 steps (longest linear sequence) from (*R*)-pulegone (**11**), and is the first total synthesis of

an isoryanodane diterpene. The concision of the synthesis derives from the convergent union of two cyclopentyl fragments of comparable complexity, followed by a carbopalladation/carbonylation cascade to form two C–C bonds and rapidly constructs the tetracyclic lactone framework of anhydroperseanol. Strategic late-stage introduction of the A-ring oxidation pattern minimized lateral redox and protecting group manipulations. This synthetic framework should provide a versatile platform for the preparation of designed isoryanodanes and further studies of their mode-of-action.

References

1. Gonzalez-Coloma, A.; Terrero, D.; Perales, A.; Escoubas, P.; Fraga, B. M. Insect antifeedant ryanodane diterpenes from *Persea indica*. *J. Agric. Food. Chem.* **1996**, *44*, 296.

2. Sutko, J. L.; Airey, J. A.; Welch, W.; Ruest, L. The pharmacology of ryanodine and related compounds. *Pharmacol. Rev.* **1997**, *49*, 53.

3. Gonzalez-Coloma, A.; Reina, M.; Gutierrez, C.; Fraga, B. M. Natural insecticides: structure diversity, effects and structure-activity relationships. A case study. In *Studies in Natural Products Chemistry*, 2002; Vol. 26, pp 849.

4. United States Environmental Protection Agency R.E.D. Facts Ryanodine. https://archive.epa.gov/pesticides/reregistration/web/pdf/2595fact.pdf (accessed Oct 2018).

5. Lahm, G. P. et al. Rynaxypyr™: a new anthranilic diamide insecticide acting at the Ryanodine receptor. In *Pesticide Chemistry: Crop Protection, Public Health, Environmental Safety*, Ohkawa, H.; Miyagawa, H.; Lee, P. W., Eds. Wiley-VCH: Weinheim, 2007; p 111.

6. Cordova, D. et al. Elucidation of the mode of action of Rynaxypyr™, a selective Ryanodine receptor activator. In *Pesticide Chemistry: Crop Protection, Public Health, Environmental Safety*, Ohkawa, H.; Miyagawa, H.; Lee, P. W., Eds. Wiley-VCH: Weinheim, 2007; pp 121.

7. Nohara, T. et al. Cinncassiol D_1 and its glucoside, novel pentacyclic diterpenes from *Cinnamomi cortex*. *Tetrahedron Lett.* **1980**, *21*, 2647.

8. Chai, X. Y. et al. Six insecticidal isoryanodane diterpenoids from the bark and twigs of *Itoa orientalis*. *Tetrahedron* **2008**, *64*, 5743.

9. Zeng, J. F. et al. Diterpenoids with immunosuppressive activities from *Cinnamomum cassia*. *J. Nat. Prod.* **2014**, *77*, 1948.

10. Ling, S. Q.; Xu, Y. N.; Gu, Y. P.; Liu, S. Y.; Tang, W. W. Toxicity and biochemical effects of itol A on the brown planthopper, *Nilaparvata lugens* (Stål) (Hemiptera: Delphacidae). *Pestic. Biochem. Physiol.* **2018**, *152*, 90.

11. Sattelle, D. B.; Cordova, D.; Cheek, T. R. Insect ryanodine receptors: molecular targets for novel pest control chemicals. *Invert. Neurosi.* **2008**, *8*, 107.

12. Koshimizu, M.; Nagatomo, M.; Inoue, M. Construction of a pentacyclic ring system of isoryanodane diterpenoids by SmI_2-mediated transannular cyclization. *Tetrahedron* **2018**, *74*, 3384.

13. Deslongchamps, P. et al. Total synthesis of ryanodol. *Can. J. Chem.* **1979**, *57*, 3348.

14. Chuang, K. V.; Xu, C.; Reisman, S. E. A 15-step synthesis of (+)-ryanodol. *Science* **2016**, *353*, 912.

15. Xu, C.; Han, A.; Virgil, S. C.; Reisman, S. E. Chemical synthesis of (+)-ryanodine and (+)-20-deoxyspiganthine. *ACS Cent. Sci.* **2017**, *3*, 278.

16. Luparia, M.; Vadala, A.; Zanoni, G.; Vidari, G. 1,2-Bisanionic coupling approach to 2,3-disubstituted cyclopentenols and cyclopentenones. *Org. Lett.* **2006**, *8*, 2147.

17. Marx, J. N.; Norman, L. R. Synthesis of (–)-acorone and related spirocyclic sesquiterpenes. *J. Org. Chem.* **1975**, *40*, 1602.

18. Shen, Y. et al. Protecting-group-free total synthesis of (–)-jiadifenolide: development of a [4+1] annulation toward multisubstituted tetrahydrofurans. *Org. Lett.* **2015**, *17*, 5480.

19. Yasuda, A.; Yamamoto, H.; Nozaki, H. Highly Stereospecific isomerization of oxiranes into allylic alcohols by means of organoaluminum amides. *Bull. Chem. Soc. Jpn.* **1979**, *52*, 1705.

20. Steves, J. E.; Stahl, S. S. Copper(I)/ABNO-catalyzed aerobic alcohol oxidation: alleviating steric and electronic constraints of Cu/TEMPO catalyst systems. *J. Am. Chem. Soc.* **2013**, *135*, 15742.

21. Iimura, S.; Overman, L. E.; Paulini, R.; Zakarian, A. Enantioselective total synthesis of guanacastepene N using an uncommon 7-*endo* Heck cyclization as a pivotal step. *J. Am. Chem. Soc.* **2006**, *128*, 13095.

22. Mewshaw, R. E. Vilsmeier reagents: preparation of β-halo-α,β-unsaturated ketones. *Tetrahedron Lett.* **1989**, *30*, 3753.

23. Helal, C. J.; Meyer, M. P. The Corey-Bakshi-Shibata reduction: mechanistic and synthetic considerations – bifuntional Lewis base catalysis and dual activation. In *Lewis Base Catalysis in Organic Synthesis*, 1st ed.; Vedejs, E.; Denmark, S. E., Eds. Wiley-VCH: Weinheim, Germany, 2016.

24. Corey, E. J.; Link, J. O. A new chiral catalyst for the enantioselective synthesis of secondary alcohols and deuterated primary alcohols by carbonyl reduction. *Tetrahedron Lett.* **1989**, *30*, 6275.

25. Nwoye, E. O.; Dudley, G. B. Synthesis of *para*-methoxybenzyl (PMB) ethers under neutral conditions. *Chem. Commun.* **2007**, 1436.

26. Wu, L. P. et al. Palladium-catalyzed carbonylative transformation of C(sp^3)-X bonds. *ACS Catalysis* **2014**, *4*, 2977.

27. Odell, L. R.; Russo, F.; Larhed, M. Molybdenum hexacarbonyl mediated CO gas-free carbonylative reactions. *Synlett* **2012**, 685.

28. Ueda, T.; Konishi, H.; Manabe, K. Palladium-catalyzed carbonylation of aryl, alkenyl, and allyl halides with phenyl formate. *Org. Lett.* **2012**, *14*, 3100.

29. Ueda, T.; Konishi, H.; Manabe, K. Palladium-catalyzed fluorocarbonylation using *N*-formylsaccharin as CO source: general access to carboxylic acid derivatives. *Org. Lett.* **2013**, *15*, 5370.

30. Jiang, X. et al. Palladium-catalyzed formylation of aryl halides with *tert*-butyl isocyanide. *Org. Lett.* **2014**, *16*, 3492.

31. Krasovskiy, A.; Kopp, F.; Knochel, P. Soluble lanthanide salts $LnCl_3$•2LiCl for the improved addition of organomagnesium reagents to carbonyl compounds. *Angew. Chem. Int. Ed.* **2006**, *45*, 497.

32. Baldwin, J. E.; Cutting, J.; Dupont, W.; Kruse, L.; Silberman, L.; Thomas, R. C. 5-*endo*-trigonal reactions: disfavored ring-closure. *J. C. S. Chem. Commun.* **1976**, 736.

33. Wolleb, H.; Carreira, E. M. Total synthesis of (+)-dendrowardol C. *Angew. Chem. Int. Ed.* **2017**, *56*, 10890.

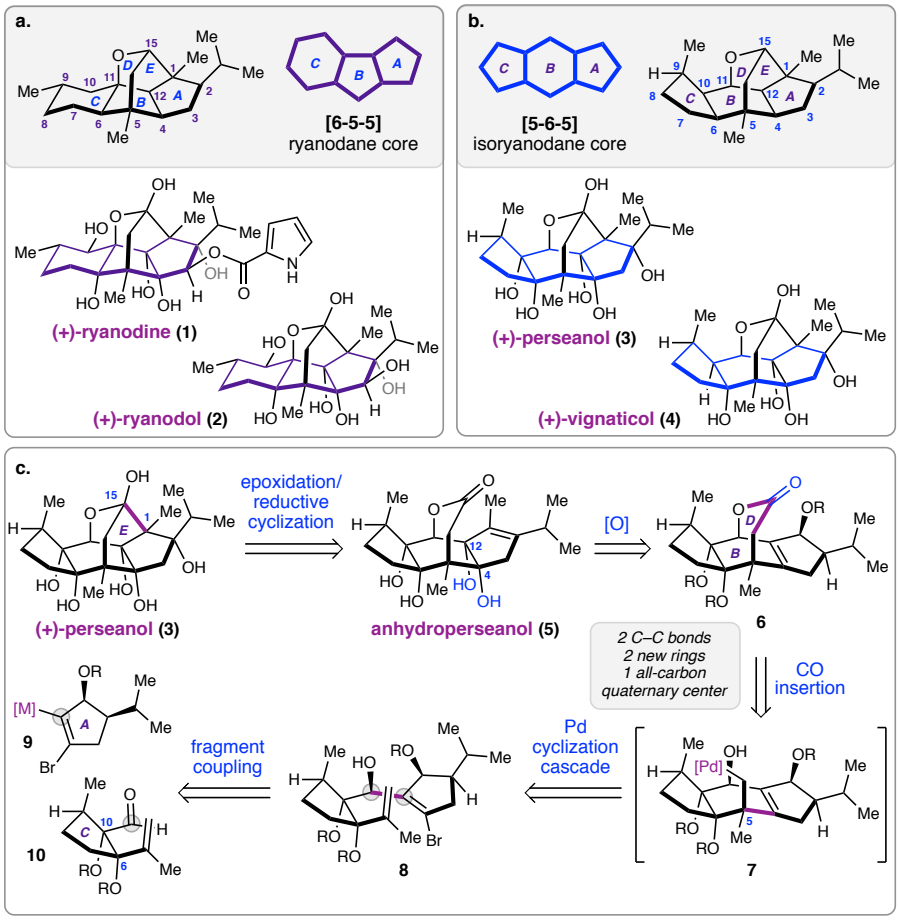

Figure 1. The ryanodane and isoryanodane diterpenes. (**a**) Chemical structure, carbon numbering, and ring system letter assignment for the ryanodane diterpenes. (**b**) Chemical structure, carbon numbering, and ring system letter assignment for the isoryanodane diterpenes. (**c**) Retrosynthetic analysis of the isoryanodane diterpene (+)-perseanol.

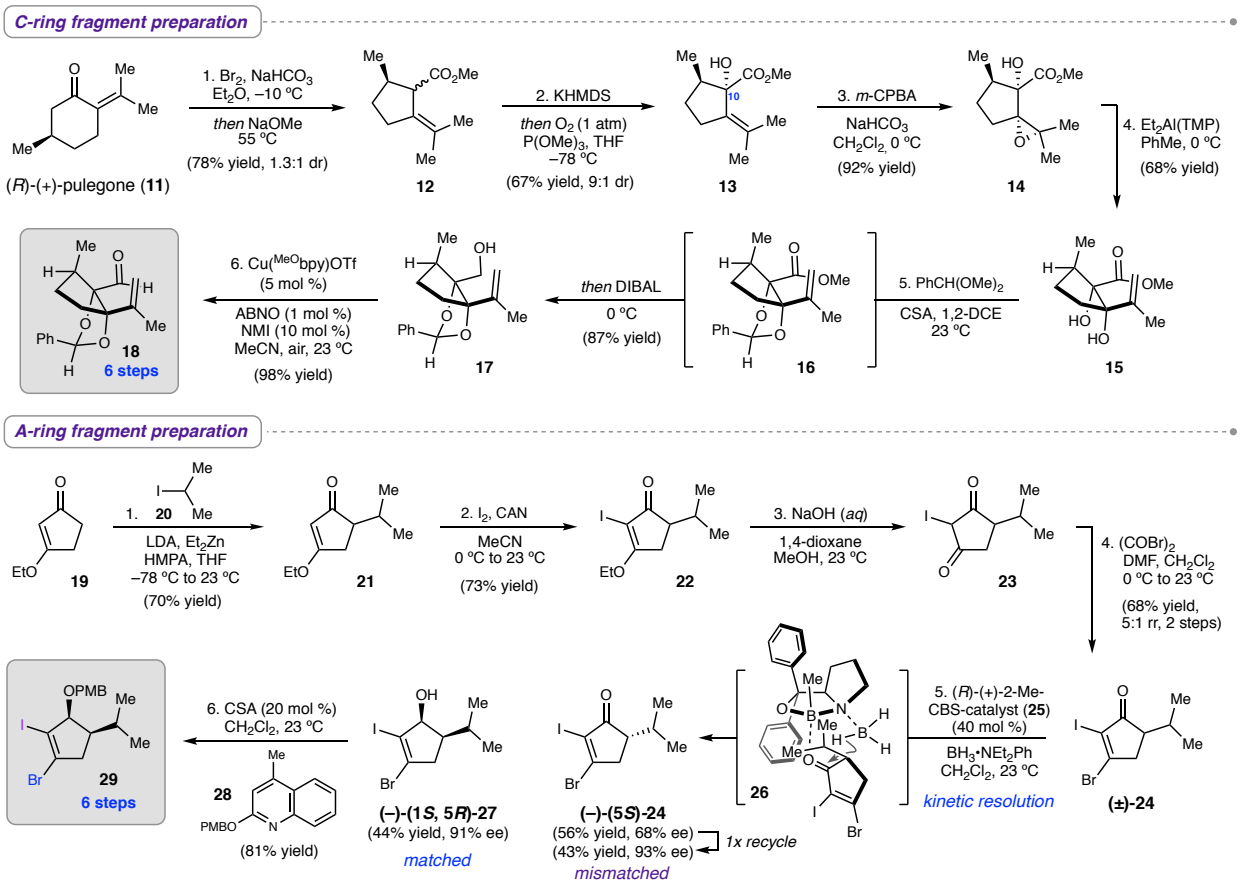

Figure 2. Fragment preparation for the synthesis of (+)-perseanol. Reagents and conditions as follows for C-ring fragment preparation: (1) Br_2 (1.1 equiv), $NaHCO_3$ (0.3 equiv), Et_2O, –10 ºC then NaOMe (2.2 equiv), MeOH, 55 ºC, 78% yield. (2) KHMDS (2.0 equiv), THF then O_2 (1 atm), $P(OMe)_3$ (2.0 equiv), –78 ºC, 67% yield. (3) *m*-CPBA (2.0 equiv), $NaHCO_3$ (4.0 equiv), CH_2Cl_2, 0 ºC, 92% yield. (4) $Et_2Al(TMP)$ (2.4 equiv), PhMe, 0 ºC, 68% yield. (5) benzaldehyde dimethyl acetal (5.0 equiv), (±)-10-camphorsulfonic acid (1.0 equiv), 1,2-dichloroethane, 23 ºC then DIBAL (9.0 equiv), 0 ºC, 87% yield. (6) $Cu(MeCN)_4OTf$ (5 mol %), 4,4'-dimethoxy-2,3'-bipyridine (5 mol %), 9-azabicyclo[3.3.1]nonane *N*-oxyl (1 mol %), 1-methyliidazole (10 mol %), air, MeCN, 23 ºC, 98% yield. Reagents and conditions as follows for A-ring fragment preparation: (1) **20** (5.0 equiv), LDA (1.1 equiv), Et_2Zn (1.05 equiv), hexamethylphosphoramide (4.5 equiv), THF, –78 ºC to 23 ºC, 70% yield. (2) I_2 (1.05 equiv), ceric ammonium nitrate (1.05 equiv), MeCN, 0 ºC to 23 ºC, 73% yield. (3) 1.0 M NaOH (*aq*) (10 equiv), 1,4-dioxane/MeOH (1:1), 23 ºC. (4) oxalyl bromide (1.5 equiv), DMF (3.0 equiv), CH_2Cl_2, 0 ºC to 23 ºC, 68% yield, 2 steps. (5) **25** (0.4 equiv), BH_3•NEt_2Ph (0.7 equiv), CH_2Cl_2, 23 ºC, 44% yield **(–)-27**, 91% ee. (6) **28** (2.0 equiv), (±)-10-camphorsulfonic acid (0.2 equiv), CH_2Cl_2, 23 ºC, 81% yield.

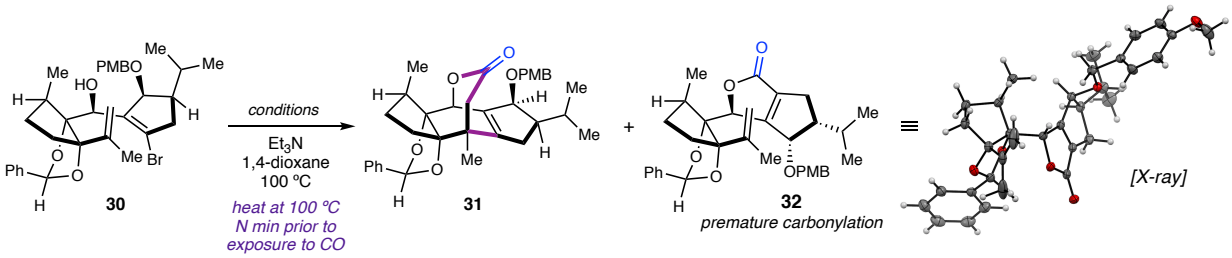

entry[a]	[M]	mol %	CO source	additive	*N* (min)	30 (%)[b]	31 (%)[b]	32 (%)[b]
1	$Pd(P(o\text{-}Tol)_3)_2$	50	CO (1 atm)	–	0	92	1	5
2	$Pd(P(o\text{-}Tol)_3)_2$	50	CO (1 atm)	–	20	67	11	15
3	$Pd(P(o\text{-}Tol)_3)_2$	120	CO (1 atm)	–	90	0	52	0
4	$Pd(P(o\text{-}Tol)_3)_2$	120	CO (10 atm)	–	90	0	53	0
5	$Pd(PPh_3)_4$	120	CO (1 atm)	–	90	23	48	13
6	$Pd(PPh_3)_4$	50	**33**	DBU	–	85	0	8
7	$Pd(PPh_3)_4$	50	**34**	–	–	90	0	0
8	$Pd(PPh_3)_4$	50	**35**	–	–	14	7	4
9	$Pd(PPh_3)_4$	50	**36**	–	–	22	31	10
10	$Pd(PPh_3)_4$	50	**36**	KF	–	1	57	14
11	$Pd(P(o\text{-}Tol)_3)_2$	50	**36**	KF	–	60	0	0
12	$PdCl_2$(dppf)	50	**36**	KF	–	80	0	0
13	$PdCl_2$(Xantphos)	50	**36**	KF	–	55	1	4

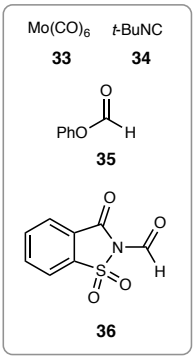

[a]Reactions performed on 0.01 mmol scale at 100 °C (0.01M).
[b]Yields determined by ^{1}H NMR versus pyrazine as an added internal standard.

Table 1. Evaluation of conditions for a Pd-catalyzed carbopalladation/carbonylation cascade.

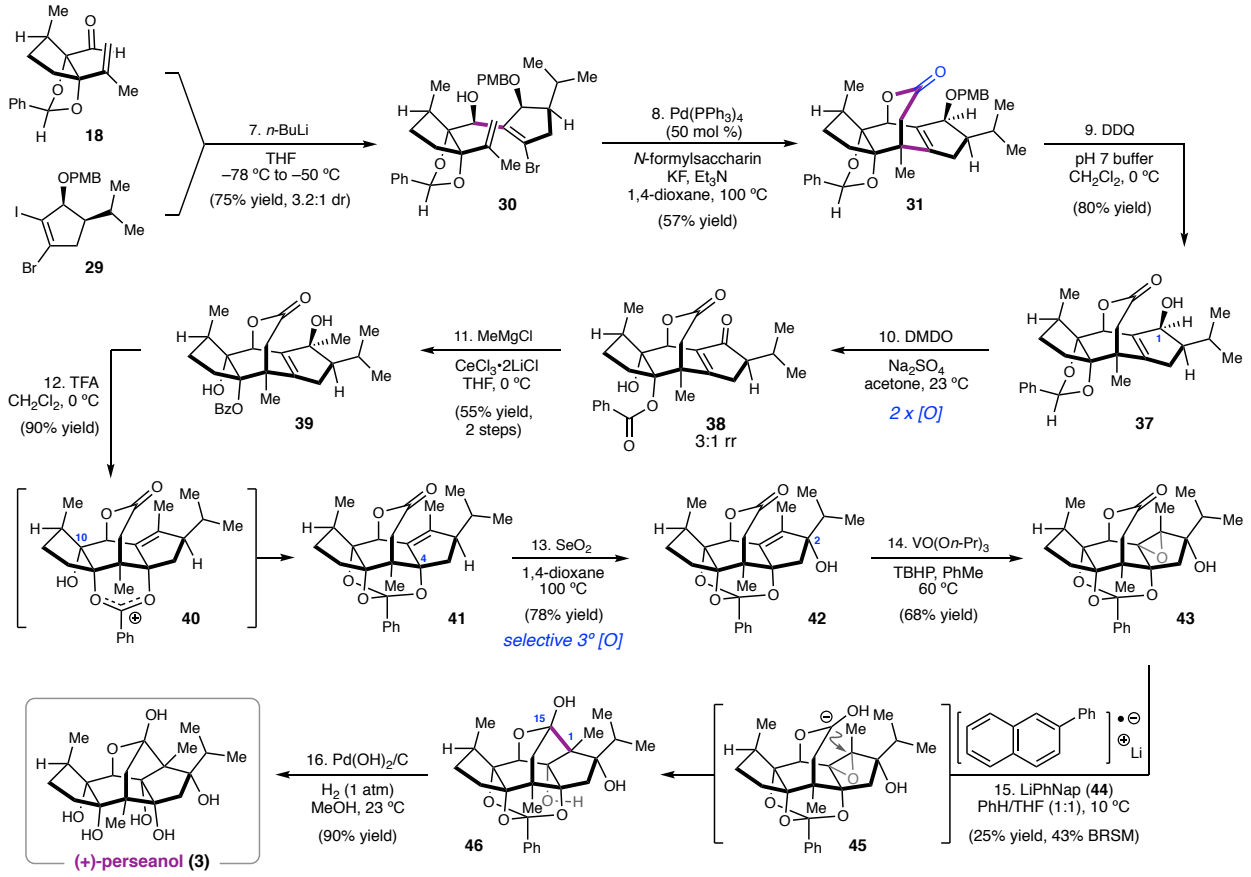

Figure 3. 16-step synthesis of (+)-perseanol. Reagents and conditions as follows: (7) 29 (1.25 equiv), *n*-butyllithium (1.25 equiv), THF, –78 °C to –50 °C, 75% yield. (8) $Pd(PPh_3)_4$ (50 mol %), *N*-formylsaccharin (1.2 equiv), KF (2.5 equiv), Et_3N (4.0 equiv), 1,4-dioxane, 100 °C, 57% yield. (9) DDQ (1.8 equiv), CH_2Cl_2/pH 7 buffer (5:1), 0 °C, 80% yield. (10) DMDO (3.0 equiv), Na_2SO_4 (200% w/w), acetone, 23 °C. (11) MeMgCl (2.0 equiv), $CeCl_3$•2LiCl (2.0 equiv), THF, 0 °C, 55% yield, 2 steps. (12) TFA (5.0 equiv), CH_2Cl_2, 0 °C, 90% yield. (13) SeO_2 (5.0 equiv), 1,4-dioxane, 100 °C, 78% yield. (14) $VO(On\text{-}Pr)_3$ (1.0 equiv), TBHP (6.0 equiv), PhMe, 60 °C, 68% yield. (15) 44 (4.5 equiv), PhH/THF (1:1), 10 °C, 25% yield, 43% BRSM. (16) $Pd(OH)_2$/C (200% w/w), H_2 (1 atm), MeOH, 90% yield.

Supplementary Information is available in the online version of the paper.

Acknowledgments. Dr. Scott Virgil and the Caltech Center for Catalysis and Chemical Synthesis are gratefully acknowledged for access to analytical equipment. We thank Mr. Larry Henling

(Caltech) and Dr. Julie Hofstra (Caltech) for X-ray data collection and data refinement, respectively, for the structure of **32** and **S21**. Prof. Yonghui Zhang (Huanzhong University of Science and Technology) is acknowledged for providing original spectral data of perseanol. Dr. Kangway Chuang (Caltech) is gratefully acknowledged for insightful contributions to the synthetic design. Fellowship support was provided by the NIH (A.H., Nos. 5T32GM007616-37 and 1F31GM120821). S.E.R. is a Heritage Medical Research Investigator. Financial support from the NIH (Nos. NIGMS RGM097582-01 and R35GM118191-01), Eli Lilly, and Novartis is gratefully acknowledged.

Author Contributions. A.H. and S.E.R. conceived this work; A.H., Y.T., and S.E.R. designed the experiments and analyzed the data; A.H. and Y.T. conducted the experiments; A.H. and S.E.R. wrote the manuscript.

Methods. Unless otherwise stated, reactions were performed under an inert atmosphere (dry Ar) with freshly dried solvents utilizing standard Schlenk techniques. Tetrahydrofuran, methylene chloride, acetonitrile, 1,4-dioxane, and toluene were dried by passing through activated alumina columns. Yields refer to chromatographically and spectroscopically (^{1}H and ^{13}C) homogeneous materials. Reagents were purchased at the highest commercial quality and used without purification, unless otherwise stated. Reactions were magnetically stirred and monitored by thin-layer chromatography. For full experimental details–including procedures for all reactions and characterization of all compounds (^{1}H NMR, ^{13}C NMR, mass spectrometry, infrared spectroscopy, retention factors)–see the Supplementary Information.

Author Information. Reprints and permissions Information is available at http://www.nature.com/reprints. The authors declare no competing interests. Correspondence and request for materials should be addressed to S.E.R (reisman@caltech.edu).

Data Availability. Characterization data for all compounds produced in this study are available in the Supplementary Information or on request from the corresponding author. Metrical parameters for the structure of **32** and **S21** are available free of charge from the Cambridge Crystallographic Data Centre (CCDC) under reference number 1909375 and 1914686, respectively.

Chapter 2

Enantioselective Diels-Alder Reactions of α-Acyloxy Enones[†]

[†]This chapter have been reproduced from: Mendoza, S. D.; Rombola, M.; Tao, Y.; Zuend, S. J.; Götz, R.; McLaughlin, M. J.; Reisman, S. E. *Org. Lett.* **2022**, *24* (21), 3802–3806.

Expanding the Chiral Monoterpene Pool: Enantioselective Diels–Alder Reactions of α-Acyloxy Enones

Skyler D. Mendoza‡[1], Michael Rombola‡[1], Yujia Tao[1], Stephan J. Zuend[2], Roland Götz[3], Martin J. McLaughlin[3], and Sarah E. Reisman*[1]

[1]The Warren and Katharine Schlinger Laboratory for Chemistry and Chemical Engineering, Division of Chemistry and Chemical Engineering, California Institute of Technology, Pasadena, California, 91125, United States

[2]BASF Corp., 46820 Fremont Boulevard, Fremont, California 94538, United States

[3]BASF SE, Carl Bosch Str. 38, Ludwigshafen 67056m Germany

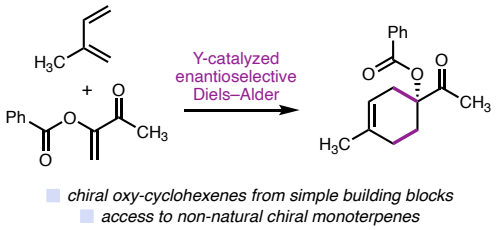

ABSTRACT: An enantioselective Diels–Alder (DA) reaction of α-acyloxy enones has been developed to synthesize chiral oxidized cyclohexenes. Yttrium(III) triflate, in conjunction with a chiral pyridinebisimidazoline (PyBim) ligand, was found to catalyze the asymmetric [4+2] cycloaddition with a variety of dienes and α-acyloxy enone dienophiles. Using this method, terpinene-4-ol, a key intermediate in the synthesis of commercial herbicide cinmethylin, can be prepared in four steps from isoprene. A combination of kinetics data and NMR studies support a mechanism involving reversible binding of dienophile to an yttrium catalyst followed by cycloaddition with a diene as the rate-determining step.

Naturally occurring monoterpenes serve as important chiral building blocks for the synthesis of natural products, medicines, and agrochemicals. For example, the monocyclic cyclohexene-containing terpenes (+)- and (–)-limonene and (+)- and (–)-carvone are inexpensive and frequently used members of the 'chiral pool'.[1] Terpinene-4-ol (T-4-ol, **2**, Figure 1a), the starting material for the BASF herbicide cinmethylin (**1**), is also a naturally occurring monoterpene; however, it is only available either as a racemate or as a 2:1 scalemic mixture of enantiomers. Given the importance of oxidized monoterpenes as entry points to higher order terpenes and other complex molecules, we sought to develop an enantioselective synthesis of **2** and related oxidized cyclohexenes that could expand the pool of chiral building blocks.

As a result of the cyclohexene motif, we envisioned that **2** could be derived from a Diels–Alder cycloadduct.[2] Despite the extensive development of enantioselective DA reactions,[3] the use of α-acyloxy enones as dienophiles remains underexplored (Figure 1b). In independent studies, teams lead by Ishihara and Hayashi have reported the chiral amine-catalyzed reaction of aldehyde **4**;[3g,3k] however, this mode of dienophile activation could not be extended to the corresponding methyl ketone **7**, as required to efficiently prepare **8**. More generally, methods to prepare cyclohexenes bearing stereogenic, fully substituted alcohols, such as that found in **2**, are limited.[3l] In this communication, we report an yttrium-catalyzed enantioselective Diels–Alder reaction between simple dienes, such as isoprene (**3a**), and α-oxygenated dienophiles (Figure 1c). This transformation provides direct access to valuable oxidized cyclohexene building blocks in enantioenriched form.

Figure 1. Motivation for Reaction Development

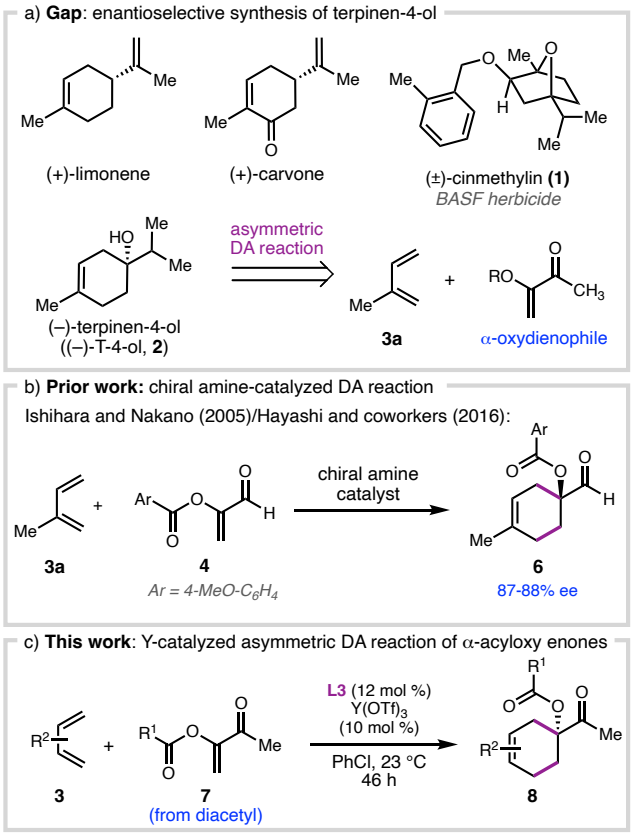

Our reaction development efforts began with isoprene (**3a**) as the diene and 3-oxobut-1-en-2-yl benzoate (**7a**) as the dienophile (Table 1). We note that **7a** can be prepared form the commercially available chemicals diacetyl and benzoyl chloride,[4] and therefore was appealing from an industrial perspective. It was hypothesized that dienophile **7a** may form a 7-membered chelate to a Lewis acidthrough its two carbonyl oxygens, which would provide a sterically well-defined environment for asymmetric induction while attenuating the resonance donating effect of the acyloxy substituent. As a result, we investigated chiral Lewis acids known to catalyze enantioselective cycloadditions of dicarbonyl electrophiles.[3e]

Table 1. Optimization of Reaction Conditions[a]

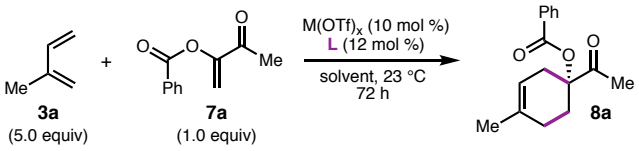

entry	$M(OTf)_x$	L	solvent	Yield (%)[b]	ee (%)[c]	rr[b]
1	$Cu(OTf)_2$	L1	CH_2Cl_2	25	–5	8:1
2	$Cu(OTf)_2$	L2	CH_2Cl_2	66	–32	>20:1
3	$Sc(OTf)_3$	L2	CH_2Cl_2	21	11	12:1
4	$Yb(OTf)_3$	L2	CH_2Cl_2	16	52	15:1
5	$Y(OTf)_3$	L2	CH_2Cl_2	75	65	15:1
6	$Y(OTf)_3$	L3	CH_2Cl_2	88	83	14:1
7	$Y(OTf)_3$	L3	TBME	77	86	10:1
8	$Y(OTf)_3$	L3	PhCl	90	90	15:1
9[d]	$Y(OTf)_3$	L3	PhCl	66	89	12:1
10[e]	$Y(OTf)_3$	L3	PhCl	51	37	11:1

[a]Reactions performed on 0.2 mmol scale. [b]Yield and rr determined by ^{1}H NMR analysis of crude reaction mixture. [c]Determined by SFC chromatography using chiral stationary phase. [d]5 mol % catalyst and 6 mol % ligand. [e]10 mol % BzOH added.

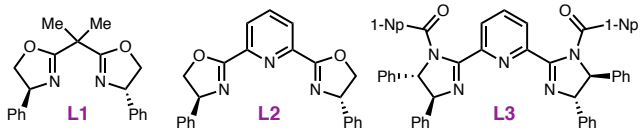

The combination of $Cu(OTf)_2$ and **L1** was found to catalyze the desired transformation; however, cycloadduct **8a** was obtained in low yield as a nearly racemic mixture (Table 1, entry 1). Whereas other bidentate ligands gave **8a** in <10% ee, the tridentate PyBox ligand **L2** gave **8a** in improved yield, ee, and regioselectivity, favoring the para cycloadduct (entry 2).[5] At this stage, we investigated alternative Lewis acids, which revealed that **L2** complexes of rare-earth salts gave significantly improved enantioselectivity (entries 3–5).[6]

Further ligand optimization determined that PyBim ligand **L3**[7] with $Y(OTf)_3$ in CH_2Cl_2 catalyzed the formation of **8a** with good conversion and 83% ee (entry 6). A solvent screen revealed that chlorobenzene – a preferred solvent in the agrochemical industry – provided the optimal combination of yield and enantioselectivity (entry 8). Use of 5 mol % catalyst resulted in slightly lower yields of the product but comparable ee (entry 9). Addition of benzoic acid (10 mol %), an impurity resulting from dienophile hydrolysis, significantly decreased the yield and ee of the product (entry 10).[8]

With optimized conditions in hand, we next interrogated the influence of the ester substituent on the yield and ee of the reaction (Figure 2). A series of benzoate esters revealed that esters with electron donating substituents in the para position perform best in terms of enantioselectivity (**8b–d**). Electron deficient benzoate esters required long reaction times to achieve high conversion and the products were formed in lower ee (**8e,f**). We hypothesized that the lower enantioselectivity may result from dienophile hydrolysis by adventitious water during the extended reaction times, which produces the corresponding benzoic acid. Given that exogenous benzoic acid was found to deactivate the catalyst and lower the ee (see Table 1, entry 10), we tested whether catalyst deactivation was operative with slow-reacting dienophiles. Indeed, the results of a same excess experiment for the reaction between **3a** and **7e** were consistent with catalyst deactivation over time.[9] Sterically encumbered aliphatic esters also performed well, giving the corresponding products in good yield and high ee (**8g–i**). The phenyl carbonate dienophile could also be used; however, the product was formed in lower yield and ee (**8j**). The reaction to give cycloadduct **8g** was scaled to 1.0 mmol with no decrease in yield or selectivity (92% yield, 86% ee, 16:1 rr).

Figure 2. Investigation of the Ester Substituent

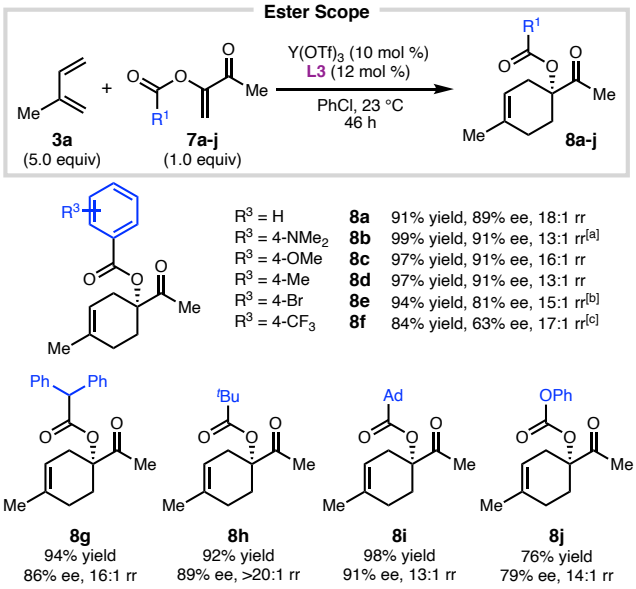

Reactions performed on 0.4 mmol scale. Isolated yields. % ee determined by SFC using chiral stationary phase. [a]Reaction time of 3 days. [b]Reaction time of 5 days. [c]Reaction time of 14 days.

Next, we investigated the diene scope (Figure 3). For these studies, dienophile **7g** was used due to its ease of handling. Although the simple 1,3-butadiene undergoes cycloaddition, the reaction was very slow, and the product (**10a**) was formed in low yield with poor ee. Substitution at the 2-position of the diene with iso-propyl is tolerated with only a minor decrease in ee (**10b**) compared to **8g**. 2,3-dimethylbutadiene was found to be an excellent substrate, providing the product **10c** in 99% yield and 97% ee. Whereas cyclopentadiene undergoes cycloaddition to form **10d** in high yield, ee, and dr favoring the endo-cycloadduct, the corresponding cyclohexa-1,3-diene is less reactive and the product is formed in lower ee (**10e**). Electron rich 2-silyloxy dienes also perform well (**10f, g**), giving products with high regioselectivity and comparable ee to **8g**. In contrast, slightly lower ee is observed when the 1-silyloxydiene is employed (**10h**).

We lastly turned to investigate different dienophiles (Figure 4). Aldehyde **11a** was found to react but gave the product **12a** with low selectivity presumably due to a lack of steric bias. In general,

increasing the steric bulk of the ketone decreased the reaction rates; attempts to perform the reaction between **11c** and acyclic dienes such as **9c** and **9f** resulted in low conversion. However, when the more reactive cyclopentadiene was used, the dienophiles **11b** and **11c** gave the respective cycloadducts in good yield, albeit with slightly lower ee than when **7g** is employed. Dienophile **11d**, with a β- methyl group, underwent the cycloaddition in good yield and ee, but only modest selectivity for the endo-diastereomer was observed (**12d**).

Figure 3. Investigation of Diene Scope

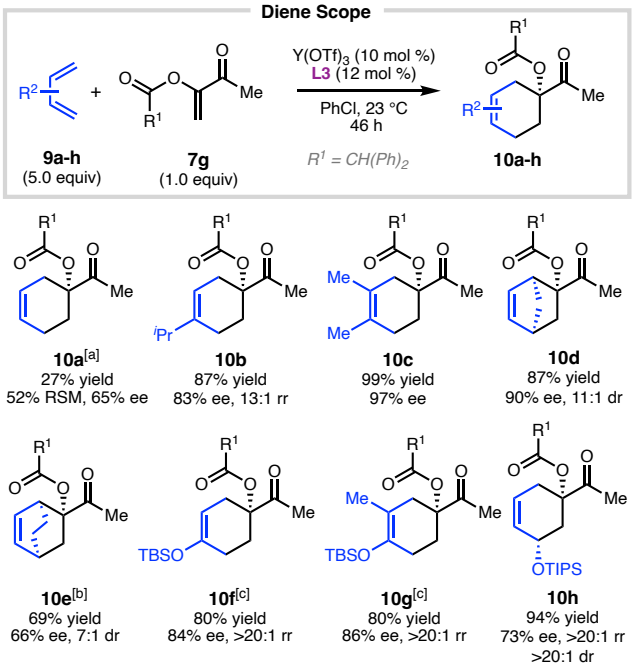

Reactions performed on 0.4 mmol scale. Isolated yields. % ee determined by SFC using chiral stationary phase. [a]Reaction time of 18 days. [b]Reaction time of 13 days. [c]Reaction performed at 0 °C.

Figure 4. Investigation of Alternative Dienophiles

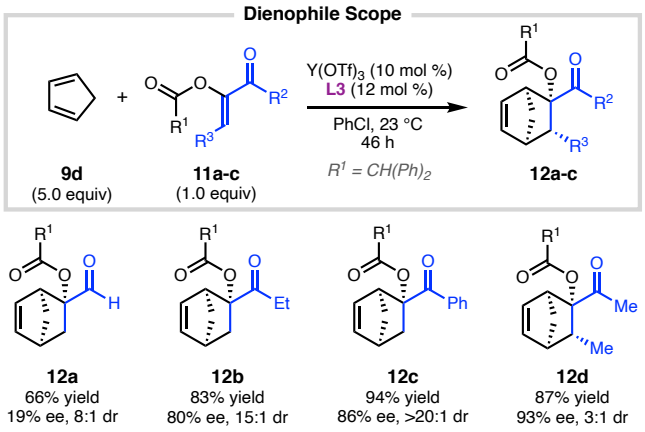

Reactions performed on 0.4 mmol scale. Isolated yields. % ee determined by SFC using chiral stationary phase.

To demonstrate the synthetic utility of these products, we elaborated **8g** to **2**, the key intermediate in the BASF synthesis of cinmethylin (Scheme 1). Cinmethylin (**1**) is a chiral terpene-derived herbicide that inhibits plant fatty acid biosynthesis. Herbicide **1** was first brought to market by Shell in 1989 for the control of grassweeds during rice cultivation[10] and was reintroduced in 2019 by BASF as Luximo™. Although cinmethylin is chiral, it is currently manufactured as a racemate;[11] however, with the changing regulatory landscape, an enantioselective synthesis is of high value. To this end, methanolysis of **8g** followed by Wittig olefination and subsequent hydrogenation afforded **2** in good yield with preservation of ee. Alternatively, the natural product (+)-andirolactone (**13**)[12] could be prepared by methanolysis of **8g** followed by reaction with Bestmann ylide,[13] also with complete retention of ee.

Scheme 1. Product Derivitization

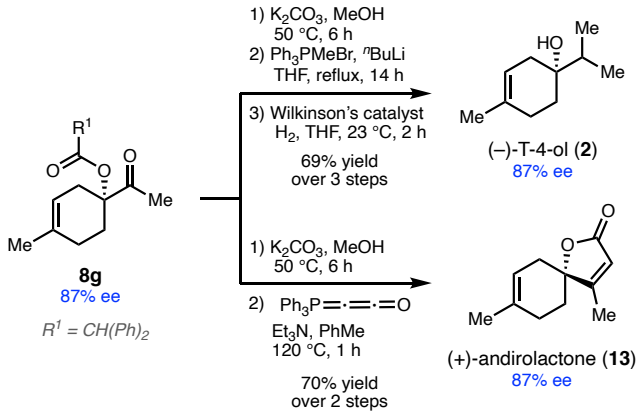

Kinetic studies were carried out on the reaction between **7d** and **9c** using variable time normalization analysis (VTNA).[14] The reaction followed an apparent first order dependence on [**L3**•$Y(OTf)_3$], first order dependence on [**9c**], and first order dependence on [**7d**].[9] These data are consistent with a mechanism involving reversible binding of **7d** to **L3**•$Y(OTf)_3$ followed by cycloaddition as the rate-determining step. ^{1}H NMR spectroscopic studies of a mixture of **L3**, $Y(OTf)_3$, and **7d** in PhCl-d5 shows no change in the chemical shifts of **7d**, suggesting the equilibrium heavily favors unbound **7d** in the presence of **L3**•$Y(OTf)_3$. In contrast to the experiments with **3a** and **7e** (vide supra), a same excess experiment revealed no significant amount of catalyst deactivation with this more rapidly reacting substrate combination.[9,15]

In summary, a Y-catalyzed Diels–Alder reaction of α-acyloxy enones has been developed. These reactions generally proceed with good enantio-, diastereo-, and regioselectivity. This method provides direct entry to enantioenriched (–)-T-4-ol (**2**), an intermediate in the synthesis of the commercial herbicide cinmethylin.[16] More generally, we anticipate that the cyclohexenes prepared by this reaction will serve as valuable chiral building blocks in the context of terpene synthesis.

ASSOCIATED CONTENT

Supporting Information

The Supporting Information is available free of charge on the ACS Publications website at DOI:

Detailed experimental procedures, compound characterization data, and ^{1}H, ^{13}C, ^{19}F NMR spectra (PDF)

AUTHOR INFORMATION

Corresponding Author

Sarah E. Reisman – *The Warren and Katharine Schlinger Laboratory for Chemistry and Chemical Engineering, Division of Chemistry and Chemical Engineering, California Institute of Technology, Pasadena, California 91125, United States;* orcid: 0000-0001-8244-9300; **Email: reisman@caltech.edu**

Authors

Skyler D. Mendoza – *The Warren and Katharine Schlinger Laboratory for Chemistry and Chemical Engineering, Division of Chemistry and Chemical Engineering, California Institute of Technology, Pasadena, California 91125, United States;* orcid: 0000-0003-1939-1884

Michael Rombola – *The Warren and Katharine Schlinger Laboratory for Chemistry and Chemical Engineering, Division of Chemistry and Chemical Engineering, California Institute of Technology, Pasadena, California 91125, United States;* orcid: **0000-0002-4402-5619**

Yujia Tao – *The Warren and Katharine Schlinger Laboratory for Chemistry and Chemical Engineering, Division of Chemistry and Chemical Engineering, California Institute of Technology, Pasadena, California 91125, United States;* orcid: 0000-0003-4615-6409

Stephan J. Zuend – BASF Corp., 46820 Fremont Boulevard, Fremont, California 94538, United States; orcid: 0000-0002-4420-000X

Roland Götz – BASF SE, Carl Bosch Str. 38, Ludwigshafen 67056, Germany

Martin J. McLaughlin – BASF SE, Carl Bosch Str. 38, Ludwigshafen 67056, Germany

Author Contributions

‡These authors contributed equally.

ACKNOWLEDGMENT

This work was financially supported by BASF (SA-9852). We thank Dr. S. Virgil (Caltech) and the Caltech Center for Catalysis and Chemical Synthesis for access to analytical equipment. Nicholas J. Fastuca (Caltech) is gratefully acknowledged for experimental help regarding kinetics experiments. Dr. Caitlin R. Lacker (Caltech) is gratefully acknowledged for discussion of substrate scope.

REFERENCES

(1) Brill, Z. G.; Condakes, M. L.; Ting, C. P; Maimone, T. J. Navigating the Chiral Pool in the Total Synthesis of Complex Terpene Natural Products *Chem. Rev.* **2017**, *117*, 11753–11795.

(2) For racemic examples using alpha-oxygenated enone dienophiles in Diels–Alder reactions, see: a) Ishibashi, Y.; Ohno, M.; Sasaki, T. Catalyzed Cycloaddition Reactions of α-silyloxy-α,β-unsaturated Ketone and Aldehyde *Tetrahedron Lett.* **1982**, *23*, 1693–1696. b) Reyes, A.; Aguilar,

R.; Munoz, A. H.; Zwick, J. C.; Rubio, M.; Escobar, J. L.; Soriano, M.; Toscano, R.; Tamariz, J. Highly Selective Diels–Alder Cycloadditions of Captodative Dienophiles 1-Acetylvinyl Arenecarboxylates to Unsymmetrically Substituted Butadienes *J. Org. Chem.* **1990**, *55*, 1024–1034. c) Andrade, R. M.; Muñoz, A. H.; Tamariz, J. 1-Acetyl-4-methyl-3-cyclohexen-1-ol, a Useful Precursor in the Synthesis of Cyclic Monoterpenes *Synth. Commun.* **1992**, *22*, 1603–1609. d) Roush, W. R.; Barda, D. A. Highly Selective Lewis Acid Catalyzed Diels–Alder Reactions of Acyclic (*Z*)-1,3-Dienes *J. Am. Chem. Soc.* **1997**, *119*, 7402–7403.

(3) a) Motoyama, Y.; Terada, M.; Mikami, K. Asymmetric Catalysis of Diels–Alder Cycloadditions by an MS-Free Binaphthol-Titanium Complex: Dramatic Effect of MS, Linear vs Positive Nonlinear Relationship, and Synthetic Applications *J. Am. Chem. Soc.* **1994**, *116*, 2812–2820. b) Hayashi, Y.; Rohde, J. J.; Corey, E. J. A Novel Chiral Super-Lewis Acidic Catalyst for Enantioselective Synthesis *J. Am. Chem. Soc.* **1996**, *118*, 5502–5503. c) Aggarwal, V. K.; Anderson, E. S.; Jones, D. E.; Obierey, K. B.; Giles, R. Catalytic Asymmetric Diels–Alder Reactions of α-Thioacrylates for the Preparation of Norbornenone *Chem. Commun.* **1998**, 1985–1986. d) Ishihara, K.; Kurihara, H.; Matsumoto, M.; Yamamoto H. Design of Brønsted Acid-Assisted Chiral Lewis Acid (BLA) Catalysts for Highly Enantioselective Diels–Alder Reactions *J. Am. Chem. Soc.* **1998**, *120*, 6920–6930. e) Evans, D. A.; Barnes, D. M.; Johnson, J. S.; Lectka, T.; Matt, P. v.; Miller, S. J.; Murry, J. A.; Norcross, R. D.; Shaughnessy, E. A.; Campos, K. R. Bis(oxazoline) and Bis(oxazolinyl)pyridine Copper Complexes as Enantioselective Diels–Alder Catalysts: Reaction Scope and Synthetic Applications *J. Am. Chem. Soc.* **1999**, *121*, 7582–7594. f) Corey, E. J.; Shibata, T.; Lee, T. W. Asymmetric Diels–Alder Reactions Catalyzed by a Triflic Acid Activated Chiral Oxazaborolidine. *J. Am. Chem. Soc.* **2002**, *124*, 3808–3809. g) Ishihara, K.; Nakano, K. Design of an Organocatalyst for the Enantioselective Diels–Alder

Reaction with α-Acyloxyacroleins *J. Am. Chem. Soc.* **2005**, *127*, 10504–10505. h) Sakakura, A.; Suzuki, K.; Ishihara, K. Enantioselective Diels–Alder Reaction of α-Acyloxyacroleins Catalyzed by Chiral 1,1'-Binaphthyl-2,2'-diammonium Salts *Adv. Synth. Catal.* **2006**, *348*, 2457–2465. i) Rickerby, J.; Vallet, M.; Bernardinelli, G.; Viton, F.; Kündig, P. E. Ruthenium–Lewis Acid Catalyzed Asymmetric Diels–Alder Reactions between Dienes and α,β-Unsaturated Ketones *Chem. Eur. J.* **2007**, *13*, 3354–3368. j) Sakakura A.; Kondo, R.; Matsumura, Y.; Akakura, M.; Ishihara, K. Rational Design of Highly Effective Asymmetric Diels–Alder Catalysts Bearing 4,4'-Sulfonamidomethyl Groups *J. Am. Chem. Soc.* **2009**, *131*, 17762–17764. k) Hayashi, Y.; Bondzic, B. P.; Yamazaki, T.; Gupta, Y.; Ogasawara, S.; Taniguchi, T.; Monde, K. Asymmetric Diels–Alder Reaction of α-Substituted and β,β-Disubstituted α,β-Enals via Diarylprolinol Silyl Ether for the Construction of All-Carbon Quaternary Stereocenters *Chem. Eur. J.* **2016**, *22*, 15874–15880. l) Ni, D.; Witherspoon, B. P.; Zhang, H.; Zhou, C.; Houk, K. N.; Brown, K. M. Stereoselective [4+2]-Cycloaddition with Chiral Alkenylboranes *Angew. Chem. Int. Ed.* **2020**, *59*, 11432–11439.

(4) Tamariz, J.; Vogel, P. New Dienophiles: 1-Acetylvinyl Arenecarboxylates. Reactivity Toward Cyclopentadiene and Exocyclic Dienes *Helv. Chim. Acta* **1981**, *64*, 188–197.

(5) Caputo, C. A.; Jones, N. D. Developments in Asymmetric Catalysis by Metal Complexes of Chiral Chelating Nitrogen-Donor Ligands *Dalton Trans.* **2007**, 4627–4640.

(6) a) Kobayashi, S.; Ishitani, H. Lanthanide(III)-Catalyzed Enantioselective Diels–Alder Reactions. Stereoselective Synthesis of Both Enantiomers by Using a Single Chiral Source and a Choice of Achiral Ligands *J. Am. Chem. Soc.* **1994**, *116*, 4083–4084. b) Keshavaraja, A.; Hegde, V. R.; Pandey, B.; Ramaswamy, A. V.; Kumar, P.; Ravindranathan, T. An Yttrium-Based Strong Lewis Acid for the Heterogeneous Catalysis of the Diels–Alder Reaction *Angew. Chem. Int. Ed.*

1995, *34*, 2143–2145. c) Spino, C.; Clouston, L. L.; Berg, D. J. Lanthanide Catalysts for the Hetero Diels–Alder Reaction: Effect of Ligand Structure and Acidity *Can. J. Chem.* **1997**, *75*, 1047–1054. d) Mikami, K.; Kotera, O.; Motoyama, Y.; Tanaka, M. Synthesis, Structure and High Catalytic Activity in the Diels–Alder Reaction of Ytterbium(III) and Yttrium(III) Bis(trifluoromethanesulfonyl)amide Complexes *Inorganic Chemistry Communications* **1998**, *1*, 10–11. e) Pellissier, H. Recent Developments in Enantioselective Yttrium-Catalyzed Transformations *Coord. Chem. Rev.* **2016**, *324*, 17–38.

(7) Bhor, S.; Anilkumar, G.; Tse, M. K.; Klawonn, M.; Döbler, C.; Bitterlich, B.; Grotevendt, A.; Beller, M. Synthesis of a New Chiral *N,N,N*-Tridentate Pyridinebisimidazoline Ligand Library and Its Application in Ru-Catalyzed Asymmetric Epoxidation *Org. Lett.* **2005**, *7*, 3393–3396.

(8) Control experiments showed that in the absence of ligand, both 10 mol % and 1 mol % $Y(OTf)_3$ catalyze the racemic background reaction. However, when neither **L3** nor $Y(OTf)_3$ were added, only trace product was formed.

(9) See Supporting information.

(10) a) Payne, G.B.; Soloway, S. B.; Powell, J. E.; Roman, S. A.; Kollmeyer, W. D. Oxabicycloalkane herbicides, EP81893, 1981. b) May, J. W.; Moncorge, J. M.; Murphy, M. W. SD 95481 a versatile new herbicide with wide spectrum crop use, Proc. – Br. Crop Prot. Conf. 1985, pp 265–270.

(11) Urch, H.; Schmitt, M.; Kolb, K.; Franz, D.; Klimov, E.; Kraus, H. Composition comprising cinmethylin-containing microparticles and a further herbicide, WO 2018/130588, 2018.

(12) Avcibasi, H.; Anil, H.; Toprak, M. Four Terpenoids from Cedrus libanotica *Phytochemistry*, **1987**, *26*, 2852–2854.

(13) Bestmann, H. J.; Sandmeier, D. Kumulierte Ylide, VI. Eine neue Synthese des (Triphenylphosphoranylinden)ketens, seines Thioanalogen und stabiler Propadienylidentriphenylphosphorane *Chem. Ber.* **1980**, *113*, 274–277.

(14) Burés, J. Variable Time Normalization Analysis: General Graphical Elucidation of Reaction Orders from Concentration Profiles *Angew. Chem. Int. Ed.* **2016**, *55*, 16084–16087.

(15) Blackmond, D. G. Kinetic Profiling of Catalyztic Organic Reactions as a Mechanistic Tool *J. Am. Chem. Soc.* **2015**, *137*, 10852–10866.

(16)A patent has been filed: Reisman, S.; Rombola, M.; Ladd, C. L.; McLaughlin, M. J.; Zuend, S.; Göetz, R. Process for the synthesis of non-racemic cyclohexenes. US Patent WO 2021/007141 A1, January 2021.

Chapter 3

An Introduction to Enterocin

3.1. Background and Significance

Polyketides are an important class of natural products, with diverse structural motifs and potent therapeutic properties.[1,2] (–)-Enterocin (**33**), also known as vulgamycin[3,3], is a polyketide natural product, first isolated from terrestrial strands of *Streptomyces* bacteria in 1976 (Figure 1).[3,3,4] By isolation chemists, enterocin (**33**) was found to be bacteriostatic against gram-negative bacteria, including *Escherichia coli* at a concentration of 4 mg/ml[3], but this result might be misreported according to a recent study by Capon and coworkers.[3] In 2020, Capon and coworkers found that enterocin (**33**) had no significant growth inhibitory activity (to 60 μM) against Gram-negative Escherichia coli ATCC11775 and Gram-positive Staphylococcus aureus ATCC 25923.[3]

Nevertheless, Enterocin (**33**) was found to have cytotoxicity against HeLa cells,[5] and possess moderate herbicidal activities.[3] Enterocin (**33**) is herbicidal towards dicotyledonous

grasses, including *Setaria sp.* at 125 - 500 g ha^{-1}, while tolerated by crops like barley, cotton, and maize.[3] There is no finding on enterocin (**33**)'s activity against fungi or yeast.

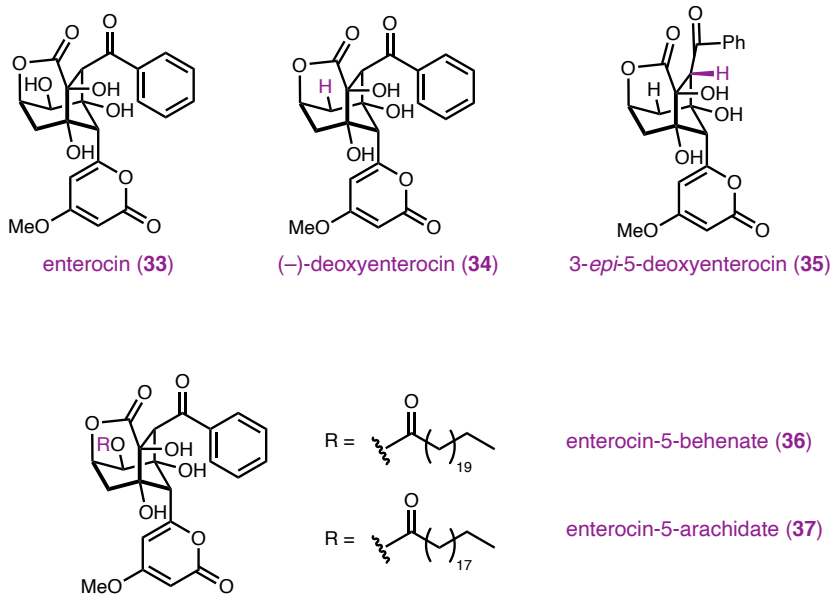

Figure 1. *Enterocin (**1**) and related natural products.*

In 1996, Australian researchers isolated enterocin (**33**) from a marine ascidian of the genus *Didemnum*.[3] This is the first report of enterocin (**33**) isolation from a non-microbial species, potentially suggesting that bacteria can produce the some of the same molecules that isolated from marine invertebrates, and there might have a symbiotic relationship between the two. Within the same paper, some enterocin-related natural products were also isolated: deoxyenterocin (**34**), and 5-acylated analogues (**36-37**) that contains long fatty acid chains (Figure 1). According to a preliminary study by Zhu and coworkers[3], **2** was found to be antiviral against the H1N1 virus with 60.6 % inhibition at 50 μg/ml, though the IC_{50} value was not determined due to lack of material. In addition, 3-*epi*-5-deoxyenterocin (**35**), an epimer of deoxygenterocin (**34**), was isolated by Davidson and coworkers.[7] This epimer (**35**) was found to have antimicrobial acitivity against *E. coli* in a paper disc diffusion assay.[7]

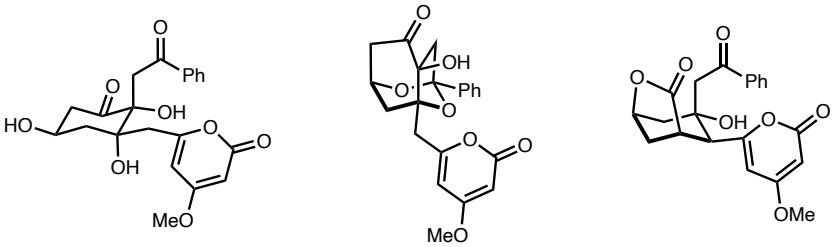

Figure 2. *Wailupemycin natural products.*

There are other three natural products isolated by Davidson and coworkers.[7] They are wailupemycins A (**38**), B(**39**), and C(**40**) (Figure 2). The shared appended α-pyrone ring feature in wailupemycin natural products potentially indicates that they are derived from the same biosynthetic pathway as enterocin (**33**).[8] Only wailupemycin A (**38**) exhibits antimicrobial activity in a paper disc diffusion assay[7], and the wailupemycins B (**39**) and C (**40**)'s bioactivities are yet to be discovered.

Structurally, enterocin (**33**) is a daunting synthetic challenge (Figure 3). It has a complicated oxygenation pattern and a near 2:1 carbon to oxygen ratio. Enterocin features a rigid and uncommon bicyclo[3.2.1]octane carbon core, decorated by 7 contiguous stereocenters and 4 free hydroxyl groups. The four free hydroxyl groups on the caged core pose significant synthetic challenge on how to install them elegantly and stereoselectively. There are two appended units in the molecule: a benzoyl group and an α-pyrone group. Overall, the high confluence of oxygenation and functional groups confers significant tactical difficulties in the design of synthetic approaches.

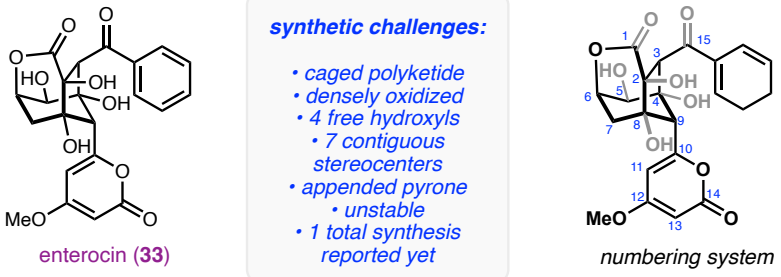

Figure 3. *Structure and synthetic challenges of enterocin.*

In addition, another major difficulty of synthetizing enterocin (**33**) chemically is that **33** is an unstable natural product. In the original isolation paper, Miyairi and coworkers[3] have noted that enterocin (**33**) was found to be stable under neutral and acidic conditions at room temperature, but was labile under basic environment. However, there was no description on the decomposition pathway of enterocin nor further investigation of the decomposed products by Miyairi and coworkers. It is not until recently that there are reports[3,9–11] on enterocin's stability and rearrangements.

3.2. Rearrangements of enterocin

In 2019, Zhang and coworkers reported the isolation of neoenterocins A and B (**41**) from enterocin producer *Streptomyces* sp. SCSIO 11863.[11] The heterologous expression, gene disruption, and isotope feeding experiments indicated that both neoenterocins A and B (**41**) were derived from the enterocin biosynthetic pathway. In the decomposition experiments, Zhang and coworkers demonstrated that enterocin (**33**) (64 mg) was converted to acid **43** (20 mg), **42** (4 mg), and neoenterocin B (**41**) (2 mg) in phosphate-buffered saline (PBS) solution (pH 9). They proposed that enterocin can undergo a series lactone-opening hydrolysis, decarboxylation, retro-aldol condensation, hemiketal formation, and dehydrations to arrive at **42**, which can be oxidized under air to neoenterocin B (**41**).

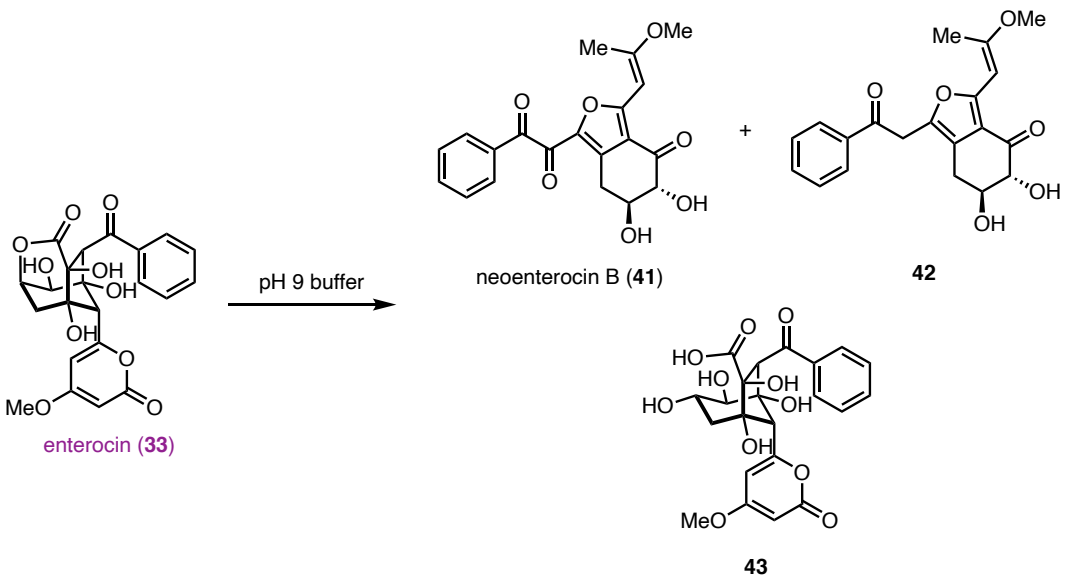

Figure 4. *Enterocin's decomposition to neoenterocin B.*

In 2020, there is a report from Piggott laboratory on (**33**)'s isomerization in different solvents. Piggott and coworkers found that enterocin (**33**) has varying degrees of decomposition when dissolving in the following solvents at room temperature over a 19-day period: water, acetone, methanol, ethanol, DMSO, dimethylformamide, pyridine, acetonitrile. Interestingly, THF, ethyl acetate, and dioxane resulted in no decomposition of enterocin (**33**). Toluene, chloroform, and dichloromethane also resulted in no decomposition, but it is because enterocin (**33**) does not dissolve in these solvents. This instability observed demonstrated that unusual lability of enterocin (**33**) and the difficulty involved in synthesizing it chemically.

As for the structures of enterocin's rearranged products in mild neutral conditions, there are three reports from Piggott laboratory[9,10] and Capon laboratory[3]. Though two laboratories have some disagreements on the structural assignments for some intermediates, one tentative rearrangement sequence was proposed by Piggott and coworkers[10] (Figure 5). First, enterocin (**33**) can epimerize to form 3-*epi*-enterocin (**35**). This epimerization was found to more likely to occur under basic conditions compared to acidic conditions. This finding therefore explains why

enterocin (**33**) is more stable under acidic over basic environments: the epimizeration is a prerequisite for further rearrangement.

Then, C5 hydroxyl group can participate in a series intramolecular nucleophilic attacks and translactonization to form hemiketal isoenterocin A (**45**). Isoenterocin A (**45**) can isomerize to isoenterocin B (**47**) either through intermediate A (**46**) or through spontaneous translactonization directly. It is important to note that Piggott and coworkers found isoenterocin B forms after isoenterocin A, although the formation of isoenterocin B (**47**) from 3-*epi*-enterocin (**35**) seems more straightforward, and validated this experimental result through DFT calculations. It is also interesting to note that isoenterocin A (**45**) is in a boat conformation, while isoenterocin B (**47**) with the 6-membered lactone present is in a pseudo-chair conformation. The distribution of isoenterocin A (**45**) and isoenterocin B (**47**) varies depending on the environmental conditions: isoenterocin A (**45**) is the dominant species in aprotic solvents, and isoenterocin B (**47**) is the dominant in protic solvents; the distribution can be further modified through pH.

Further rearrangements include equilibration between intermediate A **46** and intermediate B **49**, and then the formation of enterocinic acid A (**50**). In enterocinic acid A (**50**), the benzylic alcohol (C15 alcohol) is no longer in the correct orientation to cyclization with C1 carbonyl and therefore enterocinic acid A (**50**) does not have further isomerizations. On the other hand, enterocenic acid A (**48**) (revised structure of reported enterocin F by Capon and coworkers[3]), which was isolated before[12] from a family of bacteriocins isolated from *Enterococcus faecium*, can form under basic conditions from **49**.

This proposed rearrangement heavily reply on the agency of C5 hydoxyl group to perform intramolecular attacks to the benzylic carbonyl. Indeed, this finding is supported by comparision with deoxyenterocin (**34**), which does not have C5 hydroxyl group and does not rearrange further

after forming 3-*epi*-deoyenterocin. There is further evidence from Piggott and coworkers[9] that if they protected the key nucleophilic secondary C5 alcohol with acyl groups, the corresponding analogues have better stability than enterocin (**33**).

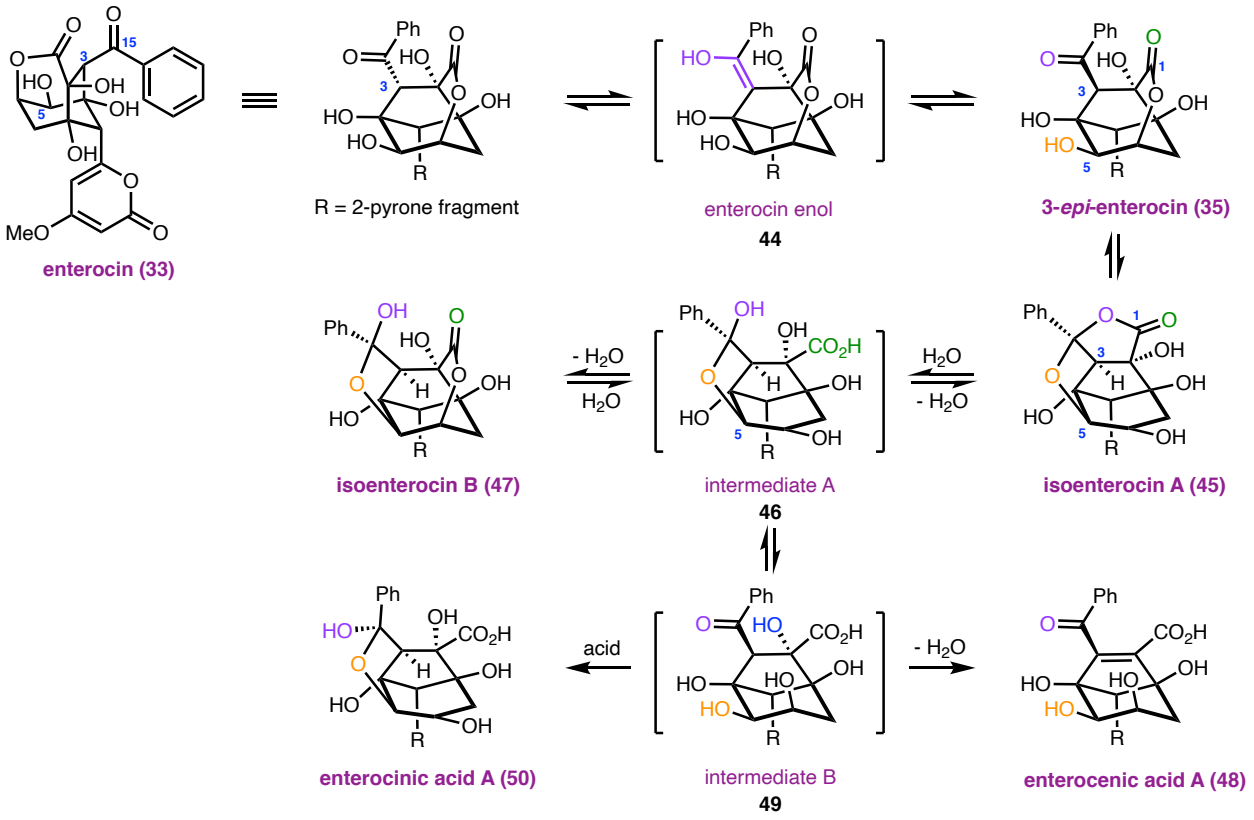

Figure 5. *Proposed rearrangement mechanism for the transformation of enterocin.*

3.3. Biosynthesis of enterocin

Unlike other polyketides that have polycyclic aromatic core structures, enterocin (**33**) is a unique polyketide natural product, featuring a caged tricyclic core. The formation of enterocin (**33**) is therefore of interests and in 2013, Moore and coworkers elucidated its biosynthetic pathway (Figure 6)[8]. Benzoate primer **52,** derived from *L*-phenylalanine, first undergoes seven iterative elongation steps by type II polyketide synthase (EncABC) and is reduced by ketoreductase EncD to afford the linear dihydrooctaketide **53**. Interestingly, enterocin (**33**) uses benzoate instead of acetate as the starter unit. Using a benzoic acid starter unit is pretty unique, as the only other

example is soraphen A[13]. Another interesting part of this biosynthesis is that while type II polyketide synthase pathways typically provide polycyclic aromatic compounds, such as tetracycline[14], **53** remarkably cyclizes into wailupemycin G (**57**) and wailupemycin F (**58**) only in minor quantities. Instead, in the presence of FAD-dependent 'favorskiiase' EncM, **21** preferentially converts into desmethyl-5-deoxyenterocin (**56**), through C2 oxidation to form triketone **54**, followed by a favorskii rearrangement, and subsequent aldol reactions. Finally, a methyltransferase (EncK) and a P450 hydroxylase (EncR) convert **52** to **33**.

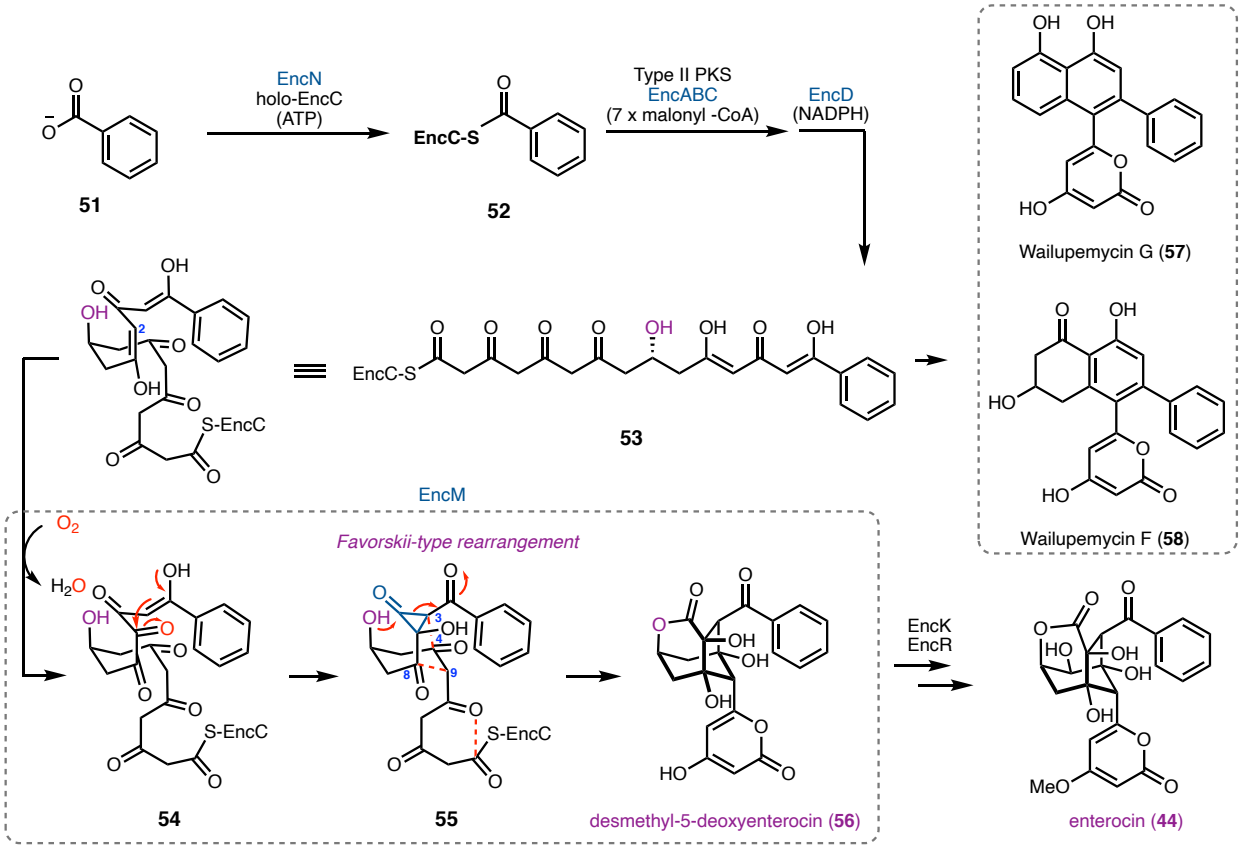

Figure 6. *Biosynthetic pathway of enterocin (**1**).*

The 'favorskii' EncM enzyme's structure was resolved and found to be a homodimer that covalently links to a flavin cofactor.[8] Compared with homologous flavin-dependent enzymes, EncM has an unusually long L-shaped ligand-binding tunnel. When octaketide **53** resides in the

L-shaped tunnel in an elongated form, the deleterious polycyclic aromatization can be avoided. Having elucidated the biosynthetic pathway, Moore lab was able to synthesize several enterocin analogs (Figure 7) on analytical scale observing by HPLC-MS, using different benzoate starter units.[15,16] EncN was found to be quite substrate specific, as evaluated by relative reactivity toward different benzoate substrate (Figure 7) and has been found to be inactive to a lot of other substrates.

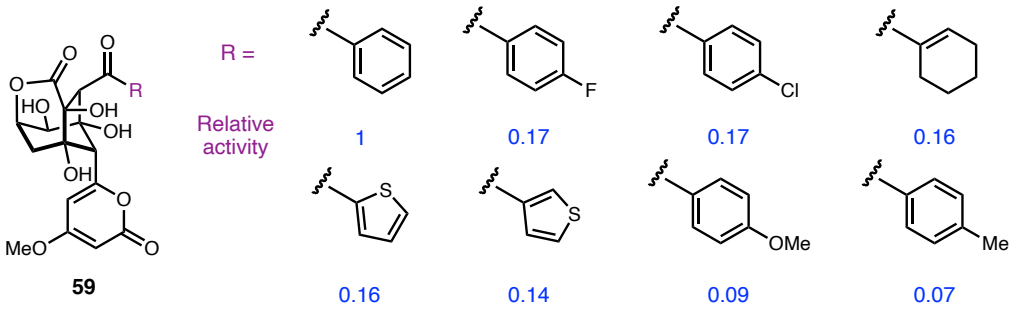

Figure 7. *Mutasynthesis of enterocin analogs and substrate specificity.*

3.4. Previous synthetic effort toward the total synthesis of enterocin

While this highly oxygenated core presents interesting yet challenging questions on introducing these functionalities selectively and compatibly, there have been much elegant and efficient synthetic effort reported toward the total synthesis of enterocin (**33**). More specifically, there are one reported total synthesis and several synthetic approaches toward the total synthesis of **33** and **34**. In 1986, Flores-Parra and Khuong-Huu prepared an early intermediate with enterocin's 2-oxabicyclo[3.3.1]nonane core.[17,18] In 2007, Chin and coworkers attempted using McMurry coupling to construct enterocin's dihydroxybicyclo[3.2.1]octane core.[19] In 2015, Bach group explored using intramolecular *meta*-photocycloaddition for the synthesis of the bicyclo[3.2.1]octane core of enterocin.[20] While these early approaches are innovative, they reached limited success in further functionalization to access enterocin (**33**).

In 2016, Bach published a synthetic approach toward the total synthesis of enterocin (**33**) (Figure 8).[21] Key to their synthetic design was the proposed construction of the C3–C4 and C8–

C9 bond via a two-fold aldol cascade, mimicking the biosynthesis. This disconnection allows the simplification of the caged enterocin core into linear precursor **60**. In the forward sense, a diastereoselective Mukaiyama aldol between silyl ketene acetal **62** and aldehyde **61** affords **63** in 85% yield. Base-mediated lactonization followed by Pd-catalyzed allylation delivered **66**. Under ozonolytic conditions, terminal alkene **66** was oxidatively cleaved and, serendipitously, the C2 position was concomitantly oxidized to install the requisite tertiary hydroxyl group. Bach's report ends with compound **67** and thus, the question of a biomimetic aldol as a method for the construction of enterocin remains unsolved.

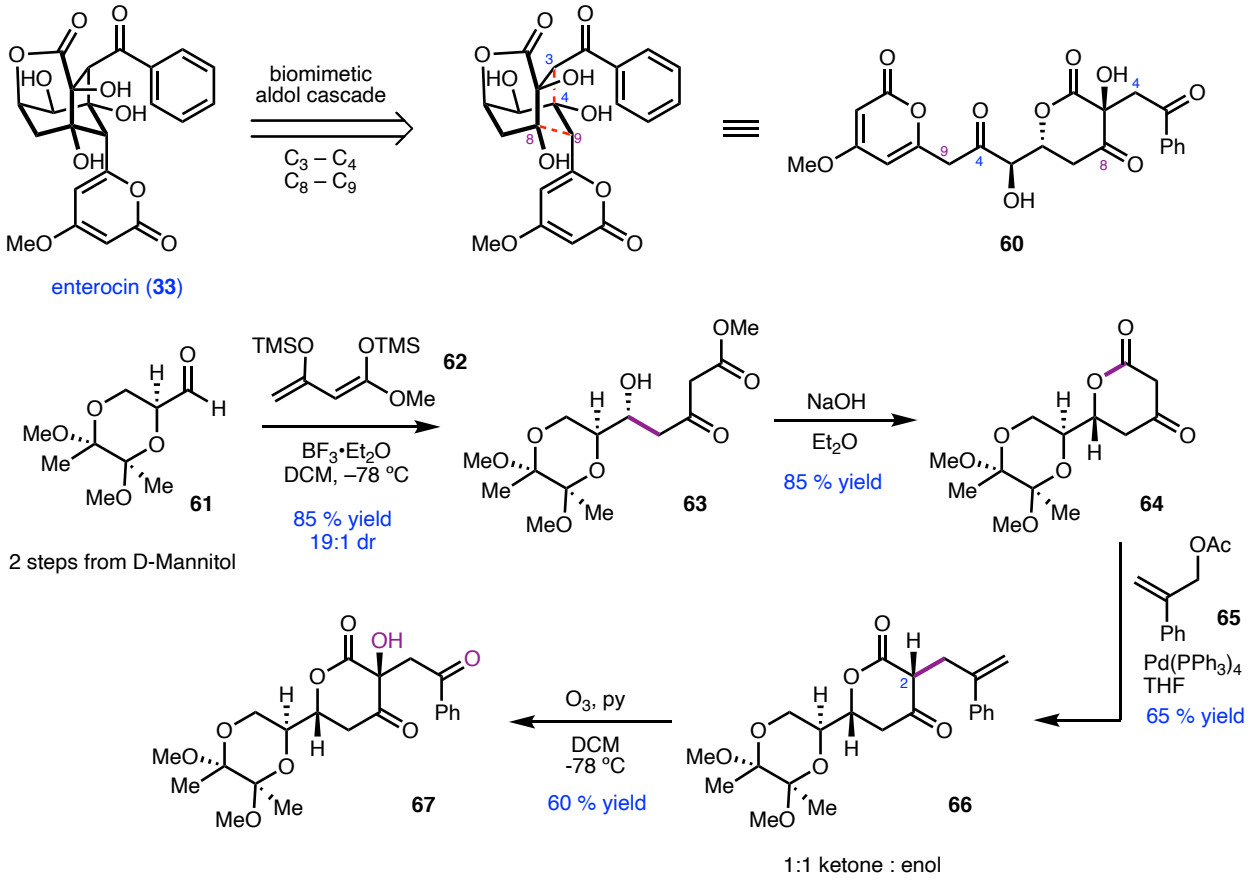

Figure 8. *2017 Bach's biomimetic two-fold aldol approach toward enterocin.*

In 2018, the Trauner lab published an approach toward enterocin (**33**) (Figure 9).[22] Hypothesizing that enterocin's lactone moiety might be unstable, they planned to install the C5

and lactone oxidations through late-stage C–H oxidations. Similar to Bach's strategy, the Trauner group disconnected the C3–C4 bond via a biomimetic aldol. Retrosynthetic reduction of diketone **69** revealed **70** as a useful intermediate, which could be accessed via an intramolecular barbier reaction of **71**. Through a key Horner-Wadsworth-Emmons reaction, fragments **72** and **73** could be coupled. Indeed, vinyl bromide **74** could be obtained in 9 steps and metalation with dialkyl cuprate (n-Bu_2CuCN•LiCN) successfully furnished the desired bicycle **75** in 70% yield. Further functionalization of the C9-C10 olefin proved challenging. It was inferred that their proposed aldol precursor might be unstable and difficult to effect in a non-enzymatic environment.

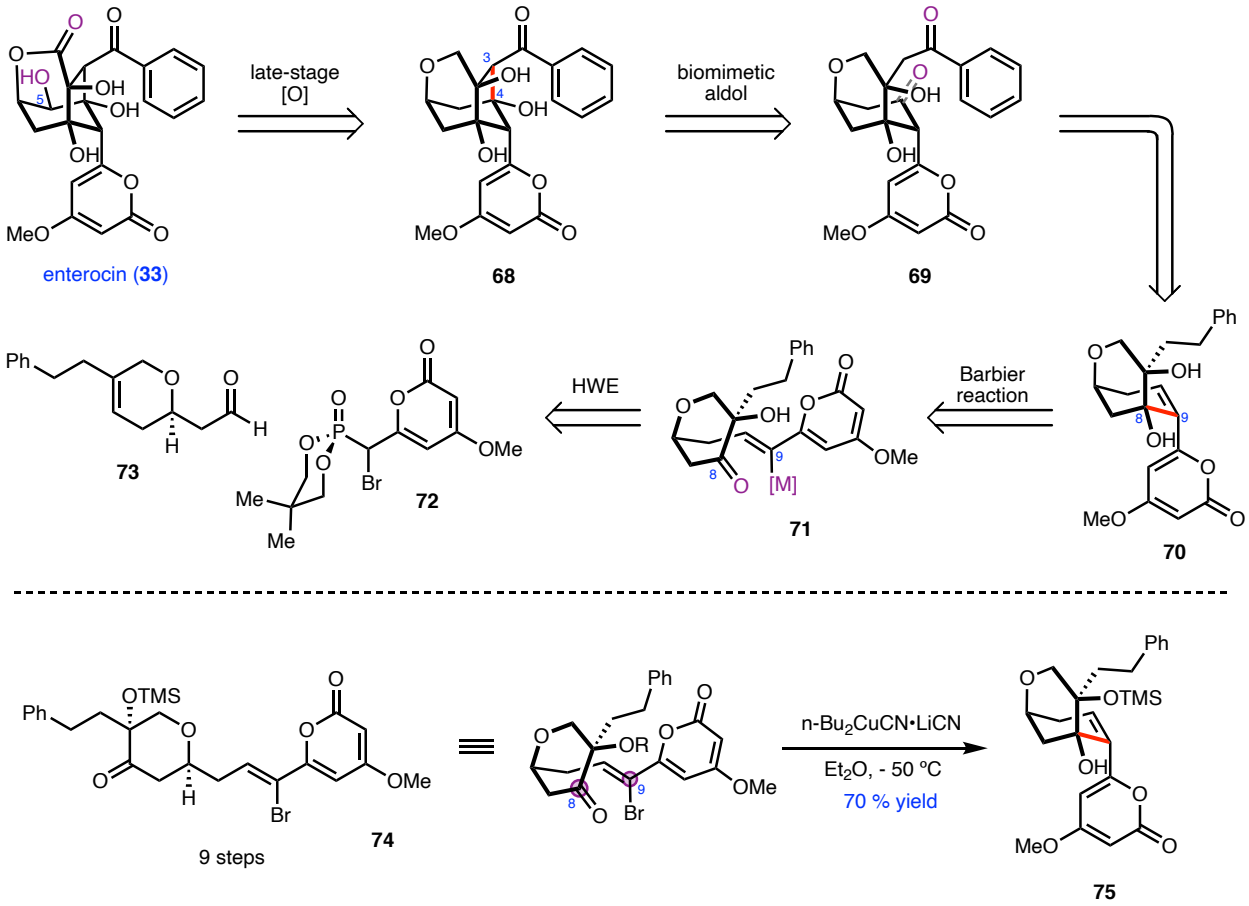

Figure 9. *2018 Trauner's aldol and cuprate addition approach toward enterocin.*

In 2019, Trauner and coworkers published another biomimetic approach toward deoxyenterocin (**34**) (Figure 10).[23] Similar to Bach's approach, they disconnected C3–C4 and C8–

C9 bonds via biomimetic aldol reactions. Retrosynthetic hydrolysis of deoxyenterocin (**34**), revealed **76** as a target linear precursor. Starting from (*S*)-epichlorohydrin, aldol precursor **76** could be accessed utilizing an acyloin coupling strategy. It is noteworthy that the benzylic position of the α-pyrone was found to be very acidic, but could be protected by a diazo group. Unfortunately, the proposed aldol cascade of **76** was unsuccessful under a variety of conditions. DFT calculations suggest that the aldol cascade is thermodynamically unfavorable.

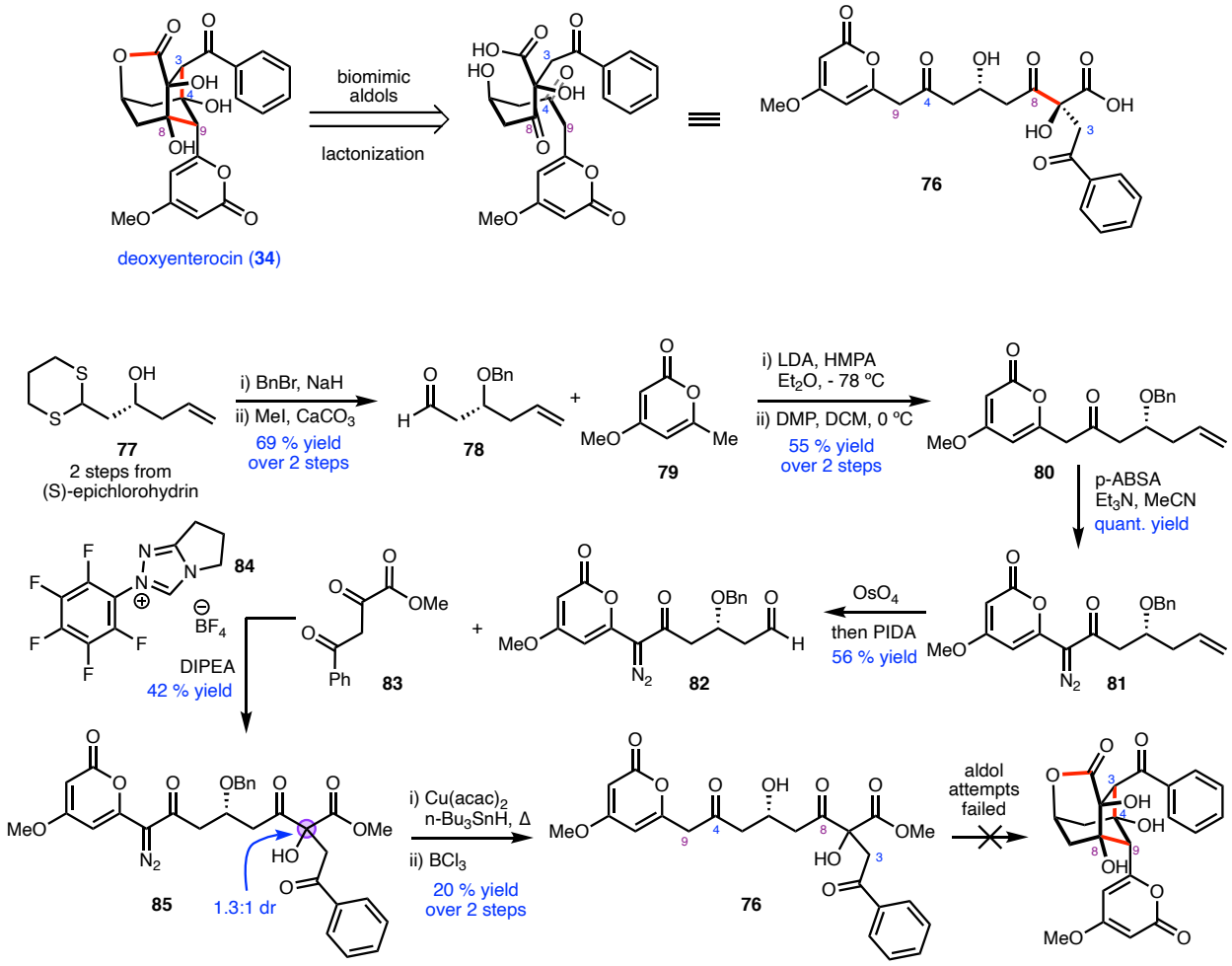

Figure 10. *2019 Trauner's biomimetic aldol approach toward deoxyenterocin.*

In 2022, Bach and coworkers reported the first and only total synthesis of enterocin (**33**).[24] The authors envisioned to use a late-stage biomimetic aldol cascade to forge the caged skeleton of **33**. This disconnection allowed them to unfold **33** into **86**, which they were able to access from L-

arabinose **90**. In acetonitrile solution, the precursor **86** cyclized into **92** as the desired aldol cascade spontaneously, albeit in modest yield. The cascade was accelerated in the presence of K_2CO_3. Bach and coworkers propose that the MEM-protected C5 alcohol in **86** is critical for the success of the biomimetic aldol cascade, as it adopts an equatorial position, conformationally favor the six-membered transition state leading to cyclization.

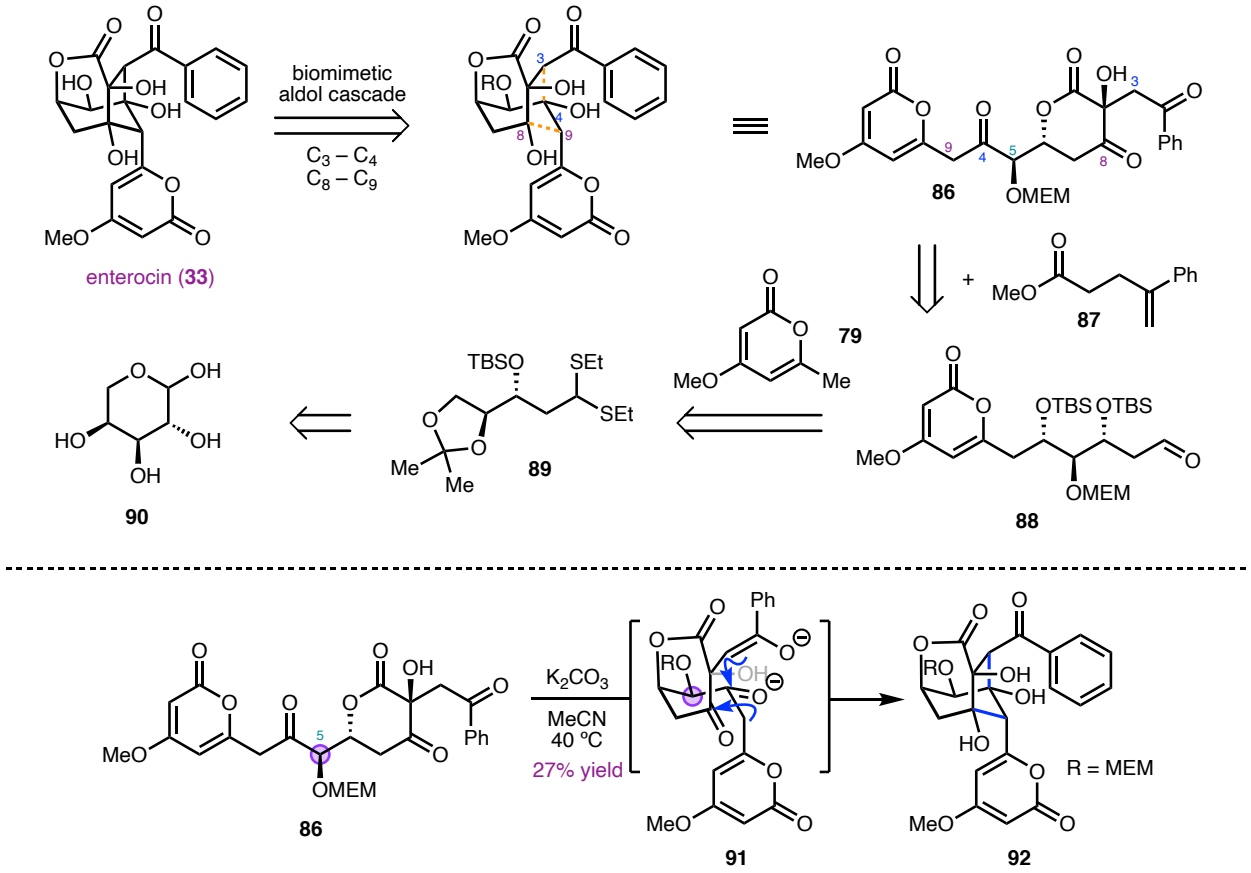

Figure 11. *2021 Bach's biomimetic total synthesis of enterocin.*

After the Bach group completed the total synthesis of **33** in 2021, they found that the synthetic enterocin has an opposite specific rotation and a different HPLC retention from the reported (–)-enterocin.[25] They also measured vibrational circular dichroism (VCD) of the synthetic enterocin, and found it to be different from the calculated VCD of (–)-enterocin. They therefore argued that (–)-enterocin's structure is *ent*-**33**. Interestingly, enterocin's derivative 5-*m*-

bromobenzoyl enterocin was analyzed through X-ray crystallography shortly after enterocin was first discovered.[4] Although the X-ray crystallography paper did not present scientific proof for the absolute configuration, the authors drew **33** as the structure of (–)-enterocin. While Bach's evidences are compelling, it would be more convincing if they were able to derivatize the synthetic enterocin to 5-*m*-bromobenzoyl enterocin and obtain a crystal structure with absolute configuration data. For clarity, we will be pursuing the synthesis of enterocin as structure **33**.

Recognizing enterocin's remarkable antibiotic properties, synthetic challenges posed by its caged and highly oxidized structure, and the elusive structure confirmation, our lab has been actively pursuing the total synthesis of enterocin antibiotics. This report will detail the synthetic efforts toward enterocin and deoxyenterocin.

3.5. References

(1) Staunton, J.; J. Weissman, K. *Nat. Prod. Rep.* **2001**, *18* (4), 380–416.

(2) Hertweck, C. *Angew. Chem. Int. Ed.* **2009**, *48* (26), 4688–4716.

(3) Salim, A. A.; Samarasekera, K.; Khalil, Z. G.; Capon, R. J. *Org. Lett.* **2020**, *22* (12), 4828–4832.

(4) Tokuma, Y.; Miyairi, N.; Morimoto, Y. *J. Antibiot. (Tokyo)* **1976**, *29* (10), 1114–1116.

(5) Xu, D.-B.; Ma, M.; Deng, Z.-X.; Hong, K. *Appl. Microbiol. Biotechnol.* **2015**, *99* (14), 5825–5832.

(6) Yaginuma, S.; Asahi, T.; Muto, N.; Hayashi, M. JP62056487A, 1987.

(7) Sitachitta, N.; Gadepalli, M.; Davidson, B. S. *Tetrahedron* **1996**, *52* (24), 8073–8080.

(8) Teufel, R.; Miyanaga, A.; Michaudel, Q.; Stull, F.; Louie, G.; Noel, J. P.; Baran, P. S.; Palfey, B.; Moore, B. S. *Nature* **2013**, *503* (7477), 552–556.

(9) Cowled, M. S.; Vuong, D.; Crombie, A.; Lacey, E.; Karuso, P.; Piggott, A. M. *Org. Biomol. Chem.* **2020**, *18* (30), 5879–5890.

(10) Cowled, M. S.; Lacey, E.; Karuso, P.; Piggott, A. M. *Org. Lett.* **2020**, *22* (24), 9688–9692.

(11) Zheng, L.; Jiang, X.; Zhang, Q.; Zhu, Y.; Zhang, H.; Zhang, W.; Saurav, K.; Liu, J.; Zhang, C. *Org. Lett.* **2019**, *21* (22), 9066–9070.

(12) Achemchem, F.; Martínez-Bueno, M.; Abrini, J.; Valdivia, E.; Maqueda, M. *J. Appl. Microbiol.* **2005**, *99* (1), 141–150.

(13) Schupp, T.; Toupet, C.; Cluzel, B.; Neff, S.; Hill, S.; Beck, J. J.; Ligon, J. M. *J. Bacteriol.* **1995**, *177* (13), 3673–3679.

(14) Hertweck, C.; Luzhetskyy, A.; Rebets, Y.; Bechthold, A. *Nat Prod Rep* **2007**, *24* (1), 162–190.

(15) Kalaitzis, J. A.; Izumikawa, M.; Xiang, L.; Hertweck, C.; Moore, B. S. *J. Am. Chem. Soc.* **2003**, *125* (31), 9290–9291.

(16) Kalaitzis, J. A.; Cheng, Q.; Thomas, P. M.; Kelleher, N. L.; Moore, B. S. *J. Nat. Prod.* **2009**, *72* (3), 469–472.

(17) Flores-Parra, A.; Khuong-Huu, F. *Tetrahedron* **1986**, *42* (21), 5925–5930.

(18) Flores-Parra, A.; Gutiérrez-Avella, D. M.; Contreras, R.; Khuong-Huu, F. *Magn. Reson. Chem.* **1989**, *27* (6), 544–555.

(19) Hong, B.-C.; Chin, S.-F. *Synth. Commun.* **1999**, *29* (18), 3097–3106.

(20) Wegmann, M.; Bach, T. *J. Org. Chem.* **2015**, *80* (3), 2017–2023.

(21) Wegmann, M.; Bach, T. *Synthesis* **2016**, *49* (01), 209–217.

(22) Rizzo, A.; Trauner, D. *Org. Lett.* **2018**, *20* (7), 1841–1844.

(23) Rizzo, A.; Mayer, R. J.; Trauner, D. *J. Org. Chem.* **2019**, *84* (3), 1162–1175.

(24) Koser, L.; Lechner, V. M.; Bach, T. *Angew. Chem. Int. Ed.* **2021**, *60* (37), 20269–20273.

(25) Koser, L.; Grassin, C.; Merten, C.; Bach, T. *Org. Lett.* **2022**, *24* (38), 6903–6907.

Chapter 4

A SeO_2 multioxidation approach toward enterocin

4.1 Retrosynthetic analysis

One of the major difficulty in chemically synthesizing enterocin is installing the rich and complex oxygenation patterns on the caged core structure, especially the three free hydroxyl groups at bridgeheads. In comtemplating routes to access enterocin, we took inspiration from an unusual step in Reisman's total synthesis of (+)-ryanodol.[1] In that synthesis, the treatment of enone **93** with SeO_2 under aqueous or anhydrous conditions yielded oxidized compounds **94** and **95**, respectively (Figure 1). While the yields are modest, this reaction provides a powerful tool to quickly construct complex oxygenation patterns. In addition, Reisman lab was able to expand the substrate scope of this SeO_2 oxidation reaction to other systems and investigate further on its mechanism.[2] Realizing this transformation can effectively install multiple oxygenation at once, we

began to be interested in how to apply this powerful methodology elegantly and efficiently. At that time, we noticed the oxygenation pattern on enterocin core matches that of the SeO_2 product: three hydroxyl groups decorating a cyclopentane ring, with two at bridgeheads (highlighted in Figure 1). This pattern recognition prompted us to explore the possibility of applying the SeO_2 multioxidation reaction on the synthesis of enterocin (**33**).

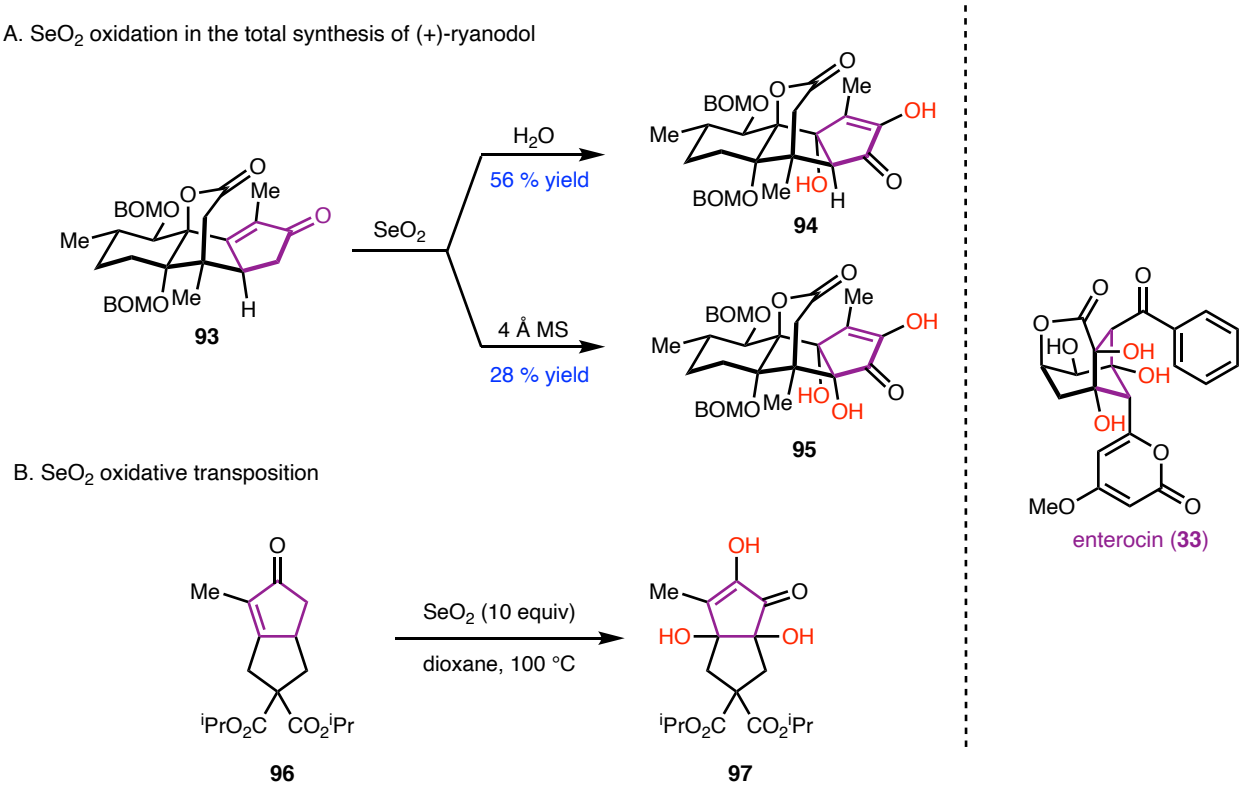

Figure 1. *Inspirations for a SeO_2 disconnection to access enterocin oxygenation patterns.*

Using the SeO_2 multioxidation as the key step, we devised the following retrosynthesis (Figure 2). We envisioned to install the benzylic oxidation through a late-stage C-H oxidation, and introduce the appended pyrone using C9 ketone as a functional handle. Next, we planned to forge C4-C5 bond through a SmI_2 reductive cyclization, and intermediate **98** can be unfolded into aldehyde **99**. The C2 and C8 hydroxyls would be planted by a SeO_2 multi-oxidation of the Pauson-Khand reaction adduct **100**. Although the SeO_2 multi-oxidation was only reported to work on [5.5]

fused bicyclic enones, and not known to be effective on a [6.5] fused bicycle system, we think this SeO_2 multi-oxidation step is early in the route enough to justify our efforts in attempting this reaction here. The enterocin system would also provide a unique insights in a better understanding of the SeO_2 multi-oxidation reaction. Next, disconnecting the ester bond would give alkyne fragment **102** [23] and alcohol fragment **103** [24], and both of them are known in literature.

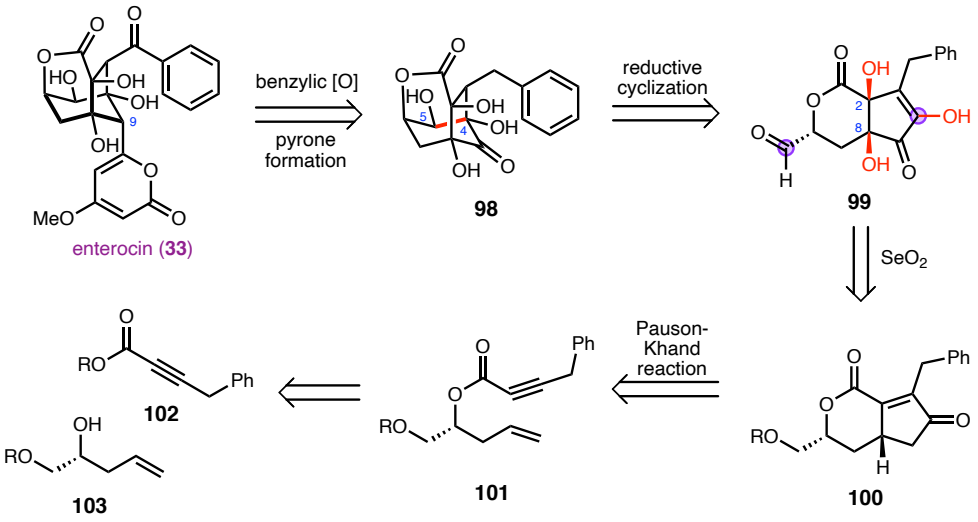

Figure 2. *Retrosynthetic analysis of enterocin.*

4.2. Results and discussion

In the forward sense, the first generation plan to access Pauson-Kand reaction precursor **109** is utilizing a DCC coupling between acid **106** and alcohol **108** (Scheme 1). Specifically, we were able to reproduce a known copper-promoted coupling[3] of ethyl propiolate **104** and benzyl chloride to afford **105** in 90 % yield on 20 g scale. A known epoxide opening[4] by vinyl Grignard adding into benzyl glycidyl ether **107** yielded alcohol fragment **108** in quantitative yield on 20 g scale. However, the initial attempts to saponify ester **105** into acid **106** via stirring with TFA or NaOH at room temperature proven fruitless. Under basic condition, a base-mediated alkyne to allene isomerization occurred on **105**, and affording allenic acid as the major product.

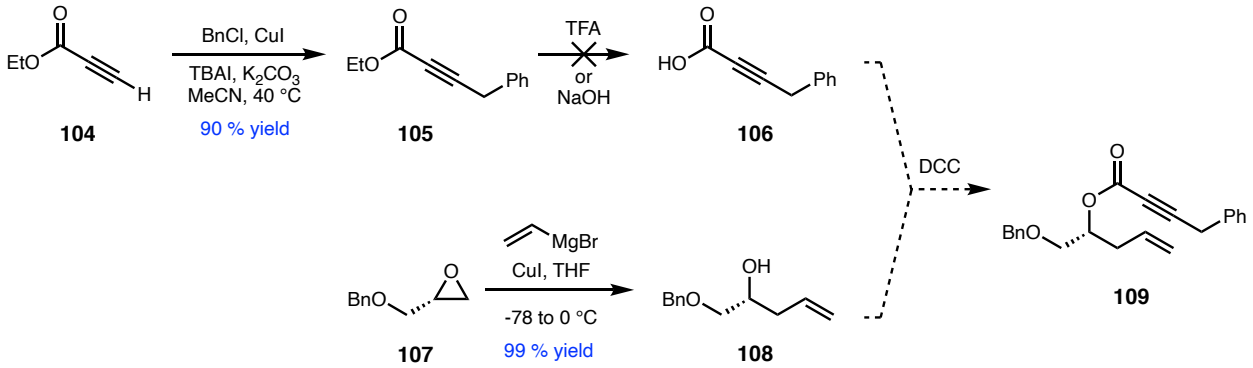

Scheme 1. *Initial attempts to assemble PKR precursor.*

Therefore, our alternative plan to circumvent the alkyne-allene isomerization problem was performing a direct transesterification between ester **105** and alcohol **108** (Scheme 2). Acid-promoted transesterification between alkyne **105** and a model system primary alcohol but-3-en-1-ol was successful. However, the same condition did not work with alcohol **108**, due to its secondary alcohol being less reactive. Fortunately, Otera's catalyst 1**21**[5,6], an organostannane transesterification catalyst, was effective in forming **119** in 68 % yield through heating **115** and 1.1 equivalence of **118** with molecular sieves in toluene at 110 ºC. With **120** at hand, the next step is performing a Pauson-Khand reaction (PKR) to access fused bicycle **122**. While the PKR reaction seems straight-forward, substrate **120** might be a challenging substrate as the alkyne is conjugated with a carbonyl, and Pauson-Khand reactions are known to be difficult for electron-deficient alkene or alkyne.[7] Nevertheless, following a Co-mediated PKR protocol for electron deficient alkyne using NMO•H_2O as the chemical promoter for CO dissociation[8], bicycle **122** was obtained in 85 % yield on 20 g scale as a single diastereomer, with C8 methine pointing down. The stereochemistry was rationalized as shown in Figure 4. The coordination of the reactant alkene to the coordinately unsaturated $Co_2(CO)_5$(alkyne) intermediate takes place from the top face. Then the insertion took place from the less hindered face (opposite from the OBn chain) of the olefin and created C8 stereocenter selectively.

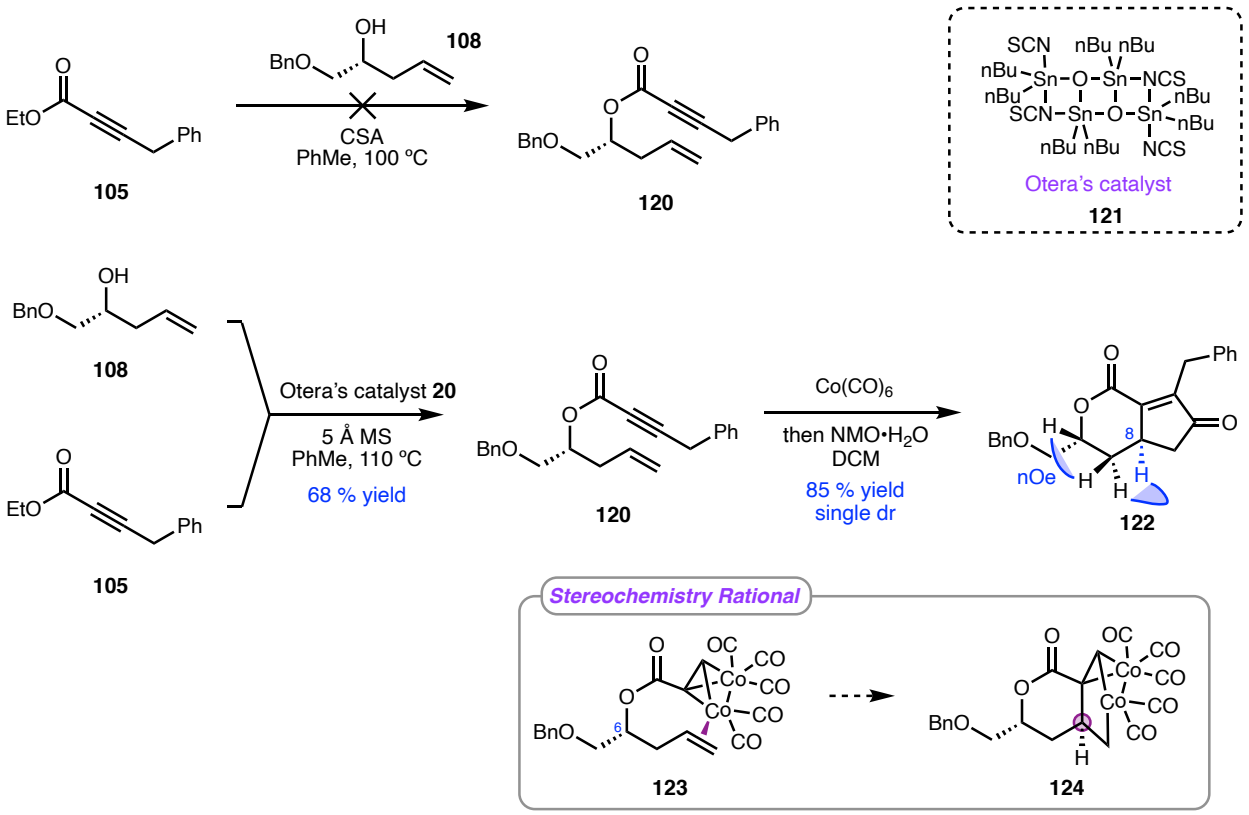

Scheme 2. *Transesterification and PKR studies.*

However, the C8 methine stereochemistry raised concerns about the next SeO_2 step. Allylic oxidations of SeO_2 are stereoretentive, because the mechanism for such reaction is SeO_2 undergoes an ene reaction to form allylseleninic acid and a subsequent [2,3]-sigmatropic rearrangement and hydrolysis furnishes the allylic alcohol.[9] In the total synthesis of (+)-ryanodol, the unusual SeO_2 is also stereoretentive.[1] When we started exploring this step, the mechanism of this multi-oxidation[2] was yet not fully understood. Therefore, it was reasonable to question that since the C8 methine is on the opposite face to the desired SeO_2 product, whether we will obtain a different diastereomer of the desired product in the SeO_2 reaction.

One solution to this stereochemistry question was to epimerize C8 methine. However, attempts to deprotonate C8 proton using KO^{t}Bu[10] was unsuccessful because the deprotonation

preferentially occurred at α-position of the enone carbonyl. We also tried different Pauson-Khand conditions[11], but the stereochemical selectivity kept the same. Therefore, we decided to investigate the feasibility of the key SeO_2 step regardless of the undesired C8 stereochemistry, before investing more time on this route.

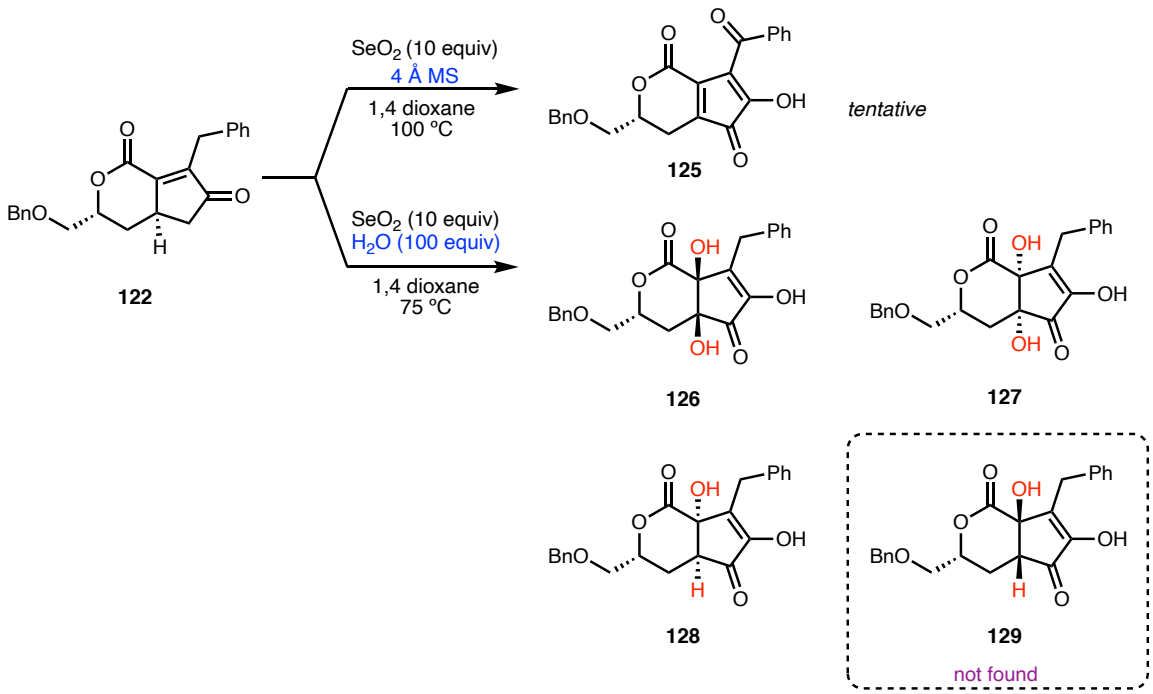

Scheme 3. *Preliminary SeO_2 reaction results.*

Following the protocols from the ryanodol synthesis[1], subjecting enone **122** to 10 equivalent SeO_2 under anhydrous condition (activated 4 Å molecular sieve) at 100 ºC for 16 hours only yielded **125** as the major product (tentative structure), with much recovered starting materials (Scheme 3). **125** is anti-aromatic and would be an interesting molecule for further investigation. Nevertheless, we treated **122** to SeO_2 under aqueous condition, and obtained the desired diol product **126** surprisingly, along with its diastereomer **127** and a monohydroxylated product **128**. The other monohydroxylated compound **129** was not found. It was to our surprise that our desired diol product was present, and we started probing the mechanism of this reaction, aiming to further optimize the reaction.

We monitored the reaction progress using NMR (Scheme 4). The tentative mechanism of the SeO_2 reaction started with enone **122** first oxidized to enediketone **130**, with C8 methine intact. Upon the addition of excess water, monohydroxylated compound **128** formed in equilibrium with hydrate **131**. We were able to cleanly isolated **128** and characterize using X-ray crystallography. The re-subjection of **128** to SeO_2 in dioxane and water under 100 ºC formed the mixture of diol diastereomer products. It was interesting to us why a mixture of diastereomers formed. If only an α oxidation occurred, then, only **127** diol diastereomer would form since only *cis*-[6.5] is allowed in this structure. Therefore, we reasoned that there is at least another pathway operating in the reaction. The other tentative mechanism is after diketone **130** formation, the C8 position can be oxidized. This oxidation would be unselective. Then an oxy-Michael reaction by water would occur on **31** to form both diol diastereomers.

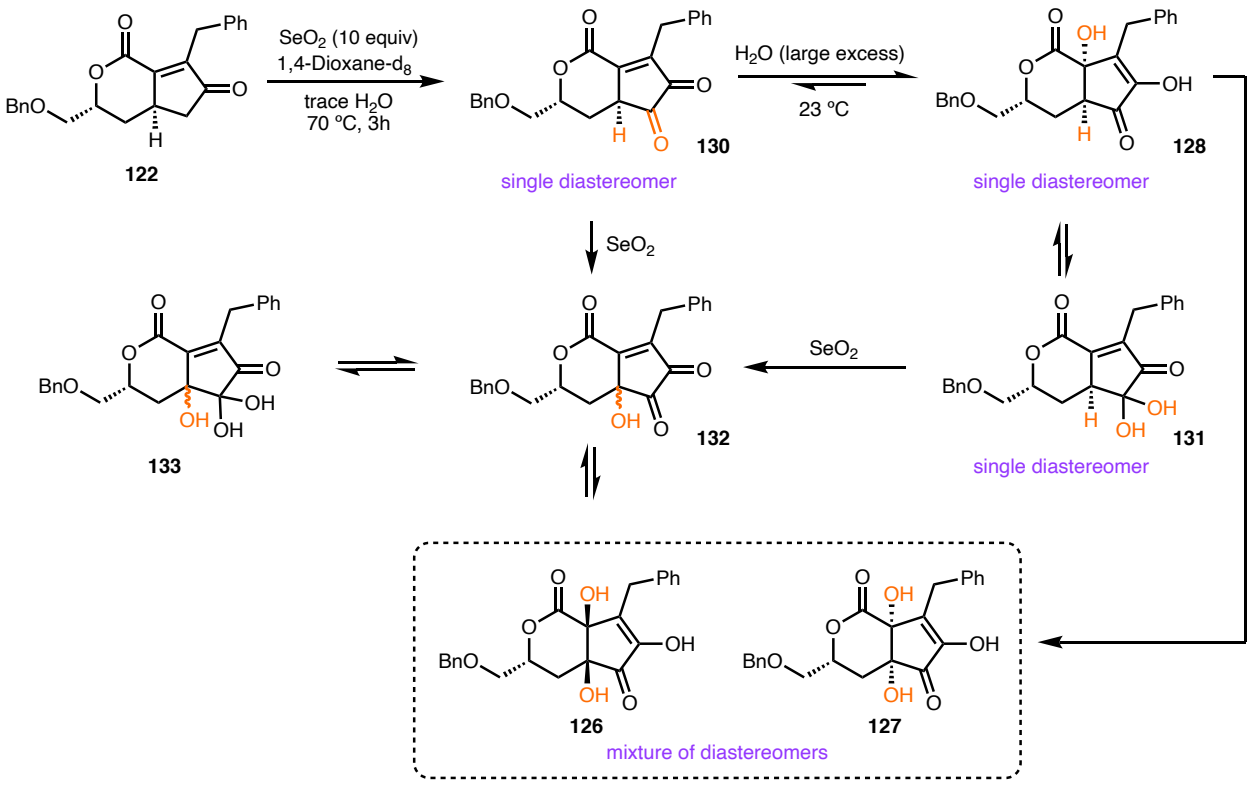

Scheme 4. *Investigation on the mechanism of SeO_2 mechanism.*

With the mechanism in mind, we aimed to optimize the reaction by reducing the amount of byproducts. The major byproducts isolated were starting material **122** and monohydroylated compound **128**. Although extended heating will eventually fully convert **122** and **128**, the yield for the desired product **126** was not improved over extended heating. Instead, we found the diol product **126** can be further oxidized under the reaction condition to acid products that we could not isolate and characterize. Therefore, the tricky part of optimizing this reaction is to find the goldilocks between full-conversion and over-reaction.

Since intermediate **128** is the major byproduct, we think maybe if we accelerate the final C8 oxidation using an additive, we will be able to reduce reaction time and improve yield (Scheme 5). After a screening of different Lewis basic additives and their ratio with SeO_2, 0.2 equivalent diisopropylethylamine was found to be effective in accelerating the final C8 oxidation. Starting material **122** and monohydroylated product **128** were fully converted, making isolation easier after the reaction. The *gem*-diol in **126** can be protected with dichlorodi*tert*-butylsilane under imidazole and DMAP in DCM to yield **134** that maps on enterocin's carbon and oxygenation patterns. Under the optimized condition, this SeO_2 reaction then diol protection sequence can be scaled up to 1 gram with 7 % yield of the desired diastereomer over 2 steps (15% for both diastereomer, 1:1 dr). Though the yield is low, the sequence provided just enough material for further investigation.

A

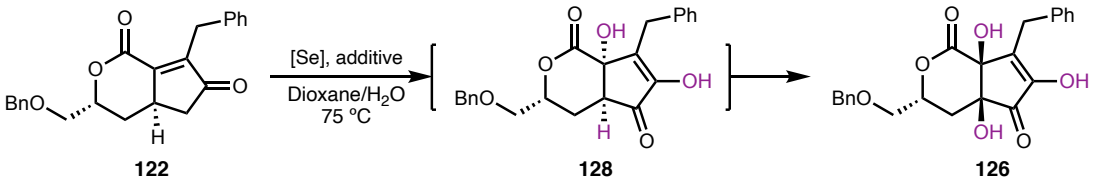

entry	[Se]	additive	result
1	SeO_2 (10 equiv)	—	Major monohydroxylated
2	SeO_2 (5 equiv)	NMO•H_2O (0.5 equiv)	diol product only
3	SeO_2 (5 equiv)	NMO•H_2O (10 equiv)	no rxn
4	SeO_2 (2 equiv)	NMO•H_2O (10 equiv)	no rxn
5	SeO_2 (8 equiv)	MPO•xH_2O (5 equiv)	slow
6	SeO_2 (8 equiv)	PNO (0.5 equiv)	slow
7	SeO_2 (8 equiv)	NMM (0.5 equiv)	little conversion
8	SeO_2 (8 equiv)	DIPEA (0.5 equiv)	fast & clean diol pdt

B

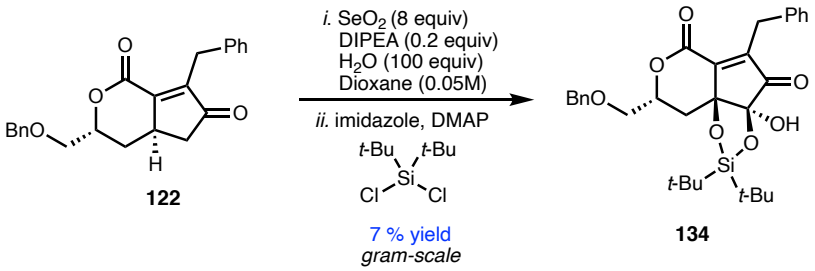

Scheme 5. *Optimization of SeO2 multioxidation.* *a) Additives effect on accelerating SeO_2 oxidation b) two-step sequence under optimized conditions.*

The next goal of this route is testing the reductive cyclization step to close C4-C5 bond and forge enterocin caged core structure. There are only two steps away from the key cyclization: benzyl deprotection and primary alcohol oxidation (Scheme 6). Canonical reductive benzyl deprotection condition resulted in the formation of byproduct **138**, due to a competing reduction of the enone. We attempted oxidation of **138** to the corresponding aldehyde, but oxidation by DMP gave a complex mixture. Among the oxidative deprotection conditions, DDQ was not effective and Bobbitt's salt slowly deprotected the silyl group. Gratifyingly, the bromine radical generated from irradiating NBS in tetrachloromethane was able to oxidize the benzylic position and the desired alcohol **135** was obtained in 85 % yield. Excess NBS and longer irradiation did not result in primary alcohol oxidation but decomposition. DMP smoothly oxidized the revealed alcohol to desired aldehyde **136**.

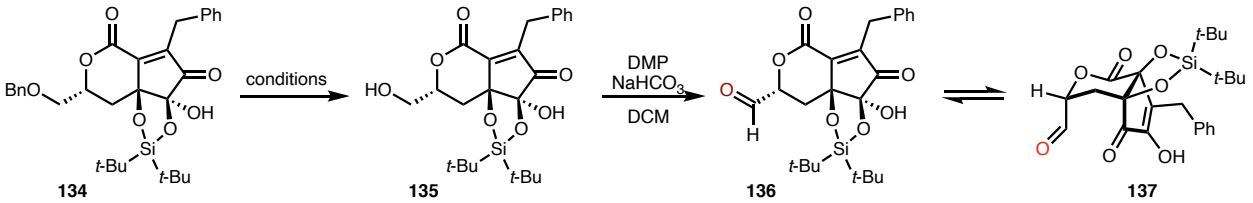

entry	conditions	result
1	Pd/C, H_2, MeOH	byproduct **138**
2	Bobbitt's salt (2 equiv), MeCN/H_2O, rt	trace conversion. [Si] deprotection
3	DDQ, pH 7 buffer, DCM, 0 °C	no reaction
4	DDQ, pH 7 buffer, DCM, 45 °C, 24h	trace conversion
5	KBr, Oxone, MeCN, rt	no reaction
6	NBS (1.3 equiv), $CaCO_3$, CCl_4/H_2O, $h\nu$*, 15 min	85 % yield
7	NBS (2.3 equiv), $CaCO_3$, CCl_4/H_2O, $h\nu$*, 1h	decomp

*: 100 W halogen lamp

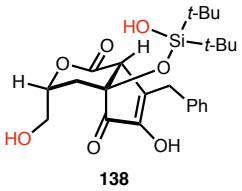

Scheme 6. *Benzyl deprotection studies and oxidation.*

With aldehyde **136** at hand, reductive cyclization to close C4-C5 bond was investigated next (Scheme 7). The plan was to generate a radical or an anion at C4 or C5 and then react to forge the bond. One of the challenges is that **136** is quite flat, and this geometry does not really allow cyclization. The hope is that aldehyde **136** may be in an equilibrium with **137** (Scheme 6) under different solvent or temperature, and C4 and C5 in **137** are close to each other. Another challenge in the design is that C3 and C5 are also electrophilic, and might interfere in the reaction. Notably, the starting aldehyde is unstable to base, protic solvents and heat, limiting the scope of reagents that can be used. Standard HAT conditions (Scheme 7, entry 1-2) led to no reaction. NHK condition (entry 3) that was inspired from a precedent[12] resulted in decomposition. Using Bu_3SnH and AIBN only led to aldehyde reduced to alcohol. Reductive aldol condition (entry 5) led to complex mixtures. Interestingly, subject **136** to freshly generated SmI_2 yielded **140** (tentative structure) in 1.6:1 dr at the secondary alcohol. The minor dr was not be isolated, because it converted to the major dr upon SiO_2, possibly via a retro-aldol/aldol pathway. This result indicated that it is feasible to generate a ketal radical from the aldehyde, but unfortunately it engaged with C9 ketone instead of C4, possibly due to their close proximity. Preliminary attempts to convert

140 to **141** using α-ketol rearrangement were not successful, possibly because **141** is strained due to the presence of the alkene.

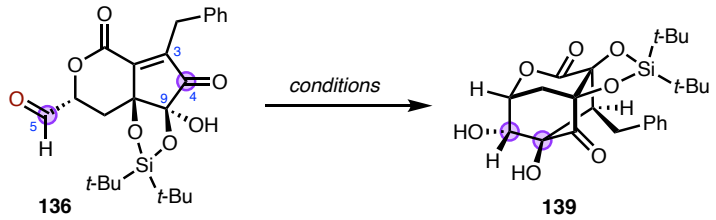

entry	condition	result
1	$Fe(acac)_3$, $PhSiH_3$, EtOH, 0 °C	Decomp
2	$Fe(acac)_3$, $PhSiH_2(Oi\text{-}Pr)$, DCM, 0 °C	No reaction
3	$CrCl_2$, DMF, *t*-BuOH, allyl bromide, 23 °C	Decomp
4	Bu_3SnH, AIBN, Dioxane, 23 °C	Aldehyde reduction
5	$P(t\text{-}Bu)_3$, H_2O, DMF, 23 °C	Decomp
6	SmI_2, THF, 0 °C	**140 (1.6:1 dr)**

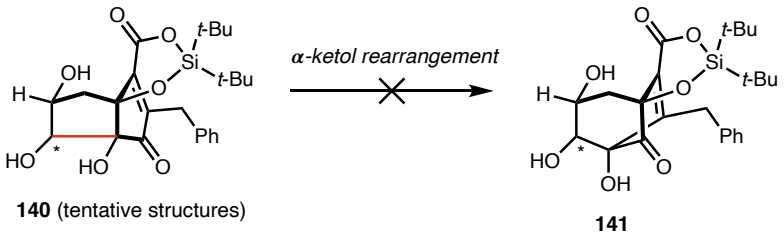

Scheme 7. *Reductive cyclization studies.*

While this route is interesting, we realize the structure geometry of **136** posed significant difficulty in forging the C4-C5 bond. We attempted installing the benzylic ketone early in the route and hoping the presence of this ketone may have an impact, but find the presence of that ketone made SeO_2 oxidation products very challenging to separate out. It was possible to introduce that benzylic oxidation as -OTBS or -OMe first, but the SeO_2 multioxidation was low yielding again and the subsequent diol protection was problematic. In addition, there were difficulties in structure determinations throughout the route as the cyclopentane ring has no proton shown in ^1H NMR, and some structures were later revised. Eventually, we decided to stop investigating this route because the low yield of the SeO_2 oxidation step cannot support subsequent investigations.

Nevertheless, we investigated other oxidation strategies[10,13,14] to oxidize C8 methine and thereby circumvent the SeO_2 oxidation. The $Pd(OH)_2$/TBHP[13] condition was interesting, as the reaction produced a mixture of C8 tertiary peroxide diastereomers. We investigated a few other unsuccessful routes but they were not characterized, and they were included in the appendix of this chapter.

4.3 Experimental Section

4.3.1 Materials and methods

Unless otherwise stated, reactions were performed under an inert atmosphere (dry N_2 or Ar) with freshly dried solvents utilizing standard Schlenk techniques. Glassware was oven-dried at 120 °C for a minimum of four hours, or flame-dried utilizing a Bunsen burner under high vacuum. Tetrahydrofuran (THF), methylene chloride (CH_2Cl_2), *N*,*N*- dimethylformamide (DMF), benzene (PhH), and toluene (PhMe) were dried by passing through activated alumina columns. Methanol (HPLC grade) was purchased from Fisher Scientific. Pyridine (Pyr) was distilled from calcium hydride immediately prior to use. All reactions were monitored by thin-layer chromatography using EMD/Merck silica gel 60 F254 pre-coated plates (0.25 mm) and were visualized by UV (254 nm), *p*-anisaldehyde, CAM, and/or $KMnO_4$ staining. Flash column chromatography was performed using silica gel (SiliaFlash® P60, particle size 40-63 microns [230 to 400 mesh]) purchased from Silicycle. ^1H and ^{13}C NMR spectra were recorded on a Bruker Avance III HD with Prodigy Cryoprobe (at 400 MHz and 101 MHz, respectively), Varian Inova 500 (at 500 MHz and 126 MHz, respectively), or Varian Inova 600 (at 600 MHz and 150 MHz, respectively), and are reported relative to internal $CHCl_3$ (^1H, $\delta = 7.26$), C_6H_6 (^1H, $\delta = 7.16$), or CD_2HOD (^1H, $\delta = 3.31$), and $CDCl_3$ (^{13}C, $\delta = 77.0$), C_6D_6 (^{13}C, $\delta = 128.0$), or CD_3OD (^{13}C, $\delta = 49.0$). Data for ^1H NMR spectra are reported as follows: chemical shift (δ ppm) (multiplicity, coupling constant (Hz),

integration). Multiplicity and qualifier abbreviations are as follows: s = singlet, d = doublet, t = triplet, q = quartet, m = multiplet, br = broad, app = apparent. IR spectra were recorded on a Perkin Elmer Paragon 1000 spectrometer and are reported in frequency of absorption (cm^{-1}). HRMS were acquired using an Agilent 6200 Series TOF with an Agilent G1978A Multimode source in electrospray ionization (ESI), atmospheric pressure chemical ionization (APCI), or mixed (MM) ionization mode. Optical rotations were measured on a Jasco P-2000 polarimeter using a 100 mm path-length cell at 589 nm. Reagents were purchased from commercial vendors as follows: ethyl propiolate was purchased from Combi blocks. Benzyl glycidyl ether, 4-Methylmorpholine N-oxide monohydrate, selenium dioxide, samarium, diiodoethane were purchased from Sigma-Aldrich. Cobalt carbonyl was purchased from Strem Chemicals.

4.3.2 Experimental procedures

Preparation of ester 120

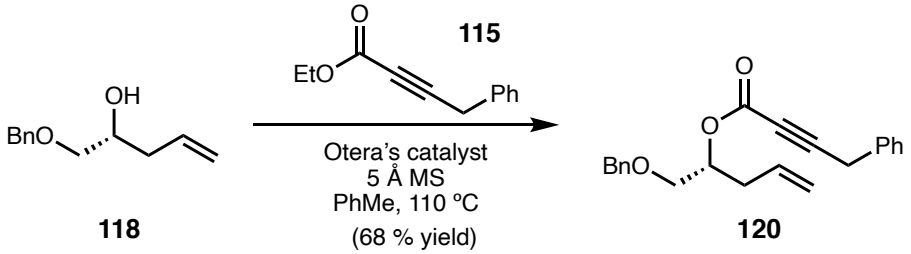

An oven-dried 200 mL round-bottom flask was charged with alcohol **118** (1.53g, 7.97 mmol, 1.5 equiv), ethyl ester **115** (1.00g, 5.31 mmol, 1 equiv), Otera's catalyst (0.31g, 0.53mmol, 10 mol%), and anhydrous toluene (53 mL). 5 g of oven-dried and then flame-dried 5Å molecular sieve powder (200% w/w of (**115** + **118**)) was added to the flask. The reaction mixture was heated to 110 ºC via an oil bath for 16 hours until complete consumption of ethyl ester **115** was observed by TLC. The reaction flask was removed from oil bath and cooled down to room temperature. The

reaction mixture was filtered over celite and the filtrate was concentrated *in vacuo*. The crude residue was purified via SiO_2 flash chromatography (3 to 5% Et_2O/hexanes) to afford ester **120** (1.21g, 3.61 mmol, 68% yield) as a colorless oil.

TLC (10% Et_2O/hexanes): R_f 0.28 (UV, $KMnO_4$).

^{1}H NMR (400 MHz, $CDCl_3$): δ 7.31 (m, 8H), 7.29 (m, 2H), 5.75 (ddt, *J* = 17.1, 10.1, 7.0 Hz, 1H), 5.18 (m, 1H), 5.1 (m, 2H), 4.57 (m, 2H), 3.75 (s, 2H), 3.57 (d, *J* = 5.0 Hz, 2H), 2.44 (m, 2H).

^{13}C NMR (101 MHz, $CDCl_3$): δ 153.38, 138.03, 134.19, 132.84, 128.91, 128.55, 128.21, 127.84, 127.79, 127.33, 118.61, 86.94, 74.92, 73.91, 73.33, 70.30, 35.32, 25.24.

FTIR(NaCl, thin film): 2238, 1710, 1645, 1390, 1248, 1051 cm^{-1}.

HRMS (ESI): calc'd for $[M+Na]^+$ 357.1461, found 357.1461.

Preparation of bicyclic enone 122

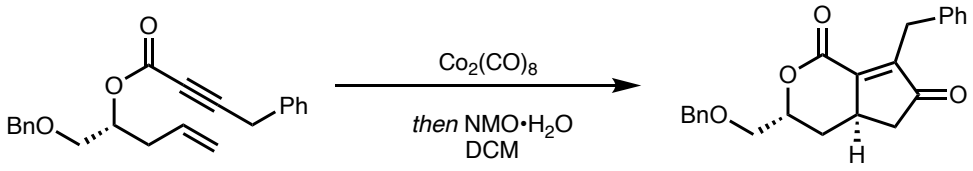

120 **122**

An oven-dried 250 mL round-bottom flask was charged with ester **120** (1.08g, 3.23 mmol, 1 equiv) and 16 mL anhydrous DCM. $Co_2(CO)_8$ (1.21g, 3.55 mmol, 1.1 equiv) was quickly added to the solution, and the stirring continued for 1 hour until TLC analysis indicated that starting material was fully consumed. The reaction mixture was diluted by adding 144 mL anhydrous DCM, and cooled to 0 ºC via an ice/water bath. Stirring was continued for 15 min prior to the addition of NMO•H_2O (0.87 g, 6.43 mmol, 2 equiv). The reaction mixture was immediately removed from the ice/water bath and the reaction was continued for 0.5 h at ambient temperature. The reaction mixture was cooled to 0 ºC via an ice/water bath again, and stirred for 15 min, prior to the addition

of NMO•H_2O (0.87 g, 6.43 mmol, 2 equiv). The reaction mixture was immediately removed from the ice/water bath and the reaction was continued for 0.5 h at ambient temperature. This procedure was repeated for 3 more times until a total of 4.37 g of NMO•H_2O (32.3 mmol, 10 equiv) was added to the reaction mixture. Stirring continued (*ca.* 1 h) until at which point TLC analysis indicated the full completion of the reaction. The mixture was filtered over celite and silica, and the filtrate was concentrated *in vacuo*. The crude residue was purified via SiO_2 flash chromatography (20 to 30% EtOAc/hexanes) to afford enone **122** (1.00g, 2.74 mmol, 85% yield) as a colorless oil, which solidified at –20 ºC.

TLC (50% EtOAc/hexanes): R_f 0.39 (UV, $KMnO_4$).

^{1}H NMR (400 MHz, $CDCl_3$): δ 4.67 (tdd, *J* = 5.6, 4.1, 2.7 Hz, 1H), 4.55 (s, 2H), 3.89 (s, 2H), 3.77 – 3.65 (m, 2H), 3.42 – 3.30 (m, 1H), 2.79 – 2.69 (m, 1H), 2.38 (ddd, *J* = 13.9, 5.9, 2.8 Hz, 1H), 2.11 – 2.01 (m, 1H), 1.84 (ddd, *J* = 13.8, 12.0, 6.1 Hz, 1H).

^{13}C NMR (101 MHz, $CDCl_3$): δ 206.38, 162.83, 152.15, 149.99, 137.85, 137.44, 129.49, 128.71, 128.60, 128.16, 127.86, 126.66, 77.57, 73.91, 71.31, 42.01, 33.16, 31.82, 29.82.

FTIR(NaCl, thin film): 2918, 2857, 2352, 1713, 1453, 1370, 1250, 1217. 1169, 1111 cm^{-1}.

HRMS (ESI): calc'd for $[M+H]^+$ 363.1591, found 363.1593.

Preparation of overoxidation product 125 (tentative structure)

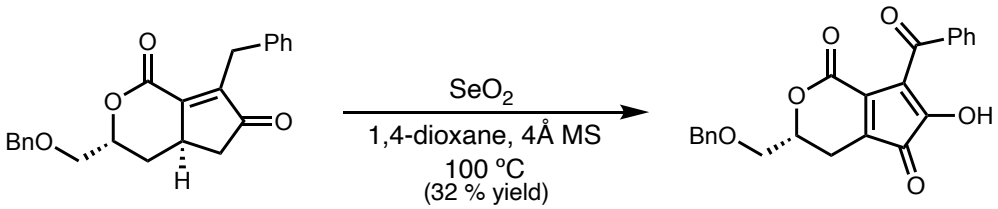

122 **125**

An oven-dried 25 mL round bottom flask was charged with bicyclic enone **122** (200 mg, 0.55 mmol, 1 equiv), SeO_2 (612 mg, 5.5 mmol, 10 equiv), 5.5 mL 1,4-dioxane and 1.2 g oven-

dried 4 Å molecular sieve. The heterogeneous mixture was heated to 100 ºC via an oil bath. Stirring was continued (*ca.* 12 h) until at which point TLC analysis indicated the full consumption of starting material. The reaction mixture was diluted with ethyl acetate, filtered over celite, and the filtrate was concentrated *in vacuo*. The crude residue was purified via SiO_2 flash chromatography (10 to 20% EtOAc/hexanes) to afford overoxidation product **125** (68 mg, 0.18 mmol, 32 % yield) as a reddish oil. Repeated SiO_2 flash chromatography might be necessary to fully remove SeO_2 derivatives.

^{1}H NMR (400 MHz, C_6D_6): 8.20 (s, 1H), 8.06 – 8.01 (m, 2H), 7.23 – 7.16 (m, 4H), 7.13 – 7.05 (m, 3H), 4.31 – 4.17 (m, 2H), 3.83 (dq, *J* = 10.8, 4.3 Hz, 1H), 3.31 – 3.16 (m, 1H), 3.10 (td, *J* = 10.4, 4.4 Hz, 1H), 2.13 – 1.90 (m, 2H).

^{13}C NMR (101 MHz, C_6D_6): δ 187.40, 185.59, 161.38, 146.42, 141.67, 139.84, 138.05, 134.07, 132.43, 131.47, 128.79, 128.73, 124.02, 77.23, 73.66, 70.62, 21.07.

Preparation of monohydroxylated 128

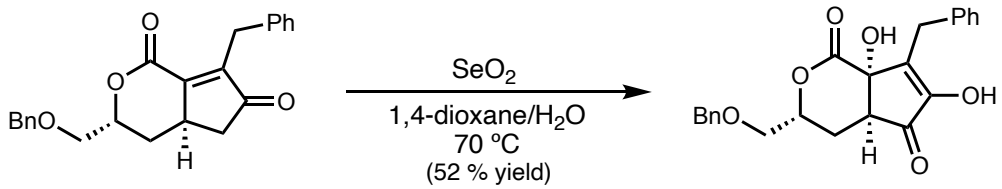

122 **128**

An oven-dried 25 mL round bottom flask was charged with bicyclic enone **122** (200 mg, 0.55 mmol, 1 equiv), SeO_2 (612 mg, 5.5 mmol, 10 equiv), 5.5 mL 1,4-dioxane and 0.55 mL H_2O. The heterogeneous mixture was heated to 70 ºC via an oil bath. Stirring was continued (*ca.* 5 h) until at which point TLC analysis indicated the full consumption of starting material. The reaction mixture was diluted with ethyl acetate, filtered over celite, and the filtrate was concentrated *in vacuo*. The crude residue was purified via SiO_2 flash chromatography (10 to 20% EtOAc/hexanes)

to afford mono-hydroxylated bicycle **128** (112 mg, 0.29 mmol, 52 % yield) as a reddish oil. Repeated SiO_2 flash chromatography might be necessary to fully remove SeO_2 derivatives.

TLC (50% EtOAc/hexanes): R_f 0.3 (UV, $KMnO_4$).

^{1}H NMR (400 MHz, $CDCl_3$): δ 7.36 – 7.15 (m, 10H), 4.55 – 4.45 (m, 2H), 4.10 (dtd, *J* = 12.0, 4.4, 1.8 Hz, 1H), 3.81 (s, 1H), 3.73 (d, *J* = 14.8 Hz, 1H), 3.64 (d, *J* = 14.8 Hz, 1H), 3.50 (d, *J* = 4.5 Hz, 2H), 2.84 (d, *J* = 5.1 Hz, 1H), 2.24 (dt, *J* = 14.6, 1.9 Hz, 1H), 2.19 – 2.08 (m, 1H), 1.64 (s, 1H).

^{13}C NMR (101 MHz, $CDCl_3$): δ 00.53, 173.12, 151.73, 141.50, 137.43, 136.75, 129.15, 128.91, 128.65, 128.12, 127.92, 127.11, 75.99, 73.77, 71.09, 48.04, 30.41, 27.84.

Preparation of di-hydroxylated bicycle 126 and 127

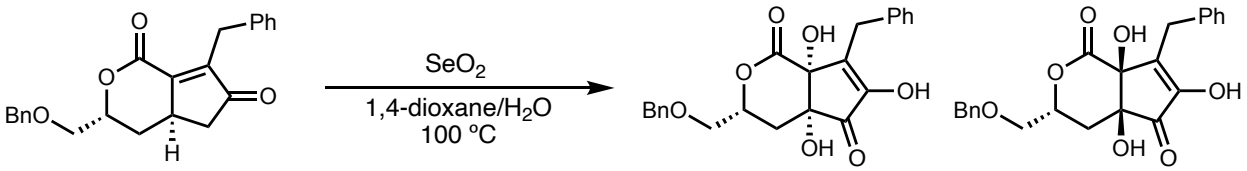

122 **127** **126**

An oven-dried 25 mL round bottom flask was charged with bicyclic enone **122** (200 mg, 0.55 mmol, 1 equiv), SeO_2 (612 mg, 5.5 mmol, 10 equiv), 5.5 mL 1,4-dioxane and 0.55 mL H_2O. The heterogeneous mixture was heated to 100 ºC via an oil bath. Stirring was continued (*ca.* 2 h) until at which point TLC analysis indicated the full consumption of starting material. The reaction mixture was diluted with ethyl acetate, filtered over celite, and the filtrate was concentrated *in vacuo*. The crude residue was purified via SiO_2 flash chromatography (20 to 40% EtOAc/hexanes) to afford di-hydroxylated bicycle **126** and **127** as inseparable mixtures of reddish oils, along with residue SeO_2 derivatives (113 mg, 0.29 mmol, 50% yield (inflated by residue SeO_2 derivatives)). The mixture was directly taken into the next step.

TLC (50% EtOAc/hexanes): R_f 0.15 (UV, $KMnO_4$).

HRMS (ESI): calc'd for $[M+NH_4]^+$ 428.1704, found 428.1704.

Preparation of dioxasilolane 134

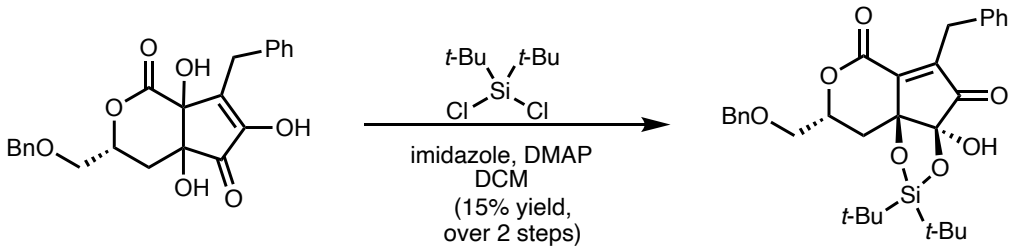

126 + 127 **134**

An oven-dried 25 mL round bottom flask was charged with di-hydroxylated bicycle **126+127** mixture (68 mg, 0.17 mmol, 1 equiv) and 1.7 mL DCM. Imidazole (34 mg, 0.5 mmol, 3 equiv) and 4-dimethylaminopyridine (2 mg, 0.017 mmol, 0.1 equiv) were added into the flask, followed by the addition of di-*tert*-butylchlorosilane (33.4 mg, 0.19 mmol, 1.1 equiv). Stirring was continued (*ca.* 18 h) until at which point TLC analysis indicated the full consumption of starting material. The reaction mixture was diluted with ethyl acetate (2 mL), and quenched with the careful addition of sat. aq. NH_4Cl (3 mL). The layers were separated and the aqueous layer was extracted with ethyl acetate (3 × 2 mL). The combined layers were washed with brine (5 mL), dried over Na_2SO_4, filtered, and concentrated *in vacuo*. The crude residue was purified via SiO_2 flash chromatography (10 to 15% EtOAc/hexanes) to afford dioxasilolane **134** (45 mg, 0.082 mmol, 15% yield over 2 steps) as a greenish oil.

TLC (20% EtOAc/hexanes): R_f 0.28 (UV, CAM, $KMnO_4$).

^{1}H NMR (400 MHz, $CDCl_3$): δ 7.48 – 7.40 (m, 2H), 7.40 – 7.26 (m, 6H), 7.25 – 7.11 (m, 3H), 5.07 (dq, *J* = 11.6, 3.7 Hz, 1H), 4.66 – 4.54 (m, 2H), 3.97 (d, *J* = 12.2 Hz, 1H), 3.84 – 3.71 (m,

3H), 3.67 (dd, *J* = 10.8, 4.1 Hz, 1H), 2.36 (dd, *J* = 14.6, 3.5 Hz, 1H), 2.22 – 2.07 (m, 1H), 1.05 (s, 9H), 0.61 (s, 9H).

^{13}C NMR (101 MHz, $CDCl_3$): δ 199.99, 161.69, 148.04, 145.74, 137.75, 135.92, 129.93, 128.67, 128.63, 128.01, 127.89, 126.90, 97.35, 82.41, 78.19, 73.83, 71.48, 32.89, 29.78, 27.10, 26.69, 20.72, 19.94.

FTIR(NaCl, thin film): 2934, 2859,1731, 1472, 1368, 1232, 1171, 1145, 1114, 1071 cm^{-1}.

HRMS (ESI): calc'd for $[M+NH_4]^+$ 568.2725, found 568.2737.

Preparation of alcohol 135

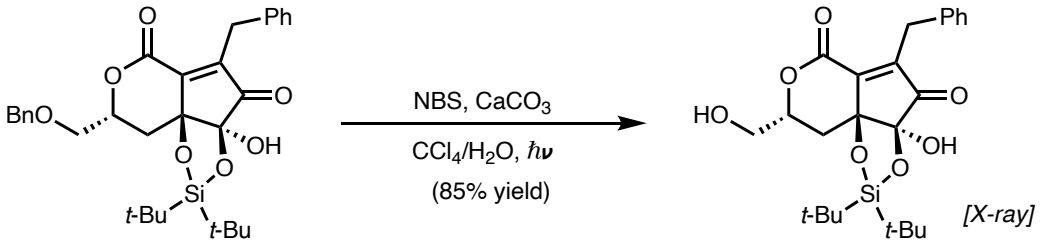

134 **135**

An oven-dried 25 mL round bottom flask was charged with benzyl ether **134** (80.0 mg, 0.145 mmol, 1 equiv), *N*-bromosuccinimide (33.6 mg, 0.189 mmol, 1.3 equiv), $CaCO_3$ (58.1 mg, 0.58 mmol, 4 equiv), 7.25 mL CCl_4 and 0.13 mL H_2O. The mixture was degassed by bubbling argon through while sonicating for 15 min. The mixture was rigorously stirred and irradiated with a 375W incandescent lamp. Irridation continued (*ca.* 45 min) until at which point TLC analysis indicated the full consumption of starting material. 200 mg of SiO_2 was added to the reaction and stirring continued for 0.5h. The reaction mixture was filtered over celite and the filtrate was concentrated *in vacuo*. The crude residue was purified via SiO_2 flash chromatography (30 to 40% EtOAc/hexanes) to afford alcohol **135** (56.9 mg, 0.123 mmol, 85% yield) as a green oil.

TLC (50% EtOAc/hexanes): R_f 0.41 (UV, $KMnO_4$).

^{1}H NMR (400 MHz, C_6D_6): δ 7.77 – 7.68 (m, 2H), 7.13 – 7.03 (m, 2H), 7.03 – 6.94 (m, 1H), 4.68 (d, *J* = 4.5 Hz, 1H), 4.06 (d, *J* = 12.1 Hz, 1H), 3.74 (d, *J* = 12.1 Hz, 1H), 3.41 – 3.32 (m, 1H), 3.07 (dd, *J* = 12.3, 4.4 Hz, 1H), 2.09 (dd, *J* = 14.6, 3.6 Hz, 1H), 1.90 (dd, *J* = 14.6, 11.9 Hz, 1H), 1.01 (s, 9H), 0.60 (s, 9H).

^{13}C NMR (101 MHz, C_6D_6): δ 199.87, 161.59, 148.10, 146.08, 136.60, 130.38, 128.95, 127.12, 97.85, 82.99, 79.53, 64.24, 32.44, 30.49, 30.02, 27.12, 26.78, 20.66, 19.95.

FTIR(NaCl, thin film): 2930, 2860, 1737, 1731, 1495, 1470, 1371, 1282, 1216, 1171 cm^{-1}.

HRMS (ESI): calc'd for $[M+H]^+$ 461.199, found 461.1993.

Preparation of aldehyde 136

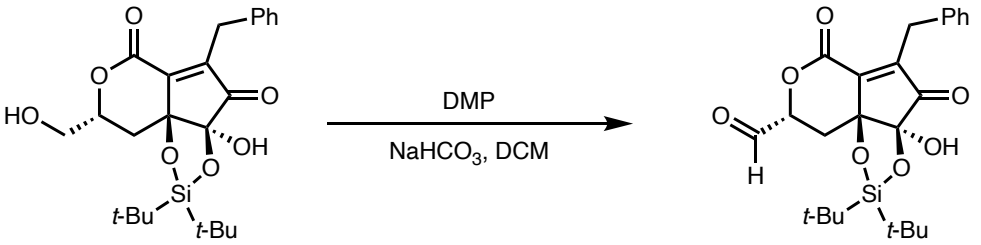

135 **136**

An oven-dried 2 dram vial was charged with alcohol **135** (10 mg, 0.022 mmol, 1 equiv), $NaHCO_3$ (10.9 mg, 0.13 mmol, 6 equiv), 1 mL DCM. The mixture was cooled to 0 ºC via ice/water bath, and stirring continued for 15min prior to the addition of Dess-Martin periodinane (55 mg, 0.13 mmol, 6 equiv). Stirring was continued (*ca.* 3h) until at which point TLC analysis indicated the full consumption of starting material. The reaction mixture was diluted with DCM, filtered over celite, and the filtrate was concentrate *in vacuo*. The crude residue was unstable to SiO_2 flash chromatography and **136** can be used directly in the next step.

TLC (50% EtOAc/hexanes): R_f 0.3 (UV, $KMnO_4$).

^{1}H NMR (400 MHz, $CDCl_3$): δ 9.83 (d, *J* = 1.0 Hz, 1H), 7.47 – 7.40 (m, 3H), 7.20 – 7.13 (m, 2H), 5.22 (ddd, *J* = 12.4, 3.8, 1.0 Hz, 1H), 3.95 (dd, *J* = 12.2, 3.4 Hz, 1H), 3.81 (dd, *J* = 12.3, 4.1 Hz, 1H), 3.49 (s, 1H), 2.58 – 2.50 (m, 1H), 2.02 – 1.94 (m, 1H), 1.03 (s, 9H), 0.65 (s, 9H).

HRMS (ESI): calc'd for $[M+H]^+$ 459.1834, found 459.1837.

Preparation of triol 140 (tentative structure)

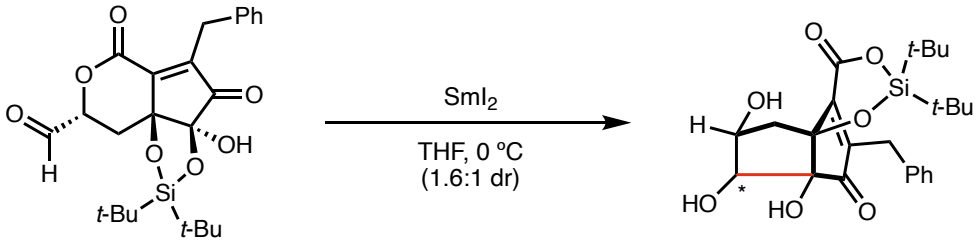

136 **140** (tentative structures)

An oven-dried 1-dram vial equipped with a stir bar was charged with aldehyde **136** (10 mg, 0.022 mmol, 1 equiv), and anhydrous THF (1 mL) and submitted to five freeze-pump-thaw cycles. The solution was cooled to 0 °C and stirred at this temperature for 15 min. Thereafter, SmI_2/THF (0.9 mL, 0.09 mmol, 4.5 equiv) was added dropwise over 5 min. The deep blue color of SmI_2 was immediately quenched upon addition of each drop. After stirring an additional 10 min at 0 °C, the resulting pale yellow solution was diluted with Et_2O (1 mL), and washed with H_2O (2 x 1 mL). The aqueous layer was back-extracted with Et_2O (2 x 1 mL), and the combined organic layers were dried over Na_2SO_4, filtered, and concentrated under reduced pressure to afford a light yellow oil. Crude NMR shows a 1.6:1 diastereomer ratio. Purification was achieved via chromatography on SiO_2 preparative TLC plate and only one of the diastereomer from the crude was shown on the preparative plate. Separation affords triol **140** (tentative structure) as a colorless oil.

Preparation of SmI_2: A 100 mL Schlenk flask containing a stir bar was charged with freshly filed Sm metal (650 mg). The system was flame-dried under high vacuum then cooled to ambient temperature before adding freshly purified 1,2-diiodoethane (700 mg). 1,2-diiodoethane (1.6 g) was dissolved in Et_2O (50 mL) and washed with sat. aq. $Na_2S_2O_3$ (3 x 10 mL) and deionized water (2 x 10 mL), dried over Na_2SO_4, filtered, and dried to 1.41 g of a white solid. The atmosphere was exchanged three times for argon. Subsequently, the flask was charged with anhydrous THF (25 mL) that had been submitted to five freeze-pump-thaw cycles. Note: The THF used for the synthesis of SmI_2 must contain <50 ppm H_2O; THF containing greater quantities of water resulted in excessive induction times for the synthesis of SmI_2. Further, residual oxygen results in formation of oxidative fragmentation products in the radical cyclization. The suspension was stirred for 2 min and the flask was cautiously and briefly (5 s) placed under partial high vacuum, then purged with argon. This process was repeated two additional times to remove ethylene gas formed from insertion of Sm metal into 1,2-diiodoethane. The resulting heterogeneous suspension was rapidly (930 rpm) stirred; after 5 min, the reaction turned dark green, and within 10 min, a dark blue color was observed. After stirring under argon for 3 h at ambient temperature, the system was cautiously and briefly placed under high vacuum, then purged with argon. This process was repeated two additional times, then stirring was halted. The mixture was allowed to settle for 15 min prior to use.

^{1}H NMR (400 MHz, $CDCl_3$): δ 7.42 – 7.27 (m, 5H), 4.66 (q, *J* = 1.2 Hz, 1H), 4.34 (d, *J* = 14.1 Hz, 1H), 3.78 (d, *J* = 14.2 Hz, 1H), 3.35 (d, *J* = 1.6 Hz, 1H), 2.41 (d, *J* = 14.8 Hz, 1H), 2.26 (dd, *J* = 14.8, 1.5 Hz, 1H), 1.03 (s, 10H), 0.96 (s, 9H).

^{13}C NMR (101 MHz, $CDCl_3$): δ 198.21, 168.48, 148.94, 137.24, 129.76, 129.65, 127.93, 86.38, 84.11, 83.50, 68.02, 34.40, 31.93, 27.62, 27.06, 20.52, 20.33.

4.4. References

(1) Chuang, K. V.; Xu, C.; Reisman, S. E. *Science* **2016**, *353* (6302), 912–915.

(2) Dibrell, S. E.; Maser, M. R.; Reisman, S. E. *J. Am. Chem. Soc.* **2020**, *142* (14), 6483–6487.

(3) Davies, K. A.; Abel, R. C.; Wulff, J. E. *J. Org. Chem.* **2009**, *74* (10), 3997–4000.

(4) Alam, M.; Wise, C.; Baxter, C. A.; Cleator, E.; Walkinshaw, A. *Org. Process Res. Dev.* **2012**, *16* (3), 435–441.

(5) Otera, J.; Danoh, N.; Nozaki, H. *J. Org. Chem.* **1991**, *56* (18), 5307–5311.

(6) Otera, J.; Danoh, N.; Nozaki, H. *Tetrahedron* **1993**, *49* (15), 3065–3074.

(7) Veretenov, A. L.; Smit, W. A.; Vorontsova, L. G.; Kurella, M. G.; Caple, R.; Gybin, A. S. *Tetrahedron Letters* **1991**, *32* (19), 2109–2112.

(8) Krafft, M. E.; Romero, R. H.; Scott, I. L. *J. Org. Chem.* **1992**, *57* (20), 5277–5278.

(9) Sharpless, K. B.; Lauer, R. F. *J. Am. Chem. Soc.* **1972**, *94* (20), 7154–7155.

(10) Zhang, W.; Ding, M.; Li, J.; Guo, Z.; Lu, M.; Chen, Y.; Liu, L.; Shen, Y.-H.; Li, A. *J. Am. Chem. Soc.* **2018**, *140* (12), 4227–4231.

(11) Yang, Z. *Acc. Chem. Res.* **2021**, *54* (3), 556–568.

(12) Preindl, J.; Leitner, C.; Baldauf, S.; Mulzer, J. *Org. Lett.* **2014**, *16* (16), 4276–4279.

(13) Darses, B.; Michaelides, I. N.; Sladojevich, F.; Ward, J. W.; Rzepa, P. R.; Dixon, D. J. *Org. Lett.* **2012**, *14* (7), 1684–1687.

(14) Williams, D. R.; Robinson, L. A.; Nevill, C. R.; Reddy, J. P. *Angew. Chem. Int. Ed.* **2007**, *46* (6), 915–918.

Appendix 1

Spectra Relevant to Chapter 4:

A SeO_2 multioxidation approach toward enterocin

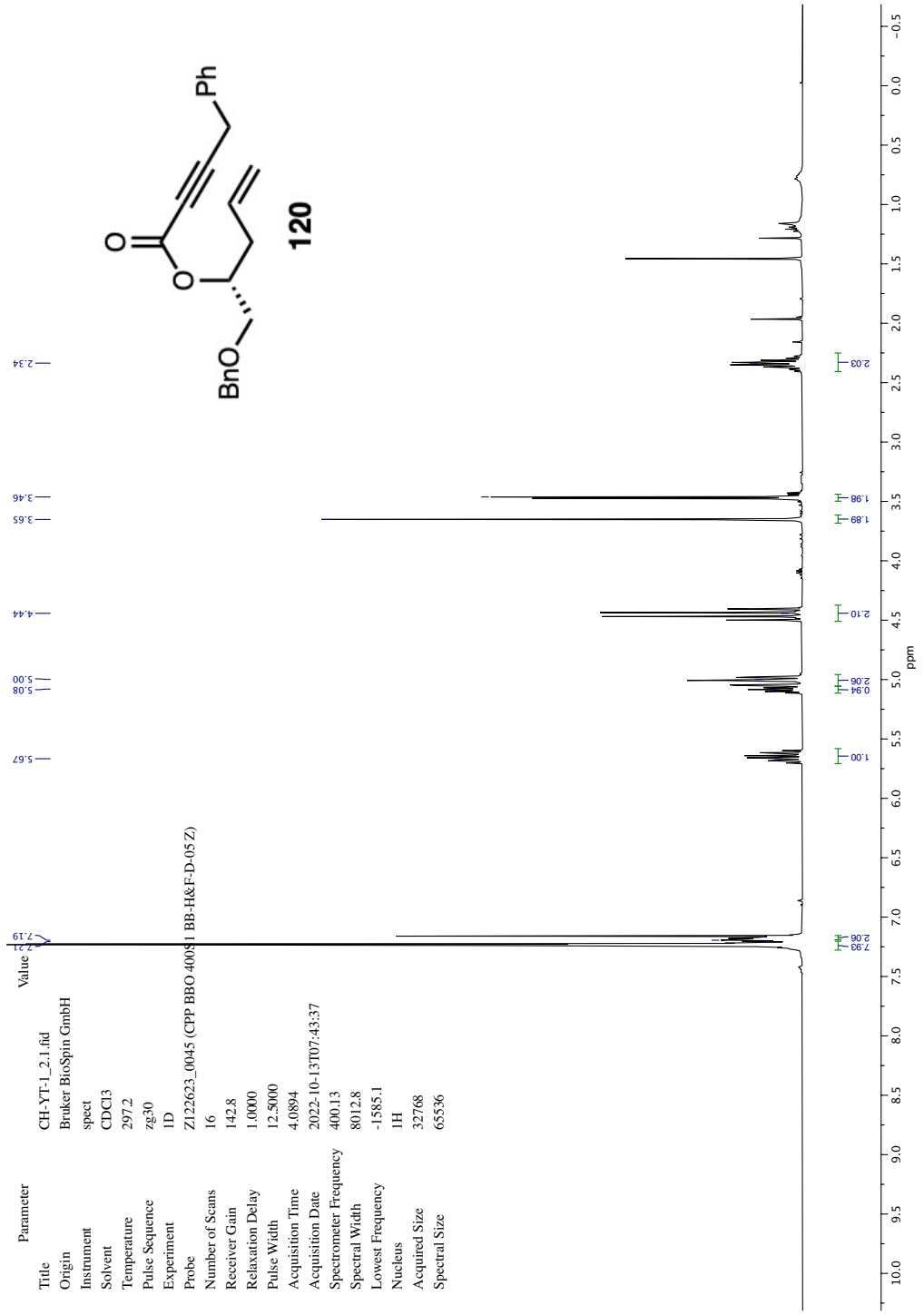
Ph
O
O
BnO
120
Parameter Value
Title CH-YT-1_2.1.fid
Origin Bruker BioSpin GmbH
Instrument spect
Solvent CDCl3
Temperature 297.2
Pulse Sequence zg30
Experiment 1D
Probe Z122623_0045 (CPP BBO 400S1 BB-H&F-D-05 Z)
Number of Scans 16
Receiver Gain 142.8
Relaxation Delay 1.0000
Pulse Width 12.5000
Acquisition Time 4.0894
Acquisition Date 2022-10-13T07:43:37
Spectrometer Frequency 400.13
Spectral Width 8012.8
Lowest Frequency -1585.1
Nucleus 1H
Acquired Size 32768
Spectral Size 65536
7.21
7.19
5.67
5.08
5.00
4.44
3.65
3.46
2.34
2.06
1.00
0.94
2.06
2.10
1.89
1.98
2.03
ppm

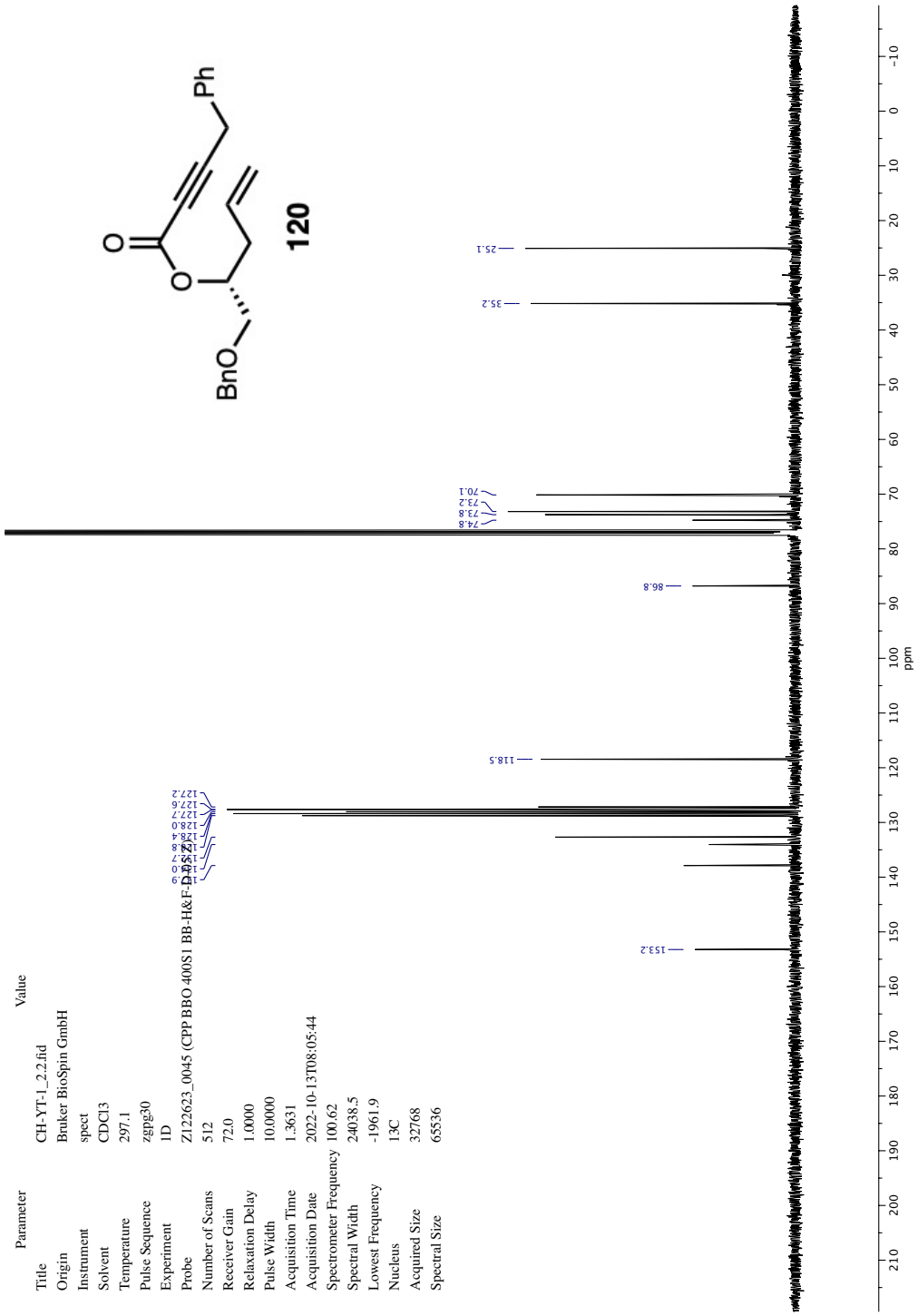

Parameter	Value
Title	CH-YT-1_2.2.fid
Origin	Bruker BioSpin GmbH
Instrument	spect
Solvent	CDCl3
Temperature	297.1
Pulse Sequence	zgpg30
Experiment	1D
Probe	Z122623_0045 (CPP BBO 400S1 BB-H&F-D-05-Z)
Number of Scans	512
Receiver Gain	72.0
Relaxation Delay	1.0000
Pulse Width	10.0000
Acquisition Time	1.3631
Acquisition Date	2022-10-13T08:05:44
Spectrometer Frequency	100.62
Spectral Width	24038.5
Lowest Frequency	-1961.9
Nucleus	13C
Acquired Size	32768
Spectral Size	65536

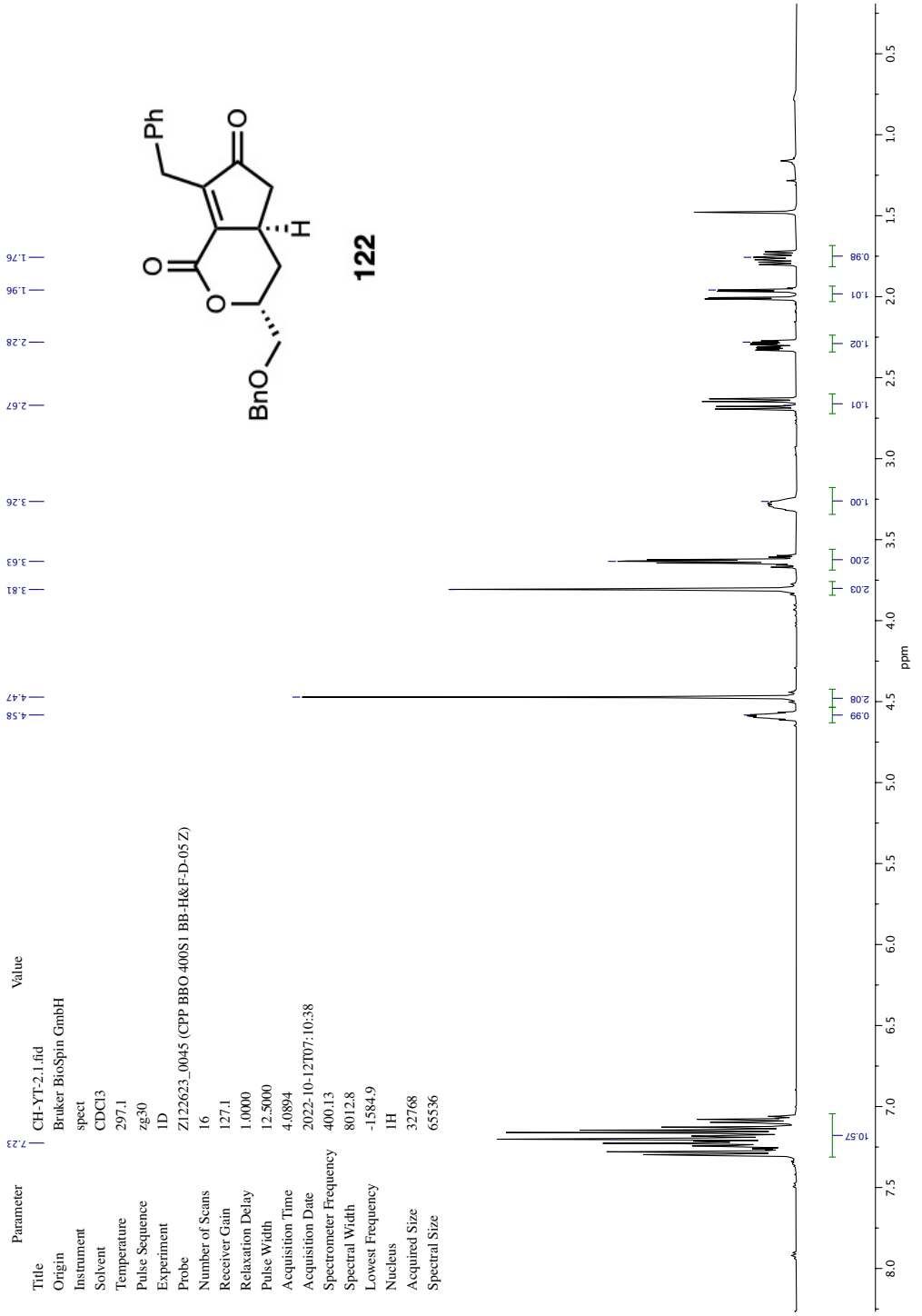

Parameter	Value
Title	CH-YT-2.1.fid
Origin	Bruker BioSpin GmbH
Instrument	spect
Solvent	CDCl3
Temperature	297.1
Pulse Sequence	zg30
Experiment	1D
Probe	Z122623_0045 (CPP BBO 400S1 BB-H&F-D-05 Z)
Number of Scans	16
Receiver Gain	127.1
Relaxation Delay	1.0000
Pulse Width	12.5000
Acquisition Time	4.0894
Acquisition Date	2022-10-12T07:10:38
Spectrometer Frequency	400.13
Spectral Width	8012.8
Lowest Frequency	-1584.9
Nucleus	1H
Acquired Size	32768
Spectral Size	65536

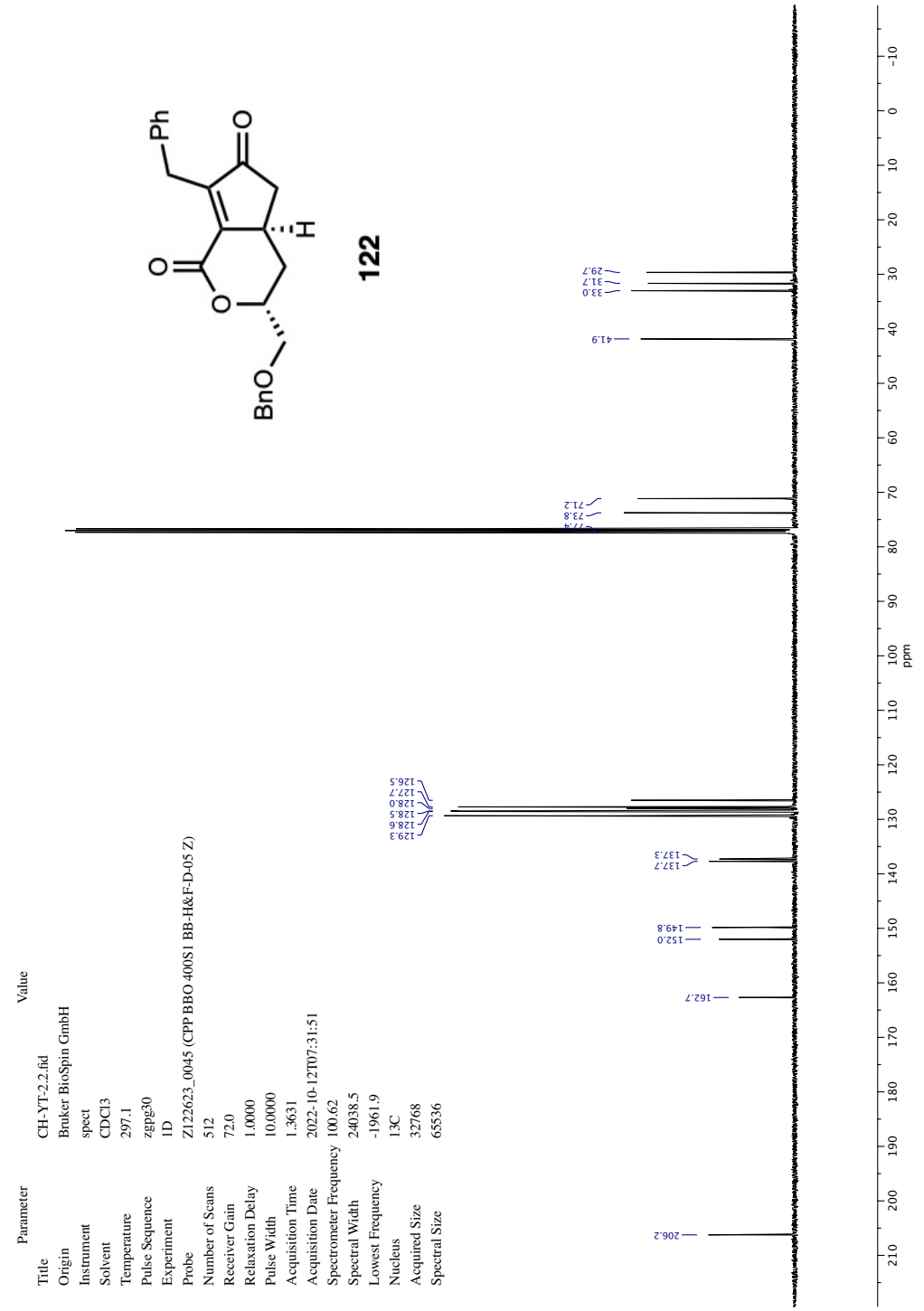

Parameter	Value
Title	CH-YT-2.2.fid
Origin	Bruker BioSpin GmbH
Instrument	spect
Solvent	CDCl3
Temperature	297.1
Pulse Sequence	zgpg30
Experiment	1D
Probe	Z122623_0045 (CPP BBO 400S1 BB-H&F-D-05 Z)
Number of Scans	512
Receiver Gain	72.0
Relaxation Delay	1.0000
Pulse Width	10.0000
Acquisition Time	1.3631
Acquisition Date	2022-10-12T07:31:51
Spectrometer Frequency	100.62
Spectral Width	24038.5
Lowest Frequency	-1961.9
Nucleus	13C
Acquired Size	32768
Spectral Size	65536

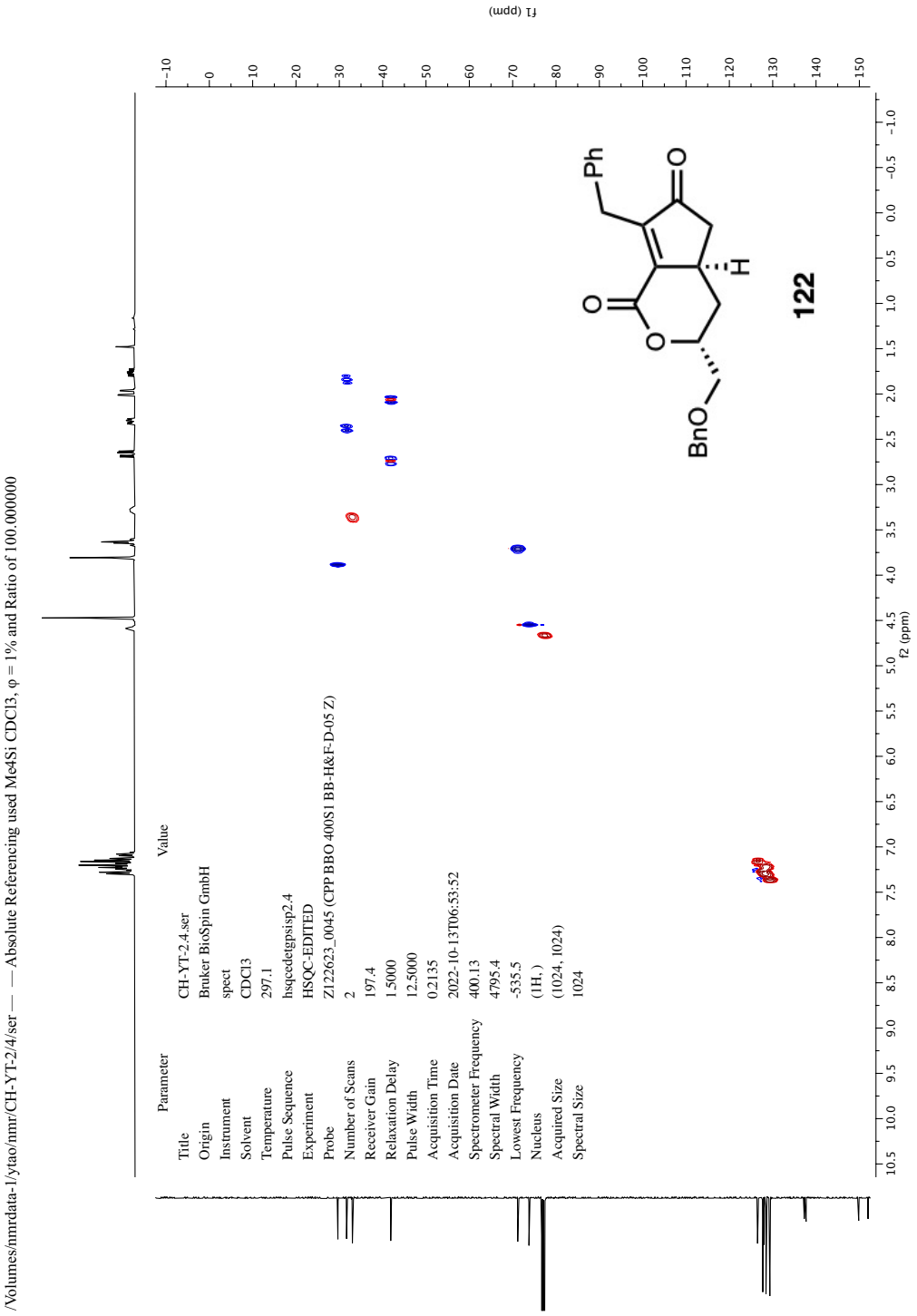
/Volumes/nmrdata-1/ytao/nmr/CH-YT-2/4/ser — — Absolute Referencing used Me4Si CDCl3, φ = 1% and Ratio of 100.000000
Parameter Value
Title CH-YT-2.4.ser
Origin Bruker BioSpin GmbH
Instrument spect
Solvent CDCl3
Temperature 297.1
Pulse Sequence hsqcedetgpsisp2.4
Experiment HSQC-EDITED
Probe Z122623_0045 (CPP BBO 400S1 BB-H&F-D-05 Z)
Number of Scans 2
Receiver Gain 197.4
Relaxation Delay 1.5000
Pulse Width 12.5000
Acquisition Time 0.2135
Acquisition Date 2022-10-13T06:53:52
Spectrometer Frequency 400.13
Spectral Width 4795.4
Lowest Frequency -535.5
Nucleus (1H,)
Acquired Size (1024, 1024)
Spectral Size 1024
f1 (ppm)
f2 (ppm)
Ph
O
O
H
O
BnO
122

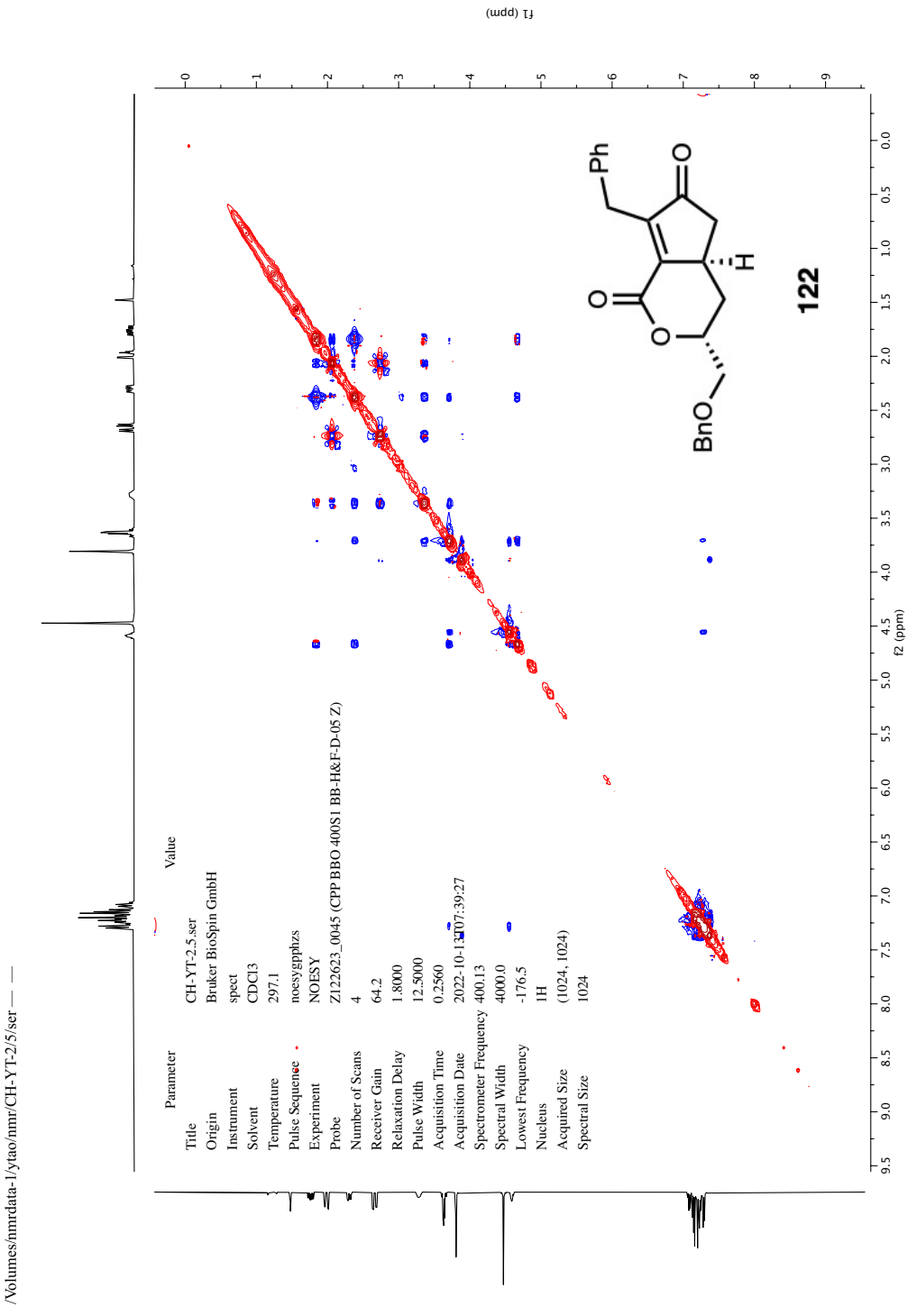
/Volumes/nmrdata-1/ytao/nmr/CH-YT-2/5/ser — —
Parameter Value
Title CH-YT-2.5.ser
Origin Bruker BioSpin GmbH
Instrument spect
Solvent CDCl3
Temperature 297.1
Pulse Sequence noesygpphzs
Experiment NOESY
Probe Z122623_0045 (CPP BBO 400S1 BB-H&F-D-05 Z)
Number of Scans 4
Receiver Gain 64.2
Relaxation Delay 1.8000
Pulse Width 12.5000
Acquisition Time 0.2560
Acquisition Date 2022-10-13T07:39:27
Spectrometer Frequency 400.13
Spectral Width 4000.0
Lowest Frequency -176.5
Nucleus 1H
Acquired Size (1024, 1024)
Spectral Size 1024
f1 (ppm)
f2 (ppm)
Ph
O
O
O
H
BnO
122

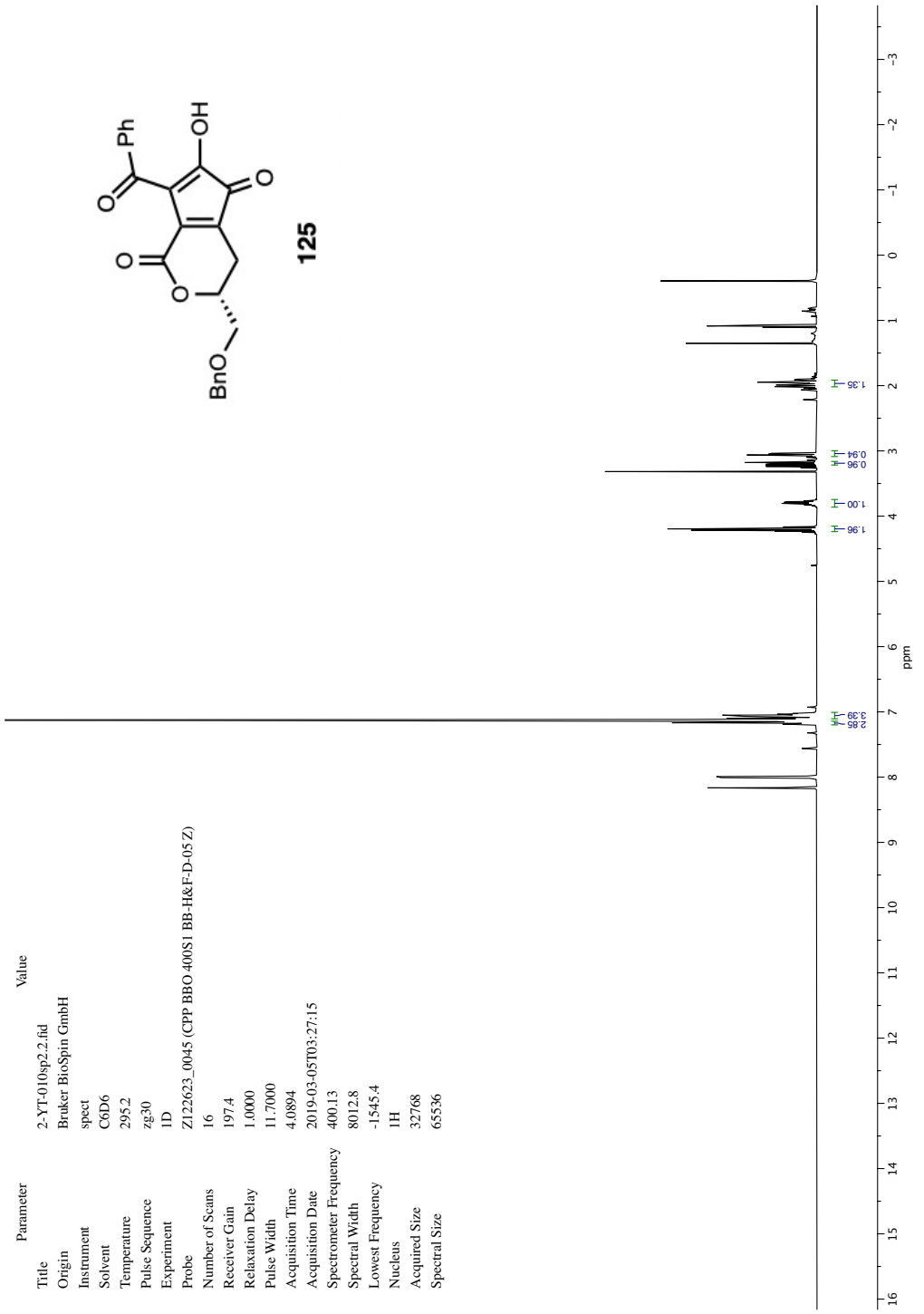

Parameter	Value
Title	2-YT-010sp2.2.fid
Origin	Bruker BioSpin GmbH
Instrument	spect
Solvent	C6D6
Temperature	295.2
Pulse Sequence	zg30
Experiment	1D
Probe	Z122623_0045 (CPP BBO 400S1 BB-H&F-D-05 Z)
Number of Scans	16
Receiver Gain	197.4
Relaxation Delay	1.0000
Pulse Width	11.7000
Acquisition Time	4.0894
Acquisition Date	2019-03-05T03:27:15
Spectrometer Frequency	400.13
Spectral Width	8012.8
Lowest Frequency	-1545.4
Nucleus	1H
Acquired Size	32768
Spectral Size	65536

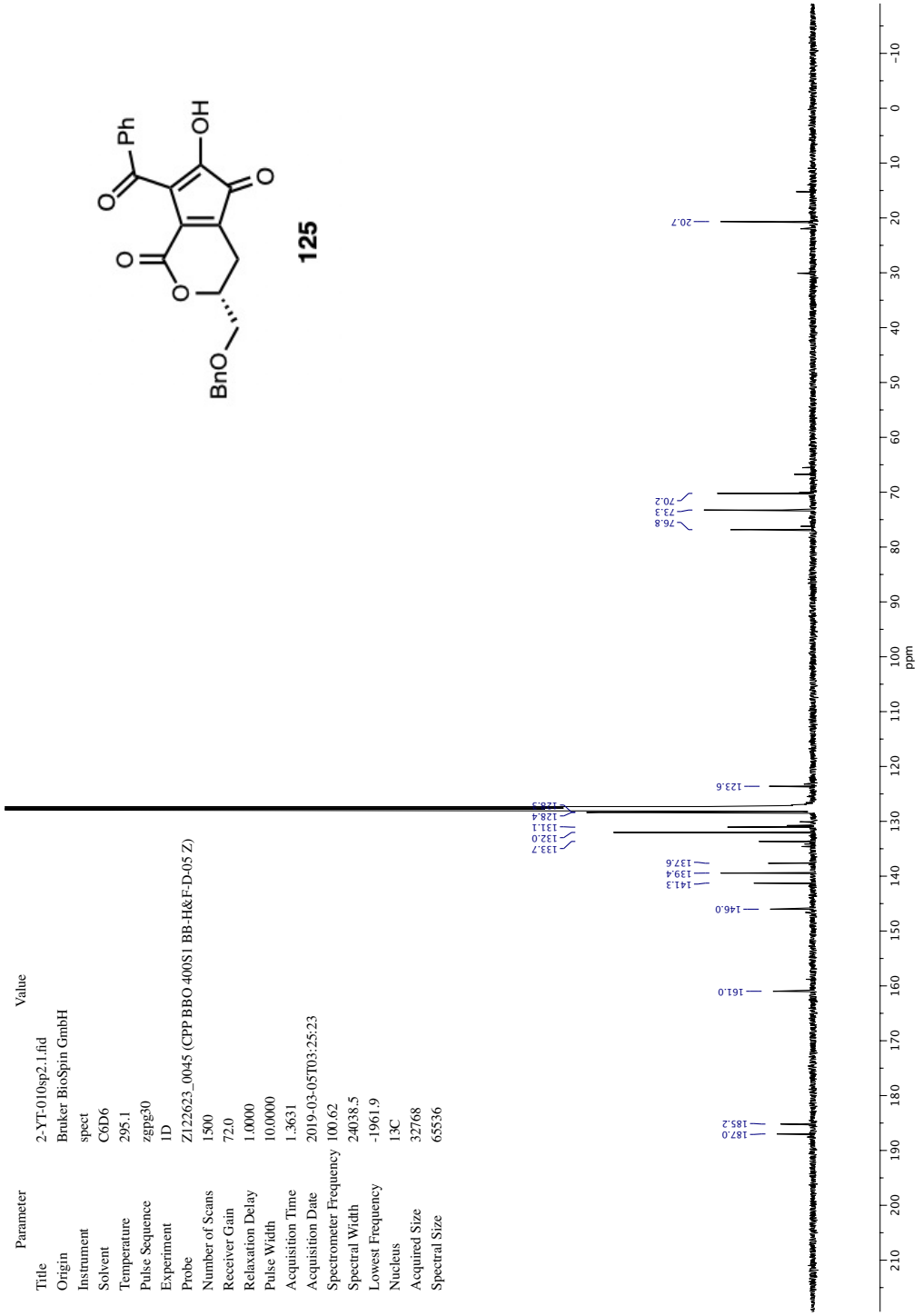

Parameter	Value
Title	2-YT-010sp2.1.fid
Origin	Bruker BioSpin GmbH
Instrument	spect
Solvent	C6D6
Temperature	295.1
Pulse Sequence	zgpg30
Experiment	1D
Probe	Z122623_0045 (CPP BBO 400S1 BB-H&F-D-05 Z)
Number of Scans	1500
Receiver Gain	72.0
Relaxation Delay	1.0000
Pulse Width	10.0000
Acquisition Time	1.3631
Acquisition Date	2019-03-05T03:25:23
Spectrometer Frequency	100.62
Spectral Width	24038.5
Lowest Frequency	-1961.9
Nucleus	13C
Acquired Size	32768
Spectral Size	65536

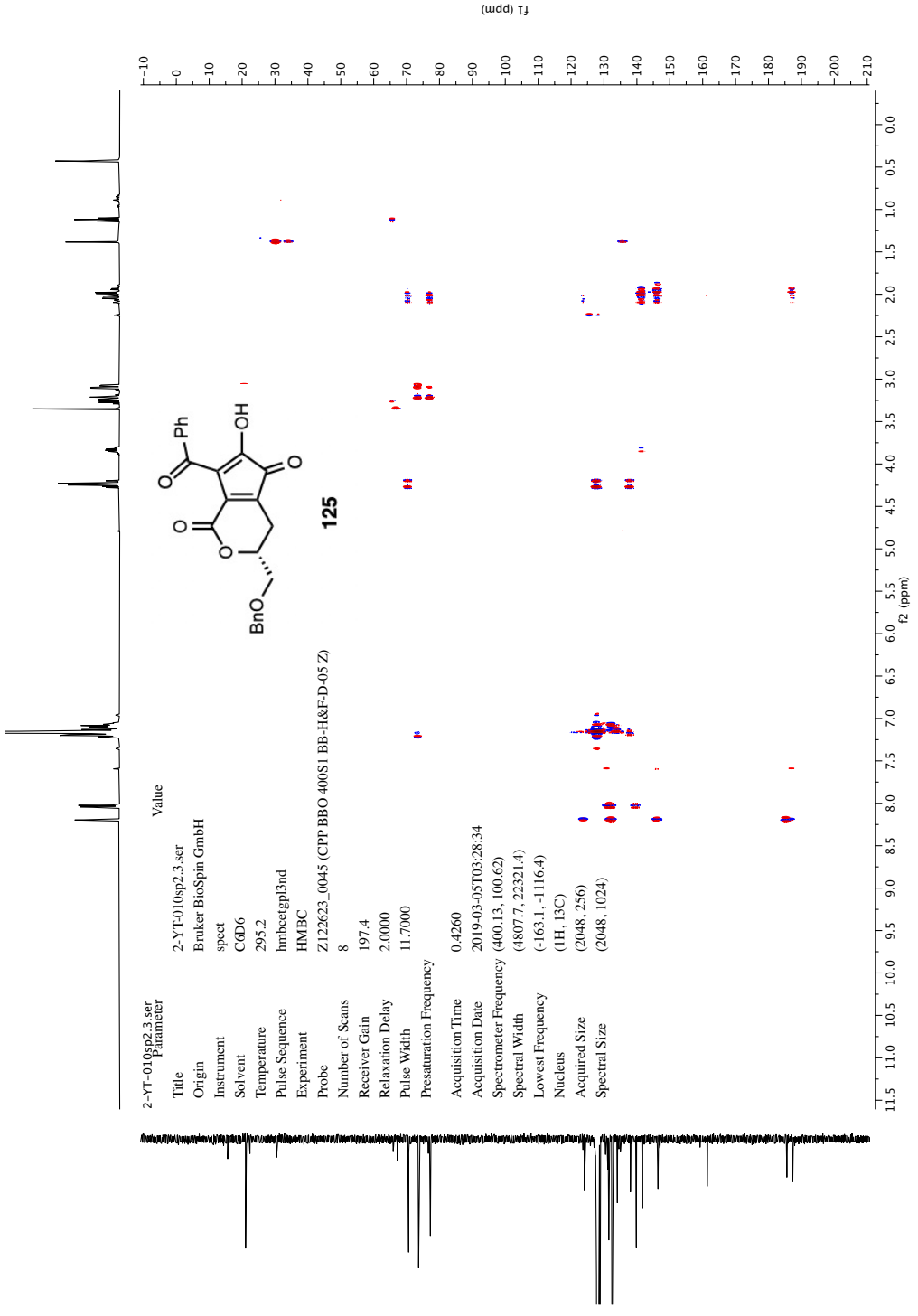
f1 (ppm)
f2 (ppm)
Ph
OH
O
O
O
O
BnO
125
2-YT-010sp2.3.ser
Parameter Value
Title 2-YT-010sp2.3.ser
Origin Bruker BioSpin GmbH
Instrument spect
Solvent C6D6
Temperature 295.2
Pulse Sequence hmbcetgpl3nd
Experiment HMBC
Probe Z122623_0045 (CPP BBO 400S1 BB-H&F-D-05 Z)
Number of Scans 8
Receiver Gain 197.4
Relaxation Delay 2.0000
Pulse Width 11.7000
Presaturation Frequency
Acquisition Time 0.4260
Acquisition Date 2019-03-05T03:28:34
Spectrometer Frequency (400.13, 100.62)
Spectral Width (4807.7, 22321.4)
Lowest Frequency (-163.1, -1116.4)
Nucleus (1H, 13C)
Acquired Size (2048, 256)
Spectral Size (2048, 1024)

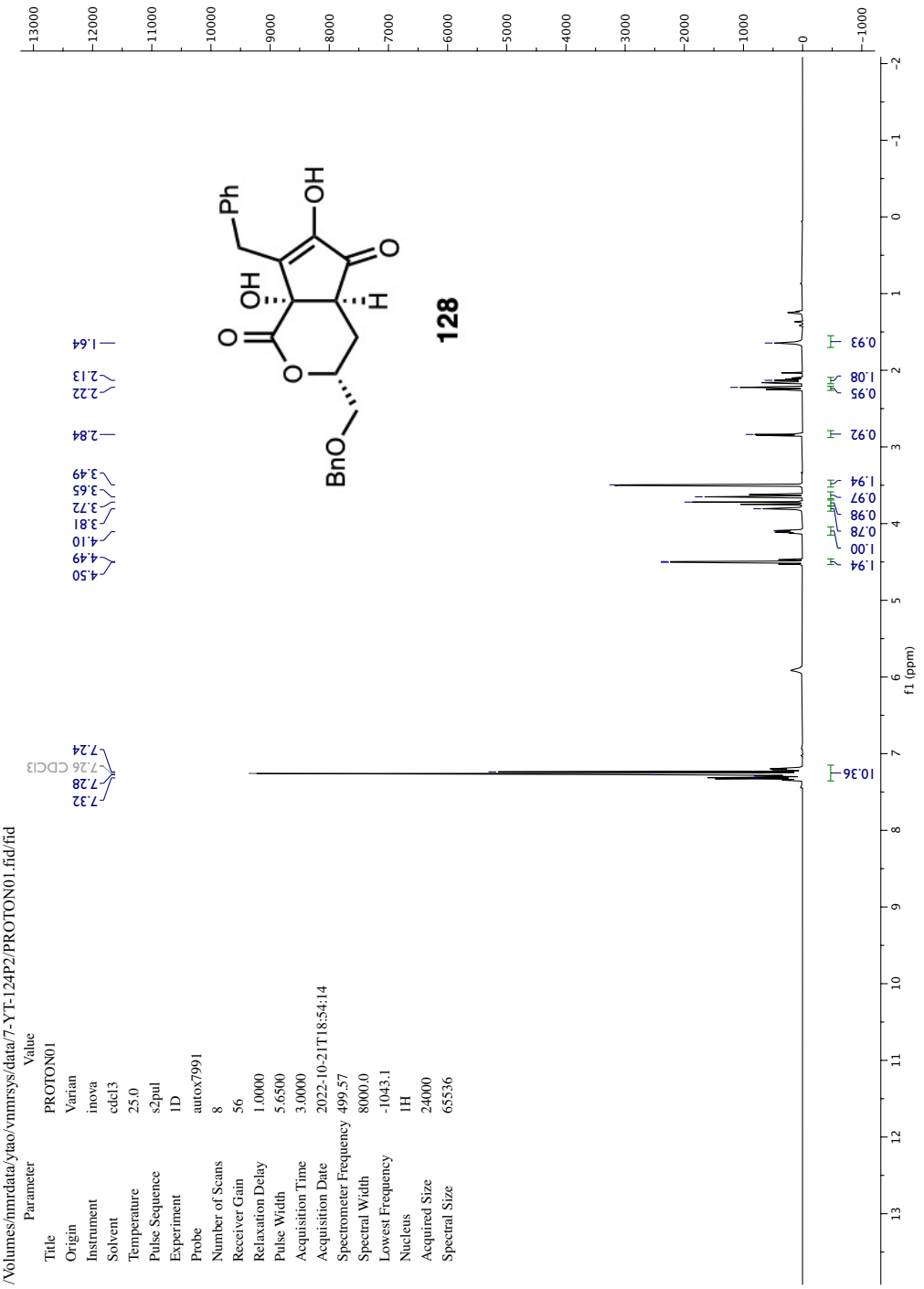
/Volumes/nmrdata/ytao/vnmrsys/data/7-YT-124P2/PROTON01.fid/fid
Parameter Value
Title PROTON01
Origin Varian
Instrument inova
Solvent cdcl3
Temperature 25.0
Pulse Sequence s2pul
Experiment 1D
Probe autox7991
Number of Scans 8
Receiver Gain 56
Relaxation Delay 1.0000
Pulse Width 5.6500
Acquisition Time 3.0000
Acquisition Date 2022-10-21T18:54:14
Spectrometer Frequency 499.57
Spectral Width 8000.0
Lowest Frequency -1043.1
Nucleus 1H
Acquired Size 24000
Spectral Size 65536
128
Ph
OH
O
OH
O
H
O
BnO
7.32
7.28
7.26 CDCl3
7.24
4.50
4.49
4.10
3.81
3.72
3.65
3.49
2.84
2.22
2.13
1.64
10.36
1.94
1.00
0.78
0.98
0.97
1.94
0.92
0.95
1.08
0.93
f1 (ppm)

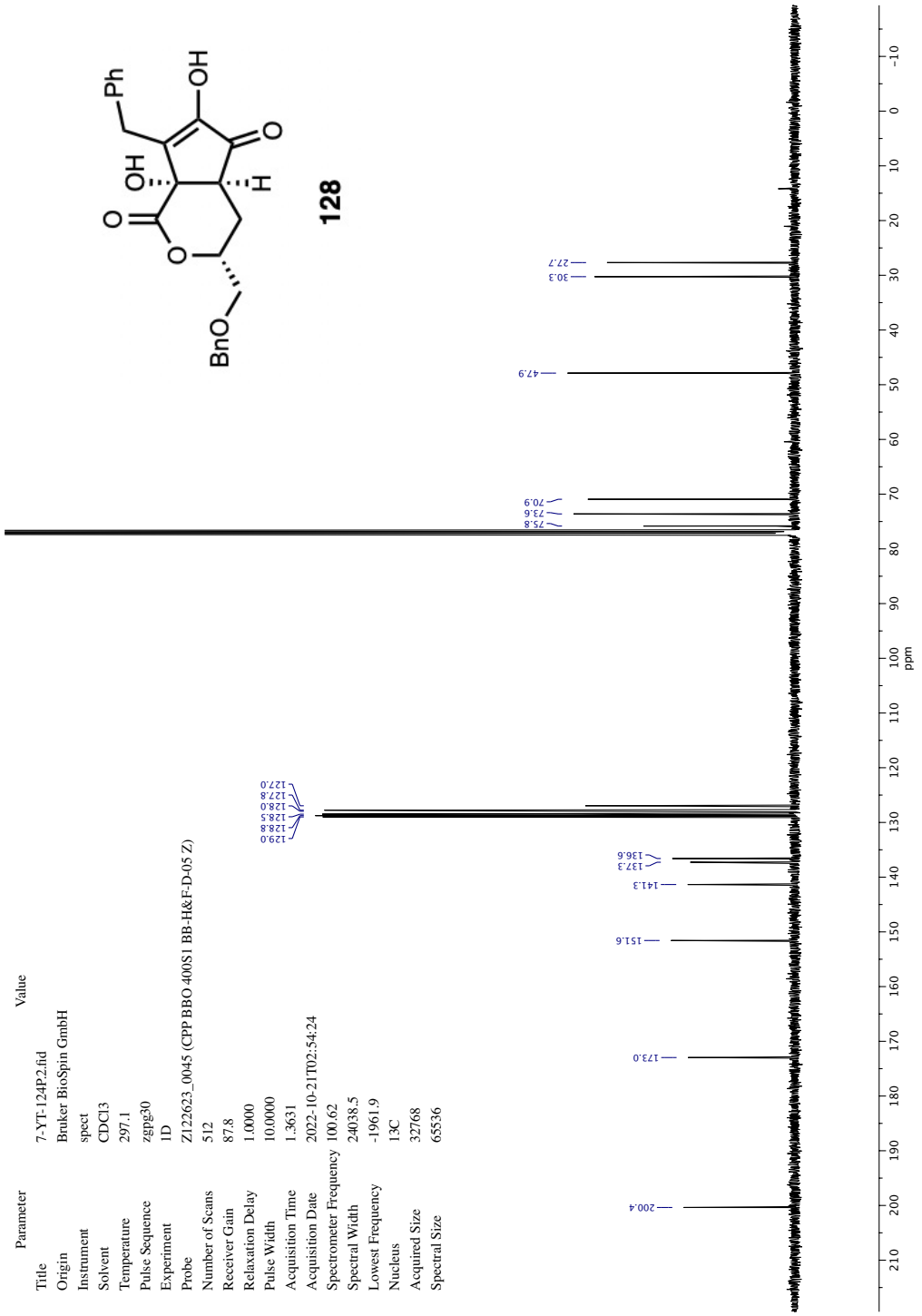
Ph
OH
O
OH
O
H
O
BnO
128
Parameter Value
Title 7-YT-124P2.fid
Origin Bruker BioSpin GmbH
Instrument spect
Solvent CDCl3
Temperature 297.1
Pulse Sequence zgpg30
Experiment 1D
Probe Z122623_0045 (CPP BBO 400S1 BB-H&F-D-05 Z)
Number of Scans 512
Receiver Gain 87.8
Relaxation Delay 1.0000
Pulse Width 10.0000
Acquisition Time 1.3631
Acquisition Date 2022-10-21T02:54:24
Spectrometer Frequency 100.62
Spectral Width 24038.5
Lowest Frequency -1961.9
Nucleus 13C
Acquired Size 32768
Spectral Size 65536
200.4
173.0
151.6
141.3
137.3
136.6
129.0
128.8
128.5
128.0
127.8
127.0
75.8
73.6
70.9
47.9
30.3
27.7
ppm

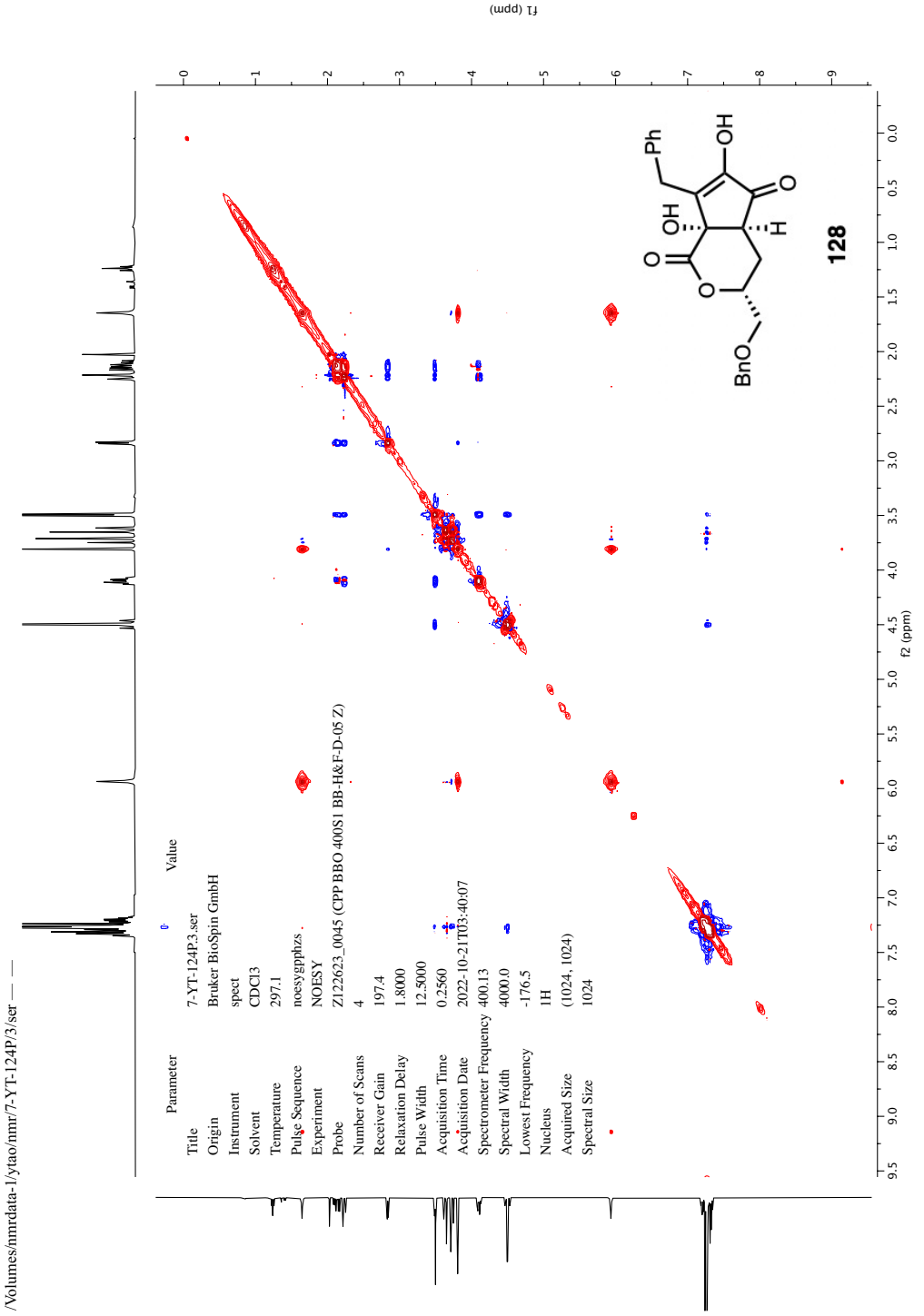
/Volumes/nmrdata-1/ytao/nmr/7-YT-124P/3/ser — —
Parameter Value
Title 7-YT-124P3.ser
Origin Bruker BioSpin GmbH
Instrument spect
Solvent CDCl3
Temperature 297.1
Pulse Sequence noesygpphzs
Experiment NOESY
Probe Z122623_0045 (CPP BBO 400S1 BB-H&F-D-05 Z)
Number of Scans 4
Receiver Gain 197.4
Relaxation Delay 1.8000
Pulse Width 12.5000
Acquisition Time 0.2560
Acquisition Date 2022-10-21T03:40:07
Spectrometer Frequency 400.13
Spectral Width 4000.0
Lowest Frequency -176.5
Nucleus 1H
Acquired Size (1024, 1024)
Spectral Size 1024
f1 (ppm)
f2 (ppm)
Ph
OH
OH
O
H
O
O
BnO
128

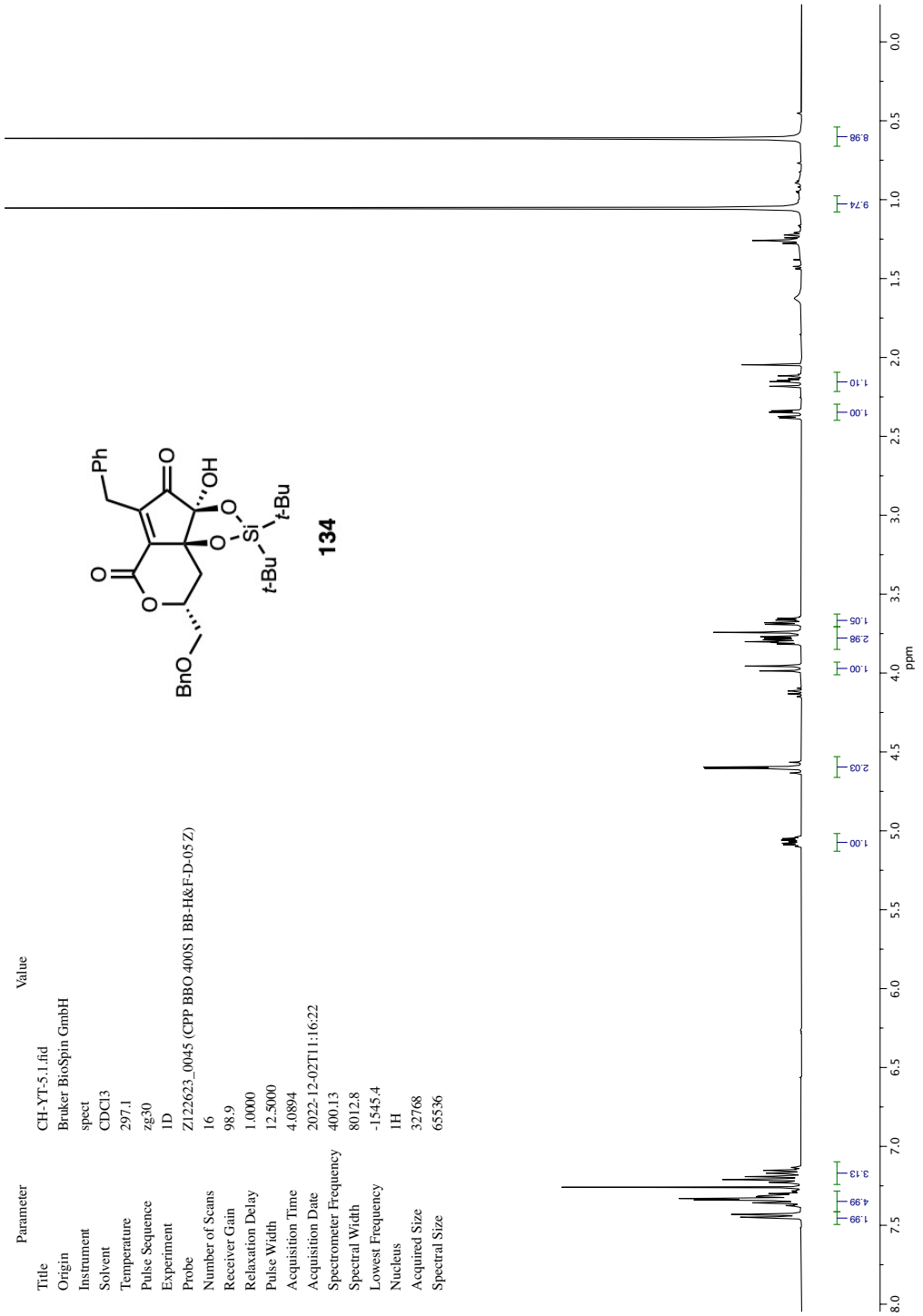

Parameter	Value
Title	CH-YT-5.1.fid
Origin	Bruker BioSpin GmbH
Instrument	spect
Solvent	CDCl3
Temperature	297.1
Pulse Sequence	zg30
Experiment	1D
Probe	Z122623_0045 (CPP BBO 400S1 BB-H&F-D-05 Z)
Number of Scans	16
Receiver Gain	98.9
Relaxation Delay	1.0000
Pulse Width	12.5000
Acquisition Time	4.0894
Acquisition Date	2022-12-02T11:16:22
Spectrometer Frequency	400.13
Spectral Width	8012.8
Lowest Frequency	-1545.4
Nucleus	1H
Acquired Size	32768
Spectral Size	65536

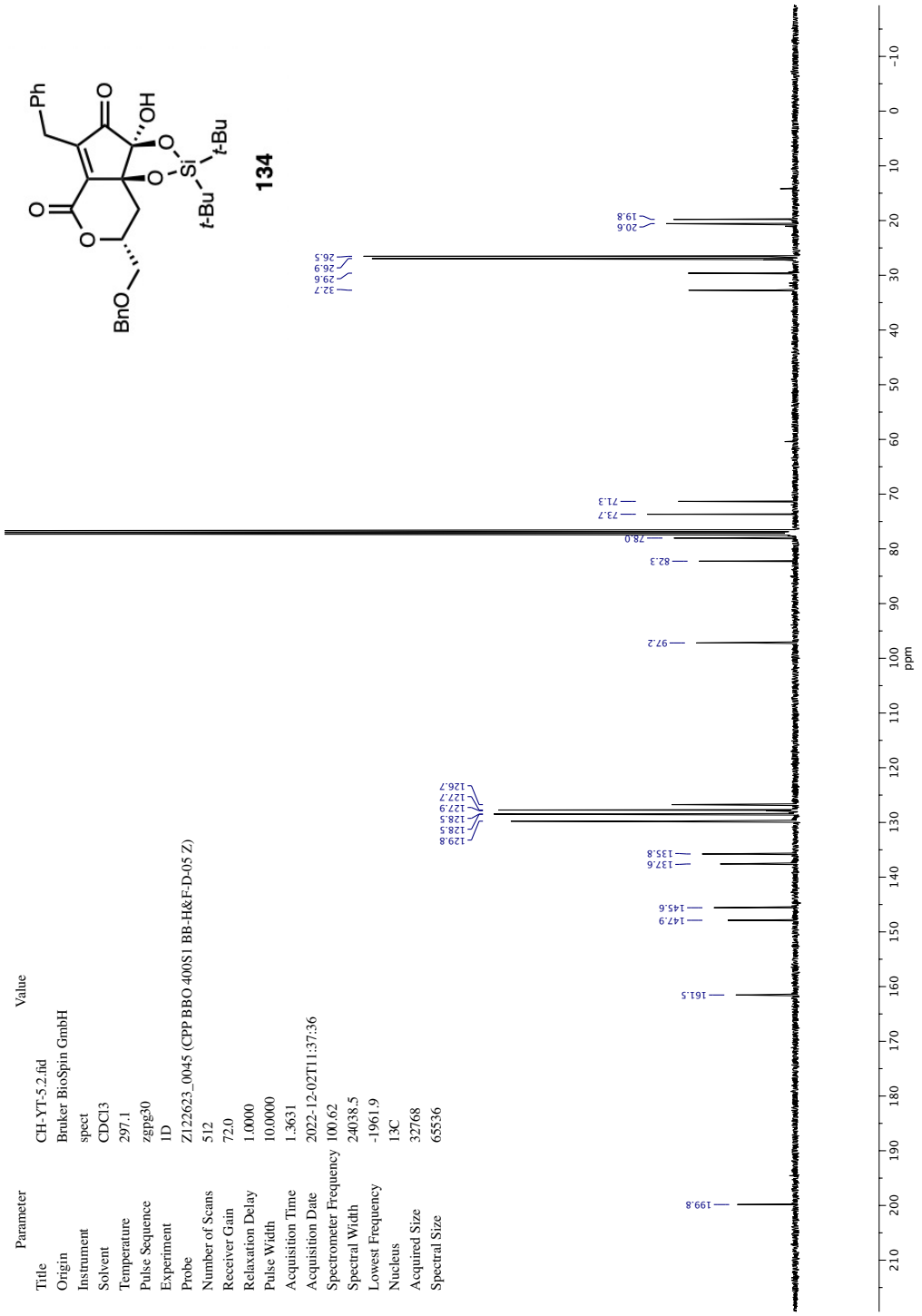
Ph
O
OH
O
O
Si
t-Bu
t-Bu
O
O
BnO
134
Parameter Value
Title CH-YT-5.2.fid
Origin Bruker BioSpin GmbH
Instrument spect
Solvent CDCl3
Temperature 297.1
Pulse Sequence zgpg30
Experiment 1D
Probe Z122623_0045 (CPP BBO 400S1 BB-H&F-D-05 Z)
Number of Scans 512
Receiver Gain 72.0
Relaxation Delay 1.0000
Pulse Width 10.0000
Acquisition Time 1.3631
Acquisition Date 2022-12-02T11:37:36
Spectrometer Frequency 100.62
Spectral Width 24038.5
Lowest Frequency -1961.9
Nucleus 13C
Acquired Size 32768
Spectral Size 65536
199.8
161.5
147.9
145.6
137.6
135.8
129.8
128.5
128.5
127.9
127.7
126.7
97.2
82.3
78.0
73.7
71.3
32.7
29.6
26.9
26.5
20.6
19.8
ppm

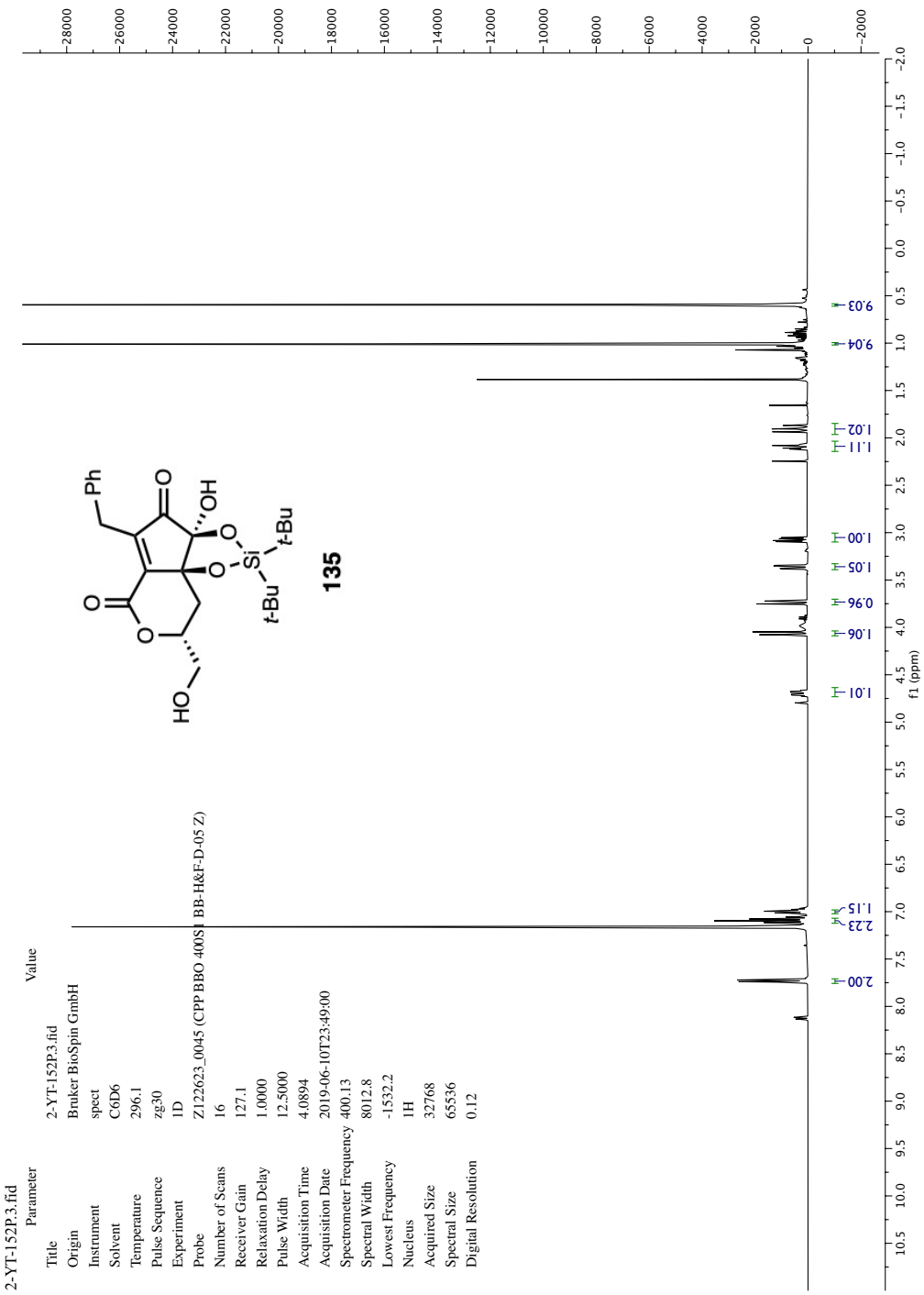
2-YT-152P3.fid
Parameter Value
Title 2-YT-152P3.fid
Origin Bruker BioSpin GmbH
Instrument spect
Solvent C6D6
Temperature 296.1
Pulse Sequence zg30
Experiment 1D
Probe Z122623_0045 (CPP BBO 400S1 BB-H&F-D-05 Z)
Number of Scans 16
Receiver Gain 127.1
Relaxation Delay 1.0000
Pulse Width 12.5000
Acquisition Time 4.0894
Acquisition Date 2019-06-10T23:49:00
Spectrometer Frequency 400.13
Spectral Width 8012.8
Lowest Frequency -1532.2
Nucleus 1H
Acquired Size 32768
Spectral Size 65536
Digital Resolution 0.12
Ph
O
OH
O
O
O
O
Si
t-Bu
t-Bu
HO
135
9.03
9.04
1.02
1.11
1.00
1.05
0.96
1.06
1.01
2.23
1.15
2.00
f1 (ppm)

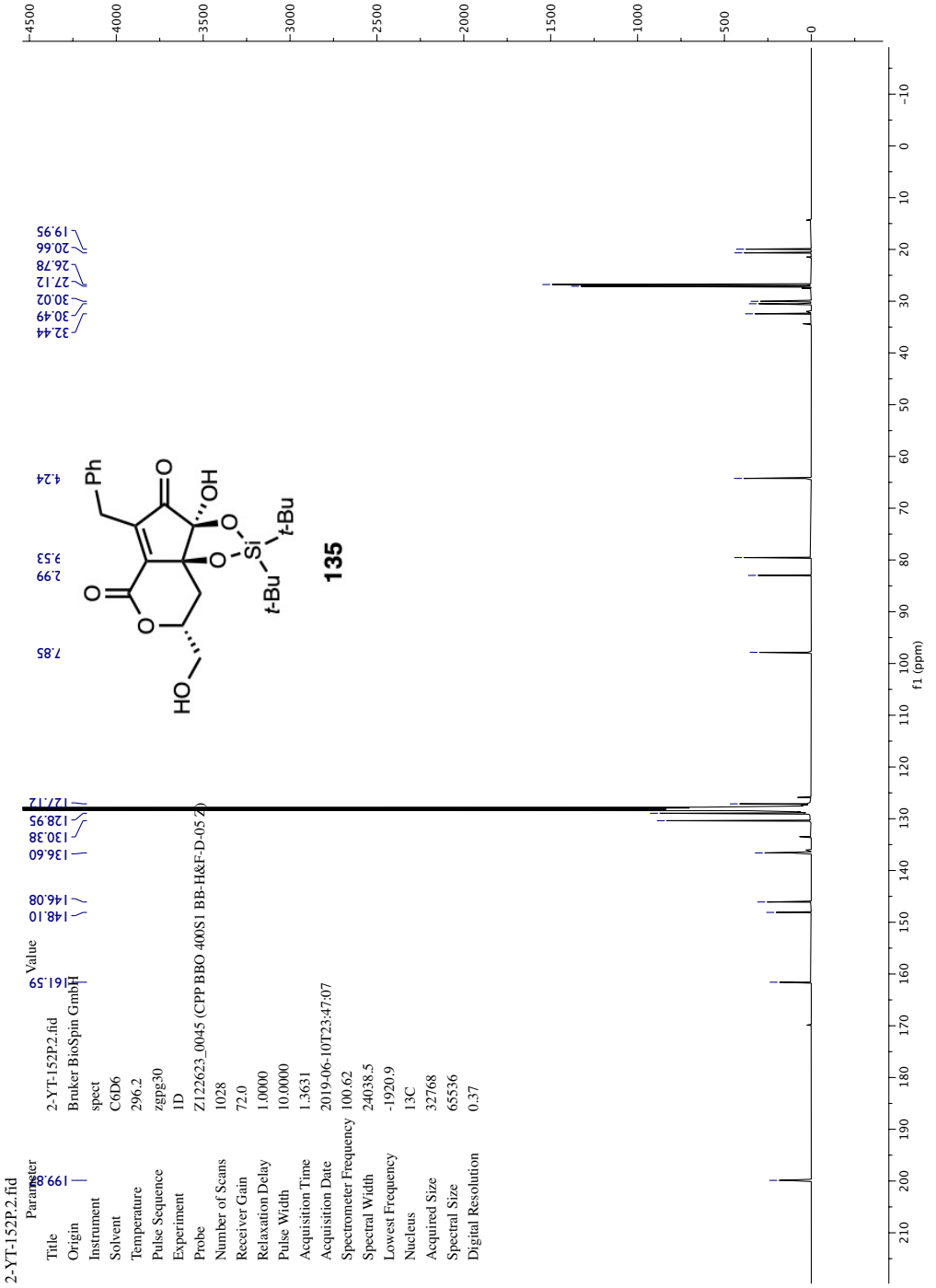
2-YT-152P2.fid
Parameter Value
Title 2-YT-152P2.fid
Origin Bruker BioSpin GmbH
Instrument spect
Solvent C6D6
Temperature 296.2
Pulse Sequence zgpg30
Experiment 1D
Probe Z122623_0045 (CPP BBO 400S1 BB-H&F-D-05 Z)
Number of Scans 1028
Receiver Gain 72.0
Relaxation Delay 1.0000
Pulse Width 10.0000
Acquisition Time 1.3631
Acquisition Date 2019-06-10T23:47:07
Spectrometer Frequency 100.62
Spectral Width 24038.5
Lowest Frequency -1920.9
Nucleus 13C
Acquired Size 32768
Spectral Size 65536
Digital Resolution 0.37
199.81
161.59
148.10
146.08
136.60
130.38
128.95
127.12
77.85
42.99
39.53
32.44
30.49
30.02
27.12
26.78
20.66
19.95
4.24
Ph
O
OH
O
O
Si
t-Bu
t-Bu
O
O
HO
135
f1 (ppm)

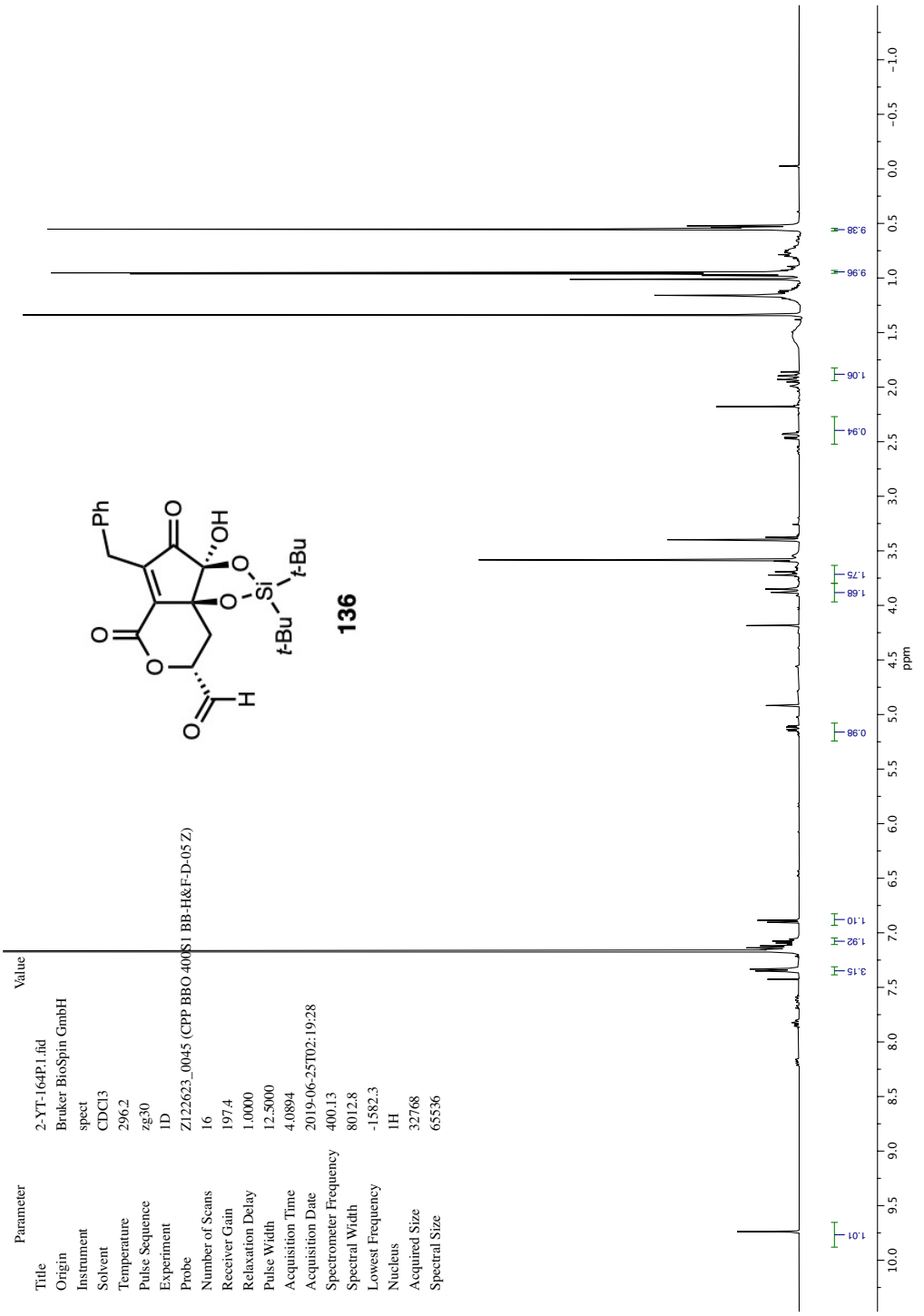
Parameter
Value
Title
2-YT-164P1.fid
Origin
Bruker BioSpin GmbH
Instrument
spect
Solvent
CDCl3
Temperature
296.2
Pulse Sequence
zg30
Experiment
1D
Probe
Z122623_0045 (CPP BBO 400S1 BB-H&F-D-05 Z)
Number of Scans
16
Receiver Gain
197.4
Relaxation Delay
1.0000
Pulse Width
12.5000
Acquisition Time
4.0894
Acquisition Date
2019-06-25T02:19:28
Spectrometer Frequency
400.13
Spectral Width
8012.8
Lowest Frequency
-1582.3
Nucleus
1H
Acquired Size
32768
Spectral Size
65536
Ph
OH
O
Si
t-Bu
t-Bu
H
136
ppm

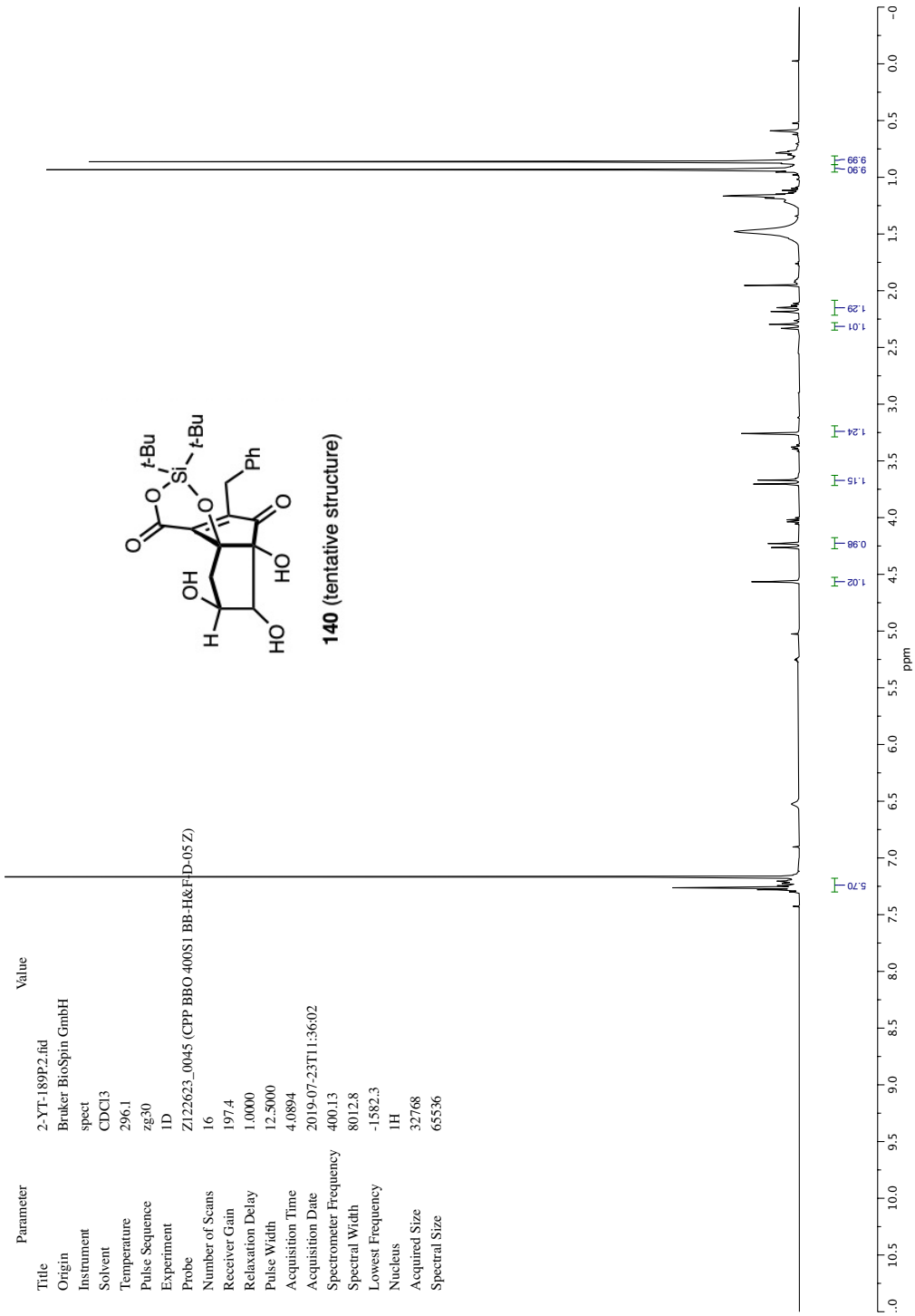
Parameter Value
Title 2-YT-189P2.fid
Origin Bruker BioSpin GmbH
Instrument spect
Solvent CDCl3
Temperature 296.1
Pulse Sequence zg30
Experiment 1D
Probe Z122623_0045 (CPP BBO 400S1 BB-H&F-D-05 Z)
Number of Scans 16
Receiver Gain 197.4
Relaxation Delay 1.0000
Pulse Width 12.5000
Acquisition Time 4.0894
Acquisition Date 2019-07-23T11:36:02
Spectrometer Frequency 400.13
Spectral Width 8012.8
Lowest Frequency -1582.3
Nucleus 1H
Acquired Size 32768
Spectral Size 65536
t-Bu
Si
t-Bu
O
O
O
Ph
O
OH
HO
H
HO
140 (tentative structure)
5.70
1.02
0.98
1.15
1.24
1.01
1.29
9.90
9.99
ppm

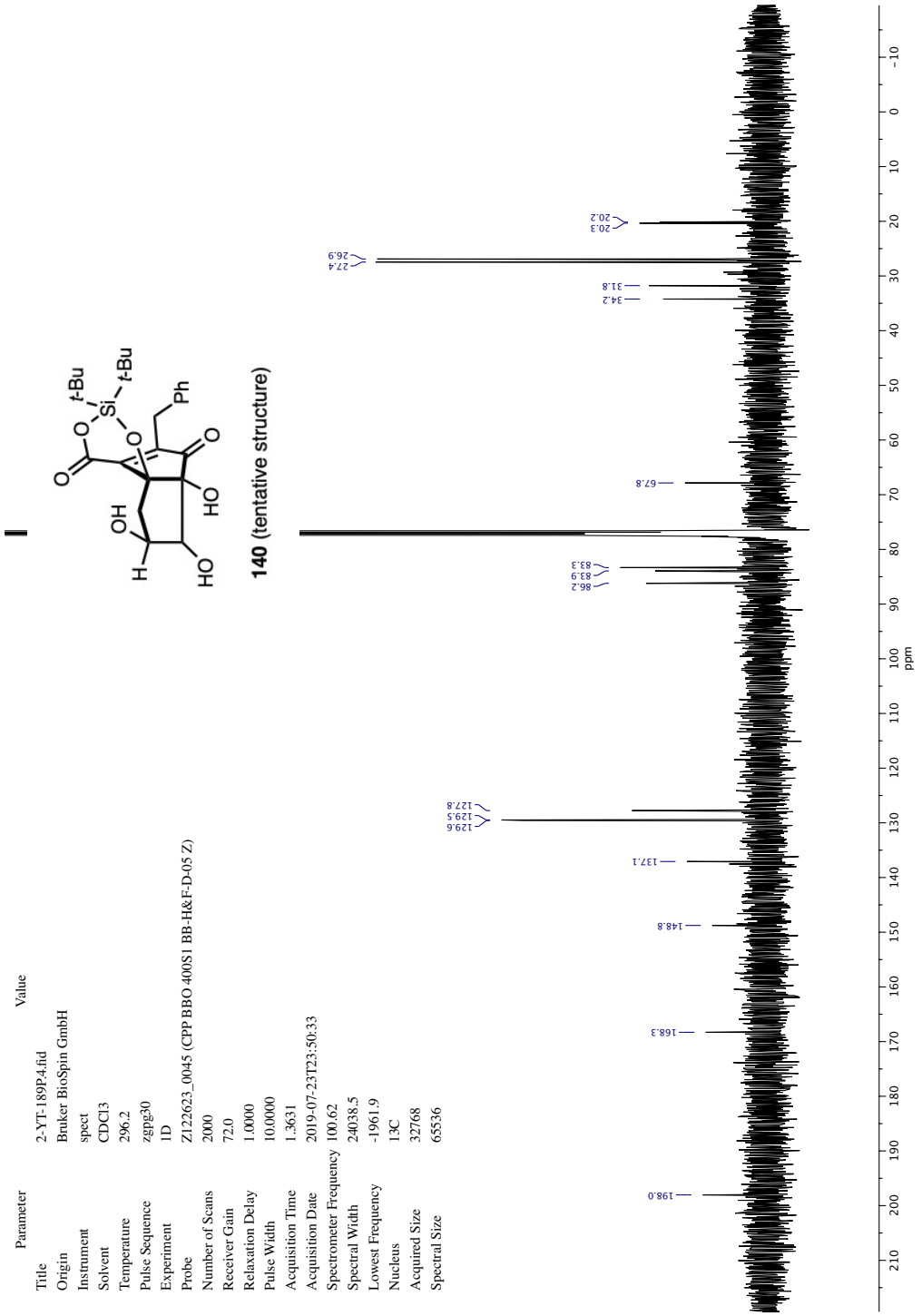
Parameter Value
Title 2-YT-189P4.fid
Origin Bruker BioSpin GmbH
Instrument spect
Solvent CDCl3
Temperature 296.2
Pulse Sequence zgpg30
Experiment 1D
Probe Z122623_0045 (CPP BBO 400S1 BB-H&F-D-05 Z)
Number of Scans 2000
Receiver Gain 72.0
Relaxation Delay 1.0000
Pulse Width 10.0000
Acquisition Time 1.3631
Acquisition Date 2019-07-23T23:50:33
Spectrometer Frequency 100.62
Spectral Width 24038.5
Lowest Frequency -1961.9
Nucleus 13C
Acquired Size 32768
Spectral Size 65536
t-Bu
Si
t-Bu
Ph
O
OH
H
HO
HO
140 (tentative structure)
198.0
168.3
137.1
148.8
129.6
129.5
127.8
86.2
83.9
83.3
67.8
27.4
26.9
34.2
31.8
20.3
20.2
ppm

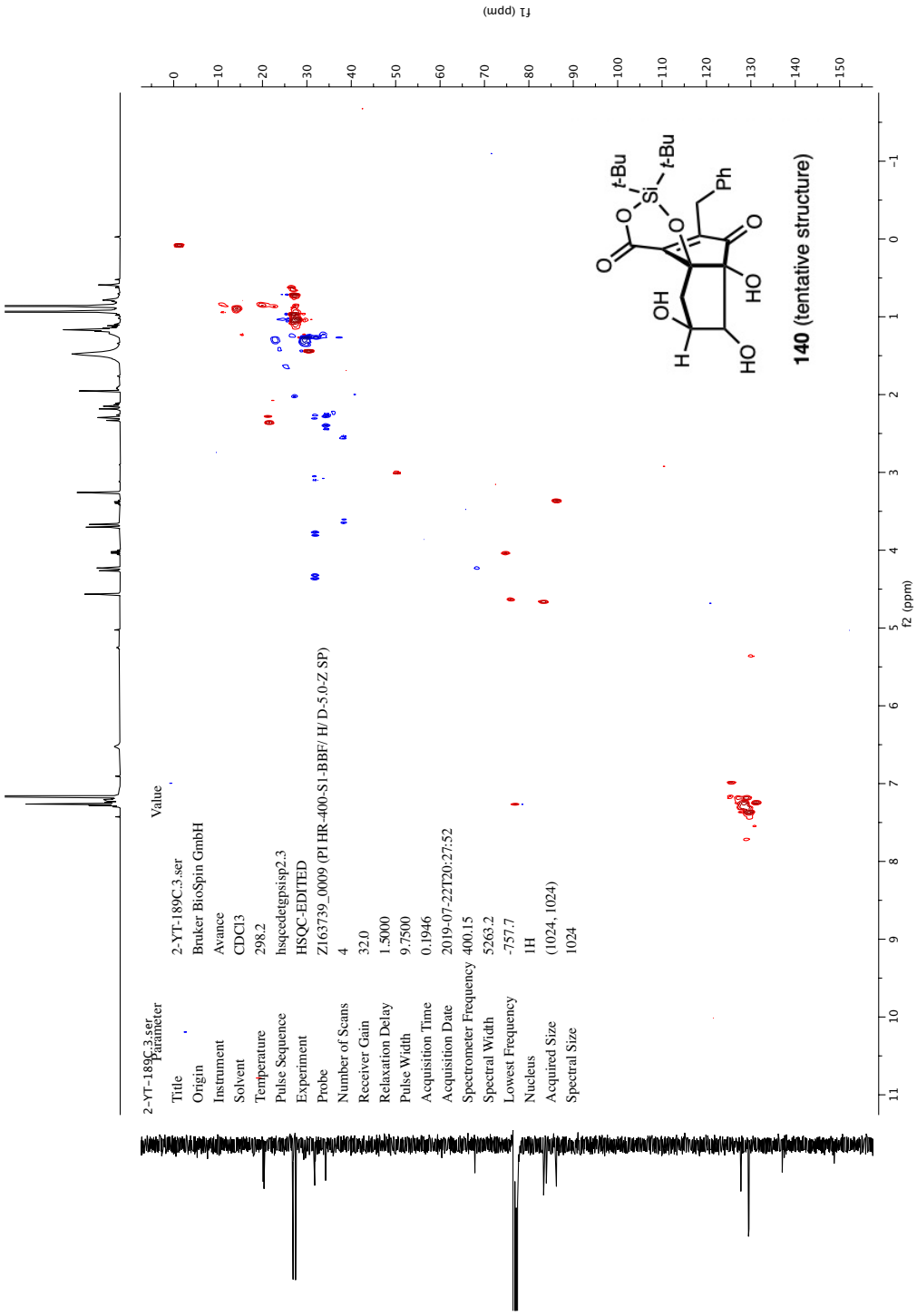
f1 (ppm)
f2 (ppm)
2-YT-189C.3.ser
Parameter Value
Title 2-YT-189C.3.ser
Origin Bruker BioSpin GmbH
Instrument Avance
Solvent CDCl3
Temperature 298.2
Pulse Sequence hsqcedetgpsisp2.3
Experiment HSQC-EDITED
Probe Z163739_0009 (PI HR-400-S1-BBF/ H/ D-5.0-Z SP)
Number of Scans 4
Receiver Gain 32.0
Relaxation Delay 1.5000
Pulse Width 9.7500
Acquisition Time 0.1946
Acquisition Date 2019-07-22T20:27:52
Spectrometer Frequency 400.15
Spectral Width 5263.2
Lowest Frequency -757.7
Nucleus 1H
Acquired Size (1024, 1024)
Spectral Size 1024
t-Bu
Si
t-Bu
Ph
O
O
O
O
OH
HO
H
HO
140 (tentative structure)

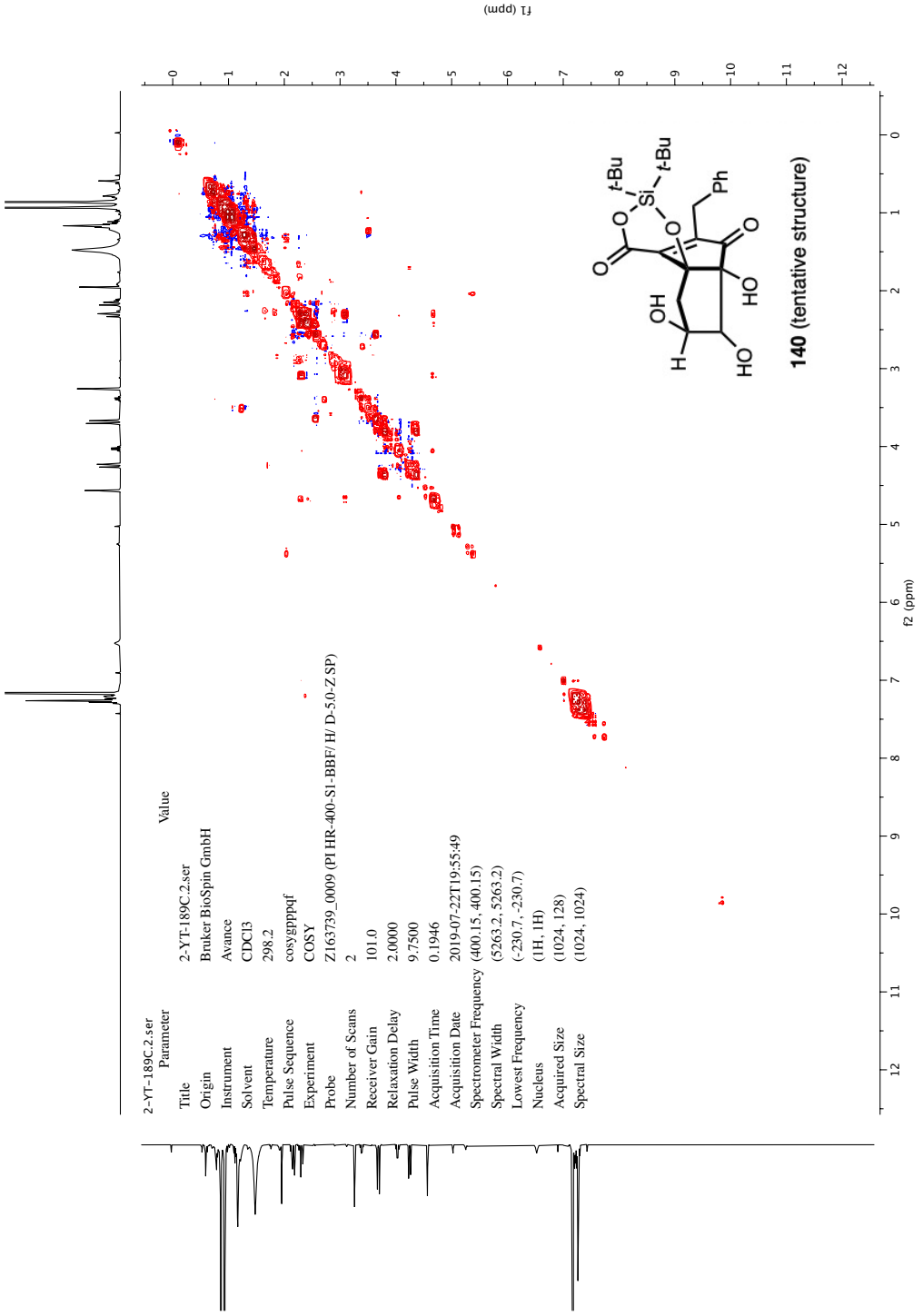
f1 (ppm)
f2 (ppm)
2-YT-189C.2.ser
Parameter Value
Title 2-YT-189C.2.ser
Origin Bruker BioSpin GmbH
Instrument Avance
Solvent CDCl3
Temperature 298.2
Pulse Sequence cosygpppqf
Experiment COSY
Probe Z163739_0009 (PI HR-400-S1-BBF/ H/ D-5.0-Z SP)
Number of Scans 2
Receiver Gain 101.0
Relaxation Delay 2.0000
Pulse Width 9.7500
Acquisition Time 0.1946
Acquisition Date 2019-07-22T19:55:49
Spectrometer Frequency (400.15, 400.15)
Spectral Width (5263.2, 5263.2)
Lowest Frequency (-230.7, -230.7)
Nucleus (1H, 1H)
Acquired Size (1024, 128)
Spectral Size (1024, 1024)
t-Bu
t-Bu
Si
O
O
O
Ph
O
OH
H
HO
HO
140 (tentative structure)

Appendix 2

X-Ray Crystallography Reports Relevant to Chapter 4:

A SeO_2 multioxidation approach toward enterocin

A2.1 X-RAY CRYSTAL STRUCTURE ANALYSIS

Low-temperature diffraction data (φ- and ω-scans) were collected on a Bruker AXS D8 VENTURE KAPPA diffractometer coupled to a PHOTON 100 CMOS detector with Cu-K_α radiation (λ = 1.54178 Å) from a $I_\mu S$ HB micro-focus sealed X-ray tube. All diffractometer manipulations, including data collection, integration, and scaling were carried out using the Bruker APEXII software.[1] Absorption corrections were applied using SADABS.[2] The structure was solved by intrinsic phasing using SHELXT[3] and refined against F^2 on all data by full-matrix least squares with SHELXL-2014[3] using established refinement techniques.[4] All non-hydrogen atoms were refined anisotropically. All hydrogen atoms were included into the model at geometrically calculated positions and refined using a riding model. The isotropic displacement parameters of all hydrogen atoms were fixed to 1.2 times the *U* value of the atoms they are linked to (1.5 times for methyl groups and hydroxyl groups). Absolute configuration was determined by anomalous dispersion.[5] Crystallographic data for **136** can be obtained free of charge from The Cambridge Crystallographic Data Centre (CCDC) via www.ccdc.cam.ac.uk/data_request/cif under CCDC deposition numbers 2259506. Graphical representation of the structures with 50% probability thermal ellipsoids was generated using Mercury visualization software.

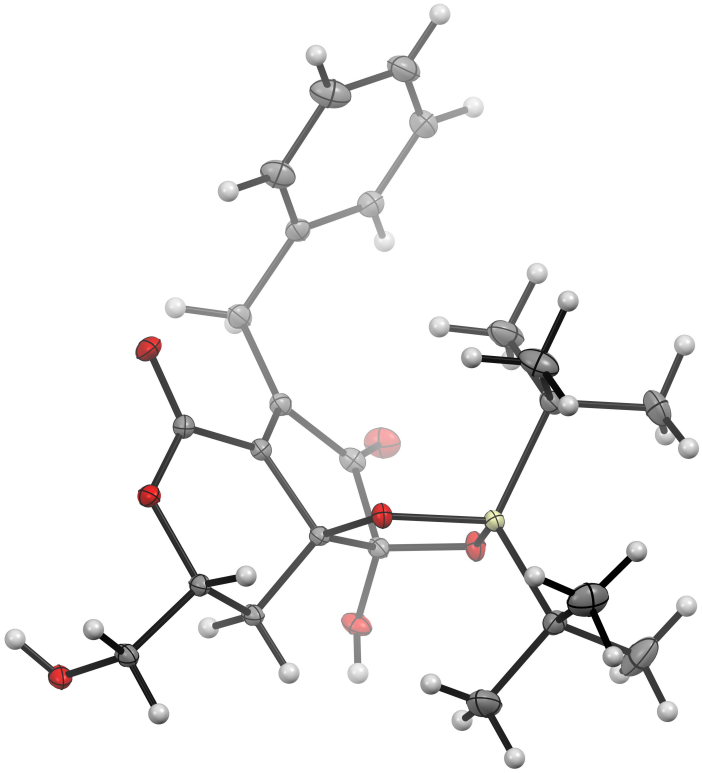

Figure A2.1. *Structure of* ***35*** *with 50% probability anisotropic displacement ellipsoids.*

Table A2.1. *Crystal data and structure refinement for* ***136****.*

Identification code	**136**
Empirical formula	$C_{24}H_{32}O_7Si$
Formula weight	460.58
Temperature/K	100.0
Crystal system	monoclinic
Space group	C2/c
a/Å	31.53(3)
b/Å	9.528(7)
c/Å	15.474(7)
α/°	90

β/°	90.92(3)
γ/°	90
Volume/Å^3	4648(6)
Z	8
ρ_{calc}g/cm^3	1.316
μ/mm^{-1}	0.143
F(000)	1968.0
Crystal size/mm^3	0.54 × 0.34 × 0.22
Radiation	MoKα (λ = 0.71073)
2Θ range for data collection/°	2.584 to 72.176
Index ranges	-51 ≤ h ≤ 45, -15 ≤ k ≤ 15, -25 ≤ l ≤ 25
Reflections collected	114658
Independent reflections	10388 [R_{int} = 0.0365, R_{sigma} = 0.0198]
Data/restraints/parameters	10388/0/297
Goodness-of-fit on F^2	1.055
Final R indexes [I>=2σ (I)]	R_1 = 0.0406, wR_2 = 0.1153
Final R indexes [all data]	R_1 = 0.0521, wR_2 = 0.1247
Largest diff. peak/hole / e Å^{-3}	0.97/-0.35

Special Refinement Details for 136

Compound **136** crystallizes in the monoclinic space group C2/c with one molecule in the unit.

A2.2 REFERENCES

1. APEX2, Version 2 User Manual, M86-E01078. Bruker Analytical X-ray Systems: Madison, WI.

2. Sheldrick, G. M. SADABS (version 2008/1): Program for Absorption Correction for Data from Area Detector Frames. University of Göttingen, 2008.
3. Sheldrick, G. M. *Acta Cryst.* **2008**, *64*, 112.
4. Müller, P. *Crystallogr. Rev.* **2009**, *15*, 57.
5. Parsons, S.; Flack, H. D.; Wagner, T. *Acta Cryst.* **2013**, *69*, 249.

Chapter 5

A radical-polar crossover annulation approach toward enterocin

5.1 Retrosynthetic analysis

After encountering difficulties in a SeO_2 multi-oxidation approach to enterocin, we started brainstorming again. When we observe enterocin (**33**) from a rotated orientation, we found that there might be some innate pseudo-symmetry within the natural product (Figure 1). Specifically, the [3.2.1]bicycle can potentially be divided into symmetrical fragments **142** and **143**. Then, the scientific question we want to explore is how to join the two pieces together.

---

† The research discussed was completed in collaboration with Dr. Simon Cooper in our laboratory.

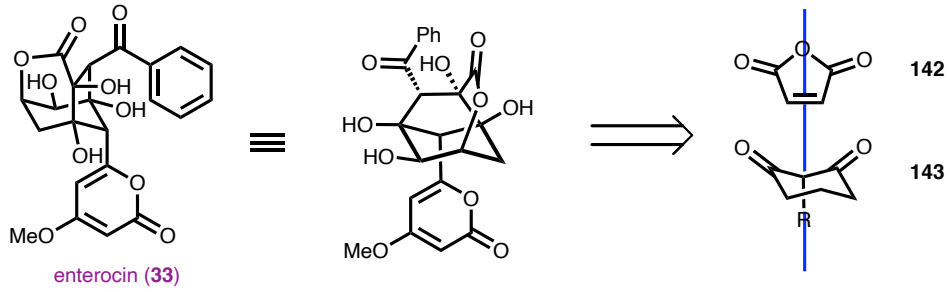

Figure 1. *Inspiration for a radical-polar crossover annulation.*

We started with literature searches on whether these types of annulation have been reported. Micalizio and coworkers reported a metallacycle-mediated annulative diketone–alkyne coupling to form five-, six-, and seven-membered highly oxygenated rings[1–3] and they also used this methodology in their synthesis of anhydroryandol[4]. Most of the examples are intramolecular coupling, but they reported this intermolecular example (Figure 2): they exposed diketone **144** to Ti(O*i*Pr)$_4$/*i*PrMgCl and 1-(Trimethylsilyl)propyne **145** and obtained cyclopentane **146** in 37% yield.

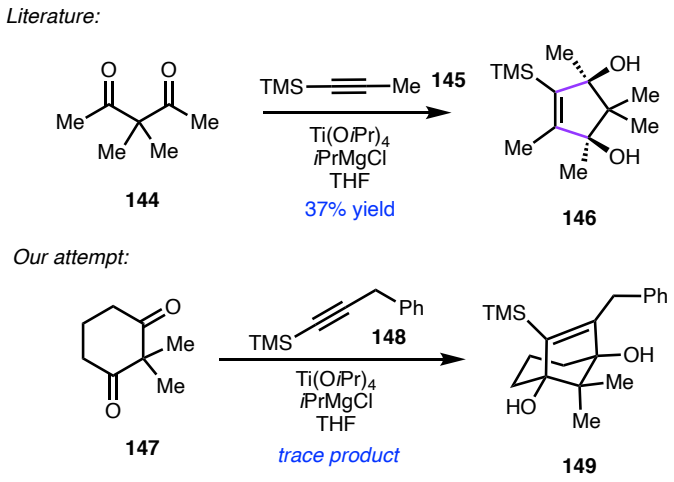

Figure 2. *Ti-mediated annulation.*

There are two major drawbacks if we were going to adopt Micalizio's methodology: 1. The substrates for this annulation requires *gem*-disubstitutions in between the two carbonyls. This features do not map onto enterocin's structure. 2. There is no reported case on making

[3.2.1]bicycles through this methodology, and the feasibility is unknown. Therefore, we prepared a model system substrate **147** and alkyne **148** (Figure 2). Under the same condition reported by Micalizio and coworkers, we found the reaction only produced trace amount of the desired bicycle product **149**. In summary, we identified a gap in the scientific literature, and decided to invent a new annulation reaction.

Conceptually, we envisioned a non-biomimetic approach to enterocin in which the core of the molecule is constructed using a radical-polar crossover reaction as an annulation step (Figure 3).[5] Retrosynthetically, this simplifies enterocin (**33**) to a cyclohexanone such as **152**, where R1 is a radical precursor. We recognized that if a carboxylic acid served as the radical precursor, **152** could map back to quinic acid (**153**). There is strong support in literature for the initial radical formation/Giese addition,[6–8] and the catalytic cycle is proposed to close by single electron reduction to form the enolate, which could then be trapped via an intramolecular aldol reaction.[9] This radical-polar crossover reaction could be developed as a new annulation method to prepare bicyclic structures with bridgehead hydroxyl groups, possibly with applications in natural product synthesis beyond enterocin (**33**).

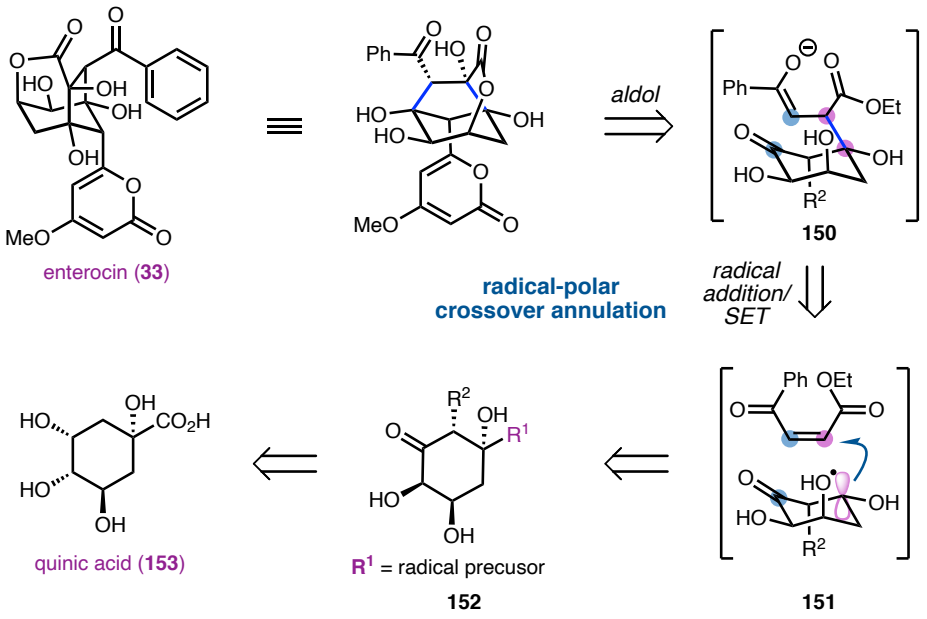

Figure 3. *Retrosynthetic analysis of enterocin.*

Looking more deeply at the key radical-polar crossover step (Figure 4), we envisioned that the reaction starts with a deprotonation, a single electron oxidation by the activated photocatalyst, and then decarboxylation to generate the stabilized radical **155**. In the presence of excess radical acceptor **156**, the newly generated radical **155** can add into the electron-deficient alkene and form a new radical **157**. Then, a single electron reduction from the reduced photocatalyst can generate enolate **158**, which may undergo facile intramolecular aldol and potentially also lactonization to form **159**. As shown in the catalytic cycle, this is an electron-neutral radical polar crossover reaction, and there is no need to addition reductant or oxidant. Precedent for decarboxylative Giese-type additions is shown in Figure 4b.[6]

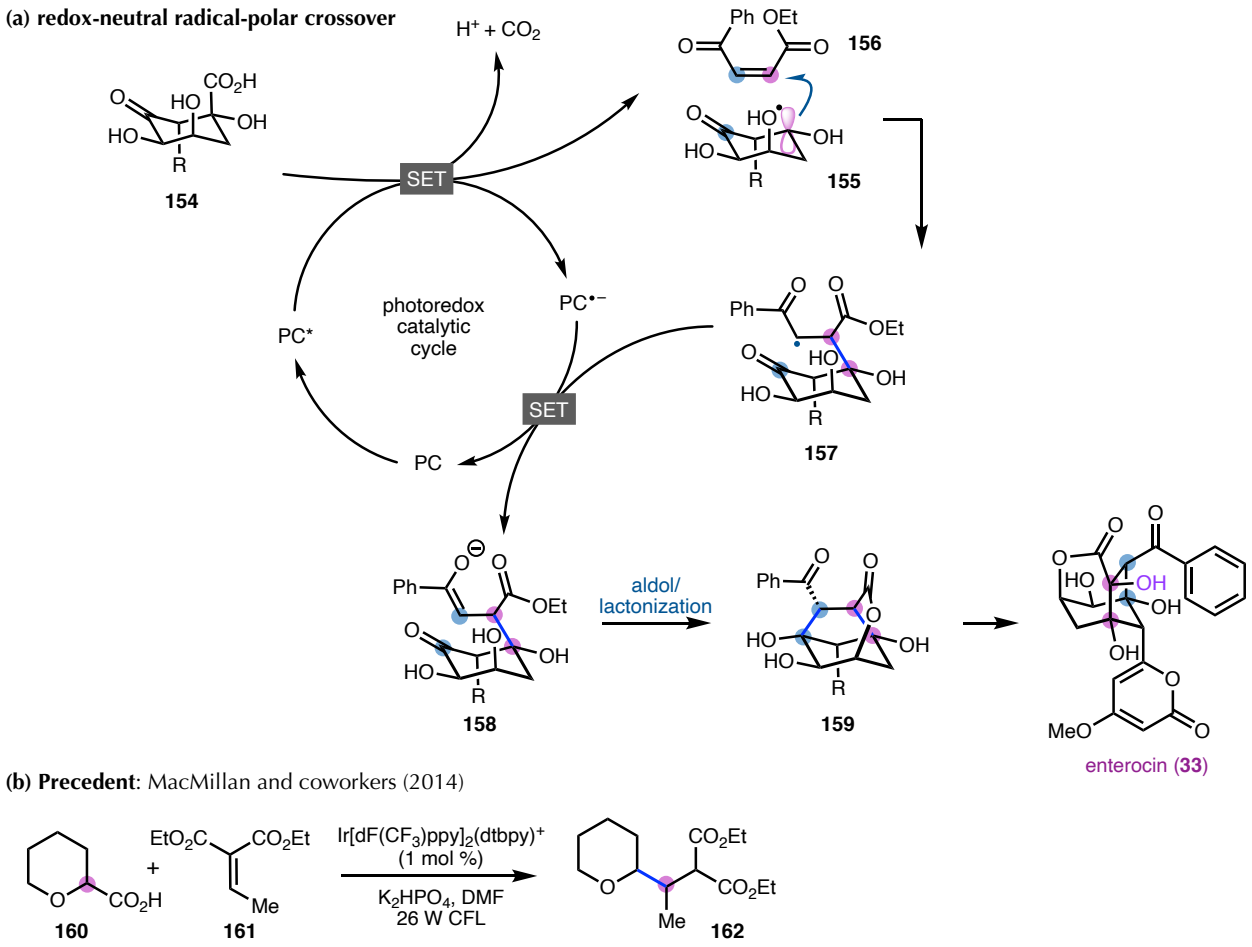

Figure 4. *Mechanism and precedents of the designed radical-polar crossover annulation.*

5.2. Results and discussion

To evaluate the feasibility of this tandem Giese addition/aldol cyclization approach, we have carried out the following preliminary studies. Irradiation of **163** (prepared in four steps from quinic acid (**153**)) and dimethyl fumarate with blue LEDs in the presence of $[Ir(dFCF_3ppy)_2dtbbpy]PF_6$ as photocatalyst and K_2HPO_4 as base gave Geise addition product **164** in 20% yield as a single diastereomer (Scheme 1). It is encouraging that the radical generation/Giese addition steps did occur, but the desired annulation product was not isolated, possibly indicating premature termination of the radical-polar crossover cascade. The result might suggest compound **164** sits in the flipped chair conformation with substituents in equatorial

position, and therefore it is conformationally difficult for intramolecular aldol to take place. It is also possible this premature termination is due to protic quenching by one of the unprotected hydroxyl. However, substrate **165**, which is in the desired conformation for the intramolecular aldol and has diol protected, also terminated early. Screening various substrates, photocatalysts, bases and solvents did not enable the intramolecular aldol reaction to occur, prompting us to explore alternative scaffolds.

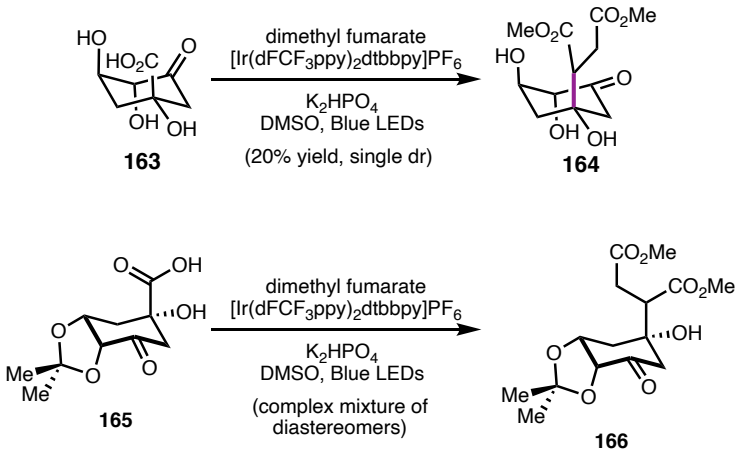

Scheme 1. *Initial attempts on radical-polar crossover reactivity.*

In light of these initial challenges, a second substrate **167** was prepared in four steps from quinic acid (**13**) to independently investigate the feasibility of the intramolecular aldol cyclization (Scheme 2). Under the reductive aldol conditions developed by Buchwald and coworkers[10], the desired [3.2.1]bicycle (**168**) was prepared in promising yield (52%) as a 6:1 mixture of diastereomers at the ester-bearing carbon. In this case, the acetonide likely reinforces the conformation with the substituents in the axial position, enabling the intramolecular aldol reaction. In summary, these two studies (Scheme 1 and 2) show that the key elementary steps in the proposed radical-polar crossover annulation are feasible.

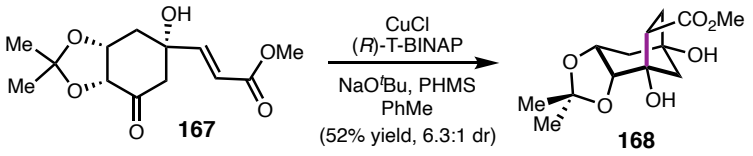

Scheme 2. *Proof-of-principle studies on the feasibility of aldol step.*

Given the exciting results with the formation of **168**, we also investigated the conjugate addition of nucleophiles to α,β- unsaturated ketone **169**, focusing on functionality that could serve as ester equivalents (Scheme 3). We surveyed a variety of ester equivalent nucleophiles on substrate **169**. Vinyl Grignard cuprate addition[11] afforded a complex mixture of products (Scheme 3, entry 1). Attempt on adding a dithiane[12] as a radical into the electron deficient alkene only produced 1,2-addition product **173** and ring expansion product **174**. We reasoned the ring expansion reaction possibly occurred through intermediate **175** that was generated from proton-coupled electron transfer (PCET) of the tertiary alcohol, similar to Knowles's report[13]. Following Overman's precedent[14], we tried to add a methyl ester radical into the alkene using photoredox condition (entry 3), but the reaction was complex. Lastly, we tried to add a cyanide group[15,16] as a masked ester and we found that successful 1,4-addition was observed to produce **177**, but the subsequent intramolecular aldol did not proceed (entry 5).

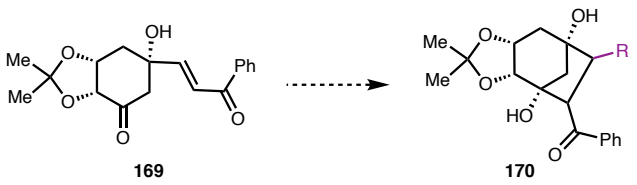

entry	conditions	result
1	 **171** CuI (10 mol%)	Product identified. Complex mixture
2	 **172** $[Ir(dFCF_3ppy)_2dtbbpy]PF_6$ K_2HPO_4 DMSO, Blue LEDs	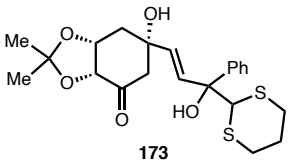 **173** 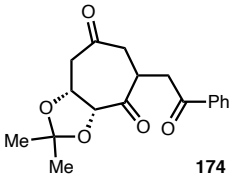 **174** via 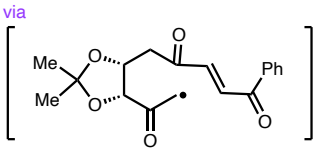 **175**
3	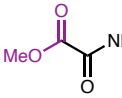 $Ru(bpy)_3(PF_6)_2$ Hantzch Ester, DIPEA DCM, blue LEDs	Complex mixture
4.	Et_2AlCN, PhMe	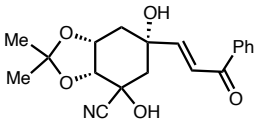 **176**
5.	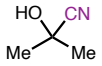 Cs_2CO_3 DCM	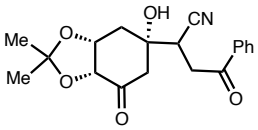 1.6:1 dr **177**

Scheme 3. *Stepwise approach to access the [3.2.1]bicycle.*

Recently, we started exploring a different mode of radical generation (Scheme 4). Following precedent from Knowles lab on light-driven proton-coupled electron transfer (PCET) activation of the O−H bond, we tested tertiary alcohol **178** and found the desired C−C *β*-scission of the resulting alkoxy radical occurred and the radical was able to engage with dimethyl fumarate. The intramolecular aldol then generate diastereomers **179** and **180** in 29% and 15% yield, respectively. We are currently working on functionalizing the bicycle products and experiment with more functionalized alkene accepters (**181-186**).

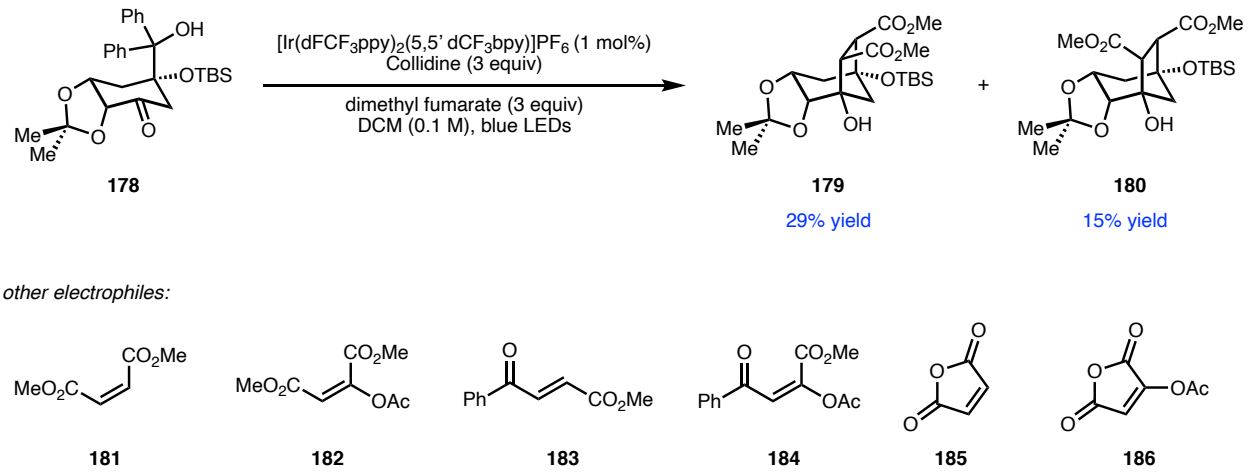

Scheme 5. *Stepwise approach to access the [3.2.1]bicycle.*

5.3 Experimental Section

5.3.1 Materials and methods

Unless otherwise stated, reactions were performed under an inert atmosphere (dry N_2 or Ar) with freshly dried solvents utilizing standard Schlenk techniques. Glassware was oven-dried at 120 °C for a minimum of four hours, or flame-dried utilizing a Bunsen burner under high vacuum. Tetrahydrofuran (THF), methylene chloride (CH_2Cl_2), *N,N*- dimethylformamide (DMF), benzene (PhH), and toluene (PhMe) were dried by passing through activated alumina columns. 2-Methyltetrahydrofuran (anhydrous, >99%, inhibitor-free) was purchased from Sigma-Aldrich and stored under argon. Methanol (HPLC grade) was purchased from Fisher Scientific. Pyridine (Pyr) was distilled from calcium hydride immediately prior to use. All reactions were monitored by thin-layer chromatography using EMD/Merck silica gel 60 F254 pre-coated plates (0.25 mm) and were visualized by UV (254 nm), *p*-anisaldehyde, CAM, and/or $KMnO_4$ staining. Flash column chromatography was performed using silica gel (SiliaFlash® P60, particle size 40-63 microns [230 to 400 mesh]) purchased from Silicycle. ^1H and ^{13}C NMR spectra were recorded on a Bruker

Avance III HD with Prodigy Cryoprobe (at 400 MHz and 101 MHz, respectively), Varian Inova 500 (at 500 MHz and 126 MHz, respectively), or Varian Inova 600 (at 600 MHz and 150 MHz, respectively), and are reported relative to internal $CHCl_3$ (^1H, $\delta = 7.26$), C_6H_6 (^1H, $\delta = 7.16$), or CD_2HOD (^1H, $\delta = 3.31$), and $CDCl_3$ (^{13}C, $\delta = 77.0$), C_6D_6 (^{13}C, $\delta = 128.0$), or CD_3OD (^{13}C, $\delta = 49.0$). Data for ^1H NMR spectra are reported as follows: chemical shift (δ ppm) (multiplicity, coupling constant (Hz), integration). Multiplicity and qualifier abbreviations are as follows: s = singlet, d = doublet, t = triplet, q = quartet, m = multiplet, br = broad, app = apparent. IR spectra were recorded on a Perkin Elmer Paragon 1000 spectrometer and are reported in frequency of absorption (cm^{-1}). HRMS were acquired using an Agilent 6200 Series TOF with an Agilent G1978A Multimode source in electrospray ionization (ESI), atmospheric pressure chemical ionization (APCI), or mixed (MM) ionization mode. Optical rotations were measured on a Jasco P-2000 polarimeter using a 100 mm path-length cell at 589 nm.

Reagents were purchased from commercial vendors as follows: $[Ir(dFCF_3ppy)_2dtbbpy]PF_6$, $[Ir(dFCF_3ppy)_2(5,5'\ dCF_3bpy)]PF_6$, copper chloride, 2,4,6-collidine, dimethyl fumarate were purchased from Sigma-Aldrich. (R)-(+)-2,2′-Bis(di-p-tolylphosphino)-1,1′-binaphthyl was purchased from Sigma-Aldrich and stored in a nitrogen-filled glovebox.

5.3.2 Experimental Procedures

Preparation of triol 164

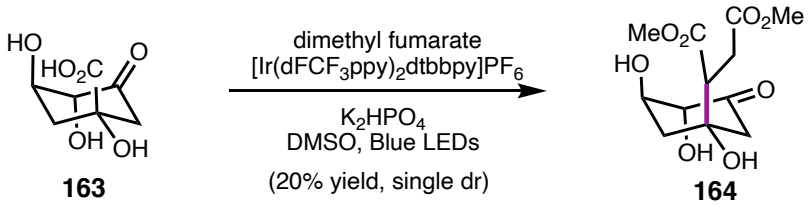

An oven-dried 2-dram vial was charged with a stir bar, acid **163** (40 mg, 0.21 mmol, 1 equiv), dimethyl fumarate (90.8 mg, 0.63 mmol, 3 equiv), $[Ir(dFCF_3ppy)_2dtbbpy]PF_6$ (2.2 mg ,0.002 mmol, 1 mol%), anhydrous K_2HPO_4 (34.8 mg, 0.63 mmol, 3 equiv), and anhydrous DMSO (0.42 mL, 0.5 M). The reaction mixture was sparged with Ar for 15 min. The vial was then irridated with 450 nm LED light for 16h, at which point TLC analysis indicated the full consumption of starting material. The reaction mixture was diluted with 3 mL diethyl ether and 2 mL sat. NH_4Cl. The layers were separated and the aqueous layer was extracted with ethyl acetate (3 × 1 mL). The combined layers were washed with brine (2 mL), dried over Na_2SO_4, filtered, and concentrated *in vacuo*. The crude residue was purified via SiO_2 flash chromatography (30 to 50% EtOAc/hexanes) to afford triol **164** (12 mg, 0.04 mmol, 20% yield) as a colorless oil.

Preparation of ketone 169

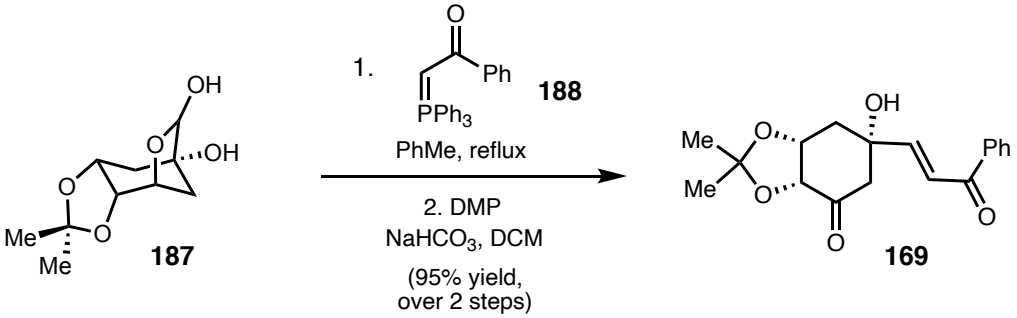

An oven-dried 25 mL round bottom flask was charged with lactol **187** (2 g, 9.25 mmol, 1 equiv), diazo **188** (3.52 g, 9.25 mmol, 1 equiv), and toluene (30 mL). The resulting solution was heated to reflux and stirred for 3 h until at which point TLC analysis indicated the full consumption of starting material. The crude mixture was concentrated *in vacuo*. The crude residue was purified via SiO_2 flash chromatography (30 to 50% EtOAc/hexanes) to remove phosphine oxide. An oven-dried 25 mL round bottom flask was charged with purified material (2.94g, 9.23 mmol, 1 equiv), $NaHCO_3$ (0.93 g, 11.1 mmol, 1.2 equiv), 90 mL DCM, and a stir bar. Then, Dess-Martin periodinane (4.7g, 11.1 mmol, 1.2 equiv) was added at room temperature. Stirring was continued (*ca.* 12h) until at which point TLC analysis indicated the full consumption of starting material. The reaction mixture was diluted with DCM, filtered over celite, and the filtrate was concentrated *in vacuo*. The crude residue was purified via SiO_2 flash chromatography (40 to 50% EtOAc/hexanes) to afford ketone **169** (2.8 g, 8.8 mmol, 95% yield) as a white solid.

TLC (50% EtOAc/hexanes): R_f 0.53 (UV, CAM).

^{1}H NMR (400 MHz, $CDCl_3$): δ 8.02 – 7.96 (m, 2H), 7.62 – 7.55 (m, 1H), 7.52 – 7.45 (m, 2H), 7.35 (d, *J* = 14.9 Hz, 1H), 6.95 (dd, *J* = 15.0, 1.3 Hz, 1H), 4.78 (ddd, *J* = 5.7, 3.6, 2.3 Hz, 1H), 4.47 (d, *J* = 5.3 Hz, 1H), 3.84 (d, *J* = 1.2 Hz, 1H), 2.80 – 2.68 (m, 2H), 2.54 – 2.46 (m, 1H), 2.41 (dd, *J* = 15.8, 3.6 Hz, 1H), 1.53 (s, 3H), 1.43 (s, 3H).

^{13}C NMR (101 MHz, $CDCl_3$): δ 204.66, 190.38, 148.84, 137.63, 133.39, 128.84, 128.81, 123.81, 110.90, 78.81, 76.15, 51.40, 36.26, 27.44, 26.03.

FTIR(NaCl, thin film): 2985, 1731, 1672, 1624, 1596, 1578, 1483, 1447, 1437, 1381 cm^{-1}.

HRMS (ESI): calc'd for $[M+Na]^+$ 339.1203, found 339.1207.

$[\alpha]_D^{25}$ = –5.6 ° (*c* = 1.00, $CHCl_3$).

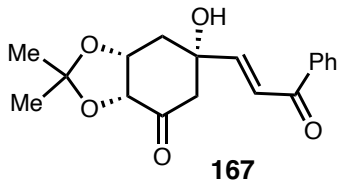

167

Compound **167** was made through a similar procedure for the preparation of compound **169**.

^{1}H NMR (400 MHz, $CDCl_3$): δ 6.86 (dd, *J* = 15.4, 1.2 Hz, 1H), 6.19 (d, *J* = 15.3 Hz, 1H), 4.78 – 4.71 (m, 1H), 4.43 (d, *J* = 5.3 Hz, 1H), 3.76 (s, 3H), 2.67 (d, *J* = 1.9 Hz, 2H), 2.45 (dq, *J* = 15.8, 2.1 Hz, 1H), 2.31 (dd, *J* = 15.8, 3.7 Hz, 1H), 1.50 (s, 3H), 1.40 (s, 3H).

^{13}C NMR (101 MHz, $CDCl_3$): δ 204.63, 167.08, 149.64, 120.36, 110.89, 78.75, 77.09, 75.56, 51.97, 51.18, 36.12, 27.41, 25.99.

FTIR(NaCl, thin film): 2921, 1721, 1652, 1436, 1369, 1318, 1202, 1172, 1153, 1131 cm^{-1}.

HRMS (ESI): calc'd for $[M+Na]^+$ 293.0996, found 293.1001.

$[\alpha]_D^{25}$ = – 7.9° (*c* = 0.5, $CHCl_3$).

Preparation of [3.2.1]bicycle 168

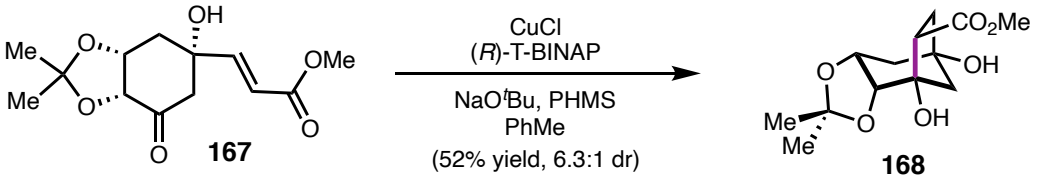

167 **168**

An oven-dried 1 dram vial was charged with a stir bar. The vial was brought into the nitrogen-filled glovebox, and (R)-*p*-tol-BINAP (15 mg, 0.022 mmol, 10 mol%) and toluene (1 mL) were added. Then, NaOt-Bu (1 mg, 0.01 mmol, 0.05 equiv) and CuCl (1.1 mg, 0.01 mmol, 0.05 equiv) were weighed into another oven-dried 1 dram vial. The toluene solution of the chiral bis-phosphine was added via pipet to the vial to dissolve the solids. The solution was stirred for 10 min and PHMS (54μL, 0.88, 4 equiv) was added to the solution. The resulting solution turned a reddish orange color. The unsaturated ester **167** (60 mg, 0.22 mmol, 1 equiv) was added to the reaction

solution in the glovebox, and the resulting solution was stirred for 20 h at room temperature until at which point TLC analysis indicated the full consumption of starting material. The reaction was quenched with sat. aq. NH_4Cl (1 mL). The layers were separated and the aqueous layer was extracted with ethyl acetate (3 × 1 mL). The combined layers were washed with brine (2 mL), dried over Na_2SO_4, filtered, and concentrated *in vacuo*. The crude residue was purified via SiO_2 flash chromatography (30 to 50% EtOAc/hexanes) to afford bicycle **168** (31 mg, 0.11 mmol, 52% yield, 6.4:1 dr) as a colorless oil.

TLC (70% EtOAc/hexanes): R_f 0.54 (UV, CAM).

^{1}H NMR (400 MHz, $CDCl_3$): δ 4.27 (td, *J* = 8.1, 5.4 Hz, 1H), 4.16 – 4.08 (m, 1H), 3.75 (s, 3H), 2.68 (dd, *J* = 9.2, 5.9 Hz, 1H), 2.23 – 2.11 (m, 4H), 1.99 – 1.89 (m, 1H), 1.78 – 1.68 (m, 1H), 1.54 (s, 3H), 1.38 (s, 3H).

^{13}C NMR (101 MHz, $CDCl_3$): δ 174.12, 111.43, 81.07, 78.52, 74.52, 72.22, 52.42, 48.14, 44.26, 43.17, 39.65, 28.46, 26.57.

FTIR(NaCl, thin film): 2952, 2925, 1731, 1437, 1325, 1365, 1329. 1310, 1203, 1167 cm^{-1}.

$[\alpha]_D^{25}$ = 0.1 ° (*c* = 1.00, $CHCl_3$).

Preparation of [3.2.1]bicycle 179 and 180

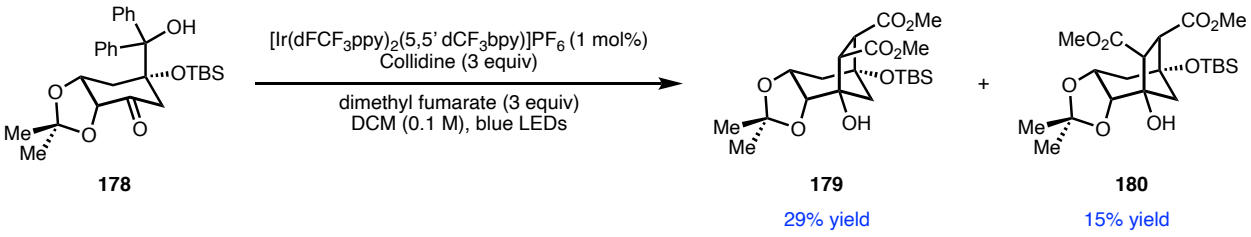

178 **179** 29% yield **180** 15% yield

An oven-dried 2-dram vial was charged with a stir bar, alcohol **178** (75 mg, 0.14 mmol, 1 equiv), dimethyl fumarate (59.7 mg, 0.42 mmol, 3 equiv), $[Ir(dFCF_3ppy)_2(5,5'\ dCF_3bpy]PF_6$ (1.6 mg, 0.001 mmol, 1 mol%), anhydrous collidine (42 mg, 0.42 mmol, 3 equiv), and anhydrous DCM

(1.4 mL, 0.1 M). The reaction mixture was sparged with Ar for 15 min. The vial was then irridated with 450 nm LED light for 16h, at which point TLC analysis indicated the full consumption of starting material. The crude mixture was concentrated *in vacuo*. The crude residue was purified via SiO_2 flash chromatography (10 to 20% Et_2O/hexanes) to afford bicycle **179** (18 mg, 0.04 mmol, 29% yield) and as bicycle **180** (3.1 mg, 0.007 mmol, 15% yield) colorless oils. Relative structure of **180** was confirmed by NOESY after an additional acylation step (TFAA, DMAP, Et_3N, DCM).

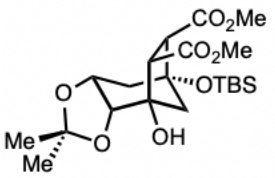

179

^{1}H NMR (400 MHz, $CDCl_3$): δ 4.33 (td, *J* = 7.8, 5.8 Hz, 1H), 4.05 (dd, *J* = 5.8, 1.3 Hz, 1H), 3.62 (s, 3H), 3.57 (d, *J* = 0.9 Hz, 3H), 3.31 (dd, *J* = 7.3, 1.7 Hz, 1H), 2.94 (dd, *J* = 7.3, 1.0 Hz, 1H), 2.13 (dd, *J* = 10.6, 1.0 Hz, 1H), 2.04 (ddd, *J* = 10.6, 2.7, 1.4 Hz, 1H), 1.97 – 1.86 (m, 1H), 1.51 (ddd, *J* = 13.6, 7.5, 1.8 Hz, 1H), 1.39 (s, 3H), 1.23 (s, 3H), 0.74 (s, 9H), 0.04 (s, 3H), -0.03 (s, 3H).
^{13}C NMR (101 MHz, $CDCl_3$): δ 172.59, 172.22, 111.00, 80.95, 78.33, 77.14, 71.28, 55.84, 52.41, 51.90, 49.89, 44.22, 42.18, 28.27, 26.30, 25.46, 17.85, -2.64, -2.68.

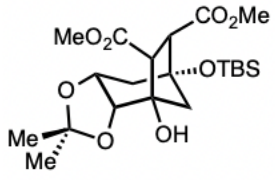

180

^{1}H NMR (400 MHz, $CDCl_3$): δ δ 4.34 – 4.25 (m, 1H), 3.96 (dd, *J* = 5.5, 1.0 Hz, 1H), 3.75 (d, *J* = 1.9 Hz, 3H), 3.68 (s, 3H), 3.65 (d, *J* = 2.9 Hz, 1H), 3.13 (d, *J* = 7.2 Hz, 1H), 2.29 – 2.24 (m, 2H), 1.78 – 1.68 (m, 1H), 1.52 (s, 3H), 1.34 (s, 3H), 0.82 (s, 9H), 0.09 (s, 3H), 0.07 (s, 3H).

^{13}C NMR (101 MHz, $CDCl_3$): δ 172.67, 171.52, 110.79, 78.45, 77.98, 77.90, 71.60, 54.02, 53.46, 52.61, 52.36, 46.64, 43.78, 28.58, 26.60, 25.62, -2.41, -2.48.

5.4. References

(1) Karmakar, R.; Rheingold, A. L.; Micalizio, G. C. *Org. Lett.* **2019**, *21* (15), 6126–6129.

(2) Millham, A. B.; Kier, M. J.; Leon, R. M.; Karmakar, R.; Stempel, Z. D.; Micalizio, G. C. *Org. Lett.* **2019**, *21* (2), 567–570.

(3) Kier, M. J.; Leon, R. M.; O'Rourke, N. F.; Rheingold, A. L.; Micalizio, G. C. *J. Am. Chem. Soc.* **2017**, *139* (36), 12374–12377.

(4) Du, K.; Kier, M. J.; Stempel, Z. D.; Jeso, V.; Rheingold, A. L.; Micalizio, G. C. *J. Am. Chem. Soc.* **2020**, *142* (30), 12937–12941.

(5) Wiles, R. J.; Molander, G. A. *Isr. J. Chem.* **2020**, *60* (3–4), 281–293.

(6) Chu, L.; Ohta, C.; Zuo, Z.; MacMillan, D. W. C. *J. Am. Chem. Soc.* **2014**, *136* (31), 10886–10889.

(7) Shu, C.; Mega, R. S.; Andreassen, B. J.; Noble, A.; Aggarwal, V. K. *Angew. Chem. Int. Ed.* **2018**, *57* (47), 15430–15434.

(8) Ji, P.; Zhang, Y.; Dong, Y.; Huang, H.; Wei, Y.; Wang, W. *Org. Lett.* **2020**, *22* (4), 1557–1562.

(9) Donabauer, K.; Maity, M.; Berger, A. L.; Huff, G. S.; Crespi, S.; König, B. *Chem. Sci.* **2019**, *10* (19), 5162–5166.

(10) Appella, D. H.; Moritani, Y.; Shintani, R.; Ferreira, E. M.; Buchwald, S. L. *J. Am. Chem. Soc.* **1999**, *121* (40), 9473–9474.

(11) Dowling, M. S.; Vanderwal, C. D. *J. Org. Chem.* **2010**, *75* (20), 6908–6922.

(12) Gualandi, A.; Matteucci, E.; Monti, F.; Baschieri, A.; Armaroli, N.; Sambri, L.; Cozzi, P. G. *Chem. Sci.* **2017**, *8* (2), 1613–1620.

(13) Zhao, K.; Yamashita, K.; Carpenter, J. E.; Sherwood, T. C.; Ewing, W. R.; Cheng, P. T. W.; Knowles, R. R. *J. Am. Chem. Soc.* **2019**, *141* (22), 8752–8757.

(14) Slutskyy, Y.; Overman, L. E. *Org. Lett.* **2016**, *18* (11), 2564–2567.

(15) Nazef, N.; Davies, R. D. M.; Greaney, M. F. *Org. Lett.* **2012**, *14* (14), 3720–3723.

(16) Provencher, B. A.; Bartelson, K. J.; Liu, Y.; Foxman, B. M.; Deng, L. *Angew. Chem.* **2011**, *123* (45), 10753–10757.

Appendix 3

Spectra Relevant to Chapter 5:

A radical-polar crossover annulation approach toward enterocin

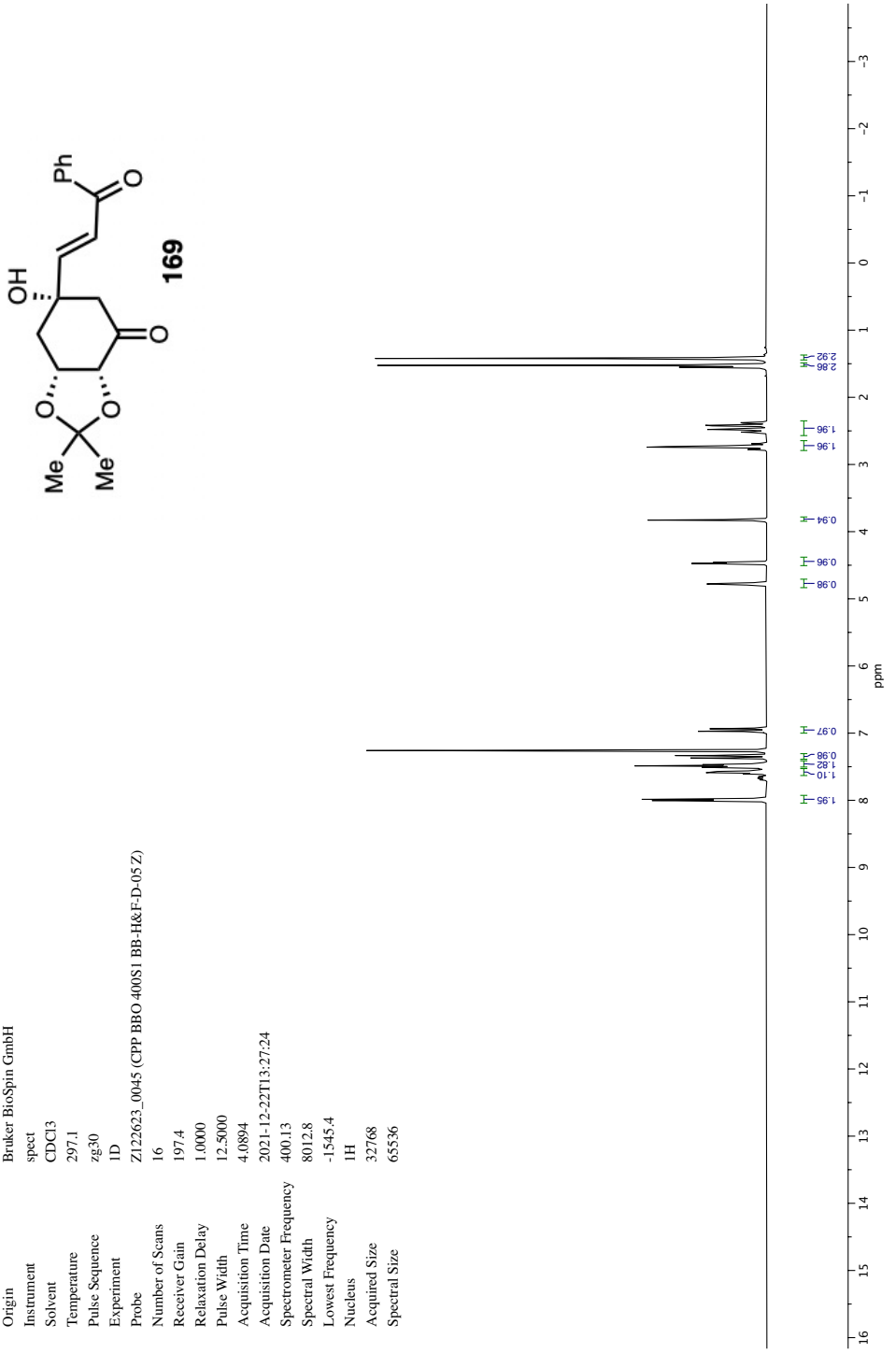

Parameter	Value
Title	6-Yt-087SM.1.fid
Origin	Bruker BioSpin GmbH
Instrument	spect
Solvent	CDCl3
Temperature	297.1
Pulse Sequence	zg30
Experiment	1D
Probe	Z122623_0045 (CPP BBO 400S1 BB-H&F-D-05 Z)
Number of Scans	16
Receiver Gain	197.4
Relaxation Delay	1.0000
Pulse Width	12.5000
Acquisition Time	4.0894
Acquisition Date	2021-12-22T13:27:24
Spectrometer Frequency	400.13
Spectral Width	8012.8
Lowest Frequency	-1545.4
Nucleus	1H
Acquired Size	32768
Spectral Size	65536

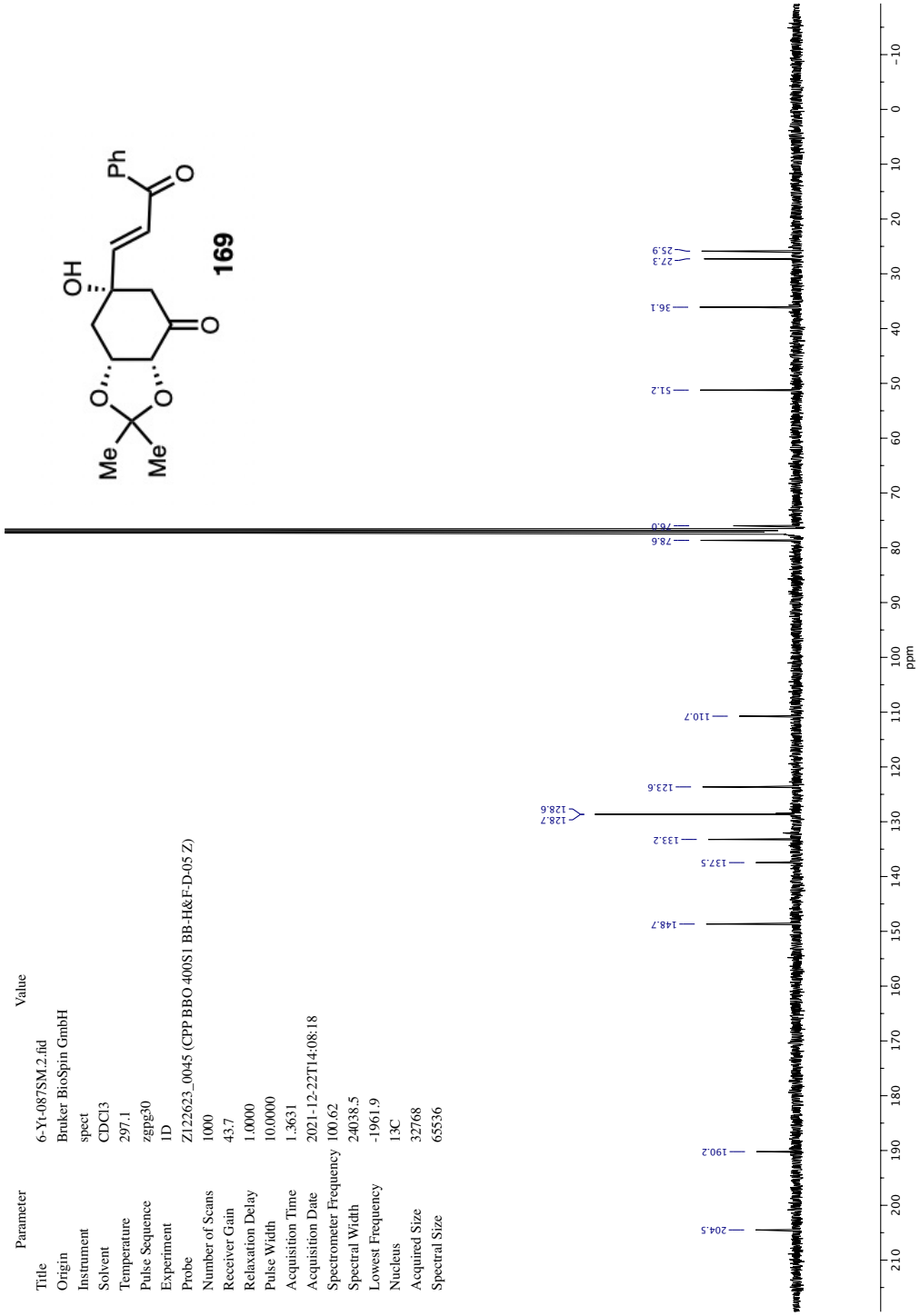

Parameter	Value
Title	6-Yt-087SM 2.fid
Origin	Bruker BioSpin GmbH
Instrument	spect
Solvent	CDCl3
Temperature	297.1
Pulse Sequence	zgpg30
Experiment	1D
Probe	Z122623_0045 (CPP BBO 400S1 BB-H&F-D-05 Z)
Number of Scans	1000
Receiver Gain	43.7
Relaxation Delay	1.0000
Pulse Width	10.0000
Acquisition Time	1.3631
Acquisition Date	2021-12-22T14:08:18
Spectrometer Frequency	100.62
Spectral Width	24038.5
Lowest Frequency	-1961.9
Nucleus	13C
Acquired Size	32768
Spectral Size	65536

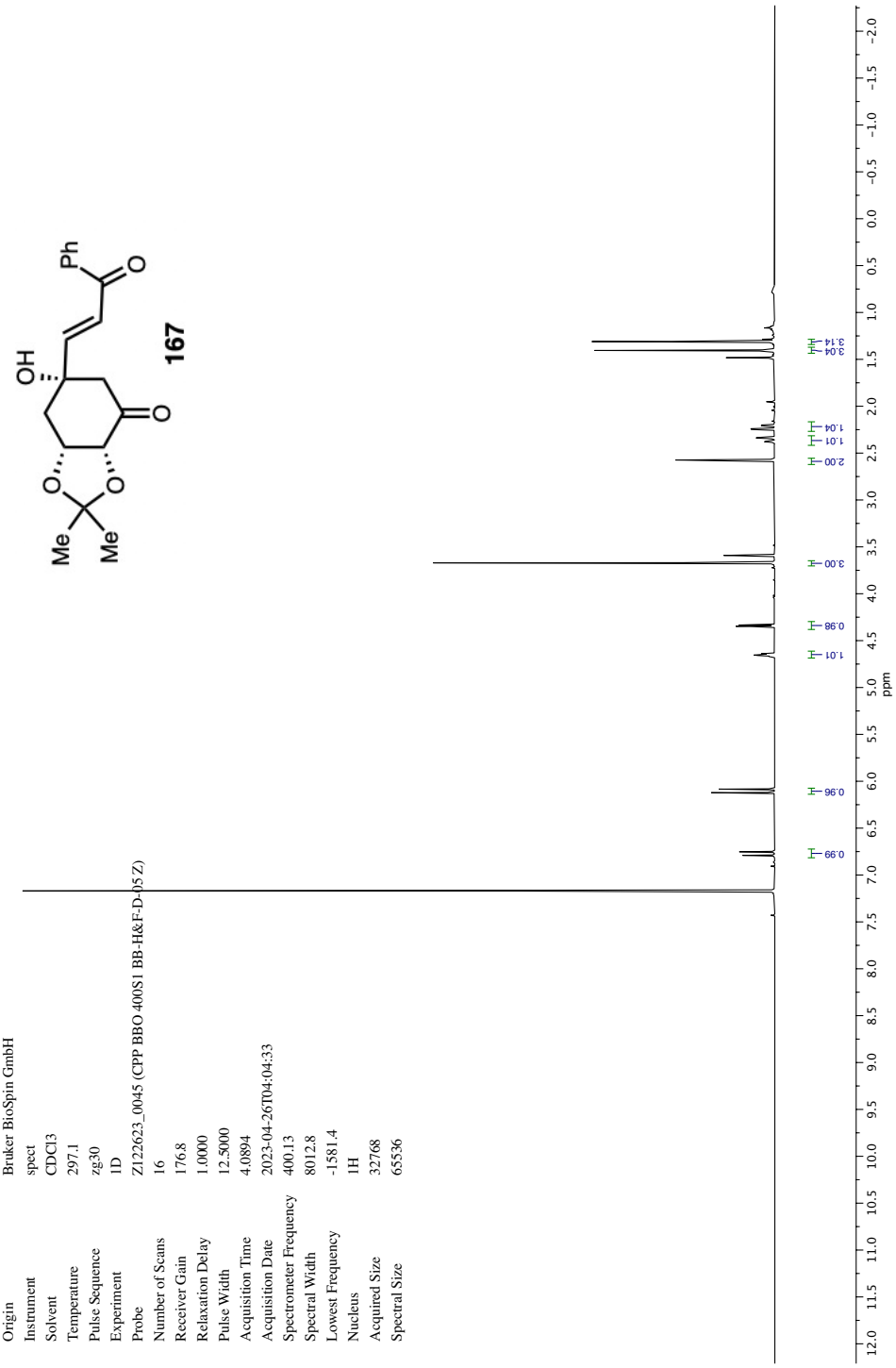
Parameter
Value
Title
CH-YT-OME2.1.fid
Origin
Bruker BioSpin GmbH
Instrument
spect
Solvent
CDCl3
Temperature
297.1
Pulse Sequence
zg30
Experiment
1D
Probe
Z122623_0045 (CPP BBO 400S1 BB-H&F-D-05 Z)
Number of Scans
16
Receiver Gain
176.8
Relaxation Delay
1.0000
Pulse Width
12.5000
Acquisition Time
4.0894
Acquisition Date
2023-04-26T04:04:33
Spectrometer Frequency
400.13
Spectral Width
8012.8
Lowest Frequency
-1581.4
Nucleus
1H
Acquired Size
32768
Spectral Size
65536
OH
Ph
O
O
O
O
Me
Me
167
0.99
0.96
1.01
0.98
3.00
2.00
1.01
1.04
3.04
3.14
ppm

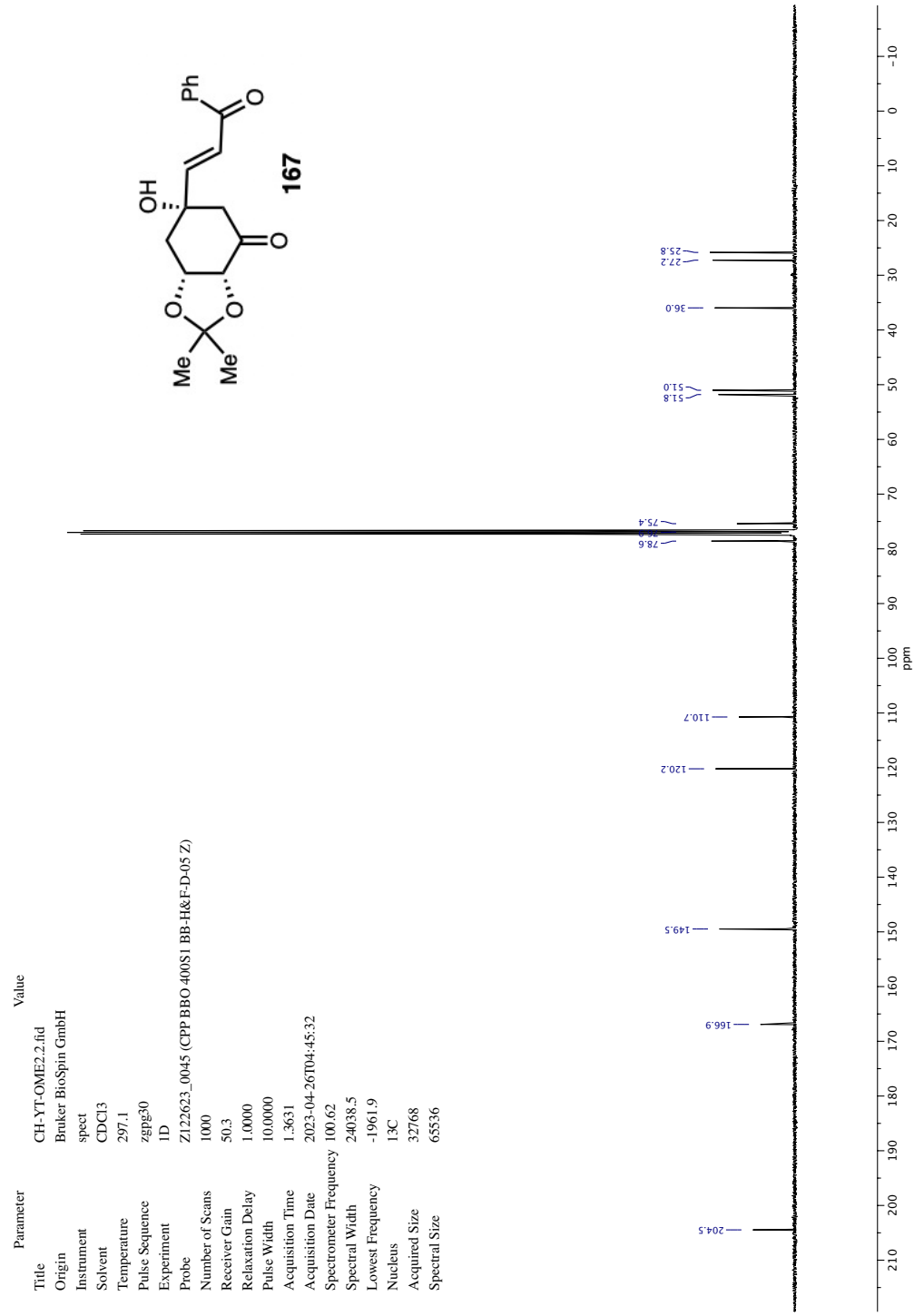

Parameter	Value
Title	CH-YT-OME2.2.fid
Origin	Bruker BioSpin GmbH
Instrument	spect
Solvent	CDCl3
Temperature	297.1
Pulse Sequence	zgpg30
Experiment	1D
Probe	Z122623_0045 (CPP BBO 400S1 BB-H&F-D-05 Z)
Number of Scans	1000
Receiver Gain	50.3
Relaxation Delay	1.0000
Pulse Width	10.0000
Acquisition Time	1.3631
Acquisition Date	2023-04-26T04:45:32
Spectrometer Frequency	100.62
Spectral Width	24038.5
Lowest Frequency	-1961.9
Nucleus	13C
Acquired Size	32768
Spectral Size	65536

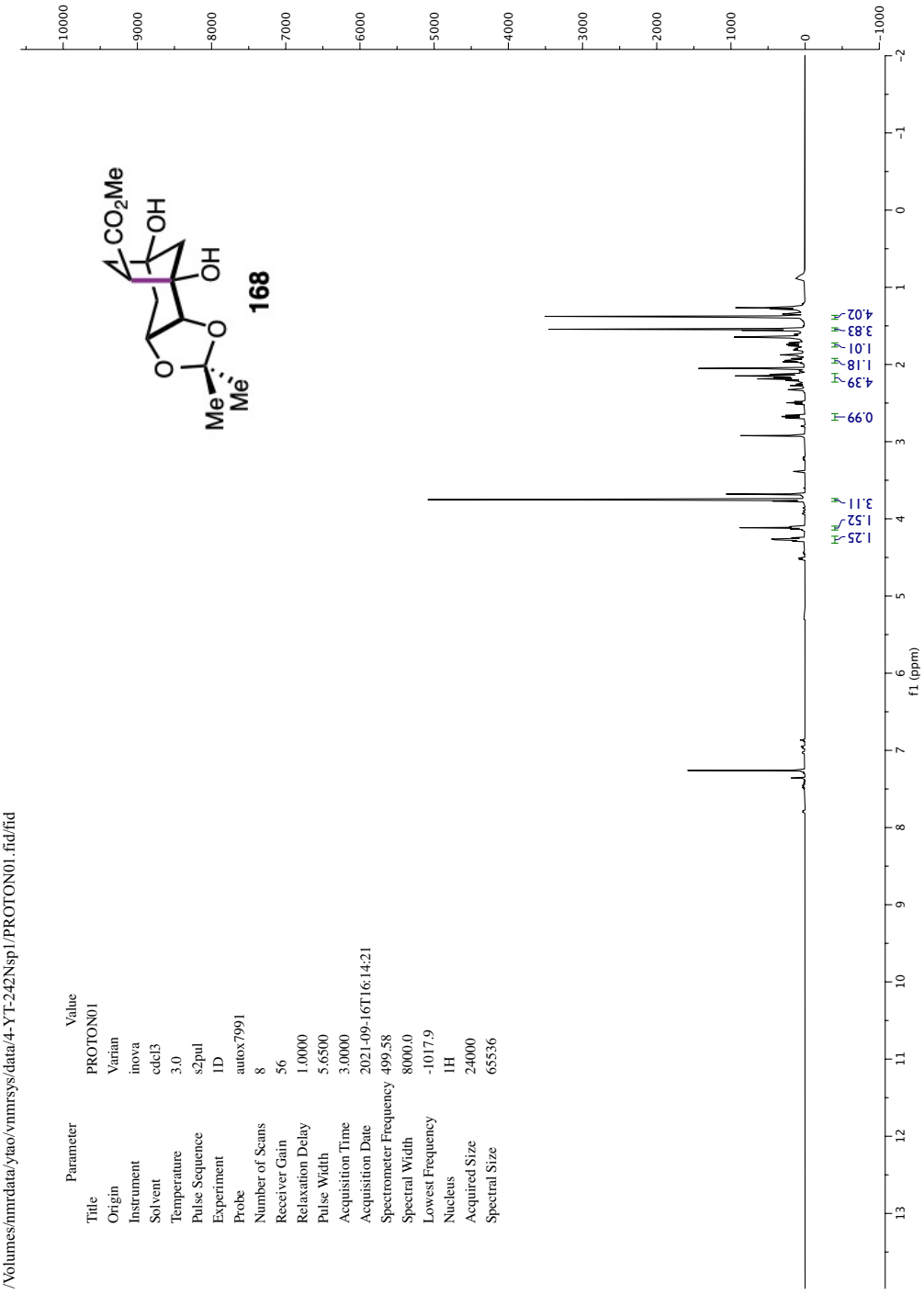
/Volumes/nmrdata/ytao/vnmrsys/data/4-YT-242Nsp1/PROTON01.fid/fid
Parameter Value
Title PROTON01
Origin Varian
Instrument inova
Solvent cdcl3
Temperature 3.0
Pulse Sequence s2pul
Experiment 1D
Probe autox7991
Number of Scans 8
Receiver Gain 56
Relaxation Delay 1.0000
Pulse Width 5.6500
Acquisition Time 3.0000
Acquisition Date 2021-09-16T16:14:21
Spectrometer Frequency 499.58
Spectral Width 8000.0
Lowest Frequency -1017.9
Nucleus 1H
Acquired Size 24000
Spectral Size 65536
CO2Me
OH
OH
O
O
Me
Me
168
4.02
3.83
1.01
1.18
4.39
0.99
3.11
1.52
1.25
f1 (ppm)

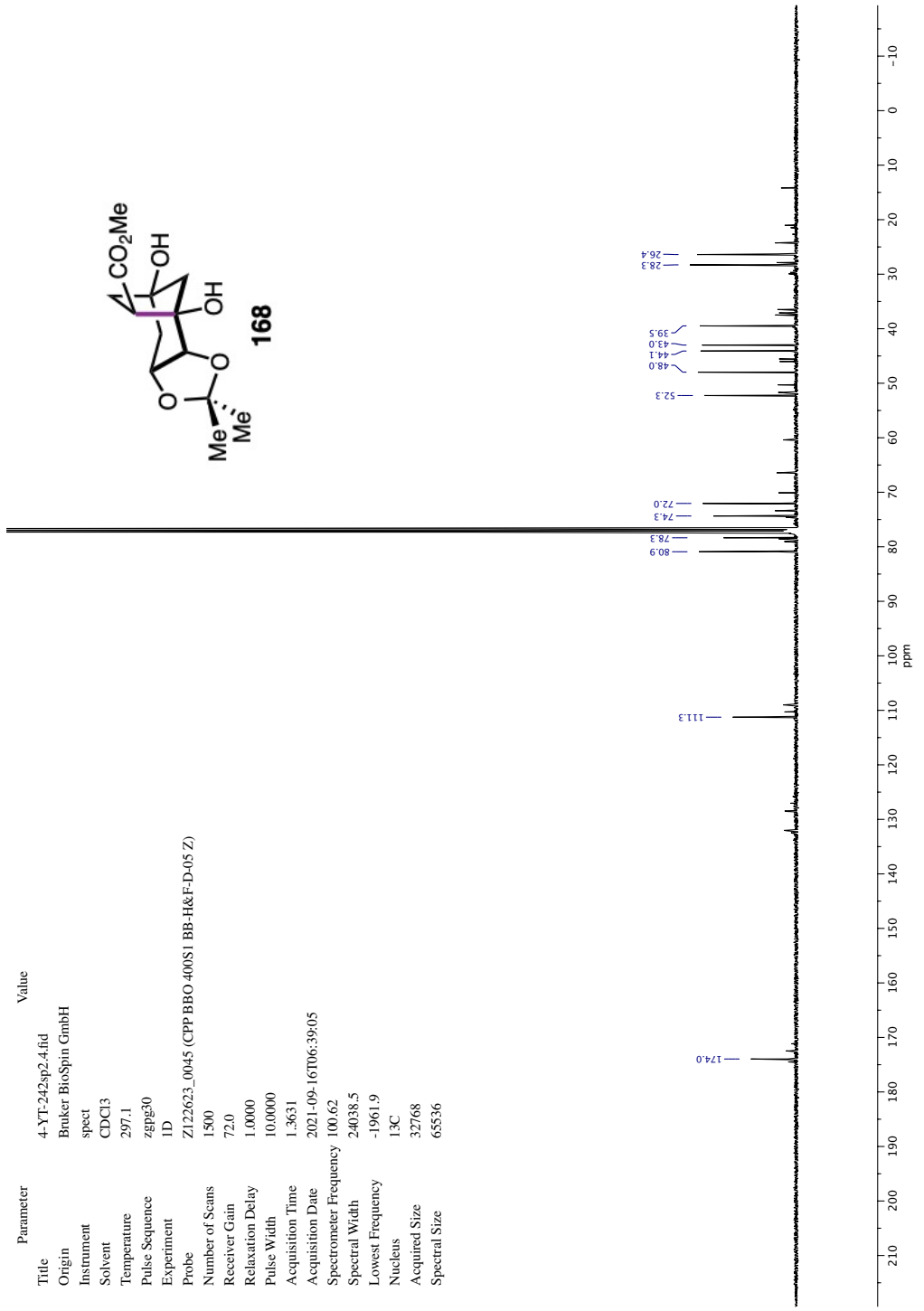

Parameter	Value
Title	4-YT-242sp2.4.fid
Origin	Bruker BioSpin GmbH
Instrument	spect
Solvent	CDCl3
Temperature	297.1
Pulse Sequence	zgpg30
Experiment	1D
Probe	Z122623_0045 (CPP BBO 400S1 BB-H&F-D-05 Z)
Number of Scans	1500
Receiver Gain	72.0
Relaxation Delay	1.0000
Pulse Width	10.0000
Acquisition Time	1.3631
Acquisition Date	2021-09-16T06:39:05
Spectrometer Frequency	100.62
Spectral Width	24038.5
Lowest Frequency	-1961.9
Nucleus	13C
Acquired Size	32768
Spectral Size	65536

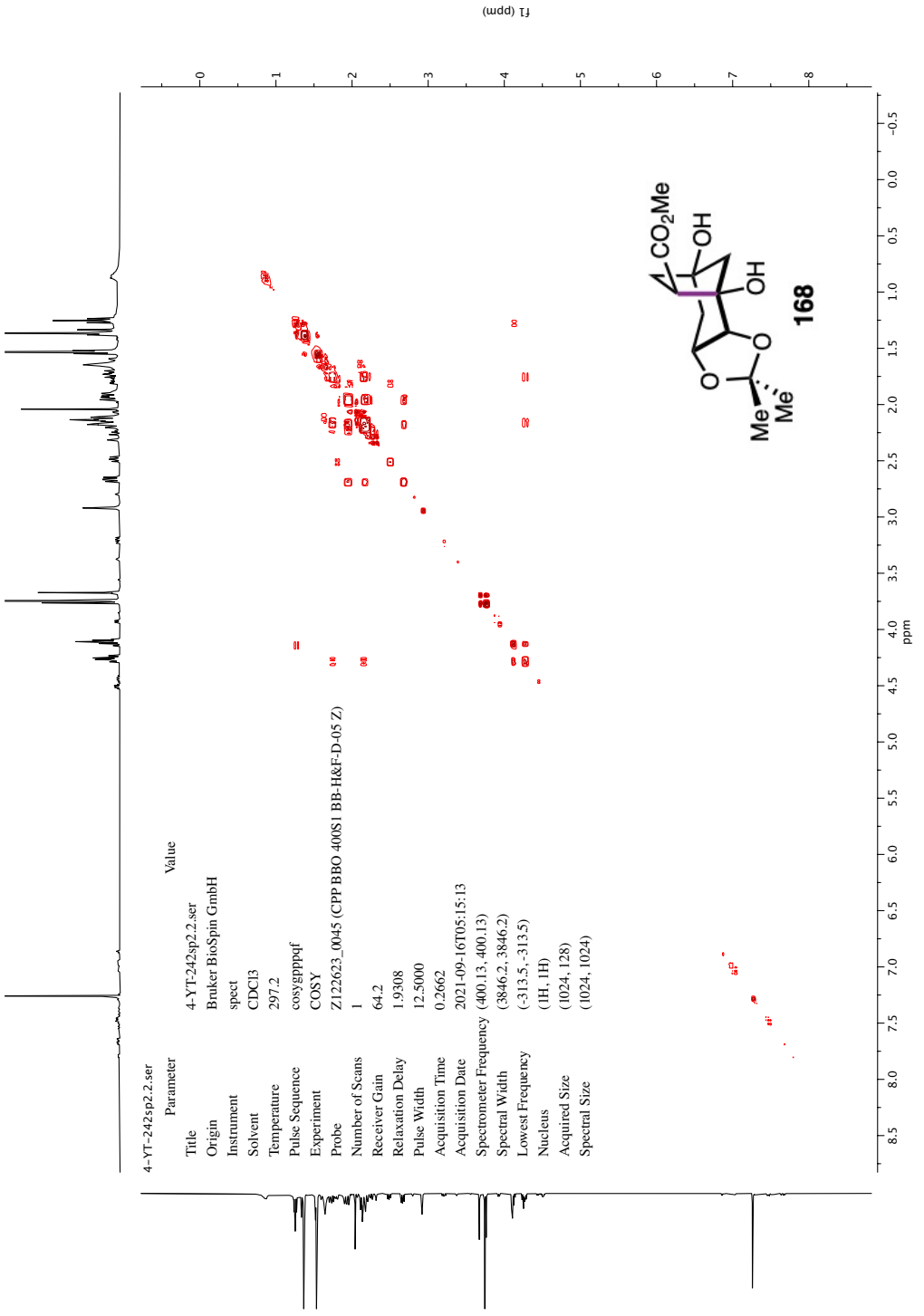
f1 (ppm)
4-YT-242sp2.2.ser
Parameter Value
Title 4-YT-242sp2.2.ser
Origin Bruker BioSpin GmbH
Instrument spect
Solvent CDCl3
Temperature 297.2
Pulse Sequence cosygpppqf
Experiment COSY
Probe Z122623_0045 (CPP BBO 400S1 BB-H&F-D-05 Z)
Number of Scans 1
Receiver Gain 64.2
Relaxation Delay 1.9308
Pulse Width 12.5000
Acquisition Time 0.2662
Acquisition Date 2021-09-16T05:15:13
Spectrometer Frequency (400.13, 400.13)
Spectral Width (3846.2, 3846.2)
Lowest Frequency (-313.5, -313.5)
Nucleus (1H, 1H)
Acquired Size (1024, 128)
Spectral Size (1024, 1024)
ppm
CO2Me
OH
OH
O
O
Me
Me
168

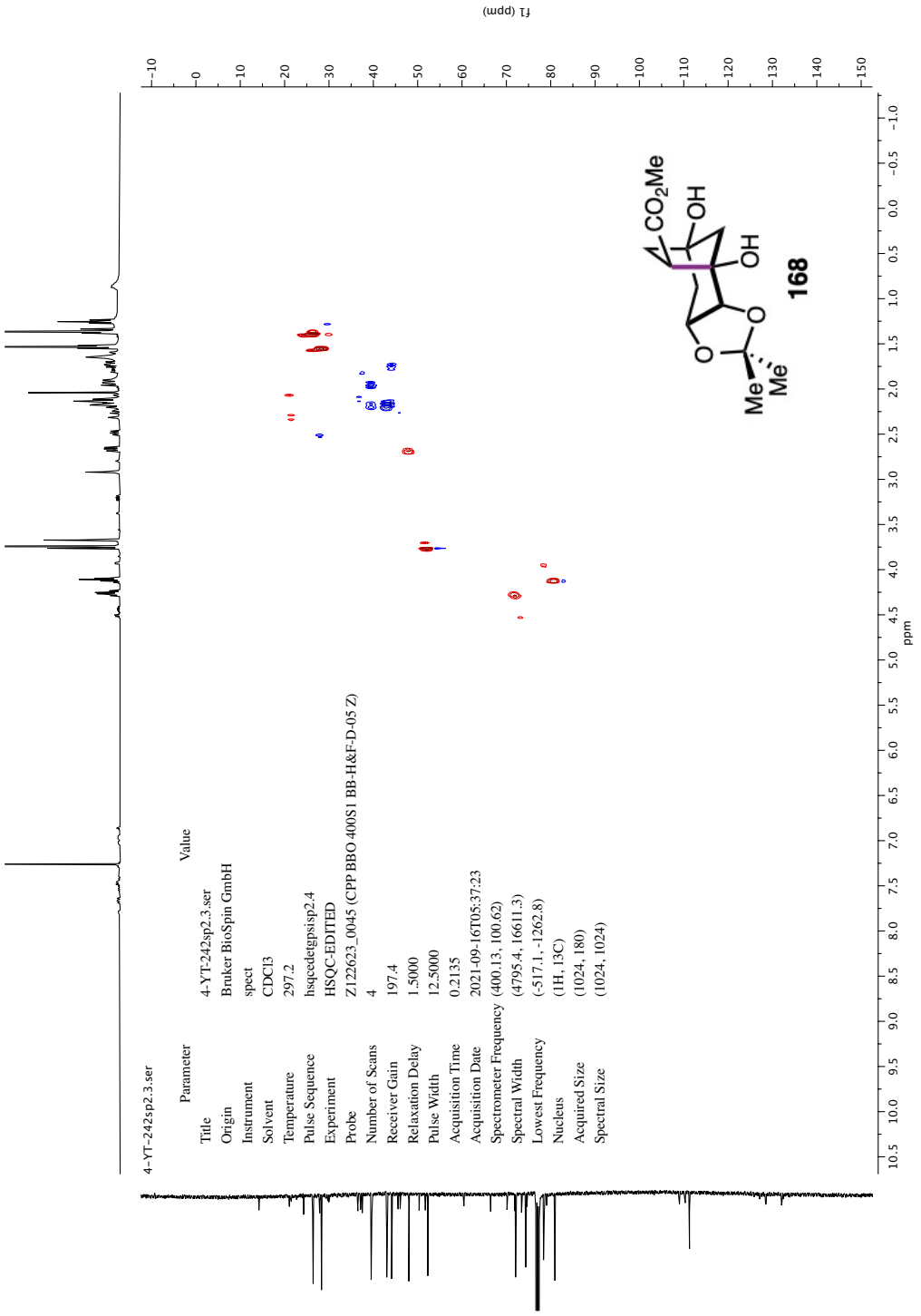
f1 (ppm)
ppm
4-YT-242sp2.3.ser
Parameter Value
Title 4-YT-242sp2.3.ser
Origin Bruker BioSpin GmbH
Instrument spect
Solvent CDCl3
Temperature 297.2
Pulse Sequence hsqcedetgpsisp2.4
Experiment HSQC-EDITED
Probe Z122623_0045 (CPP BBO 400S1 BB-H&F-D-05 Z)
Number of Scans 4
Receiver Gain 197.4
Relaxation Delay 1.5000
Pulse Width 12.5000
Acquisition Time 0.2135
Acquisition Date 2021-09-16T05:37:23
Spectrometer Frequency (400.13, 100.62)
Spectral Width (4795.4, 16611.3)
Lowest Frequency (-517.1, -1262.8)
Nucleus (1H, 13C)
Acquired Size (1024, 180)
Spectral Size (1024, 1024)
CO2Me
OH
OH
O
O
Me
Me
168

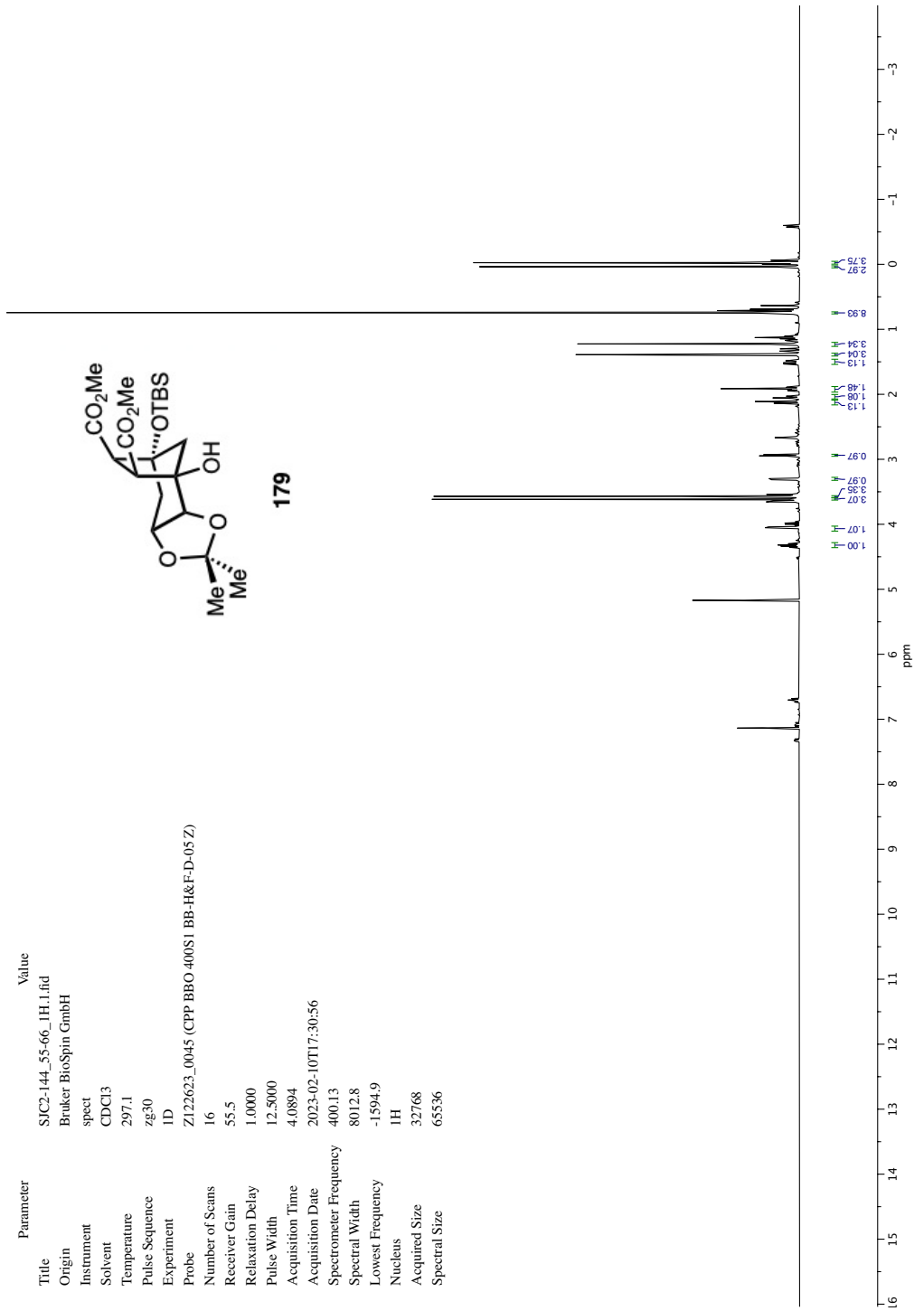

Parameter	Value
Title	SJC2-144_55-66_1H.1.fid
Origin	Bruker BioSpin GmbH
Instrument	spect
Solvent	CDCl3
Temperature	297.1
Pulse Sequence	zg30
Experiment	1D
Probe	Z122623_0045 (CPP BBO 400S1 BB-H&F-D-05 Z)
Number of Scans	16
Receiver Gain	55.5
Relaxation Delay	1.0000
Pulse Width	12.5000
Acquisition Time	4.0894
Acquisition Date	2023-02-10T17:30:56
Spectrometer Frequency	400.13
Spectral Width	8012.8
Lowest Frequency	-1594.9
Nucleus	1H
Acquired Size	32768
Spectral Size	65536

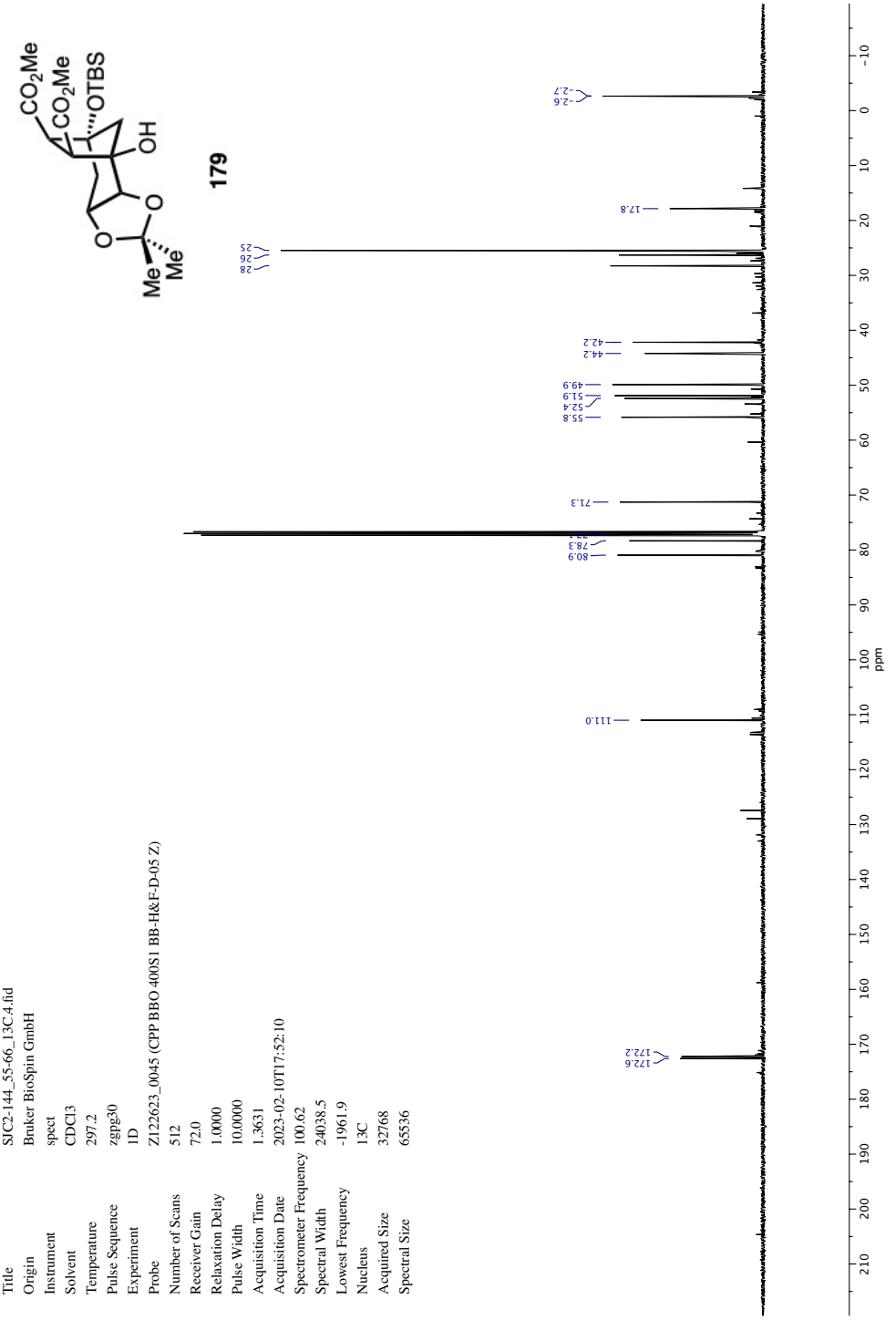

Parameter	Value
Title	SJC2-144_55-66_13C.4.fid
Origin	Bruker BioSpin GmbH
Instrument	spect
Solvent	CDCl3
Temperature	297.2
Pulse Sequence	zgpg30
Experiment	1D
Probe	Z122623_0045 (CPP BBO 400S1 BB-H&F-D-05 Z)
Number of Scans	512
Receiver Gain	72.0
Relaxation Delay	1.0000
Pulse Width	10.0000
Acquisition Time	1.3631
Acquisition Date	2023-02-10T17:52:10
Spectrometer Frequency	100.62
Spectral Width	24038.5
Lowest Frequency	-1961.9
Nucleus	13C
Acquired Size	32768
Spectral Size	65536

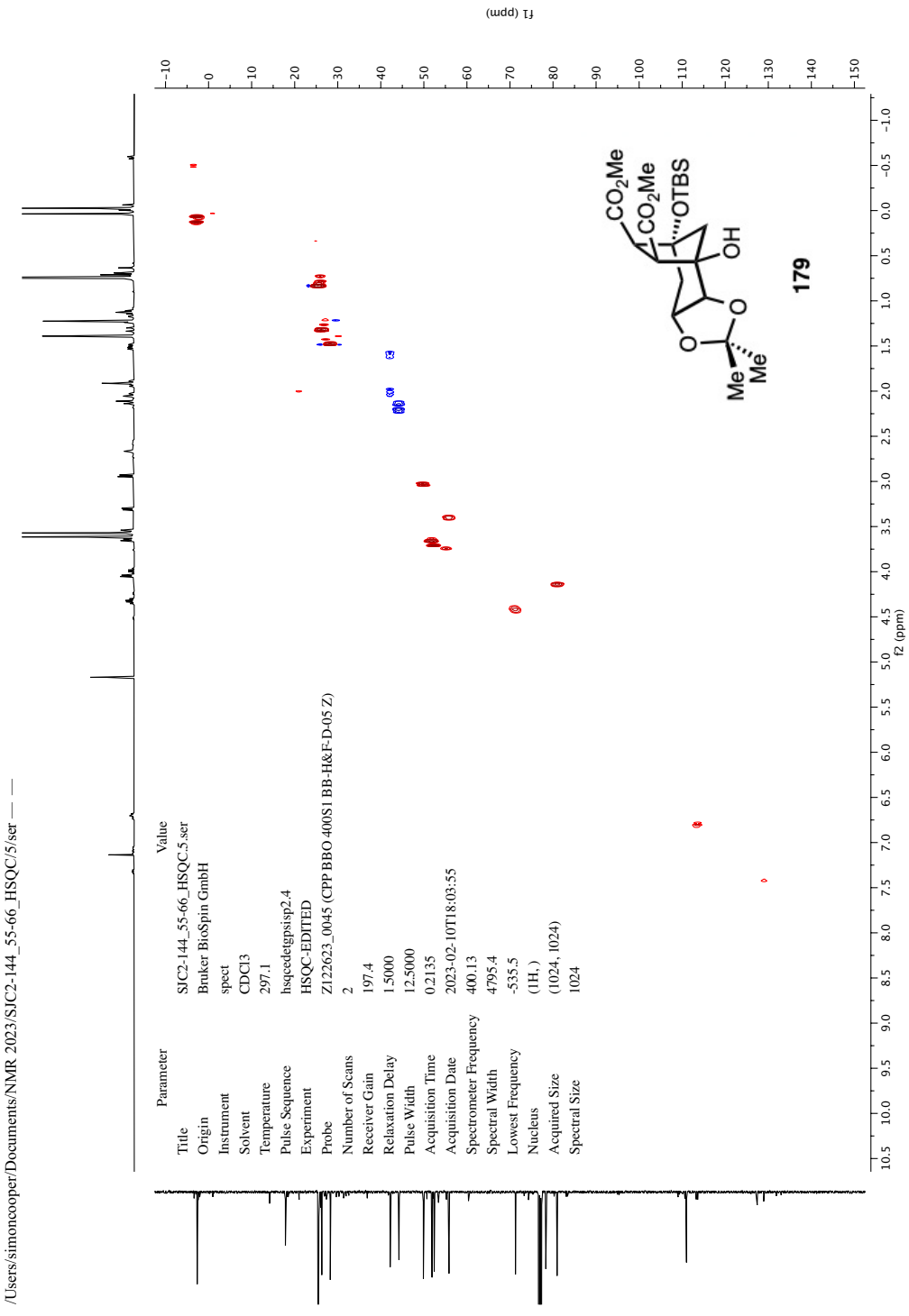
/Users/simoncooper/Documents/NMR 2023/SIC2-144_55-66_HSQC/5/ser — —
Parameter Value
Title SIC2-144_55-66_HSQC.5.ser
Origin Bruker BioSpin GmbH
Instrument spect
Solvent CDCl3
Temperature 297.1
Pulse Sequence hsqcedetgpsisp2.4
Experiment HSQC-EDITED
Probe Z122623_0045 (CPP BBO 400S1 BB-H&F-D-05 Z)
Number of Scans 2
Receiver Gain 197.4
Relaxation Delay 1.5000
Pulse Width 12.5000
Acquisition Time 0.2135
Acquisition Date 2023-02-10T18:03:55
Spectrometer Frequency 400.13
Spectral Width 4795.4
Lowest Frequency -535.5
Nucleus (1H,)
Acquired Size (1024, 1024)
Spectral Size 1024
f1 (ppm)
f2 (ppm)
CO2Me
CO2Me
OTBS
OH
Me
Me
179

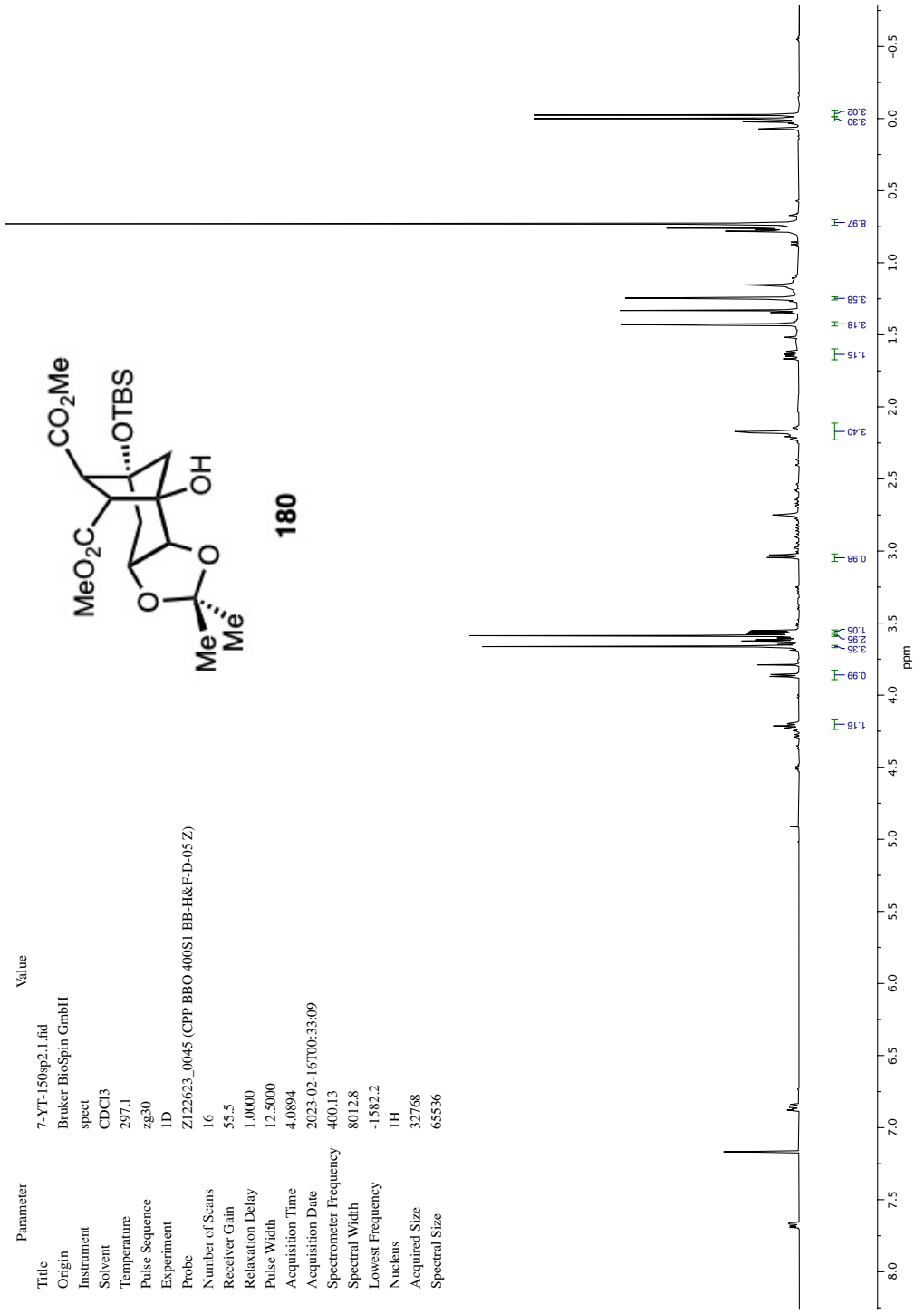

Parameter	Value
Title	7-YT-150sp2.1.fid
Origin	Bruker BioSpin GmbH
Instrument	spect
Solvent	CDCl3
Temperature	297.1
Pulse Sequence	zg30
Experiment	1D
Probe	Z122623_0045 (CPP BBO 400S1 BB-H&F-D-05 Z)
Number of Scans	16
Receiver Gain	55.5
Relaxation Delay	1.0000
Pulse Width	12.5000
Acquisition Time	4.0894
Acquisition Date	2023-02-16T00:33:09
Spectrometer Frequency	400.13
Spectral Width	8012.8
Lowest Frequency	-1582.2
Nucleus	1H
Acquired Size	32768
Spectral Size	65536

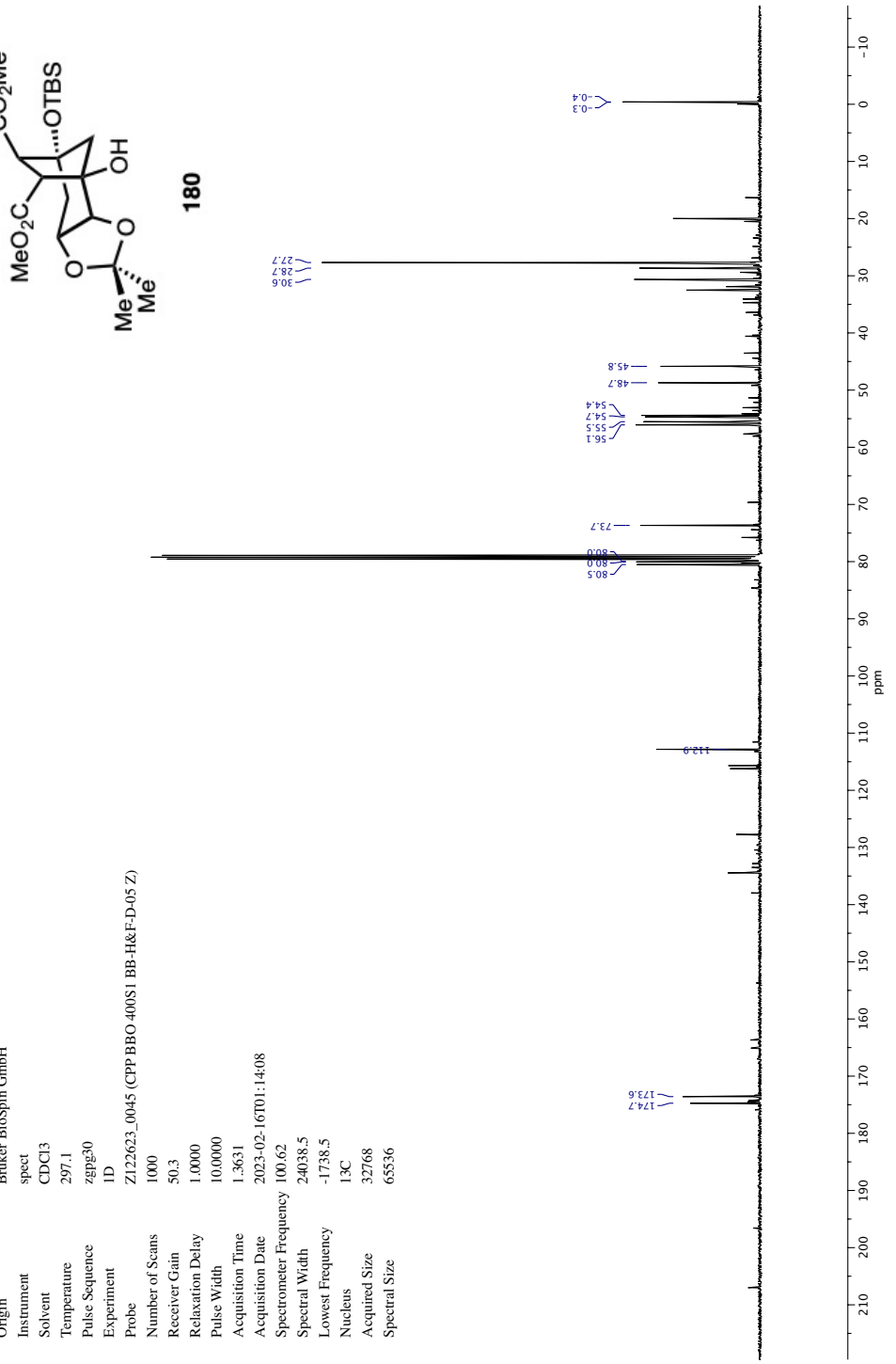

Parameter	Value
Title	7-YT-150sp2.2.fid
Origin	Bruker BioSpin GmbH
Instrument	spect
Solvent	CDCl3
Temperature	297.1
Pulse Sequence	zgpg30
Experiment	1D
Probe	Z122623_0045 (CPP BBO 400S1 BB-H&F-D-05 Z)
Number of Scans	1000
Receiver Gain	50.3
Relaxation Delay	1.0000
Pulse Width	10.0000
Acquisition Time	1.3631
Acquisition Date	2023-02-16T01:14:08
Spectrometer Frequency	100.62
Spectral Width	24038.5
Lowest Frequency	-1738.5
Nucleus	13C
Acquired Size	32768
Spectral Size	65536

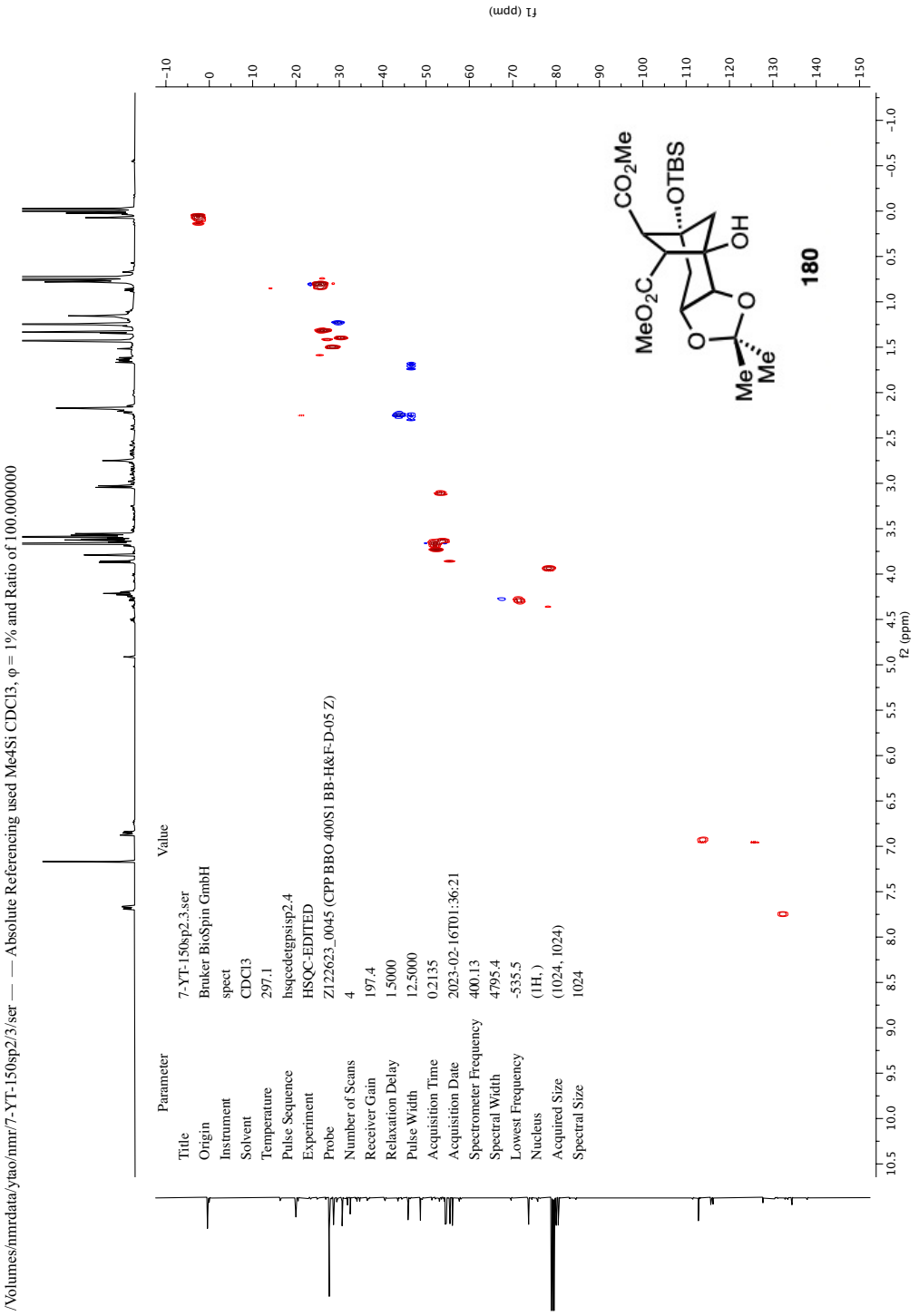
/Volumes/nmrdata/ytao/nmr/7-YT-150sp2/3/ser — — Absolute Referencing used Me4Si CDCl3, φ = 1% and Ratio of 100.000000
Parameter Value
Title 7-YT-150sp2.3.ser
Origin Bruker BioSpin GmbH
Instrument spect
Solvent CDCl3
Temperature 297.1
Pulse Sequence hsqcedetgpsisp2.4
Experiment HSQC-EDITED
Probe Z122623_0045 (CPP BBO 400S1 BB-H&F-D-05 Z)
Number of Scans 4
Receiver Gain 197.4
Relaxation Delay 1.5000
Pulse Width 12.5000
Acquisition Time 0.2135
Acquisition Date 2023-02-16T01:36:21
Spectrometer Frequency 400.13
Spectral Width 4795.4
Lowest Frequency -535.5
Nucleus (1H,)
Acquired Size (1024, 1024)
Spectral Size 1024
f1 (ppm)
f2 (ppm)
CO2Me
OTBS
MeO2C
OH
O
O
Me
Me
180

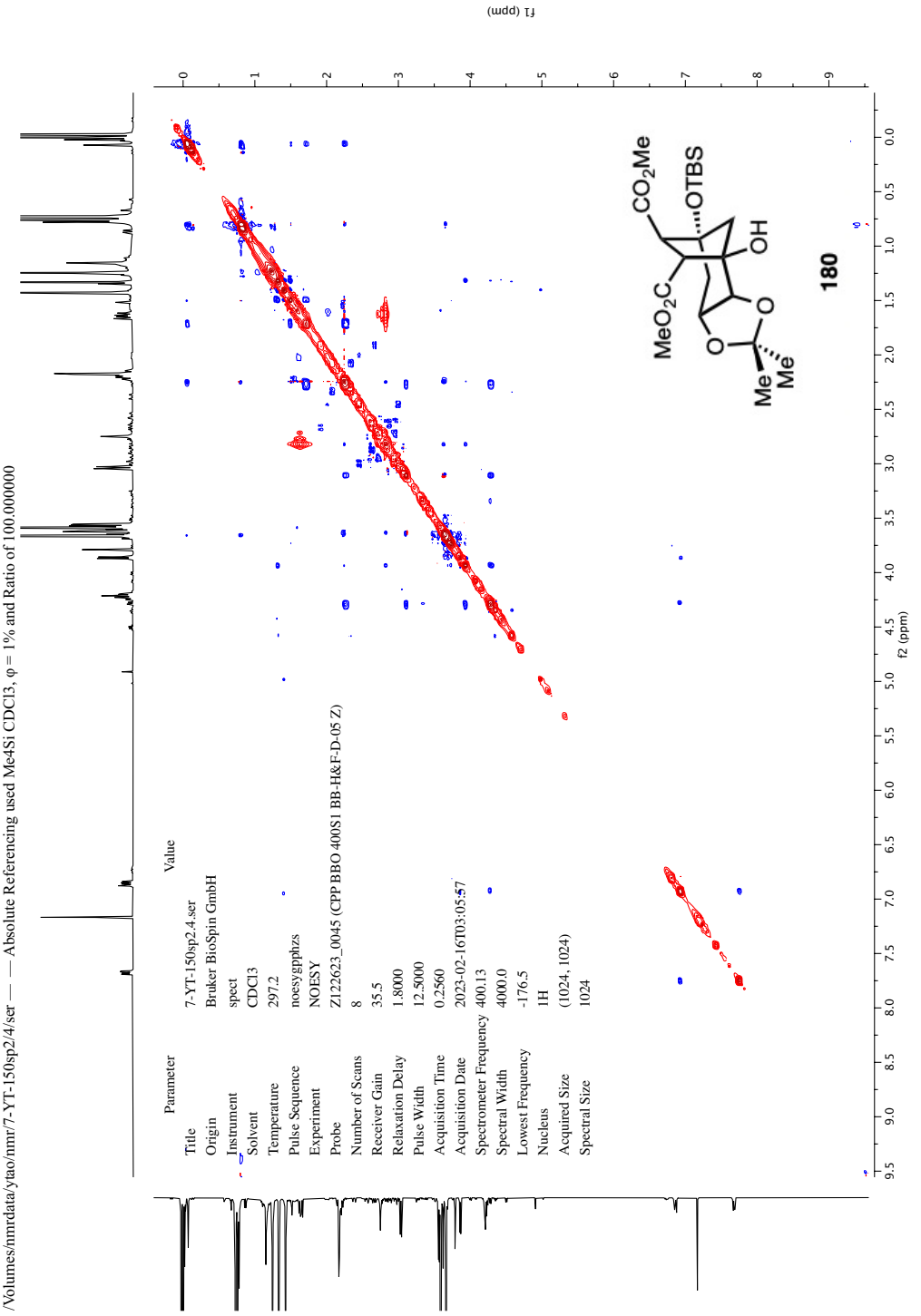
/Volumes/nmrdata/ytao/nmr/7-YT-150sp2/4/ser — — Absolute Referencing used Me4Si CDCl3, φ = 1% and Ratio of 100.000000
Parameter Value
Title 7-YT-150sp2.4.ser
Origin Bruker BioSpin GmbH
Instrument spect
Solvent CDCl3
Temperature 297.2
Pulse Sequence noesygpphzs
Experiment NOESY
Probe Z122623_0045 (CPP BBO 400S1 BB-H&F-D-05 Z)
Number of Scans 8
Receiver Gain 35.5
Relaxation Delay 1.8000
Pulse Width 12.5000
Acquisition Time 0.2560
Acquisition Date 2023-02-16T03:05:57
Spectrometer Frequency 400.13
Spectral Width 4000.0
Lowest Frequency -176.5
Nucleus 1H
Acquired Size (1024, 1024)
Spectral Size 1024
f1 (ppm)
f2 (ppm)
CO2Me
OTBS
OH
MeO2C
O
Me
Me
180

Chapter 6

An intermolecular aldol approach toward enterocin

6.1 Retrosynthetic analysis

Through our explorations of different strategies, we started to realize that the four free hydroxyl groups have been one of the most difficult features to synthesize enterocin (**33**). The radical-polar crossover strategy was able to elegantly address the installation of two of the free hydroxyl groups (C4 and C8), but the question on how to oxidize C2 position stereoselectively and chemoselectively has always been challenging to answer. With this question in mind, we started to think that we should increase the oxidation state of C2 carbon at an early stage. Therefore, we devised a novel route (Figure 1) to access enterocin (**33**).

Retrosynthetically (Figure 1), a biomimetic aldol step[1] from **189** was designed to furnished the natural product enterocin (**33**). This aldol presumably will proceed spontaneously, as demonstrated by Bach and coworkers[2] in their biomimetic total synthesis of enterocin. Next, we envisioned to introduce the acetophenone piece through an intermolecular aldol reaction: enolate **191** can add into the electrophilic C2 carbonyl. This way, we solved the problem on how to install the C2 alcohol as well. The ketolactone in **190** can be accessed through alkene oxidation from dihydropyran **192**, which can be eventually traced back to quinic acid (**153**).

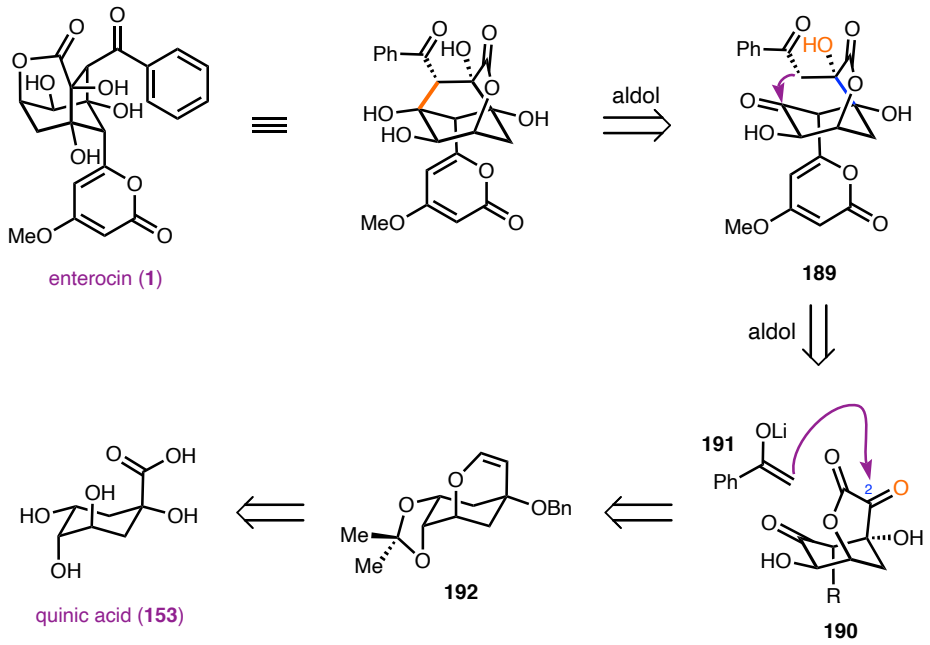

Figure 1. *Retrosynthetic analysis of enterocin.*

This route was partially inspired by Trauner's total synthesis of tetrodotoxin (Figure 2).[3] They were able to perform a cycloisomerization reaction[4,5] to form dihydropyran **193**, by generating a metallo-vinylidene carbene from alkyne **194** with catalyst $CpRu(PPh_3)_2Cl$.[6] They found they were able to turn the Ru cycloisomerization catalyst into an oxidant in the prescence of Oxone and a cosolvent mixture, and oxidize the alkene into hydroxyl lactone **195**.

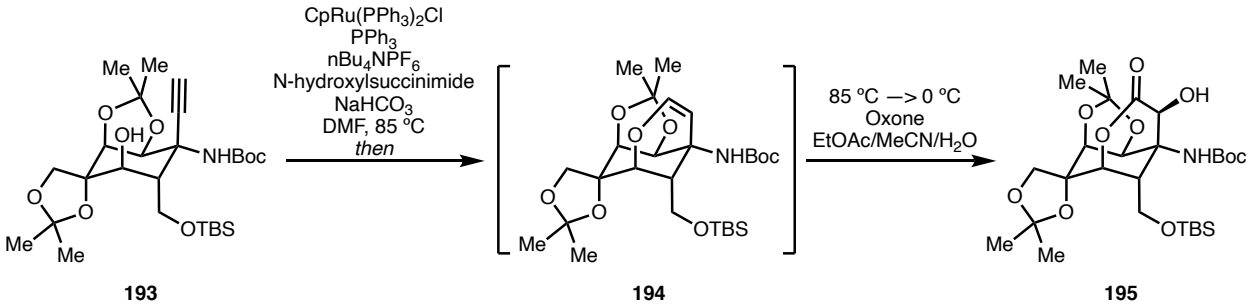

Figure 2. *Inspiration on accessing the ketolactone.*

In Trauner's report[3], they were able to control the oxidation to stop at the hydroxyl lactone stage **195**, but with excess Oxone and prolonged reaction time, ketolactone was isolated too. Therefore, we envisioned that we might be able to employ the same strategy to access the ketolactone **190** through an alkyne intermediate.

6.2. Results and discussion

At the beginning, we aimed to access the ketolactone **121** as soon as possible, and test the following intermolecular aldol reaction. Starting with quinic acid (**153**), lactone **196** was prepared in two steps following literature precedent (Scheme 1).[7] Selective DIBAL reduction of lactone **196** to the corresponding lactol **197** (mixture of diastereomers) in 88% yield and subsequent homologation via an Ohira-Bestmann reaction provided alkyne **199** in 75% yield.

We then attempted the cycloisomerization reaction using $CpRu(PPh_3)_2Cl$ as the catalyst.[6] The reaction proceeded smoothly, affording dihydropyran **200** in 64% yield. We tried to follow Trauner's protocol and add Oxone at the end of the isomerization reaction, but the expected oxidation did not occur. We also treated isolated dihydropyran **200** with Oxone under the reported conditions[8,9], and the reaction provided a complex mixture of products at varied oxidation states. We were able to identify desired ketolactone **201**, ketolactol, and hydroxyllactone in the complex, but the yields for each were low and cannot support further investigation.

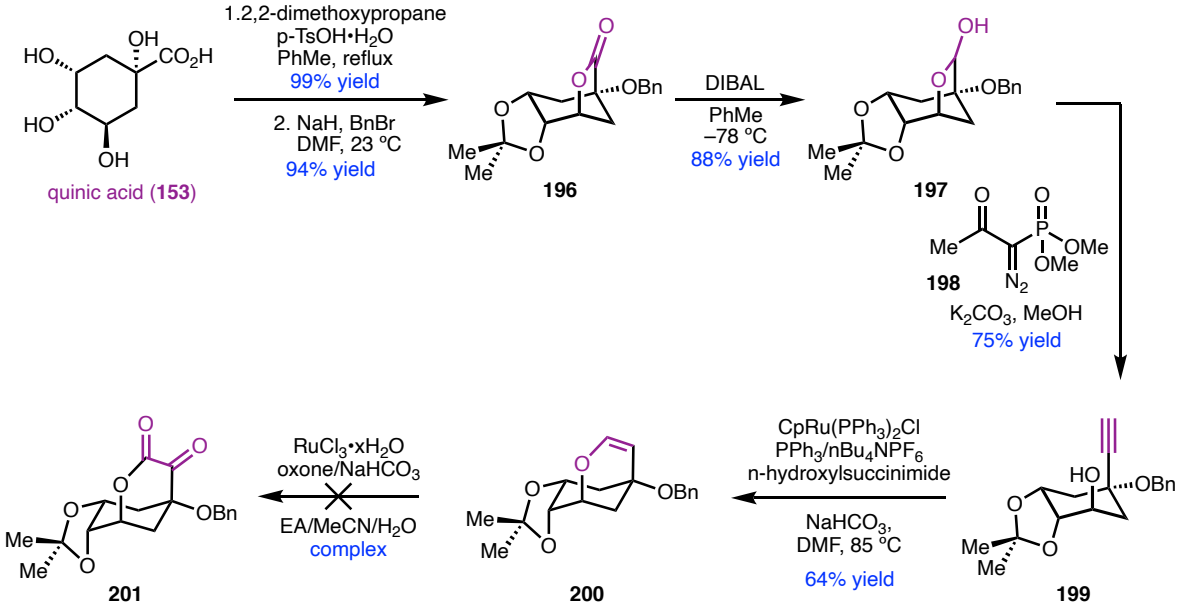

Scheme 1. *Attempts to access ketolactone.*

After the unsuccessful alkene oxidation, we became curious on whether this alkene can undergo intermolecular cyclopropanation reaction with diazo **202**. The cyclopropane product **203** might be an interesting substrate as the cyclopropane may be opened through an oxygen nucleophile and the resultant enolate can participate in the biomimetic aldol reaction. Unfortunately, no reactivity was observed in the cyclopropanation screen with different catalysts (Scheme 2).

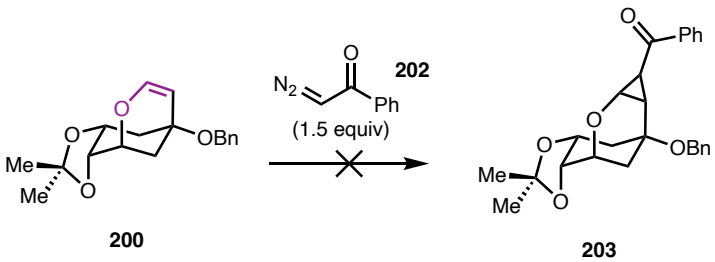

	conditions	results
1	$Rh_2(OAc)_4$, PhMe, 80 °C	no reaction
2	$Cu(acac)_2$, PhMe, 80 °C	no reaction
3	$Rh_2(OAc)_4$, DCM, 23 °C	no reaction
4	$Rh_2(cap)_4$, DCM, 23 °C	no reaction
5	Rh_2(*s*-DOSP)$_4$, DCM, 23 °C	no reaction

Scheme 2. *Intermolecular cyclopropanation attempts.*

Then, we started exploring alternative routes (Scheme 3) to access the ketolactone **201**. Specifically, we started to question whether accessing it through the dihydropyran intermediate **200** is really necessary. Instead, oxidation of alkyne **199** to ketoester might be easier than the oxidation of alkene **200** to ketolactone, as fewer number of oxidation needs to occur. Following precedents from Wu and coworkers[10], we first perfomed a bromination and then oxidation using $KMnO_4$ to access the desired ketolactone **201**. Interestingly, the major product of the oxidation was actually lactone **196**, although ketoester **205** was produced. Although the mechanism for such net decarbonylation was not exactly known[11], we reasoned that the secondary alcohol might be a bad actor, interrupting the oxidation reaction. We also attempted other oxidation methods such as direct oxidation of alkyne using $KMnO_4/NaIO_4$[12] or through a photoredox methodology using CuI/2-pinolinic acid/blue LEDs[13], but neither gave desired ketolactone **201** product.

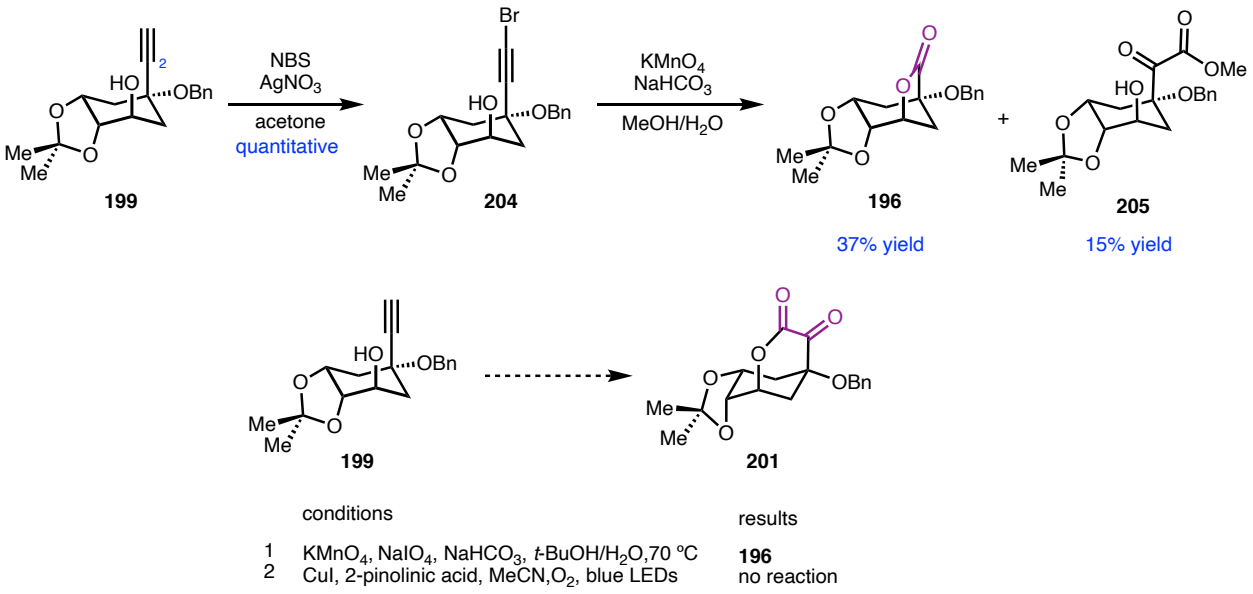

Scheme 3. *Alkyne oxidation attempts.*

Having identified that the secondary alcohol might play a role in generating lactone **196** as an oxidation product, we decided to protect it with an acetate group prior to the alkyne oxidation (Scheme 4). Indeed, the subsequent alkyne oxidation proceeded smoothly, affording ketoester **208**

in 85% yield over two steps from alkyne **206**. We next examined the key intermolecular aldol step between ketoester **208** and acetophenone. Gratifyingly, the reaction was successful in the first attempt, providing alcohol **209** in 88% yield as a single diastereomer.

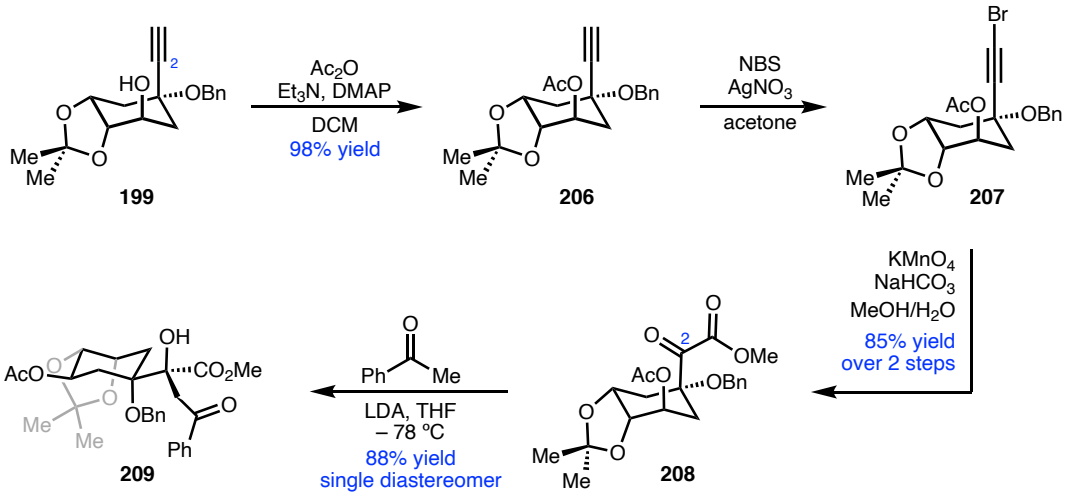

Scheme 4. *Successful intermolecular aldol.*

As we analyze the transition state model for the intermolecular aldol reaction (Figure 3), it was surprising that a single diastereomer product was obtained. According to the Zimmerman-Traxler model, the transition state **210** (left) produced the product in the reaction, and therefore should be much more favorable than **211** (right). However, the steric environment for the incoming acetophenone in **210** is not much different to that in **211**, as the purple methylene is essentiallly very similar to the orange methylene. We reasoned that there might be chelation occurring that direct the stereoselectivity observed. However, the exact reason warrants further investigation potentially through computational studies.

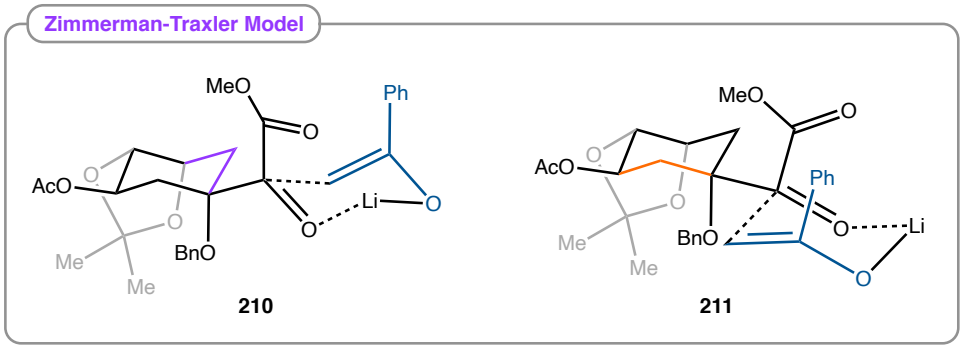

Figure 3. *Zimmerman-Traxler Model for intermolecular aldol.*

Gratifyingly, the single diastereomer obtained from the intermolecular aldol reaction is the desired diastereomer. Next, we aimed to deprotect the secondary alcohol (shown in purple) in **209** and perform a lactonization on it with the methyl ester (Scheme 5). The reason why we chose using an acetate protecting group earlier is that we think we can use the same condition for the deprotection and lactonization and cut down one step. We tried the canonical acetate deprotection condition K_2CO_3/MeOH, but a retro-aldol occurred, extruding the acetophenone fragment and leading to the formation of **213**. Acidic condition (CSA/MeOH) resulted in acetate and acetonide deprotections, and an etherification between the secondary and tertiary alcohols to form **214**. These investigations indicated the sensitive nature of **209**, and we started looking into more mild conditions for transestification. Eventually, Otera's catalyst [14,15] was used to convert **209** into **212** in 94% yield. MeOH was first added in the first part of the reaction and it can perform the first transestification with the acetate group to reveal the secondary alcohol. Then, the reaction vial was opened to let MeOH evapoarate and additional Otera's catalyst was added. The second transesterification therefore proceeded between the secondary alcohol and the methyl ester. Otera's catalyst facilitates the reaction like a Lewis acid catalyst. We were able to crystallize the lactone product **212** and obtained an X-ray confirmation of its structure and sterochemistry.

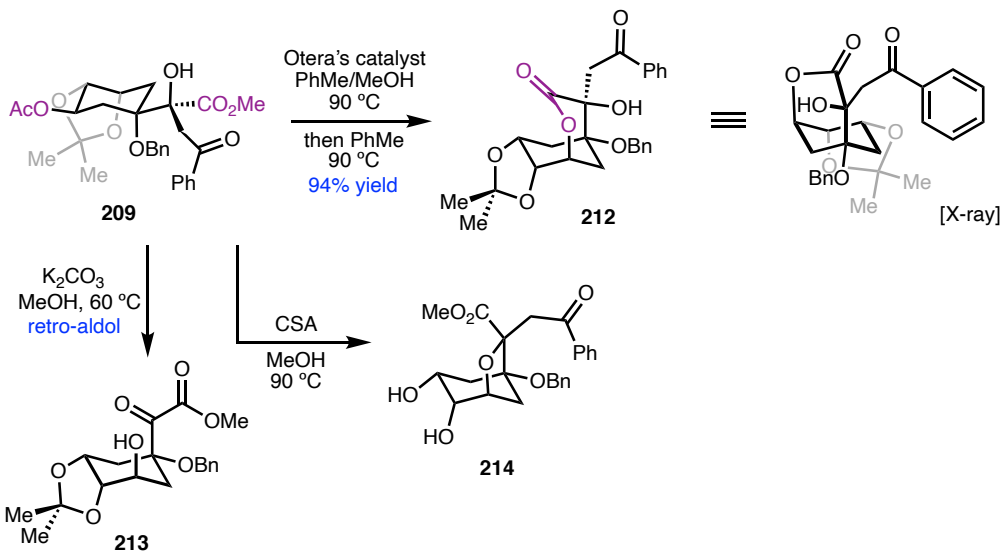

Scheme 5. *Lactonization attempts.*

Having obtained the desired lactone **212**, we next aimed to install the pyrone fragment and then test the intramolecular aldol to forge the caged core (Scheme 6). To achieve that, we think the first step is to deprotect the acetonide and oxidize C4 alcohol to a ketone. Then, α-functionization of the ketone can introduce the pyrone. Therefore, we proceeded with acid-mediated acetonide deprotection, giving diol **215** in 93% yield from **212**. Direct oxidations of the diol (DMP, PIDA/ABNO, Swern oxidation, Stahl oxidation, etc.) afforded complex mixtures of products. Therefore, we had to explore selective protection of C5 alcohol and then oxidation of C4 alcohol. Unfortunately, C4 alcohol is less sterically encumbered, and silyl protection conditions (TBSCl/DMAP/imidazole) provided exclusively C4-OTBS product. Using a less sterically bulky silyl protecting agent TMSCl, we still obtained only C4-OTBS product, along with double protection product with C4 and C5 alcohols both capped with TMS protecting groups. To overcome this selectivity, we drew inspiration from studies of regioselective opening of acetal-like cyclic orthoesters to selective form axial esters.[16,17] Conversion of diol **215** to the orthobenzoate followed by acidic hydrolysis gave **216** as a 1:0.7 mixture of isomers. The poor

regioselectivity can be rationalized by the twisted-boat conformation of **215**, which renders the C4 hydroxyl group pseudoequatorial with poor discrimination from the C5 hydroxyl.

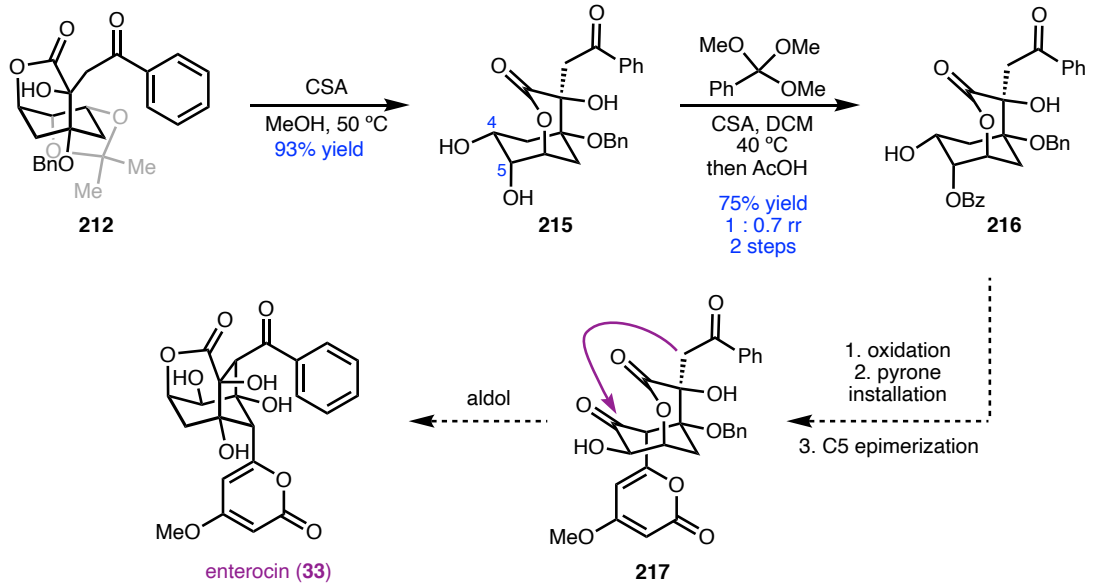

Scheme 6. *Endgame plan.*

With **216** in hand, we envision that introduction of the pyrone fragment could occur by first oxidation of the C4 alcohol followed by α-functionalization (Scheme 6). Subsequent deoxygenation or epimerization at C5 could lead to deoxyenterocin (**2**) or enterocin (**1**), respectively. Lastly, we anticipate that a biomimetic aldol reaction to connect C3 and C4, following precedent from Bach[2], could complete the synthesis.

6.3 Alternative route for pyrone installation

Though a late-stage introduction of the appended pyrone is still under investigation, we have found that late-stage intermediates become increasingly fragile as their complexity increases: they are both prone to rearrangement and unstable to isolation. The difficulty of handling late-stage compounds significantly limits the reactions that we are able to explore for pyrone installation. Therefore, we devised an alternative route in which a precursor to the pyrone is installed at an early stage. The ideal functional group handle for pyrone formation would be an

aldehyde or alkyne equivalent (Scheme 7), which could be converted to the desired pyrone through intermolecular aldol reaction[18,19](Scheme 7A) or metal-mediated cyclization[20,21](Scheme 7B), respectively.

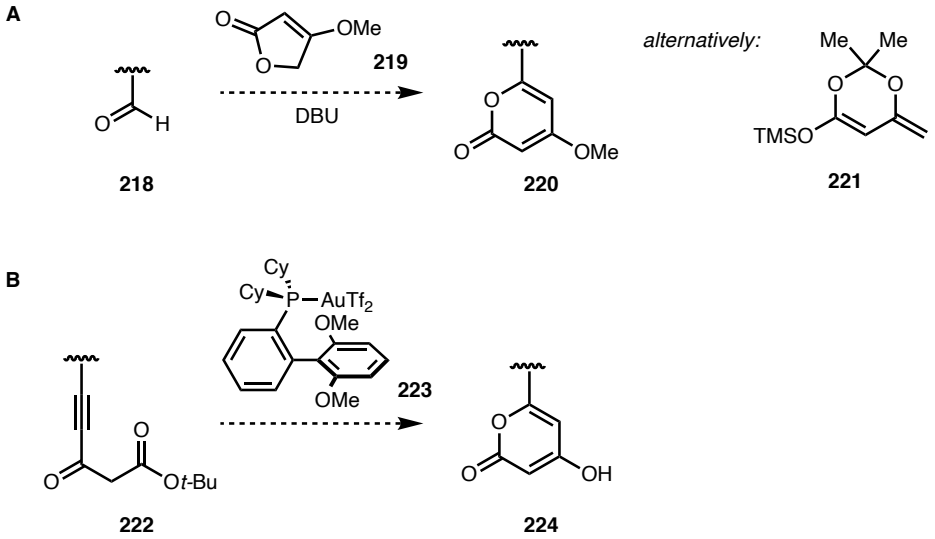

***Scheme 7**. Pyrone formation plan.*

Next, we surveyed a few quinic acid derived substrates for installing the functional handle for the pyrone early in the synthesis. We envisioned to functionalize the carbon that attaches to the pyrone ring through α-functionalization of ketone. However, one interesting challenge for these quinic acid derived substrates is that there is usually a β-tertiary alcohol that is prone to elimination. For instance, we investigated α-functionalization of ketone **169** (Scheme 8). Attempts of enolization of the ketone or generating a silyl enol ether resulted in β-tertiary alcohol elimination. α-bromination and α-oxidation also resulted in β-tertiary alcohol elimination or a complex mixture. Eventually, we were able to solve this problem by accessing lactone **227**. Once again, we need to enolize the ketone and there is a β-tertiary alcohol, but this time the β-tertiary alcohol is at bridgehead position and the lactone locks the geometry, making it unable to eliminate.

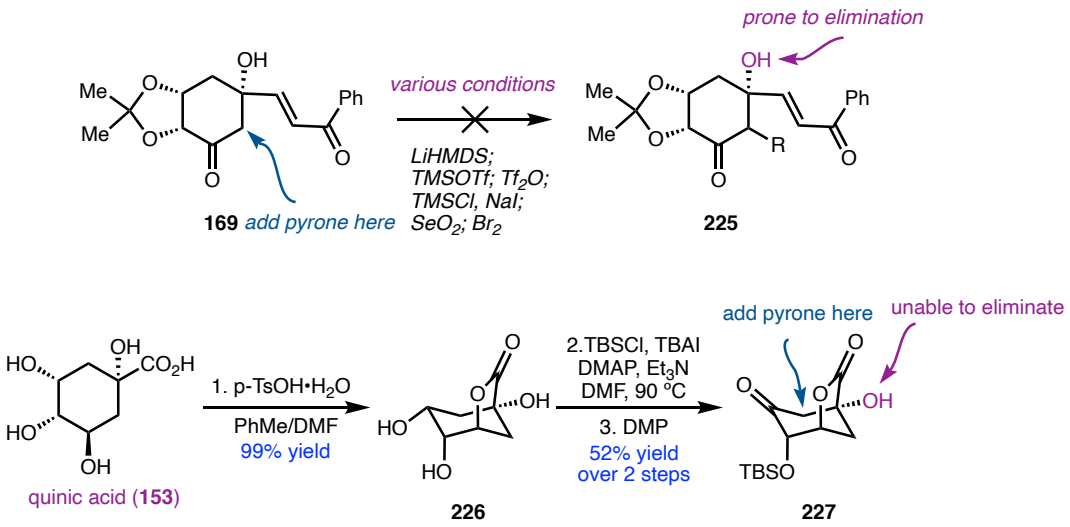

Scheme 8. *Looking for α-functionalization substrates.*

Having identified the desirable substrate **227** to work with, we started exploring the α-functionalization (Scheme 9). With the tertiary alcohol unprotected, we found excess LiHMDS did not result in desired enolization, possibly because the tertiary alkoxy anion is too adjacent to the α position. Nevertheless, α-bromination using bromine • 1,4-dioxane complex proceeded smoothly[22], affording **229** in 98% yield as a single diastereomer. **229** can be purified through column chromatography but also usually clean enough to be used in the next steps. The neat part of this α-bromination reaction is that the single diastereomer obtained has the bromide pointing down, which is on same face of the desired pyrone ring. Therefore, we started exploring whether we can leverage this stereoselective α-bromination to functionalize the α-position as an aldehyde or alkyne equivalent. We investigated various methodologies to generate an α-radical or a metal-enolate from **229** and then trap with different electrophiles (Scheme 9). A Keck radical allylation proceeded stereoselectively, furnishing **240** (**230** with R = allyl) in 95% yield as a single diastereomer. We also attempted photoredox chemistry to generate the α-radical and react with different electrophiles, including a pyrone fragement **232**. Unfortunately, these attempts gave inconsistent results and low yields of the products. Some conditions (Scheme 9, table 2, entry 7,

10) provided alkenyl products, but the reactions were messy and the products were not characterized.

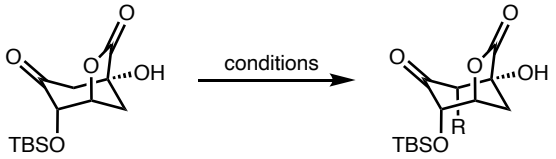

227 **228**

	conditions	results
1	LiHMDS, formaldehyde	no reaction
2	Br_2•dioxane	R= Br, 98% yield, single diastereomer

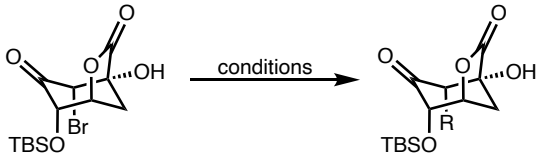

229 **230**

	conditions	results
1	*t*BuNC, AIBN, PhMe, 90 ºC	complex mixture
2	*t*BuNC, AIBN, Bu_3SnH, PhMe, 90 ºC	debromination
3	allyl$SnBu_3$, AIBN, PhMe, 90 ºC	R = allyl, 95% yield, single diastereomer
4	**231**, AIBN, PhMe, 120 ºC	no reaction
5	$Pd(PPh_3)_4$, $PhB(OH)_2$, K_3PO_4•H_2O, THF, 80 ºC	complex mixture
6	**232**, $Ir(ppy)_3$, Na_2CO_3, MeCN, blue Kessil	complex mixture
7	**233**, $Ir(ppy)_3$, Na_2CO_3, MeCN, blue Kessil	tentative 38% yield of an alkene product
8	tBuNC, $Ir(ppy)_3$, Na_2CO_3, MeCN, blue Kessil	complex mixture
9	**234**, $Ir(ppy)_3$, Na_2CO_3, MeCN, blue Kessil	19% debromination, no alkene product
10	**235**, $Ir(ppy)_3$, Na_2CO_3, MeCN, blue Kessil	combined 34% yield of 2 alkene products
11	**236**, $Ir(ppy)_3$, Na_2CO_3, MeCN, blue Kessil	tentative 11% yield of an alkene product

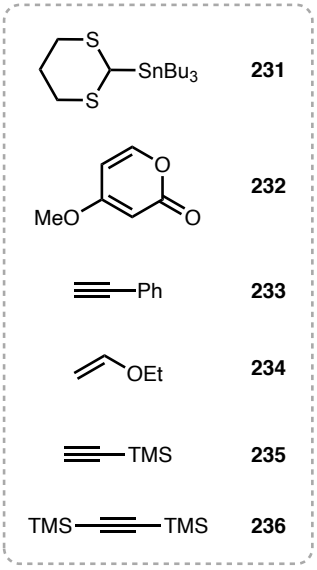

Scheme 9. *α-functionalization attempts through α-bromination.*

In addition to attempts on α-functionalization through a radical mechanism, we also investigated the more tranditional two electron pathway to introduce a functional handle (scheme 10). After MOM protection of the tertiary alcohol, the α-position can be enolized by LiHMDS. In a deuterium quenching study (Scheme 10, entry 1), 34% of the material has deuterium incorporation. Interestingly, there is only one diastereomer formed, similar to the α-bromination reaction. This LiHMDS enolization is very time-sensitive, as a prolonged exposure (>10 min) of starting material **237** to the base will result in decomposition. We were able to make enol triflate smoothly, although the attempt to add a radical into the enol triflate[23] did not give any reactivity.

In addition, we surveyed a variety of electrophiles (Scheme 10, entry 4-8) that can bring in an aldehyde or an alcohol products, but most of the reactions had no reactivities or low yields.

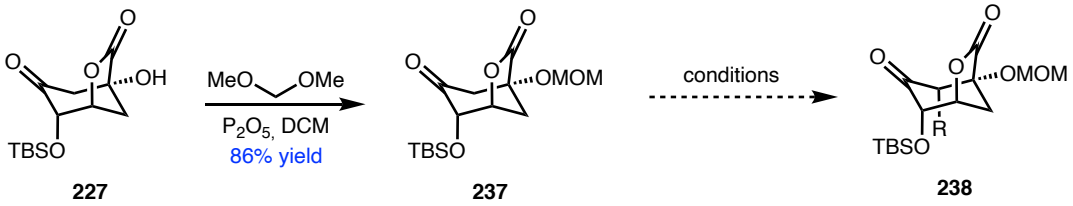

227 **237** **238**

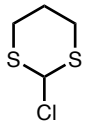

239

	conditions	results
1	LiHMDS, THF, 0 ºC, AcOD	34% D incorporation, single diastereomer
2	LiHMDS, Comin's reagent, THF, 0 ºC	76% yield of triflate
3	LiHMDS, Comin's reagent, THF, 0 ºC; dimethoxymethane, AIBN, 90 ºC	No conversion of triflate
4	LiHMDS, formaldehyde, THF, 0 ºC	No reaction
5	LiHMDS, ethyl formate, THF, 0 ºC	No reaction
6	LiHMDS, 2,2,2-trifluroethyl formate, THF, 0 ºC	No reaction
7	LiHMDS, trimethylorthoformate, BF_3*OEt_2, THF, 0 ºC	No reaction
8	LiHMDS, **239**, THF, 0 ºC	tentative 34% yield of 2 diasteromers

Scheme 10. *α-functionalization attempts through enolate chemistry.*

Though a more extensive screen of conditions and electrophiles is underway, we are concurrently testing the subsequent steps of the route using ketone **240**, in which an allyl group serves as the functional handle for pyrone formation (Scheme 11). Starting from ketone **240**, we focused on making a ketoester moiety similar to the previous substrate **208** (Scheme 4). However, when we started planning the subsequent reactions by transferring the chemistry from the previous route, we found the plan is pretty steppy (Scheme 11A). First, the route requires ketone protection, as the lactone reduction will possibly reduce ketone as well. Then, the lactol needs to be converted to alkyne, and the alkyne oxidation by $KMnO_4$ will possibly affect the allyl alkene too. In summary, this route will be around 8 steps and there are multiple interfering reactivities.

When we examine the goal of this route again, we found that all we want from the sequence is convert the lactone to the ketoester. The net reaction for this conversion is adding an ester unit into the lactone. We therefore started exploring an umplung addition using an ester equivalent nucleophile (Scheme 11B). Tris(methylthio)methane **245**[24] was investigated first. The lithiation

and nucleophilic addition into the lactone proceeded, and the desired product **246** was obtained, albeit in only 8% yield. We think this is still a promising result, as the nucleophile selectively added into the lactone, but not the ketone, possibly because the ketone is more stereically congested and the lacton is strained. Interestingly, we analyzed the reaction and found there were 34% recovered starting material **244** and 24% dimethylthioketone **247**. There is also literature precedent for the formation of dithiolated products.[25] The mechanism for the formation is that the desired product **246** can possibly undergo further reaction with a second molecule of lithiated nucleophile, and then generate an enolate, which was quenched to arrive at **247**.

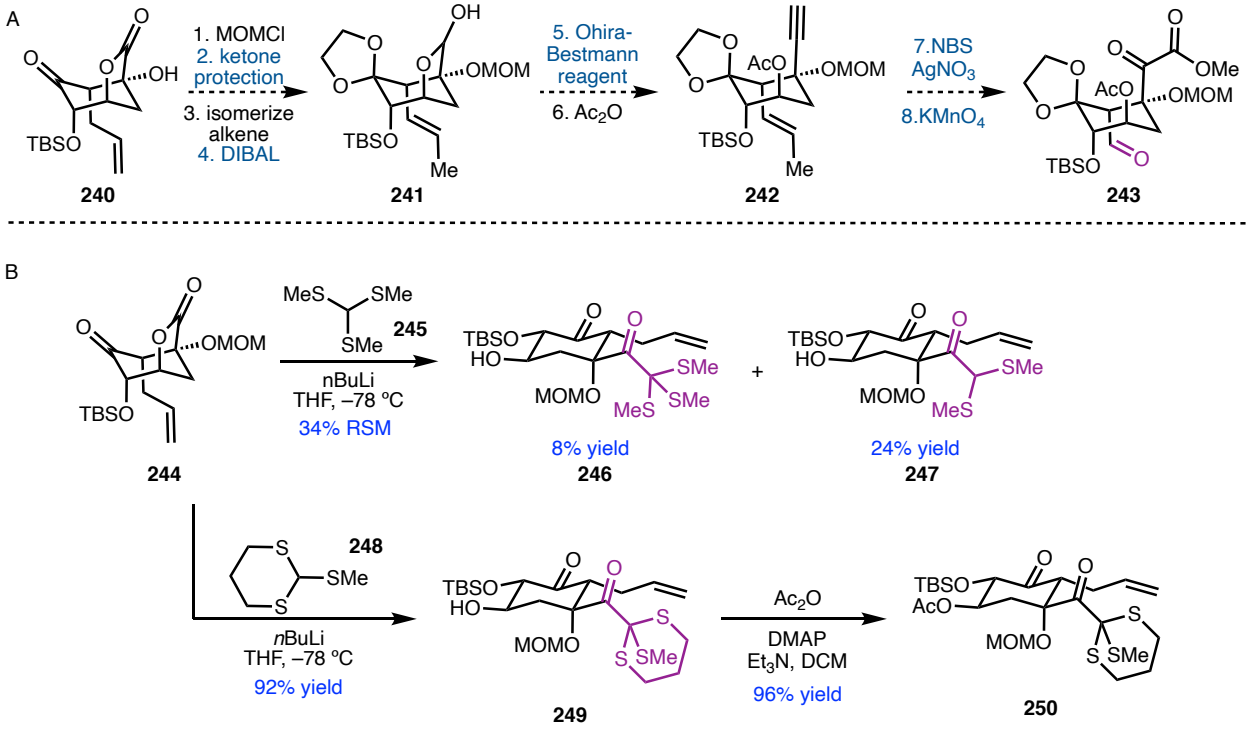

Scheme 11. *Dithiane nucleophiles addition.*

We came up with several solutions to the problem of **247** was formed as the major product (Scheme 11B). Initially, we tried running the reaction at lower temperature, such as at –96 ºC to prevent this further reaction of **246** to **247**. However, the product ratio did not have any substantial changes. Next, we attempted adding a thiol transfer agent at the end of the reaction, such as N-

(methylthio)phthalimide, and possibly react with the enolate intermediate. Unfortunately, the reaction still favored the formation of **247**. Eventually, we started looking into alternative nucleophiles to tris(methylthio)methane **245**.[26] We found that a bulkier lithiated trithioorthoester nucleophile **248**[27] was able to add into the lactone in 92% yield, and the subsequent acetylation proceeded cleanly. There are other ester equvalent nucleophiles that we found in literature but did not test. I will list them here for readers' reference: tris(phenylthio)methane[28], tris(cyclohexylthio)methane[29], Oguro anion[30,31], trithiabicyclo[2.2.2]octane[32], Bode salt[33,34], etc.

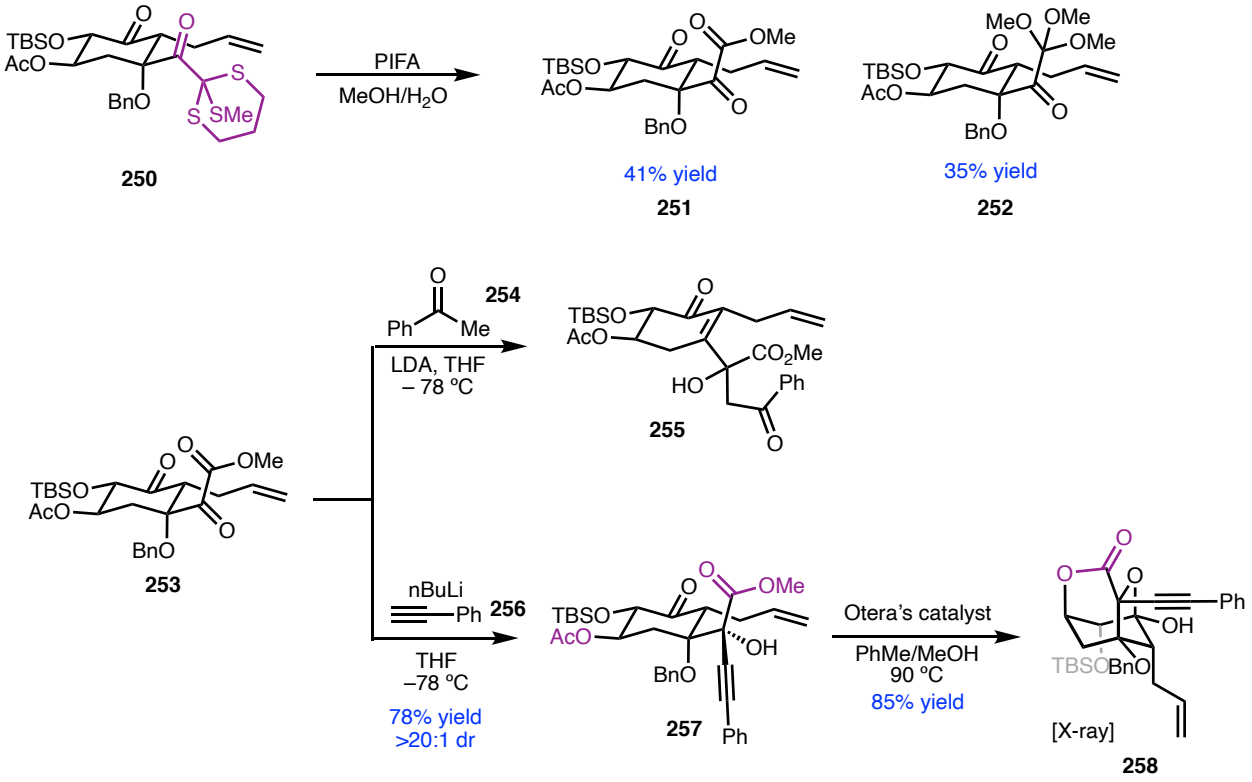

Scheme 12. *Nucleophile addition into the ketoester.*

Subsequent deprotection of **250** was achieved by PIFA[35], giving ketoester **251** in 41% yield, due to the formation of ketotrimethylorthoester **252** as a major side product. Interestingly, the HgO/$HgCl_2$ deprotection condition on **250** produced a complex mixture of products. However, on substrate **249** (Scheme 11) where the secondary alcohol is unprotected, HgO/$HgCl_2$ deprotection proceeded cleanly, but then the acetylation favorably protects the lactol over the secondary alcohol.

Therefore, we had to proceed with the PIFA condition. We did a screen of MeOH/H_2O ratio, but ketotrimethylorthoester **252** has always been a major side product. Switching MeOH with MeCN, we were able to obtain the thioester equivalent of **251** in 76% yield. With ketoester **251** in hand, addition of acetophenone enolate produced enone **255**, with the tertiary alcohol eliminated. We varied the addition sequence, equivalence of the enolate, and temperature, but this elimination has always occurred, indicating the sensitive nature of our highly oxidized substrates. Nevertheless, we used a less basic nucleophile lithium phenylacetylide to add into ketoester **253**, and the reaction delivered tertiary alcohol **257** as a single diastereomer in 78% yield. This stereoselectivity possibly came from allyl group blocking the back face for nucleophile attacks. Exposure of **257** to Otera's catalyst provided lactone **258**, whose structure was confirmed by X-ray crystallography.

In summary, we developed two routes to access the core structure of enterocin with requisite oxidations and functional handle for the pyrone. Future studies will [1] target the formation of the appended pyrone ring, [2] adjust C5 hydroxyl group stereochemistry, [3] effect an intramolecular aldol cyclization to access enterocin (1), and [4] develop the radical-polar crossover reaction into a separate methodology.

6.4 Experimental Section

6.4.1 Materials and methods

Unless otherwise stated, reactions were performed under an inert atmosphere (dry N_2 or Ar) with freshly dried solvents utilizing standard Schlenk techniques. Glassware was oven-dried at 120 °C for a minimum of four hours, or flame-dried utilizing a Bunsen burner under high vacuum. Tetrahydrofuran (THF), methylene chloride (CH_2Cl_2), *N*,*N*- dimethylformamide (DMF), benzene (PhH), and toluene (PhMe) were dried by passing through activated alumina columns. 2-Methyltetrahydrofuran (anhydrous, >99%, inhibitor-free) was purchased from Sigma-Aldrich and

stored under argon. Methanol (HPLC grade) was purchased from Fisher Scientific. Pyridine (Pyr) was distilled from calcium hydride immediately prior to use. All reactions were monitored by thin-layer chromatography using EMD/Merck silica gel 60 F254 pre-coated plates (0.25 mm) and were visualized by UV (254 nm), *p*-anisaldehyde, CAM, and/or $KMnO_4$ staining. Flash column chromatography was performed using silica gel (SiliaFlash® P60, particle size 40-63 microns [230 to 400 mesh]) purchased from Silicycle. ^1H and ^{13}C NMR spectra were recorded on a Bruker Avance III HD with Prodigy Cryoprobe (at 400 MHz and 101 MHz, respectively), Varian Inova 500 (at 500 MHz and 126 MHz, respectively), or Varian Inova 600 (at 600 MHz and 150 MHz, respectively), and are reported relative to internal $CHCl_3$ (^1H, $\delta = 7.26$), C_6H_6 (^1H, $\delta = 7.16$), or CD_2HOD (^1H, $\delta = 3.31$), and $CDCl_3$ (^{13}C, $\delta = 77.0$), C_6D_6 (^{13}C, $\delta = 128.0$), or CD_3OD (^{13}C, $\delta = 49.0$). Data for ^1H NMR spectra are reported as follows: chemical shift (δ ppm) (multiplicity, coupling constant (Hz), integration). Multiplicity and qualifier abbreviations are as follows: s = singlet, d = doublet, t = triplet, q = quartet, m = multiplet, br = broad, app = apparent. IR spectra were recorded on a Perkin Elmer Paragon 1000 spectrometer and are reported in frequency of absorption (cm^{-1}). HRMS were acquired using an Agilent 6200 Series TOF with an Agilent G1978A Multimode source in electrospray ionization (ESI), atmospheric pressure chemical ionization (APCI), or mixed (MM) ionization mode. Optical rotations were measured on a Jasco P-2000 polarimeter using a 100 mm path-length cell at 589 nm.

Reagents were purchased from commercial vendors as follows: Silver triflate was purchased from Strem Chemicals. Diisobutylaluminium hydride, acetic anhydride, Potassium Permanganate, n-butyllithium (2.5 M in hexane), (Bis(trifluoroacetoxy)iodo)benzene were purchased from Sigma-Aldrich. 1,3-dithiane was purchased from Combi blocks.

6.4.2 Experimental procedures

Preparation of lactone 259

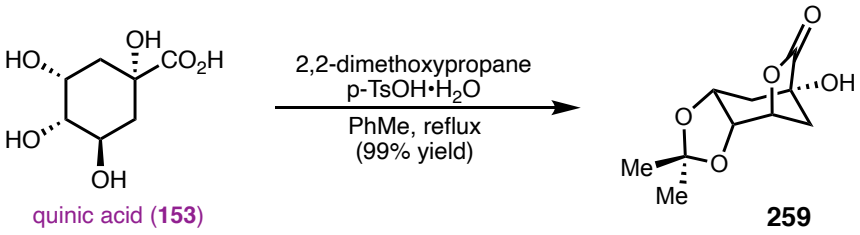

quinic acid (**153**) **259**

A suspension of D-(−)-quinic acid (**6**) (15 g, 80 mmol, 1 equiv), 2,2-dimethoxypropane (30 mL, 240 mmol, 3 equiv), and *p*-TsOH·H_2O (0.15 g, 0.8 mmol, 0.01 equiv) in toluene (100 mL) was stirred for 1 h under reflux. Cool to room temperature, and the solvent was removed *in vacuo*. Product was directly taken into the next step. NMR spectra of lactone **259** match what was reported in literature.[36]

Preparation of benzyl ether 196

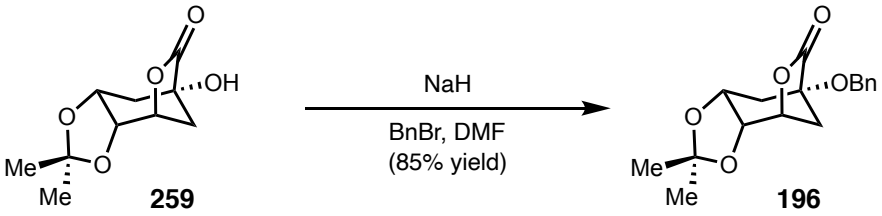

259 **196**

NaH (4 g, 60% suspension in oil, 93.3 mmol, 2 equiv) was washed with *n*-hexane (2 × 5 mL) under argon and suspended in DMF (20 mL) at 0 °C. Then a solution of **259** (10 g, 46.7 mmol, 1 equiv) in DMF (50 mL) was added dropwise during 30 min with stirring. Then, benzyl bromide (16 g, 93.3 mmol, 2 equiv) was added dropwise over 30 min. The reaction mixture was warmed to room temperature and stirred for 19 h and then quenched by slowly adding saturated aqueous NH_4Cl (20 mL) at 0 °C. The mixture was extracted with diethyl ether (3 × 40 mL) and the combined organic layers were dried with Na_2SO_4. After filtration and evaporation of the solvents, the residue

was purified by chromatography on silica (10 to 20% EtOAc/hexane) to yield **196** (12.6 g, 85%) as a colorless solid. NMR spectra of lactone **196** match what was reported in literature.[7]

Preparation of lactol 197

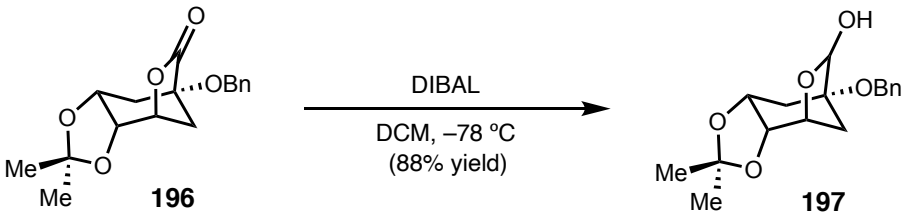

An oven-dried 500 mL round-bottom flask was charged with benzyl ether **196** (12 g, 39.4 mmol, 1 equiv) and 131 mL anhydrous DCM. The reaction mixture was cooled to –78 ºC via acetone/dry ice bath, and the stirring continued for 15 min. Then, DIBAL solution (1M in hexane, 39.4 mL, 39.4 mmol, 1 equiv) was added dropwise. Stirring continued (*ca.* 1h) until TLC analysis indicated that starting material was fully consumed. The reaction mixture was next *carefully* treated with EtOAc (50 mL) followed by sat. aq. Rochelle's salt (100 mL). The cooling bath was removed and the mixture was vigorously stirred for 1h at ambient temperature. The resulting two layers were separated and the aqueous layer extracted with EtOAc (4 × 80 mL). The combined organic layers were washed with brine (80 mL), dried over Na_2SO_4, filtered, and concentrated *in vacuo*. The crude residue was purified by SiO_2 flash chromatography (30 to 40 % EtOAc/hexanes) to afford alcohol **197** (10.6 g, 34.7 mmol, 5:1 dr, 88% yield) as a white solid.

TLC (50% EtOAc/hexanes): R_f 0.36 (UV, CAM).

^{1}H NMR (400 MHz, $CDCl_3$):

<u>*Major diastereomer:*</u> δ 7.38 – 7.27 (m, 5H), 4.93 (d, *J* = 4.4 Hz, 1H), 4.60 – 4.52 (m, 2H), 4.51 – 4.45 (m, 1H), 4.40 (ddd, *J* = 6.4, 2.9, 0.6 Hz, 1H), 4.16 (ddd, *J* = 6.7, 2.9, 1.3 Hz, 1H), 3.33 (d, *J*

= 4.5 Hz, 1H), 2.36 – 2.27 (m, 2H), 2.22 (ddd, *J* = 14.8, 7.3, 2.1 Hz, 1H), 2.15 – 2.07 (m, 1H), 1.51 (s, 3H), 1.32 (s, 3H).

Minor diastereomer: δ 7.40 – 7.22 (m, 1H), 5.33 (dd, *J* = 3.8, 0.9 Hz, 0.2H), 4.68 (ddd, *J* = 8.2, 6.6, 4.0 Hz, 0.2H), 4.59 – 4.52 (m, 0.4H), 4.28 (dd, *J* = 5.9, 2.8 Hz, 0.2H), 4.23 (ddd, *J* = 6.5, 2.9, 1.2 Hz, 0.2H), 3.52 – 3.48 (m, 0.2H), 2.79 (ddd, *J* = 13.7, 8.2, 2.6 Hz, 0.2H), 2.35 – 2.30 (m, 0.4H), 1.96 (ddd, *J* = 13.7, 4.0, 0.9 Hz, 0.2H), 1.55 – 1.48 (m, 0.6H), 1.32 (t, *J* = 1.1 Hz, 0.6H).

^{13}C NMR (101 MHz, $CDCl_3$):

Major diastereomer: δ 137.71, 128.67, 128.09, 127.95, 109.26, 100.04, 81.11, 76.43, 75.31, 72.09, 67.10, 35.03, 29.03, 27.28, 24.57.

Minor diastereomer: δ 138.50, 128.53, 127.75, 127.63, 109.72, 101.40, 81.31, 76.43, 75.96, 72.68, 66.78, 34.38, 32.50, 27.64, 24.93.

HRMS (ESI): calc'd for $[M+Na]^+$ 329.1359, found 329.1362.

Preparation of alkyne 199

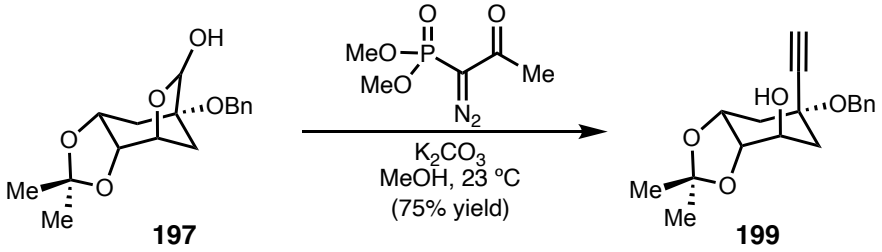

An oven-dried 250 mL round bottom flask was charged with lactol **197** (5.70 g, 18.6 mmol, 1 equiv), Bestmann-Ohira reagent[37] (4.65 g, 24.2 mmol, 1.3 equiv), and 100 mL anhydrous MeOH. K_2CO_3 (5.14 g, 37.2 mmol, 2 equiv) was slowly added to the solution. The reaction mixture was stirred at ambient temperature (*ca.* 6 h) until at which point TLC analysis indicated the full consumption of starting material. The reaction mixture was filtered over celite and SiO_2 pads, and the filtrate was concentrated *in vacuo*. The crude residue was purified via SiO_2 flash

chromatography (30 to 40% EtOAc/hexanes) to afford alkyne **199** (4.22 g, 14.0 mmol, 75% yield) as a colorless oil.

TLC (50% EtOAc/hexanes): R_f 0.36 (UV, CAM).

^{1}H NMR (400 MHz, $CDCl_3$): δ 7.41 – 7.26 (m, 5H), 4.69 – 4.58 (m, 2H), 4.40 (td, *J* = 5.4, 3.9 Hz, 1H), 4.14 (ddq, *J* = 10.1, 7.2, 5.0 Hz, 1H), 3.95 (dd, *J* = 7.1, 5.7 Hz, 1H), 2.59 (s, 1H), 2.58 (m, 1H), 2.36 (ddd, *J* = 13.7, 4.5, 2.1 Hz, 1H), 2.11 (dd, *J* = 15.3, 5.2 Hz, 1H), 1.82 (dd, *J* = 13.7, 10.8 Hz, 1H), 1.47 (s, 3H), 1.37 (s, 3H).

^{13}C NMR (101 MHz, $CDCl_3$): δ 138.48, 128.39, 128.07, 127.63, 109.28, 84.72, 80.31, 74.10, 73.17, 71.69, 68.29, 66.37, 41.20, 36.05, 28.45, 26.15.

FTIR(NaCl, thin film): 3409, 2931, 2355, 2108, 1379, 1298, 1239, 1220, 1160, 1051 cm^{-1}.

HRMS (ESI): calc'd for $[M+H]^+$ 303.1591, found 303.1592.

$[\alpha]_D^{25}$ = –60.7 ° (*c* = 1.00, $CHCl_3$).

Preparation of acetate 206

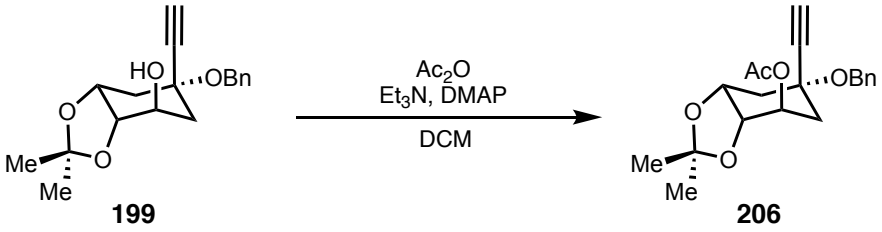

An oven-dried 250 mL round bottom flask was charged with alkyne **199** (4.22 g, 14.0 mmol, 1 equiv), acetic anhydride (15.9 mL, 16.8 mmol, 1.2 equiv), and 90 mL anhydrous DCM. 4-dimethylaminopyridine (171 mg, 1.40 mmol, 0.1 equiv) and Et_3N (2.93 mL, 21.0 mmol, 1.5 equiv) were next added to the solution. The reaction mixture was stirred at ambient temperature (*ca.* 1 h) until at which point TLC analysis indicated the full consumption of starting material. The reaction was quenched with sat. aq. NH_4Cl (50 mL). The layers were separated and the aqueous layer was

extracted with ethyl acetate (3 × 50 mL). The combined layers were washed with brine (80 mL), dried over Na_2SO_4, filtered, and concentrated *in vacuo*. The crude residue was clean enough to be directly taken into the next step.

TLC (30% EtOAc/hexanes): R_f 0.56 (UV, CAM).

Preparation of bromoalkyne 207

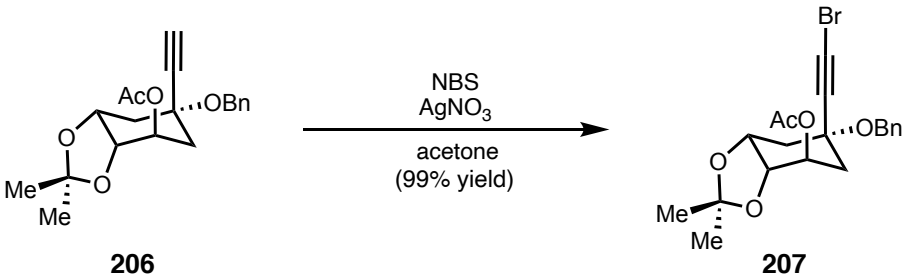

206 **207**

An oven-dried 200 mL round bottom flask was charged with acetate **206** (4.77 g, 13.9 mmol, 1 equiv) and 69 mL anhydrous acetone. The round bottom flask was wrapped with foil to minimize light exposure. *N*-bromosuccinimide (2.97 g, 16.7 mmol, 1.2 equiv) and $AgNO_3$ (708 mg, 4.17 mmol, 0.3 equiv) were added into the reaction mixture. Stirring was continued (*ca.* 40 min) until at which point TLC analysis indicated the full consumption of starting material. The reaction mixture was diluted with ethyl acetate (30 mL), and quenched with distilled water (50 mL). The layers were separated and the aqueous layer was extracted with ethyl acetate (3 × 30 mL). The combined layers were washed with brine (30 mL), dried over Na_2SO_4, filtered, and concentrated *in vacuo*. The crude residue was purified via SiO_2 flash chromatography (10 to 20% EtOAc/hexanes) to afford bromoalkyne **207** (5.83 g, 13.8 mmol, 99% yield) as a yellowish oil.

TLC (20% EtOAc/hexanes): R_f 0.35 (UV, CAM).

^{1}H NMR (400 MHz, $CDCl_3$): δ 7.43 – 7.23 (m, 5H), 5.25 (ddd, *J* = 10.6, 7.1, 4.2 Hz, 1H), 4.64 (s, 2H), 4.41 (td, *J* = 5.4, 3.6 Hz, 1H), 4.07 (dd, *J* = 7.1, 5.6 Hz, 1H), 2.57 (ddd, *J* = 15.3, 3.7, 2.1

Hz, 1H), 2.48 (ddd, *J* = 13.7, 4.3, 2.1 Hz, 1H), 2.12 (m, 1H), 2.08 (s, 3H), 1.80 (dd, *J* = 13.7, 10.5 Hz, 1H), 1.44 (s, 3H), 1.34 (s, 3H).

^{13}C NMR (101 MHz, $CDCl_3$): δ 170.34, 138.29, 128.32, 127.93, 127.49, 109.46, 80.64, 76.65, 73.12, 72.55, 70.46, 66.52, 46.22, 37.76, 36.68, 28.10, 26.08, 21.36.

FTIR(NaCl, thin film): 2983, 2932, 2198, 1740, 1496, 1453, 1370, 1368, 1241, 1178 cm^{-1}.

HRMS (ESI): calc'd for $[M+H]^+$ 423.0802, found 423.0806.

$[\alpha]_D^{25}$ = –60.9° (*c* = 1.0, $CHCl_3$).

Preparation of ketoester 208

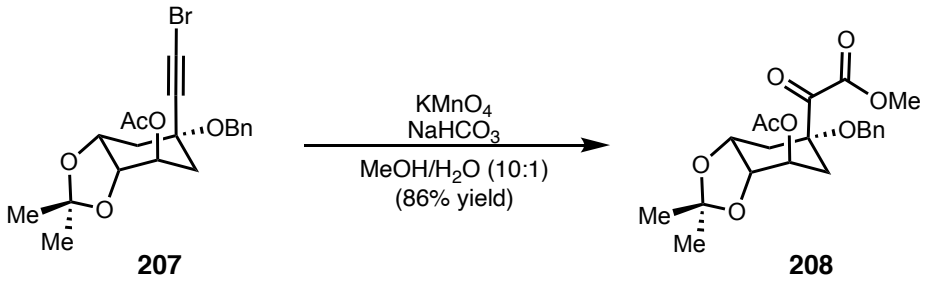

An oven-dried 500 mL round bottom flask was charged with bromoalkyne **207** (5.83 g, 13.8 mmol, 1 equiv), $NaHCO_3$ (580 mg, 6.90 mmol, 0.5 equiv), $MgSO_4$ (4.98 g, 41.4 mmol, 3 equiv), 173 mL MeOH and 17 mL H_2O. The reaction mixture was stirred for 30 min before cooling to 0 ºC via ice/water bath. The reaction mixture was allowed to stir at 0 ºC for 15 min prior to the addition of $KMnO_4$ (6.54 g, 41.4 mmol, 3 equiv). Stirring was continued (*ca.* 1.5 h) until at which point TLC analysis indicated the full consumption of starting material. The reaction mixture was filtered over celite. The filtreate was then diluted with ethyl acetate (50 mL), and quenched with sat. aq. $NaHCO_3$ (100 mL) and sat. aq. $Na_2S_2O_3$ (50 mL). The layers were separated and the aqueous layer was extracted with ethyl acetate (3 × 80 mL). The combined layers were washed with brine (80 mL), dried over Na_2SO_4, filtered, and concentrated *in vacuo*. The crude residue was

purified via SiO_2 flash chromatography (20 to 25% EtOAc/hexanes) to afford ketoester **208** (4.82 g, 11.9 mmol, 86% yield) as a white solid.

TLC (30% EtOAc/hexanes): R_f 0.40 (UV, CAM).

^{1}H NMR (400 MHz, $CDCl_3$): δ 7.34 – 7.26 (m, 5H), 5.34 (ddd, *J* = 11.0, 7.3, 3.9 Hz, 1H), 4.63 (d, *J* = 10.1 Hz, 1H), 4.51 (td, *J* = 5.3, 3.3 Hz, 1H), 4.46 (d, *J* = 10.2 Hz, 1H), 4.08 (dd, *J* = 7.3, 5.6 Hz, 1H), 3.72 (s, 3H), 2.58 (dt, *J* = 15.8, 2.8 Hz, 1H), 2.51 (ddd, *J* = 13.7, 4.0, 2.3 Hz, 1H), 2.27 (dd, *J* = 15.7, 5.0 Hz, 1H), 2.07 (s, 3H), 1.86 (dd, *J* = 13.8, 10.9 Hz, 1H), 1.49 (s, 3H), 1.36 (s, 3H).

^{13}C NMR (101 MHz, $CDCl_3$): δ 198.89, 170.32, 164.90, 137.36, 128.45, 127.85, 127.78, 109.66, 82.48, 76.57, 72.81, 70.07, 67.86, 52.83, 33.53, 30.41, 28.16, 26.05, 21.30.

FTIR(NaCl, thin film): 2985, 2935, 1744, 1454, 1434, 1370, 1286, 1239, 1182, 1125 cm^{-1}.

HRMS (ESI): calc'd for $[M+H]^+$ 407.1700, found 407.1705.

$[\alpha]_D^{25}$ = –34.1° (*c* = 1.0, $CHCl_3$)

Preparation of alcohol 209

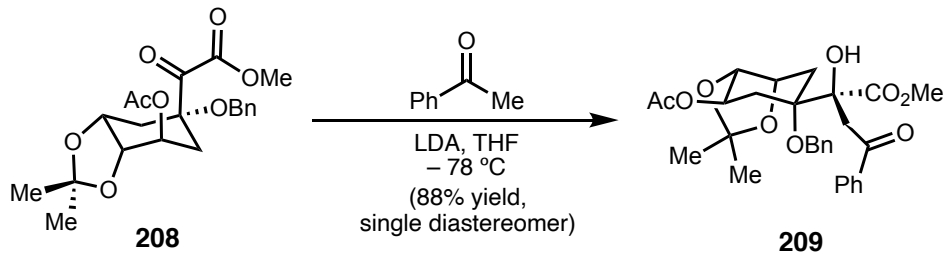

An oven-dried, 100 mL round-bottomed flask was treated with freshly distilled *i*Pr_2NH (0.42 mL, 2.95 mmol, 1.2 equiv) and anhydrous THF (15 mL). The solution was cooled to 0 ºC via an ice/water bath and stirring was continued for 15 min prior to the dropwise addition of *n*-BuLi (2.5 M in hexanes, 1.18 mL, 2.95 mmol, 1.2 equiv) via syringe. Upon complete addition, the

reaction was continued for 30 min to produce LDA, which was then further cooled to –78 ºC via a dry ice/acetone bath. To the cooled solution was added acetophenone (0.32 mL, 2.70 mmol, 1.1 equiv) dropwise at –78 ºC. The reaction was continued at –78 ºC for 1 h prior to the dropwise addition of ketoester **208** (1.00 g, 2.46 mmol, 1.0 equiv) in anhydrous THF (10 mL) dropwise via syringe. Stirring was continued (*ca.* 15 min) until at which point TLC analysis indicated the full consumption of starting material. The reaction mixture was diluted with ethyl acetate (15 mL), and quenched with sat. aq. NH_4Cl (30 mL). The layers were separated and the aqueous layer was extracted with ethyl acetate (3 × 30 mL). The combined layers were washed with brine (30 mL), dried over Na_2SO_4, filtered, and concentrated *in vacuo*. The crude residue was purified via SiO_2 flash chromatography (20 to 25% EtOAc/hexanes) to afford alcohol **209** (1.14 g, 2.16 mmol, 88% yield) as a white solid.

TLC (30% EtOAc/hexanes): R_f 0.25 (UV, CAM).

^{1}H NMR (400 MHz, $CDCl_3$): δ 7.93 – 7.86 (m, 2H), 7.63 – 7.53 (m, 1H), 7.50 – 7.37 (m, 4H), 7.34 – 7.28 (m, 2H), 7.25 – 7.18 (m, 1H), 5.26 (ddd, *J* = 12.4, 8.5, 3.9 Hz, 1H), 4.96 (d, *J* = 11.2 Hz, 1H), 4.85 (d, *J* = 11.2 Hz, 1H), 4.49 (td, *J* = 5.6, 3.3 Hz, 1H), 4.20 (s, 1H), 4.08 (dd, *J* = 8.5, 5.9 Hz, 1H), 3.89 (d, *J* = 17.8 Hz, 1H), 3.74 (s, 3H), 3.45 (d, *J* = 17.8 Hz, 1H), 2.54 (ddt, *J* = 17.7, 13.2, 2.6 Hz, 2H), 2.10 (s, 3H), 1.66 – 1.56 (m, 2H), 1.35 (d, *J* = 6.6 Hz, 6H).

^{13}C NMR (101 MHz, $CDCl_3$): δ 199.56, 174.27, 170.57, 139.18, 136.37, 133.81, 128.69, 128.14, 127.24, 126.97, 109.14, 81.92, 80.13, 73.15, 72.06, 66.60, 52.95, 42.70, 32.47, 29.70, 27.73, 25.70, 21.36.

FTIR(NaCl, thin film): 2984, 2933, 1733, 1681, 1597, 1580, 1497, 1449, 1367, 1240 cm^{-1}.

HRMS (ESI): calc'd for $[M+NH_4]^+$ 544.2541, found 544.2546.

$[\alpha]_D^{25}$ = –53.0° (*c* = 1.0, $CHCl_3$).

Preparation of lactone 212

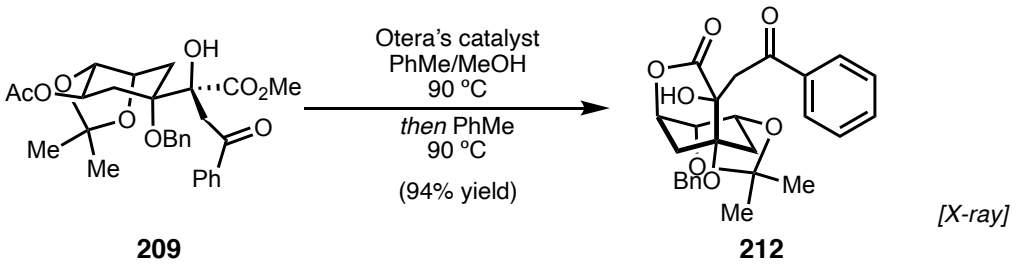

209 **212**

An oven-dried, 100 mL round-bottomed flask was charged with alcohol **209** (1.02 g, 1.94 mmol, 1 equiv), Otera's catalyst (232 mg, 0.387 mmol, 0.2 equiv), 32 mL toluene, and 8 mL MeOH. The solution was heated to 90 ºC via an oil bath. Stirring was continued (*ca.* 12 h) until at which point TLC analysis indicated the full consumption of starting material. The reaction mixture was cooled down to ambient temperature and concentrated *in vacuo*. To the residue, Otera's catalyst (116 mg, 0.194 mmol, 0.1 equiv) and 32 mL toluene were added. The solution was heated to 100 ºC via an oil bath. Stirring was continued (*ca.* 12 h) until at which point TLC analysis indicated the full consumption of the intermediate spot. The reaction mixture was cooled down to ambient temperature and concentrated *in vacuo*. The crude residue was purified via SiO_2 flash chromatography (20 to 30% EtOAc/hexanes) to afford lactone **212** (825 mg, 1.82 mmol, 94% yield) as a white solid. **212** was crystallized and characterized by X-ray crystallography.

TLC (30% EtOAc/hexanes): R_f 0.33 (UV, CAM).

^{1}H NMR (400 MHz, $CDCl_3$): δ 7.92 – 7.85 (m, 2H), 7.62 – 7.53 (m, 1H), 7.50 – 7.40 (m, 2H), 7.26 (s, 5H), 6.89 (s, 1H), 4.64 (t, *J* = 5.3 Hz, 2H), 4.45 (ddd, *J* = 6.6, 4.5, 3.2 Hz, 1H), 4.22 (dt, *J* = 6.5, 1.9 Hz, 1H), 3.58 (d, *J* = 16.2 Hz, 1H), 3.32 (d, *J* = 16.2 Hz, 1H), 2.98 – 2.87 (m, 1H), 2.44 – 2.29 (m, 2H), 1.93 – 1.83 (m, 1H), 1.54 (s, 3H), 1.37 (s, 3H).

^{13}C NMR (101 MHz, $CDCl_3$): δ 203.27, 170.86, 138.88, 137.44, 133.79, 128.79, 128.48, 128.44, 127.49, 127.23, 109.61, 81.71, 76.32, 75.45, 73.63, 71.28, 65.61, 34.09, 32.07, 27.07, 24.65, 20.31.

FTIR(NaCl, thin film): 2986, 2933, 1742, 1664, 1596, 1579, 1496, 1449, 1382, 1346 cm^{-1}.

HRMS (ESI): calc'd for $[M+H]^+$ 453.1908, found 453.1913.

$[\alpha]_D^{25}$ = 14.5° (*c* = 1.0, $CHCl_3$).

Preparation of diol 215

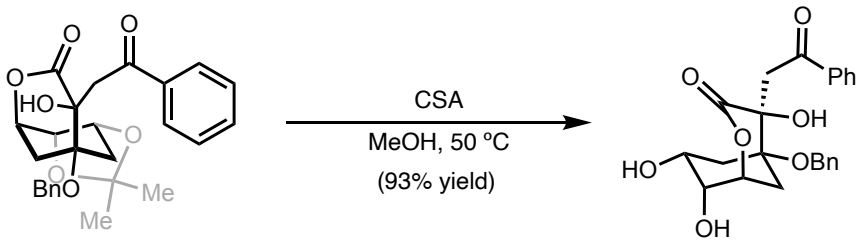

212 **215**

An oven-dried, 50 mL round-bottomed flask was charged with lactone **212** (300 mg, 0.66 mmol, 1 equiv), Camphorsulfonic acid (30.8 mg, 0.13 mmol, 0.2 equiv) and 13 mL MeOH. The solution was heated to 50 ºC via an oil bath. Stirring was continued (*ca.* 1 h) until at which point TLC analysis indicated the full consumption of starting material. The reaction mixture was cooled down to ambient temperature and concentrated *in vacuo*. The crude residue was purified via SiO_2 flash chromatography (50 to 60% EtOAc/hexanes) to afford diol **215** (254 mg, 0.62 mmol, 93% yield) as a white solid.

TLC (70% EtOAc/hexanes): R_f 0.37 (UV, CAM).

^{1}H NMR (400 MHz, $CDCl_3$): δ 7.94 – 7.82 (m, 2H), 7.57 (ddt, *J* = 8.0, 6.9, 1.2 Hz, 1H), 7.46 – 7.42 (m, 2H), 7.31 – 7.27 (m, 5H), 6.63 (s, 1H), 4.85 – 4.75 (m, 2H), 4.63 (d, *J* = 11.3 Hz, 1H), 4.02 (q, *J* = 3.4 Hz, 1H), 3.80 (ddd, *J* = 11.7, 9.5, 5.9 Hz, 1H), 3.62 (d, *J* = 16.0 Hz, 1H), 3.24 (d,

J = 16.0 Hz, 1H), 2.88 (ddd, *J* = 13.0, 4.6, 2.3 Hz, 1H), 2.73 (d, *J* = 2.7 Hz, 1H), 2.38 (d, *J* = 6.7 Hz, 1H), 2.34 – 2.23 (m, 1H), 2.15 – 2.09 (m, 1H).

^{13}C NMR (101 MHz, $CDCl_3$): δ 202.90, 171.81, 138.68, 137.46, 133.87, 128.79, 128.59, 128.52, 127.69, 127.51, 80.36, 76.97, 76.09, 67.78, 66.07, 64.73, 35.47, 35.28, 23.32.

FTIR(NaCl, thin film): 3438, 2925, 1735, 1663, 1596, 1578, 1496, 1449, 1356, 1218 cm^{-1}.

HRMS (ESI): calc'd for $[M+H]^+$ 413.1595, found 413.1600.

$[\alpha]_D^{25}$ = 24.9° (*c* = 1.0, $CHCl_3$).

Preparation of diol 26

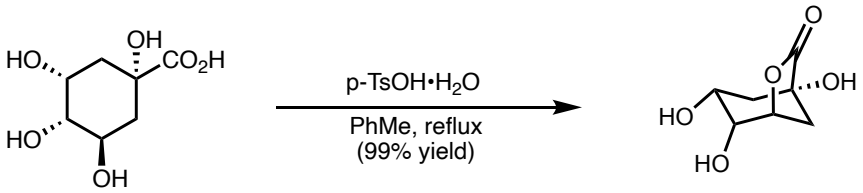

quinic acid (**153**) **226**

A solution of (−)-quinic acid (20 g, 104 mmol, 1 equiv) and *p*-toluenesulfonic acid (0.2 g, 1 mmol, 0.5 mol%) in 200 mL of anhydrous toluene was stirred under reflux for 24 h. The mixture was allowed to reach room temperature, neutralized with solid $NaHCO_3$, and the mixture was filtered over celite. The solution was concentrated *in vacuo*. The residue was dissolved in acetone, filtrated, and the filtrate was concentrated *in vacuo* to give **226** as a white solid in quantitative yield. Spectral data of diol **226** matched that was previously reported.[38]

Preparation of monosilyl ether 260

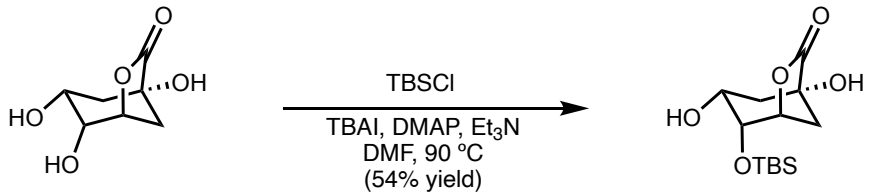

226 **260**

To a stirred solution of the diol **226** (10 g, 0.057 mol, 1 equiv), DMAP (0.97 g, 8 mmol, 0.14 equiv) and *tert*-butylammonium iodide (1.06 g, 2.85 mmol, 0.05 equiv) in dry DMF (100 mL) and dry triethylamine (9.5 mL, 0.068 mol, 1.2 equiv) at room temperature under argon was added *tert*-butyldimethylsilyl chloride (9.9g, 0.065 mol, 1.15 equiv). The resultant solution was heated at 90 ºC for 24 h, and after cooling was diluted with ethyl acetate (100 mL) and filtered over Celite. The solution was washed successively with 1M HCl (100 mL). The combined organic layers were washed with brine (100 mL), dried over Na_2SO_4, filtered, and concentrated *in vacuo*. The crude residue was purified by SiO_2 flash chromatography (50 to 75 % Et_2O/hexanes) to afford monosilyl ether **260** (8.8 g, 30.8 mmol, 54% yield) as white needles. Spectral data of monosilyl ether **260** matched that was previously reported.[22]

Preparation of ketone 227

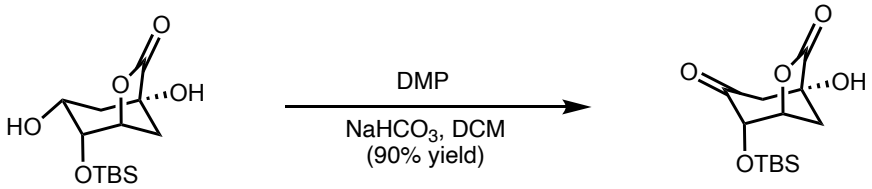

260 **227**

An oven-dried 250 mL round bottom flask was charged with alcohol **260** (8.8 g, 30.8 mmol, 1 equiv), $NaHCO_3$ (3.1 g, 37 mmol, 1.2 equiv), 100 mL DCM, and a stir bar. Then, Dess-Martin periodinane (16 g, 37 mmol, 1.2 equiv) was added at room temperature. Stirring was continued

(*ca.* 12h) until at which point TLC analysis indicated the full consumption of starting material. The reaction mixture was diluted with DCM, filtered over celite, and the filtrate was concentrated *in vacuo*. The crude residue was purified via SiO_2 flash chromatography (20 to 30% EtOAc/hexanes) to afford ketone **227** (7.9 g, 27 mmol, 90% yield) as a white solid. Spectral data of monosilyl ether **227** matched that was previously reported.[22]

Preparation of bromo ketone 229

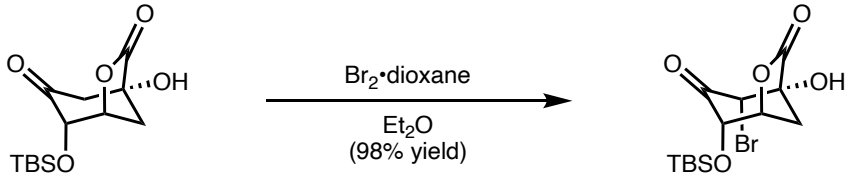

227 **229**

To a stirred solution of the ketone **227** (5 g, 17.4 mmol, 1 equiv) in dry diethyl ether (150 mL) under argon was added freshly made dioxane dibromide (4.7 g, 19.1 mmol, 1.1 equiv). The red solution was stirred at room temperature until decoloration (2 h), diluted with diethyl ether (100 mL) and washed successively with sat. aqueous $Na_2S_2O_3$ (30 mL), sat. aqueous sodium bicarbonate (60 mL). The combined organic layers were washed with brine (100 mL), dried over Na_2SO_4, filtered, and concentrated *in vacuo*. The product **229** (white needles) was clean enough to be used in the next step. **229** can be recrystallized from hexanes for purification. Spectral data of bromo ketone **229** matched that was previously reported.[22]

Preparation of allyl ketone 240

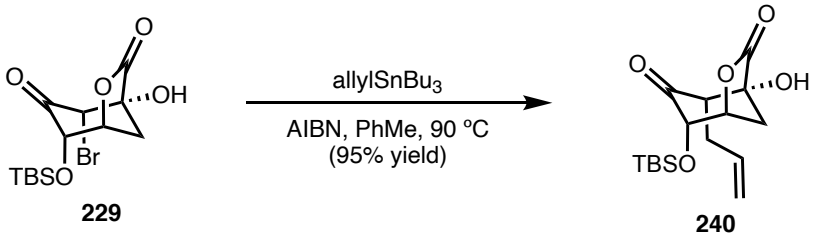

229 **240**

A solution of the α-bromoketone **229** (1 g, 2.7 mmol, 1 equiv) in dry toluene (50 mL), under inert atmosphere, was treated allyltributyltin (0.92 mL, 2.97 mmol, 1.1 equiv) and AIBN (0.2 M in toluene, 2 mL, 0.4 mmol, 0.15 equiv). The resultant reaction mixture was deoxygenated by bubbling argon through it for 30 min. and then heated at 90 ºC for 14 h. After cooling at room temperature, the solvent was evaporated and the crude product was purified by flash chromatography eluting with ethyl acetate-hexane (5:95) to yield the α-allyl ketone **240** (837 mg, 95% yield) as beige solid. Spectral data of allyl ketone **240** matched that was previously reported.[22]

Preparation of MOM ether 244

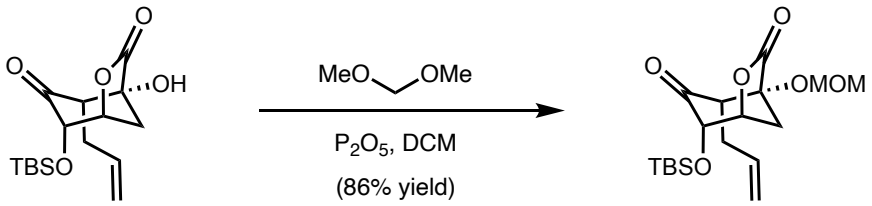

240 **244**

Anhydrous phosphorous pentoxide (8.8 g, 200% w/w) was added to a solution of lactone **240** (4.4 g, 13.5 mmol, 1 equiv) and dimethoxymethane (12 mL, 135 mmol, 10 equiv) in anhydrous DCM (50 mL). The mixture was stirred under N_2 at room temperature for 1 h. Another portion of phosphorous pentoxide (8.8 g, 200% w/w) was added and the mixture stirred for a further 1 h and TLC analysis indicated the complete consumption of starting material. The mixture was diluted with diethyl ether (50 mL) and the solution phase was poured into a 250 mL round bottom flask.

The remaining solid was washed with diethyl ether (20 mL) and the solution was added to the 250 mL round bottom flask. The mixture was then quenched with saturated aqueous $NaHCO_3$ solution (50 mL). The organic phase was separated and the aqueous layer was washed with diethyl ether (2 X 30 mL). The combined organic extracts were dried (Na_2SO_4) and the solvent removed in vacuo to afford **244** as a white solid (4.3 g, 11.6 mmol, 86% yield)

TLC (20% EtOAc/hexanes): R_f 0.52 (UV, CAM).

^{1}H NMR (400 MHz, $CDCl_3$): δ 5.83 – 5.68 (m, 1H), 5.12 – 5.01 (m, 2H), 4.90 – 4.80 (m, 2H), 4.69 – 4.60 (m, 1H), 3.99 – 3.93 (m, 1H), 3.45 (s, 3H), 2.86 – 2.81 (m, 2H), 2.80 – 2.70 (m, 1H), 2.51 (dddt, *J* = 13.4, 9.6, 7.5, 1.0 Hz, 1H), 0.89 (s, 9H), 0.14 (s, 3H), 0.10 (s, 3H).

^{13}C NMR (101 MHz, $CDCl_3$): δ 203.72, 174.75, 134.36, 117.69, 93.57, 78.43, 74.59, 71.85, 57.40, 56.61, 32.50, 28.17, 25.71, 18.14, -4.62, -5.49.

FTIR(NaCl, thin film): 2953, 2931, 2857, 1800, 1732, 1642, 1471, 1463, 1442, 1362 cm^{-1}.

HRMS (ESI): calc'd for $[M+H]^+$ 371.1884, found 371.1888.

$[\alpha]_D^{25}$ = –27.4 ° (*c* = 1.0, $CHCl_3$).

Preparation of benzyl ether 261

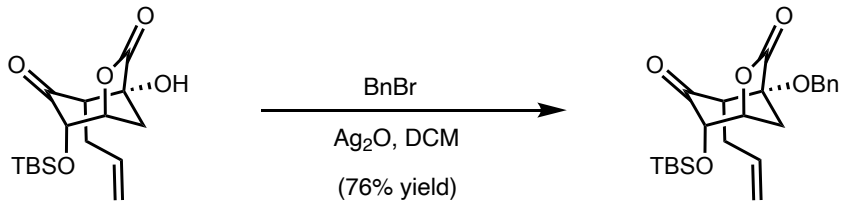

240 **261**

An oven-dried 100 mL round-bottom flask was charged with lactone **240** (800 mg, 2.45 mmol, 1 equiv) and 50 mL anhydrous DCM. Then, Ag_2O (1.7 g, 7.3 mmol, 3 equiv) and BnBr (1.47 mL, 12.3 mmol, 5 equiv) were added. Stirring continued for 3 days until TLC analysis indicated the

complete consumption of starting material. The reaction mixture was next diluted with EtOAc (20 mL), followed by filtration over a celite plug. The solution was concentrated *in vacuo*. The crude residue was purified by SiO_2 flash chromatography (10 to 20 % EtOAc/hexanes) to afford benzyl ether **261** (775 mg, 1.8 mmol, 76% yield) as a colorless oil.

TLC (20% EtOAc/hexanes): R_f 0.5 (UV, CAM).

^{1}H NMR (400 MHz, $CDCl_3$): δ 7.42 – 7.29 (m, 5H), 5.85 – 5.67 (m, 1H), 5.10 – 5.00 (m, 2H), 4.74 (d, *J* = 10.9 Hz, 1H), 4.67 – 4.62 (m, 2H), 4.58 – 4.49 (m, 1H), 4.00 (dt, *J* = 4.1, 1.2 Hz, 1H), 2.92 – 2.77 (m, 3H), 2.73 – 2.61 (m, 1H), 2.60 – 2.44 (m, 1H), 0.92 – 0.88 (m, 9H), 0.15 (s, 3H), 0.12 (s, 3H).

^{13}C NMR (101 MHz, $CDCl_3$): δ 203.77, 174.64, 137.41, 134.29, 128.67, 128.16, 127.82, 117.82, 79.20, 74.43, 72.01, 67.27, 56.92, 32.32, 28.02, 25.72, 18.16, -4.59, -5.19.

Preparation of 2-methylthio-1,3-dithiane 248

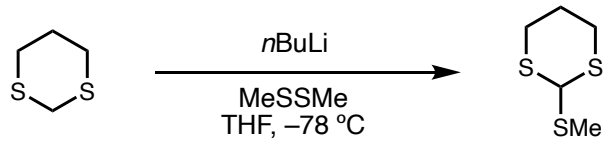

262 **248**

An oven-dried 250 mL round-bottom flask was charged with 1,3-dithiane **262** (1.5 g, 12.4 mmol, 1 equiv) and 60 mL anhydrous THF. The reaction mixture was cooled to –30 ºC via acetone/dry ice bath, and the stirring continued for 15 min. Then, *n*-BuLi solution (2.5M in hexane, 5.2 mL, 13.1 mmol, 1.05 equiv) was added dropwise at –30 ºC. Stirring continued at –30 ºC for 1h. The reaction mixture was further cooled to –78 ºC via acetone/dry ice bath, and the stirring continued for 15 min. MeSSMe (1.65 mL, 18.6 mmol, 1.5 equiv) in 30 mL anhydrous THF was cooled to –78 ºC and cannulated into the 250 mL flask dropwise. Stirring continued at –78 ºC for

1h. The flask was allowed to warm to room temperature and stirring continued overnight (*ca.* 12h). The reaction mixture was next treated with EtOAc (50 mL) followed by sat. aq. NH_4Cl (100 mL). The resulting two layers were separated and the aqueous layer extracted with EtOAc (3 × 50 mL). The combined organic layers were washed with brine (80 mL), dried over Na_2SO_4, filtered, and concentrated *in vacuo*. The crude residue was purified by Kugelrohr distillation. Residue 1,3-dithiane **73** first sublimed at 100 ºC under high vacuum. 2-methylthio-1,3-dithiane **248** (1.2 g, 58% yield) was afforded at 120 ºC under high vacuum. Spectral data of 2-methylthio-1,3-dithiane **248** matched that was previously reported.[27]

Preparation of ketone 249

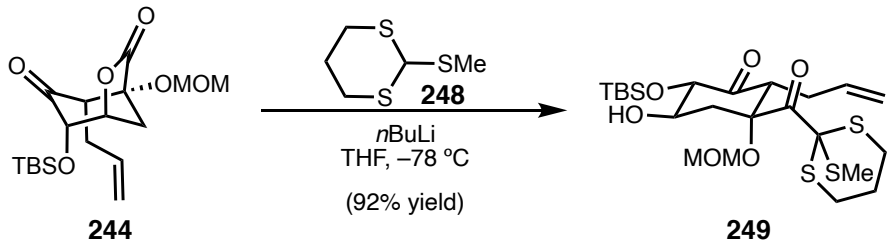

An oven-dried 25 mL round-bottom flask was charged with 2-methylthio-1,3-dithiane **248** (163 mg, 0.98 mmol, 1.1 equiv) and 4 mL anhydrous THF. The reaction mixture was cooled to –78 ºC via acetone/dry ice bath, and the stirring continued for 15 min. Then, *n*-BuLi solution (2.5M in hexane, 0.4 mL, 1.02 mmol, 1.15 equiv) was added dropwise. Stirring continued for 20 min at –78 ºC. Lactone **244** (330 mg, 0.89 mol, 1 equiv) in 4 mL anhydrous THF was added dropwise via cannula over 15 min, [Note: Lactone **244** was azeotroped with PhH three times immediately prior to use], before another portion of THF (1 mL) was used to render the transfer quantitative. After another 10 min at –78 ºC, TLC analysis indicated the complete consumption of starting material. The reaction mixture was quenched with the addition of sat. aq. NH_4Cl (10 mL) and then warmed to ambient temperature and diluted with Et_2O (10 mL). The layers were separated and the aqueous

layer was extracted with Et_2O (3 × 10 mL). The combined organic layers were washed with brine (30 mL), dried over Na_2SO_4, filtered, and concentrated *in vacuo*. The crude residue was purified by SiO_2 flash chromatography (10 to 20 % EtOAc/hexanes) to afford ketone **249** (440 mg, 0.82 mmol, 92% yield) as a colorless oil.

TLC (20% EtOAc/hexanes): R_f 0.42(UV, CAM).

^{1}H NMR (400 MHz, $CDCl_3$): δ 5.77 (dddd, *J* = 17.4, 10.2, 7.2, 6.1 Hz, 1H), 5.02 (dt, *J* = 17.2, 1.6 Hz, 1H), 4.96 (ddt, *J* = 10.2, 2.1, 1.1 Hz, 1H), 4.84 (d, *J* = 7.6 Hz, 1H), 4.63 (d, *J* = 7.6 Hz, 1H), 4.18 (dd, *J* = 8.9, 1.2 Hz, 1H), 4.10 (ddd, *J* = 14.6, 7.8, 3.4 Hz, 1H), 3.45 (dd, *J* = 7.6, 2.7 Hz, 1H), 3.32 – 3.13 (m, 6H), 2.99 – 2.64 (m, 5H), 2.52 – 2.45 (m, 1H), 2.09 – 2.01 (m, 1H), 1.98 (s, 3H), 1.92 – 1.79 (m, 2H), 0.92 (d, *J* = 0.8 Hz, 9H), 0.15 (s, 3H), 0.02 (s, 3H).

^{13}C NMR (101 MHz, $CDCl_3$): δ 202.34, 195.42, 136.37, 116.47, 93.27, 89.39, 83.85, 72.81, 67.39, 56.33, 55.83, 37.90, 27.87, 27.80, 27.56, 26.04, 24.23, 18.67, 16.72, -4.12, -5.19.

FTIR(NaCl, thin film): 2951, 2926, 1739, 1682, 1641, 1505, 1471, 1422, 1360, 1256 cm^{-1}.

HRMS (ESI): calc'd for $[M+H]^+$ 537.1829, found 537.1824.

$[\alpha]_D^{25}$ = –0.7 ° (*c* = 1.0, $CHCl_3$).

Preparation of acetate 250

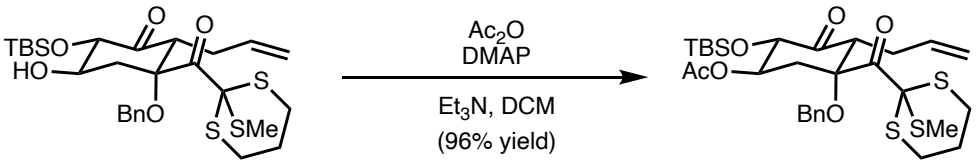

249 **250**

An oven-dried 50 mL round bottom flask was charged with ketone **249** (560 mg, 0.96 mmol, 1 equiv), acetic anhydride (0.11 mL, 1.15 mmol, 1.2 equiv), and 19 mL anhydrous DCM. 4-dimethylaminopyridine (11.7 mg, 0.096 mmol, 0.1 equiv) and Et_3N (0.2 mL, 1.44 mmol, 1.5

equiv) were next added to the solution. The reaction mixture was stirred at ambient temperature (*ca.* 1 h) until at which point TLC analysis indicated the full consumption of starting material. The reaction was quenched with sat. aq. NH_4Cl (10 mL). The layers were separated and the aqueous layer was extracted with ethyl acetate (3 × 10 mL). The combined layers were washed with brine (10 mL), dried over Na_2SO_4, filtered, and concentrated *in vacuo*. The crude residue was clean enough to be directly taken into the next step.

TLC (20% EtOAc/hexanes): R_f 0.36 (UV, CAM).

^{1}H NMR (400 MHz, $CDCl_3$): δ 7.43 – 7.35 (m, 2H), 7.29 (ddd, *J* = 8.0, 7.1, 1.0 Hz, 2H), 7.25 – 7.20 (m, 1H), 5.86 (dddd, *J* = 17.6, 10.1, 7.5, 6.1 Hz, 1H), 5.08 (dq, *J* = 17.2, 1.5 Hz, 1H), 5.02 – 4.89 (m, 2H), 4.66 (d, *J* = 10.7 Hz, 1H), 4.39 – 4.32 (m, 2H), 3.45 – 3.31 (m, 2H), 3.25 (dd, *J* = 14.5, 5.0 Hz, 1H), 3.08 (ddd, *J* = 14.6, 11.6, 8.8 Hz, 2H), 2.89 (dddd, *J* = 13.8, 4.8, 3.2, 1.2 Hz, 1H), 2.85 – 2.63 (m, 2H), 2.12 (s, 3H), 2.10 – 2.04 (m, 1H), 2.03 (s, 3H), 1.99 – 1.81 (m, 1H), 0.89 (s, 9H), 0.13 (s, 3H), 0.01 (s, 3H).

^{13}C NMR (101 MHz, $CDCl_3$): δ 200.81, 192.88, 170.47, 137.72, 136.63, 128.21, 127.56, 127.46, 116.58, 87.01, 80.15, 74.26, 67.33, 66.20, 55.67, 35.18, 28.34, 27.87, 27.25, 25.75, 24.33, 21.30, 18.67, 16.64, -4.32, -5.40.

FTIR(NaCl, thin film): 2927, 2855, 1743, 1689, 1644, 1538, 1496, 1489, 1360, 1231 cm^{-1}.

HRMS (ESI): calc'd for $[M+ NH_4]^+$ 642.2408, found 642.2413.

$[\alpha]_D^{25}$ = –83.3° (*c* = 1.0, $CHCl_3$).

Preparation of ketoester 251

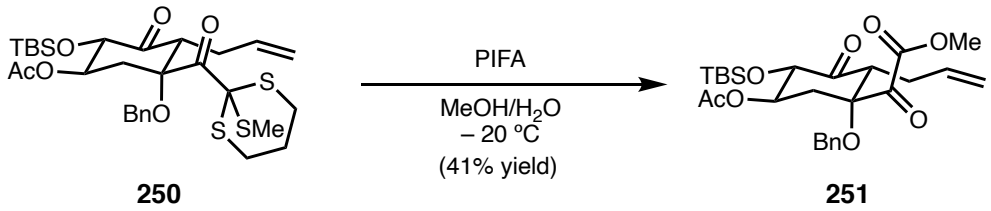

250 **251**

An oven-dried 25 mL round bottom flask was charged with ketone **250** (135 mg, 0.22 mmol, 1 equiv),12 mL MeOH, and 1 mL distilled water. The reaction mixture was cooled to –20 ºC using dry ice/acetone bath and stirring continued for 15 min. (Bis(trifluoroacetoxy)iodo)benzene (PIFA) (278 mg, 0.65 mmol, 3 equiv) was added in three portions over 1h at –20 ºC. Stirring continued until at which point TLC analysis indicated the full consumption of starting material. The reaction was quenched with sat. aq. $NaHCO_3$ (10 mL) and sat. aq. $Na_2S_2O_3$ (5 mL). The layers were separated and the aqueous layer was extracted with ethyl acetate (3 × 10 mL). The combined layers were washed with brine (10 mL), dried over Na_2SO_4, filtered, and concentrated *in vacuo*. The crude residue was purified by SiO_2 flash chromatography (10 to 20 % EtOAc/hexanes) to afford ketoester **251** (46 mg, 0.089 mmol, 41% yield) as a colorless oil.

TLC (20% EtOAc/hexanes): R_f 0.25 (UV, CAM).

^{1}H NMR (400 MHz, $CDCl_3$): δ 7.36 – 7.27 (m, 5H), 5.79 – 5.64 (m, 1H), 5.04 – 4.96 (m, 2H), 4.95 (d, *J* = 1.3 Hz, 1H), 4.68 (s, 2H), 4.40 (dd, *J* = 9.7, 1.1 Hz, 1H), 3.84 (s, 3H), 3.21 (ddd, *J* = 8.3, 4.0, 1.1 Hz, 1H), 2.90 – 2.76 (m, 2H), 2.53 (dd, *J* = 14.1, 11.6 Hz, 1H), 2.10 (s, 3H), 2.07 – 1.97 (m, 1H), 0.91 (s, 9H), 0.15 (s, 3H), 0.03 (s, 3H).

^{13}C NMR (101 MHz, $CDCl_3$): δ 201.01, 193.77, 170.28, 162.68, 137.30, 136.12, 128.34, 127.69, 127.36, 117.26, 85.30, 80.08, 73.86, 66.50, 54.89, 53.37, 32.71, 27.57, 25.73, 21.13, 18.67, -4.36, -5.40.

FTIR(NaCl, thin film): 2924, 2853, 1739, 1731, 1455, 1361, 1289, 1229, 1169, 1131 cm^{-1}.

HRMS (ESI): calc'd for $[M+NH_4]^+$ 536.2674, found 536.2679.

$[\alpha]_D^{25}$ = –28.7 ° (*c* = 0.3, $CHCl_3$).

Preparation of propargyl alcohol 257

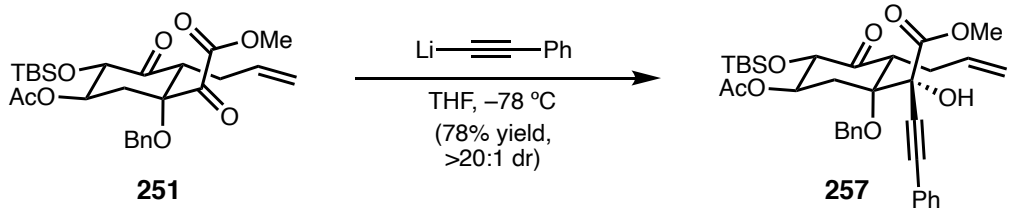

An oven-dried 1 dram vial was charged with ketoester **251** (10 mg, 0.0192 mmol, 1 equiv) [Note: ketoester **251** was azeotroped with PhH three times immediately prior to use], and 0.4 mL anhydrous THF. The reaction mixture was cooled to –78 ºC via acetone/dry ice bath, and the stirring continued for 15 min. Then, lithium phenylacetylene solution (0.4 M in THF, 51 µL, 0.02 mmol, 1.05 equiv) was added dropwise. Stirring continued for 20 min at –78 ºC until TLC analysis indicated the complete consumption of starting material. The reaction mixture was quenched with the addition of sat. aq. NH_4Cl (1 mL) and then warmed to ambient temperature and diluted with Et_2O (1 mL). The layers were separated and the aqueous layer was extracted with Et_2O (3 × 1 mL). The combined organic layers were washed with brine (2 mL), dried over Na_2SO_4, filtered, and concentrated *in vacuo*. The crude residue was purified by SiO_2 flash chromatography (10 to 20 % EtOAc/hexanes) to afford alcohol **257** (7.6 mg, 0.015 mmol, 78% yield, > 20:1 dr) as a colorless oil.

TLC (20% EtOAc/hexanes): R_f 0.31 (UV, CAM).

^{1}H NMR (400 MHz, $CDCl_3$): δ 7.45 – 7.28 (m, 10H), 5.85 – 5.70 (m, 1H), 5.09 (dd, *J* = 11.1, 1.4 Hz, 1H), 5.02 – 4.87 (m, 4H), 4.29 (dd, *J* = 9.8, 1.4 Hz, 1H), 3.96 – 3.91 (m, 3H), 3.86 (d, *J* = 1.4

Hz, 1H), 3.34 (dd, *J* = 14.8, 4.9 Hz, 1H), 2.72 (d, *J* = 4.5 Hz, 3H), 2.49 (ddd, *J* = 14.9, 11.8, 1.3 Hz, 1H), 2.11 (s, 3H), 0.90 (s, 9H), 0.14 (s, 3H), 0.01 (s, 3H).

^{13}C NMR (101 MHz, $CDCl_3$): δ 02.37, 170.59, 170.45, 137.65, 137.31, 131.90, 129.41, 128.61, 128.53, 127.79, 127.39, 121.55, 115.68, 88.64, 86.61, 82.83, 79.84, 76.02, 73.56, 66.19, 56.39, 54.29, 33.78, 27.27, 25.76, 21.26, 18.69, -4.31, -5.40.

FTIR(NaCl, thin film): 2928, 2854, 1741, 1636, 1540, 1490, 1456, 1359, 1237, 1162 cm^{-1}.

HRMS (ESI): calc'd for $[M+K]^+$ 659.2437, found 659.2442.

$[\alpha]_D^{25}$ = –50.9 ° (*c* = 0.5, $CHCl_3$).

Preparation of lactone 258

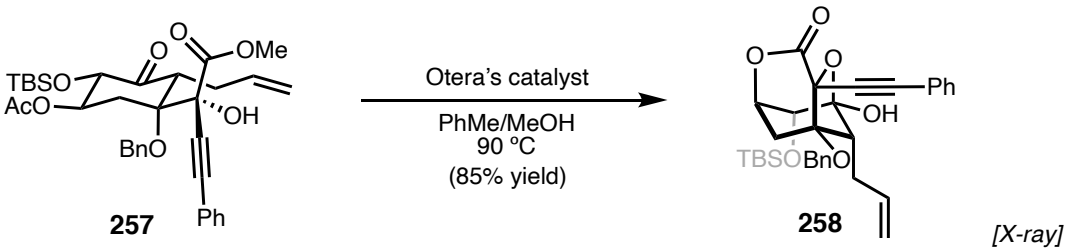

An oven-dried, 100 mL round-bottomed flask was charged with alcohol **257** (7.6 mg, 0.015 mmol, 1 equiv), Otera's catalyst (4.5 mg, 0.0075 mmol, 0.5 equiv), 0.2 mL toluene, and 50 µL MeOH. The solution was heated to 90 ºC via an oil bath. Stirring was continued (*ca.* 12 h) until at which point TLC analysis indicated the full consumption of starting material. The reaction mixture was cooled down to ambient temperature and concentrated *in vacuo*. The crude residue was purified via SiO_2 flash chromatography (10 to 20% EtOAc/hexanes) to afford lactone **258** (7 mg, 0.013 mmol, 85% yield) as a white solid. **258** was crystallized and characterized by X-ray crystallography.

TLC (30% EtOAc/hexanes): R_f 0.7 (UV, CAM).

^{1}H NMR (400 MHz, $CDCl_3$): δ 7.36 – 7.27 (m, 7H), 7.26 – 7.18 (m, 3H), 6.10 – 5.96 (m, 1H), 5.18 (dq, *J* = 17.2, 1.6 Hz, 1H), 5.09 (ddt, *J* = 10.1, 2.1, 1.1 Hz, 1H), 4.74 – 4.64 (m, 3H), 4.43 (q, *J* = 2.9 Hz, 1H), 3.94 (q, *J* = 1.7 Hz, 1H), 2.99 (s, 1H), 2.86 – 2.74 (m, 1H), 2.61 (ddt, *J* = 8.9, 5.5, 1.9 Hz, 1H), 2.55 – 2.41 (m, 3H), 2.39 – 2.30 (m, 1H), 2.30 – 2.21 (m, 1H), 0.92 (s, 9H), 0.16 (d, *J* = 6.2 Hz, 6H).

^{13}C NMR (101 MHz, $CDCl_3$): δ 168.65, 137.83, 136.44, 132.32, 129.11, 128.50, 128.22, 127.73, 127.10, 121.77, 116.92, 104.15, 91.78, 85.61, 81.35, 80.71, 76.62, 73.21, 67.39, 53.45, 28.56, 27.85, 25.84, 18.09, -4.44, -5.24.

FTIR(NaCl, thin film): 2926, 2855, 2356, 2344, 2329, 1734, 1669, 1648, 1623, 1578 cm^{-1}.

HRMS (ESI): calc'd for $[M+H]^+$ 547.251, found 547.2505.

$[\alpha]_D^{25}$ = –5.8 ° (*c* = 0.1, $CHCl_3$).

6.5. References

(1) Teufel, R.; Miyanaga, A.; Michaudel, Q.; Stull, F.; Louie, G.; Noel, J. P.; Baran, P. S.; Palfey, B.; Moore, B. S. *Nature* **2013**, *503* (7477), 552–556.

(2) Koser, L.; Lechner, V. M.; Bach, T. *Angew. Chem. Int. Ed.* **2021**, *60* (37), 20269–20273.

(3) Konrad, D. B.; Rühmann, K.-P.; Ando, H.; Hetzler, B. E.; Strassner, N.; Houk, K. N.; Matsuura, B. S.; Trauner, D. *Science* **2022**, *377* (6604), 411–415.

(4) Trost, B. M.; Rhee, Y. H. *J. Am. Chem. Soc.* **1999**, *121* (50), 11680–11683.

(5) McDonald, F. E.; Reddy, K. S.; Díaz, Y. *J. Am. Chem. Soc.* **2000**, *122* (18), 4304–4309.

(6) Zacuto, M. J.; Tomita, D.; Pirzada, Z.; Xu, F. *Org. Lett.* **2010**, *12* (4), 684–687.

(7) Schwardt, O.; Koliwer-Brandl, H.; Zimmerli, R.; Mesch, S.; Rossato, G.; Spreafico, M.; Vedani, A.; Kelm, S.; Ernst, B. *Bioorg. Med. Chem.* **2010**, *18* (20), 7239–7251.

(8) Plietker, B. *J. Org. Chem.* **2004**, *69* (24), 8287–8296.

(9) Plietker, B. *J. Org. Chem.* **2003**, *68* (18), 7123–7125.

(10) Li, L.-S.; Wu, Y.-L. *Tetrahedron Lett.* **2002**, 4.

(11) Han, Q.; Yang, L.; Liu, Y.; Wang, Y.; Qiao, C.; Song, J.; Xu, L.; Yang, D.; Chen, S.; Xu, H. *Planta Med.* **2006**, *72* (03), 281–284.

(12) Morita, M.; Kojima, S.; Ohkubo, M.; Koshino, H.; Hashizume, D.; Hirai, G.; Maruoka, K.; Sodeoka, M. *Isr. J. Chem.* **2017**, *57* (3–4), 309–318.

(13) Kumar Das, D.; Pampana, V. K. K.; Chu Hwang, K. *Chem. Sci.* **2018**, *9* (37), 7318–7326.

(14) Otera, J.; Dan-oh, N.; Nozaki, H. *Tetrahedron* **1993**, *49* (15), 3065–3074.

(15) Otera, J.; Danoh, N.; Nozaki, H. *J. Org. Chem.* **1991**, *56* (18), 5307–5311.

(16) Godage, H. Y.; Riley, A. M.; Woodman, T. J.; Thomas, M. P.; Mahon, M. F.; Potter, B. V. L. *J. Org. Chem.* **2013**, *78* (6), 2275–2288.

(17) King, J. F.; Allbutt, A. D. *Can. J. Chem.* **1970**, *48* (11), 1754–1769.

(18) Zhao, Y.-M.; Maimone, T. J. *Angew. Chem. Int. Ed.* **2015**, *54* (4), 1223–1226.

(19) Sato, M.; Sakaki, J.; Sugita, Y.; Yasuda, S.; Sakoda, H.; Kaneko, C. *Tetrahedron* **1991**, *47* (30), 5689–5708.

(20) Preindl, J.; Jouvin, K.; Laurich, D.; Seidel, G.; Fürstner, A. *Chem. - Eur. J.* **2016**, *22* (1), 237–247.

(21) Qiu, S.-Q.; Ahmad, T.; Xu, Y.-H.; Loh, T.-P. *J. Org. Chem.* **2019**, *84* (11), 6729–6736.

(22) Manthey, M. K.; González-Bello, C.; Abell, C. *J. Chem. Soc. Perkin 1* **1997**, No. 5, 625–628.

(23) Lee, J. Y.; Lim, K.-C.; Meng, X.; Kim, S. *Synlett* **2010**, *2010* (11), 1647–1650.

(24) Funk, R. L.; Knapp, S. In *Encyclopedia of Reagents for Organic Synthesis*; John Wiley & Sons, Ltd, 2007.

(25) Barbero, M.; Cadamuro, Si.; Degani, I.; Dughera, S.; Fochi, R. *J. Org. Chem.* **1995**, *60* (19), 6017–6024.

(26) J. Procter, D. *J. Chem. Soc. Perkin 1* **2001**, *0* (4), 335–354.

(27) Page, P. C. B.; Wilkes, R. D.; Witty, M. J. .

(28) Yates, P.; Seif-El-Nasr, A.; Stanton, J.; Krepinsky, J. J. *Can. J. Chem.* **1991**, *69* (3), 415–422.

(29) Liu, Y.; Chen, G.; Chen, X.; Chen, S.-X.; Gan, L.-S.; Yuan, T. *J. Nat. Prod.* **2018**, *81* (9), 2115–2119.

(30) Ogura, K. *Pure Appl. Chem.* **1987**, *59* (8), 1033–1039.

(31) Ogura, K.; McKinney, J. A.; Fujiwara, K. In *Encyclopedia of Reagents for Organic Synthesis*; John Wiley & Sons, Ltd, 2009.

(32) Valiulin, R. A.; Kutateladze, A. G. *J. Org. Chem.* **2008**, *73* (1), 335–338.

(33) Ju, L.; Lippert, A. R.; Bode, J. W. *J. Am. Chem. Soc.* **2008**, *130* (13), 4253–4255.

(34) Haughey, M. B.; Christensen, K. E.; Poole, D. L.; Donohoe, T. J. *Chem. Sci.* **2021**, *12* (40), 13392–13397.

(35) Stork, G.; Zhao, K. *Tetrahedron Lett.* **1989**, *30* (3), 287–290.

(36) Kawashima, H.; Sakai, M.; Kaneko, Y.; Kobayashi, Y. *Tetrahedron* **2015**, *71* (16), 2387–2392.

(37) Müller, S.; Liepold, B.; Roth, G. J.; Bestmann, H. J. *Synlett* **1996**, *1996* (06), 521–522.

(38) Sánchez-Abella, L.; Fernández, S.; Armesto, N.; Ferrero, M.; Gotor, V. *J. Org. Chem.* **2006**, *71* (14), 5396–5399.

Appendix 4

Spectra Relevant to Chapter 6:

An intermolecular aldol approach toward enterocin

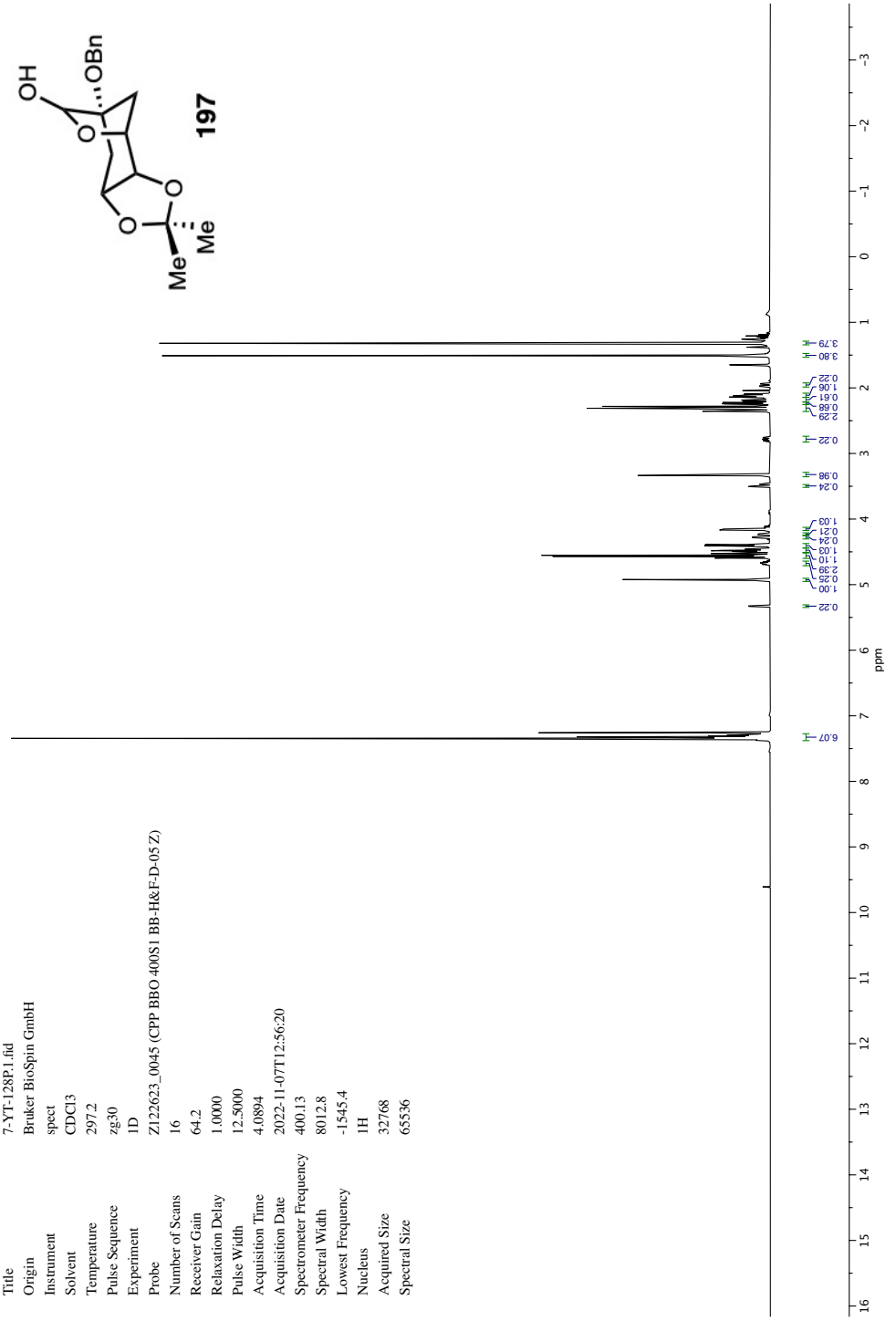

Parameter	Value
Title	7-YT-128P1.fid
Origin	Bruker BioSpin GmbH
Instrument	spect
Solvent	CDCl3
Temperature	297.2
Pulse Sequence	zg30
Experiment	1D
Probe	Z122623_0045 (CPP BBO 400S1 BB-H&F-D-05 Z)
Number of Scans	16
Receiver Gain	64.2
Relaxation Delay	1.0000
Pulse Width	12.5000
Acquisition Time	4.0894
Acquisition Date	2022-11-07T12:56:20
Spectrometer Frequency	400.13
Spectral Width	8012.8
Lowest Frequency	-1545.4
Nucleus	1H
Acquired Size	32768
Spectral Size	65536

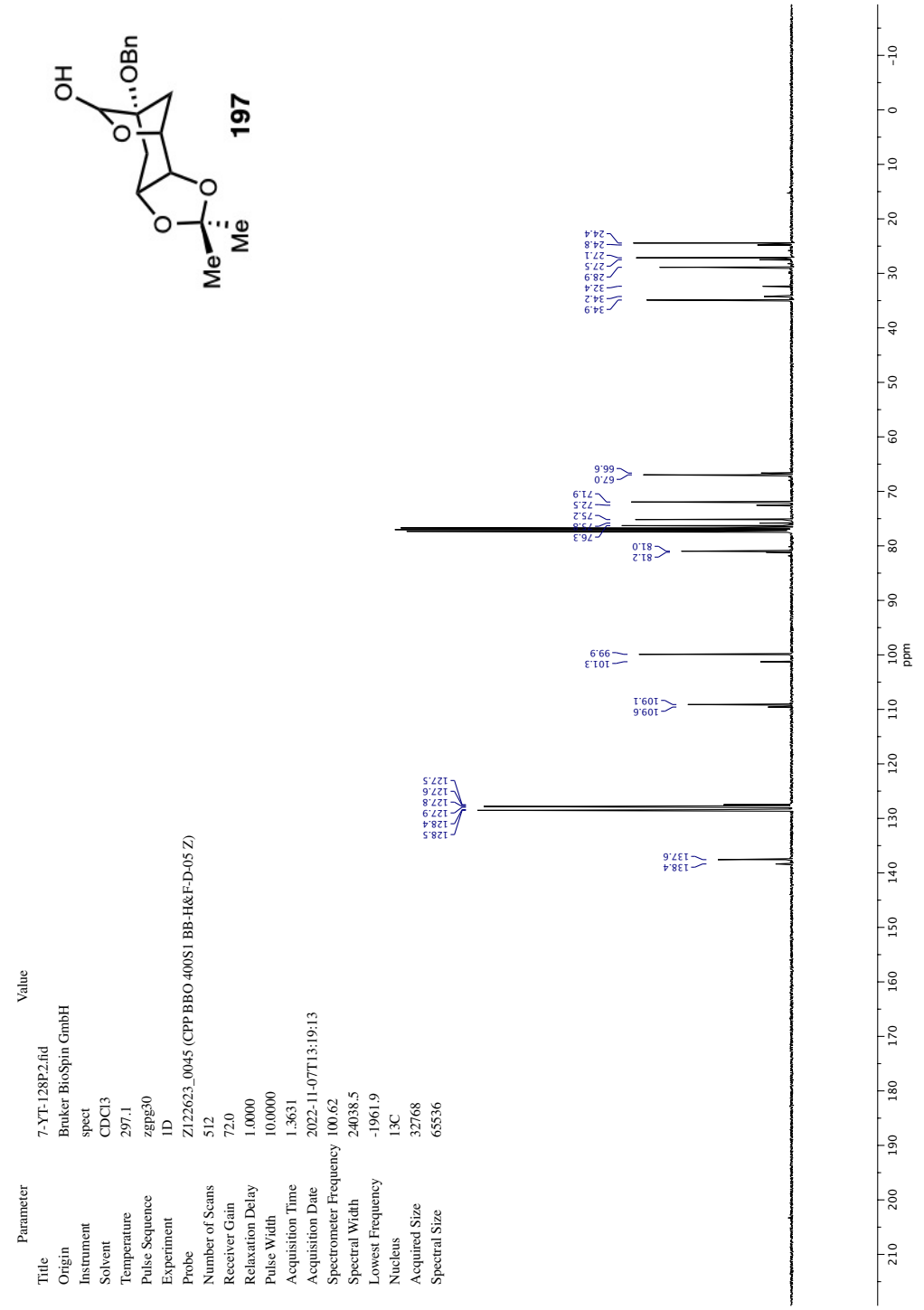
OH
OBn
Me
Me
197
Parameter Value
Title 7-YT-128P2.fid
Origin Bruker BioSpin GmbH
Instrument spect
Solvent CDCl3
Temperature 297.1
Pulse Sequence zgpg30
Experiment 1D
Probe Z122623_0045 (CPP BBO 400S1 BB-H&F-D-05 Z)
Number of Scans 512
Receiver Gain 72.0
Relaxation Delay 1.0000
Pulse Width 10.0000
Acquisition Time 1.3631
Acquisition Date 2022-11-07T13:19:13
Spectrometer Frequency 100.62
Spectral Width 24038.5
Lowest Frequency -1961.9
Nucleus 13C
Acquired Size 32768
Spectral Size 65536
128.5
128.4
127.9
127.8
127.6
127.5
138.4
137.6
109.6
109.1
101.3
99.9
81.2
81.0
76.3
75.2
72.5
71.9
67.0
66.6
34.9
34.2
32.4
28.9
27.5
27.1
24.8
24.4
ppm

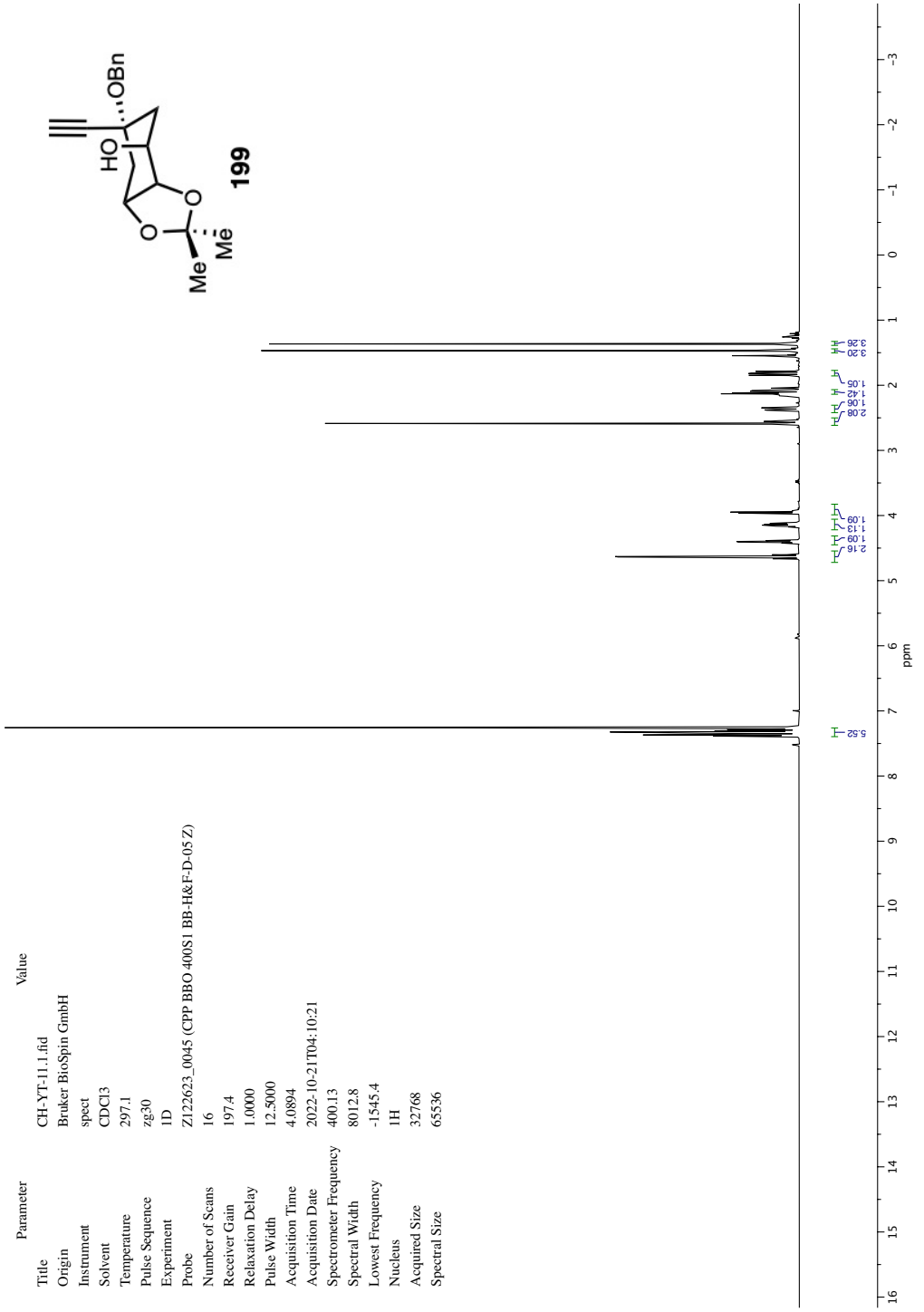

Parameter	Value
Title	CH-YT-11.1.fid
Origin	Bruker BioSpin GmbH
Instrument	spect
Solvent	CDCl3
Temperature	297.1
Pulse Sequence	zg30
Experiment	1D
Probe	Z122623_0045 (CPP BBO 400S1 BB-H&F-D-05 Z)
Number of Scans	16
Receiver Gain	197.4
Relaxation Delay	1.0000
Pulse Width	12.5000
Acquisition Time	4.0894
Acquisition Date	2022-10-21T04:10:21
Spectrometer Frequency	400.13
Spectral Width	8012.8
Lowest Frequency	-1545.4
Nucleus	1H
Acquired Size	32768
Spectral Size	65536

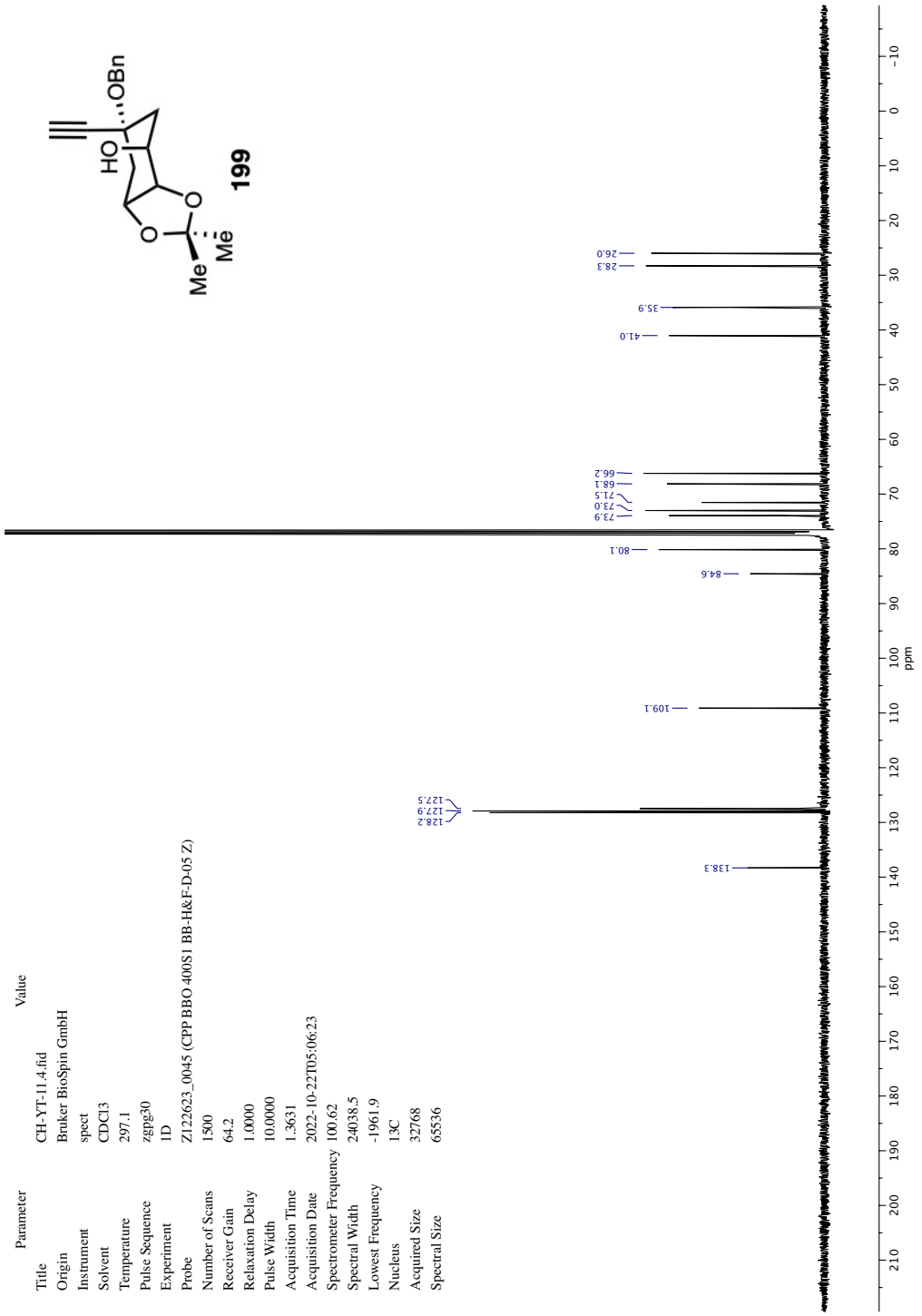

Parameter	Value
Title	CH-YT-11.4.fid
Origin	Bruker BioSpin GmbH
Instrument	spect
Solvent	CDCl3
Temperature	297.1
Pulse Sequence	zgpg30
Experiment	1D
Probe	Z122623_0045 (CPP BBO 400S1 BB-H&F-D-05 Z)
Number of Scans	1500
Receiver Gain	64.2
Relaxation Delay	1.0000
Pulse Width	10.0000
Acquisition Time	1.3631
Acquisition Date	2022-10-22T05:06:23
Spectrometer Frequency	100.62
Spectral Width	24038.5
Lowest Frequency	-1961.9
Nucleus	13C
Acquired Size	32768
Spectral Size	65536

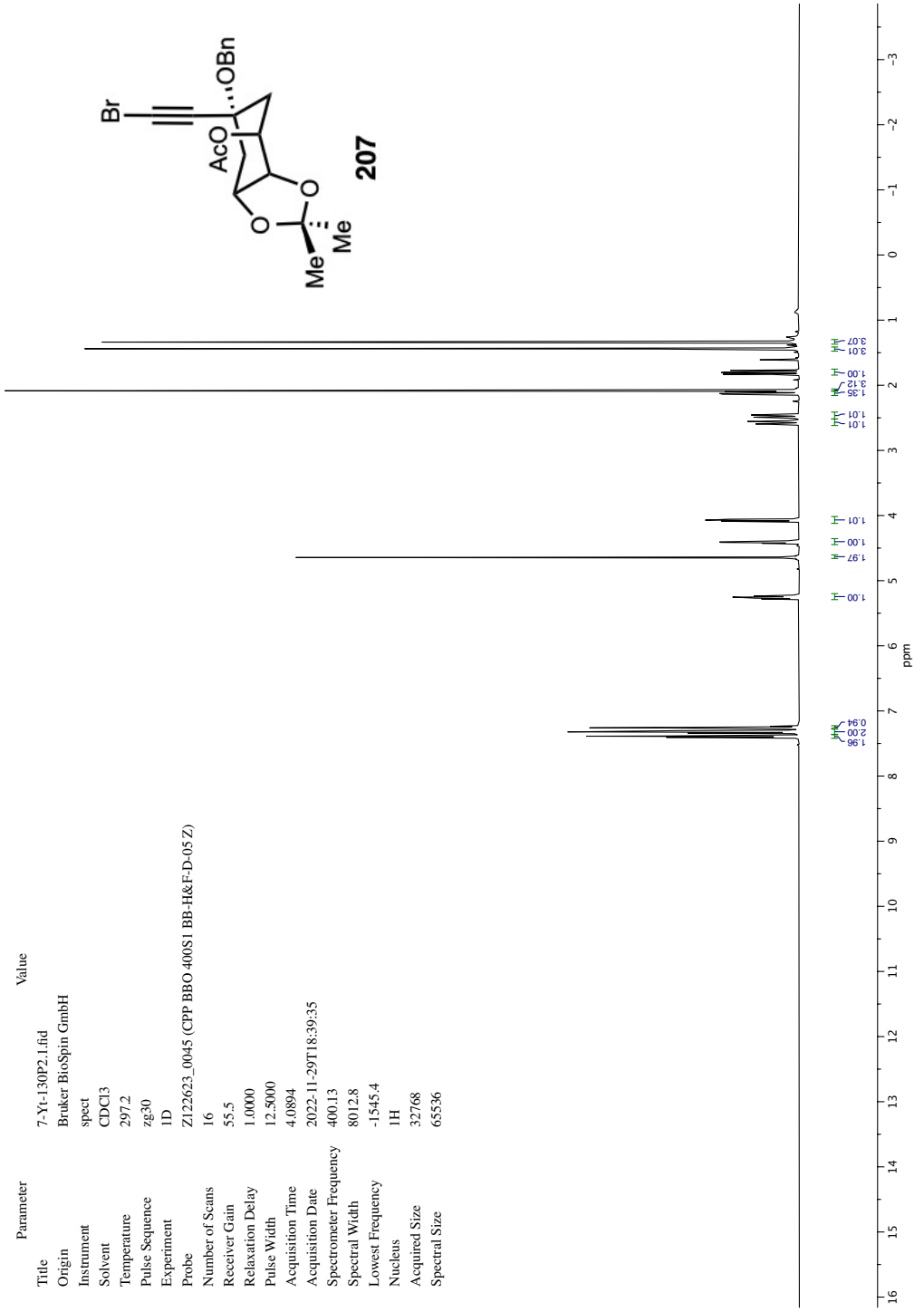

Parameter	Value
Title	7-Yt-130P2.1.fid
Origin	Bruker BioSpin GmbH
Instrument	spect
Solvent	CDCl3
Temperature	297.2
Pulse Sequence	zg30
Experiment	1D
Probe	Z122623_0045 (CPP BBO 400S1 BB-H&F-D-05 Z)
Number of Scans	16
Receiver Gain	55.5
Relaxation Delay	1.0000
Pulse Width	12.5000
Acquisition Time	4.0894
Acquisition Date	2022-11-29T18:39:35
Spectrometer Frequency	400.13
Spectral Width	8012.8
Lowest Frequency	-1545.4
Nucleus	1H
Acquired Size	32768
Spectral Size	65536

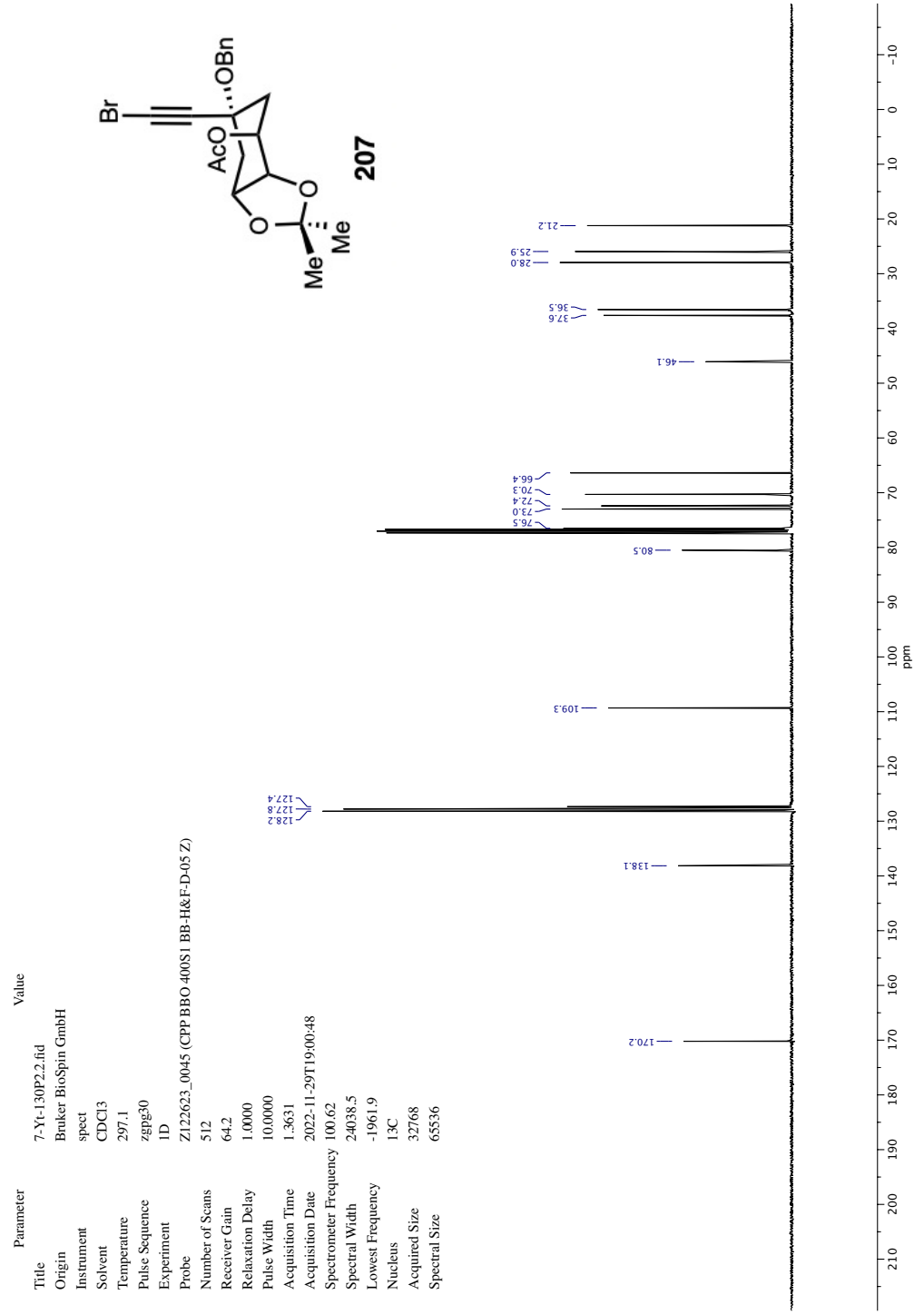
Br
AcO
OBn
Me
Me
207
Parameter Value
Title 7-Yt-130P2.2.fid
Origin Bruker BioSpin GmbH
Instrument spect
Solvent CDCl3
Temperature 297.1
Pulse Sequence zgpg30
Experiment 1D
Probe Z122623_0045 (CPP BBO 400S1 BB-H&F-D-05 Z)
Number of Scans 512
Receiver Gain 64.2
Relaxation Delay 1.0000
Pulse Width 10.0000
Acquisition Time 1.3631
Acquisition Date 2022-11-29T19:00:48
Spectrometer Frequency 100.62
Spectral Width 24038.5
Lowest Frequency -1961.9
Nucleus 13C
Acquired Size 32768
Spectral Size 65536
170.2
138.1
128.2
127.8
127.4
109.3
80.5
76.5
73.0
72.4
70.3
66.4
46.1
37.6
36.5
28.0
25.9
21.2
ppm

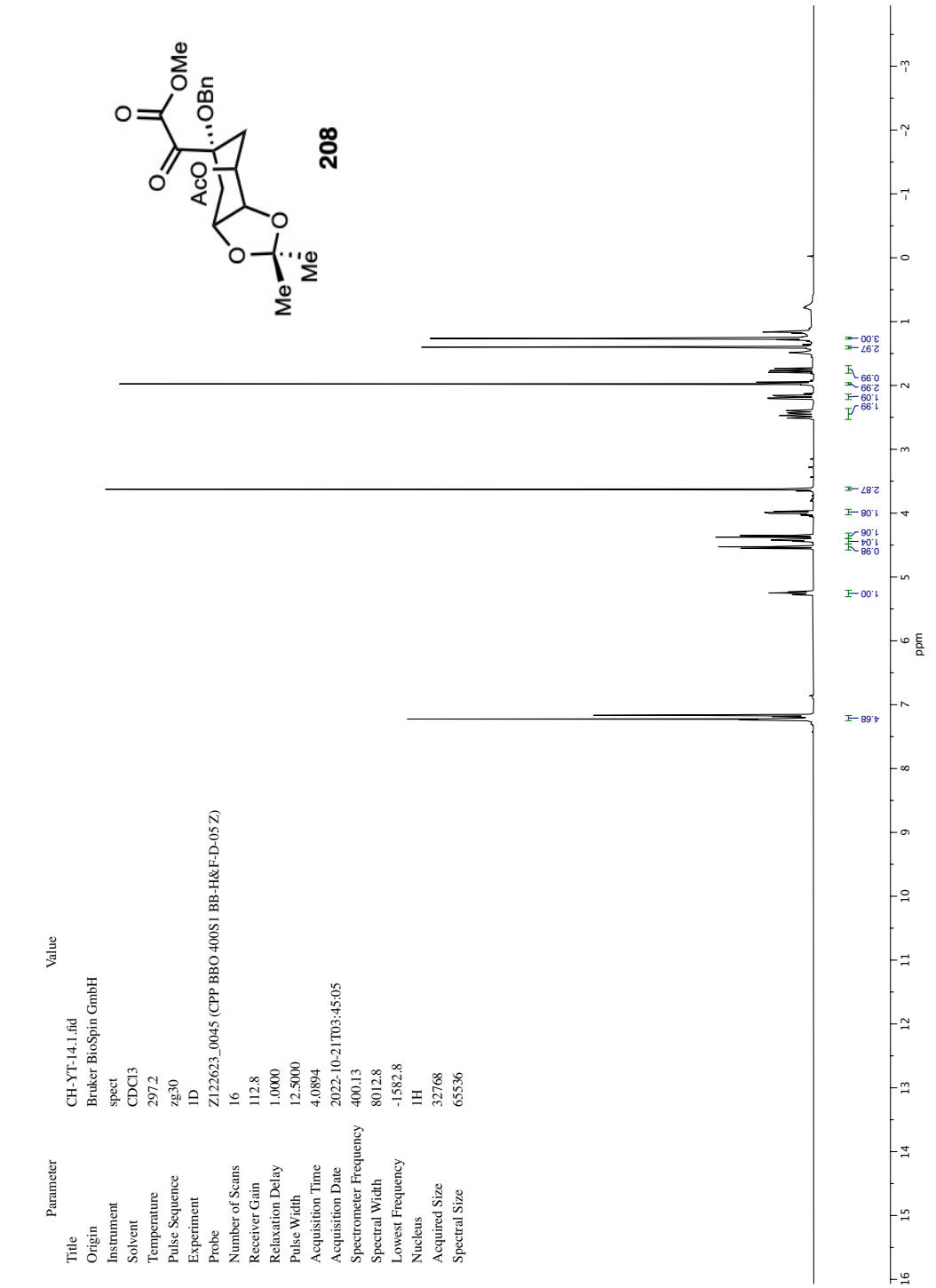

Parameter	Value
Title	CH-YT-14.1.fid
Origin	Bruker BioSpin GmbH
Instrument	spect
Solvent	CDCl3
Temperature	297.2
Pulse Sequence	zg30
Experiment	1D
Probe	Z122623_0045 (CPP BBO 400S1 BB-H&F-D-05 Z)
Number of Scans	16
Receiver Gain	112.8
Relaxation Delay	1.0000
Pulse Width	12.5000
Acquisition Time	4.0894
Acquisition Date	2022-10-21T03:45:05
Spectrometer Frequency	400.13
Spectral Width	8012.8
Lowest Frequency	-1582.8
Nucleus	1H
Acquired Size	32768
Spectral Size	65536

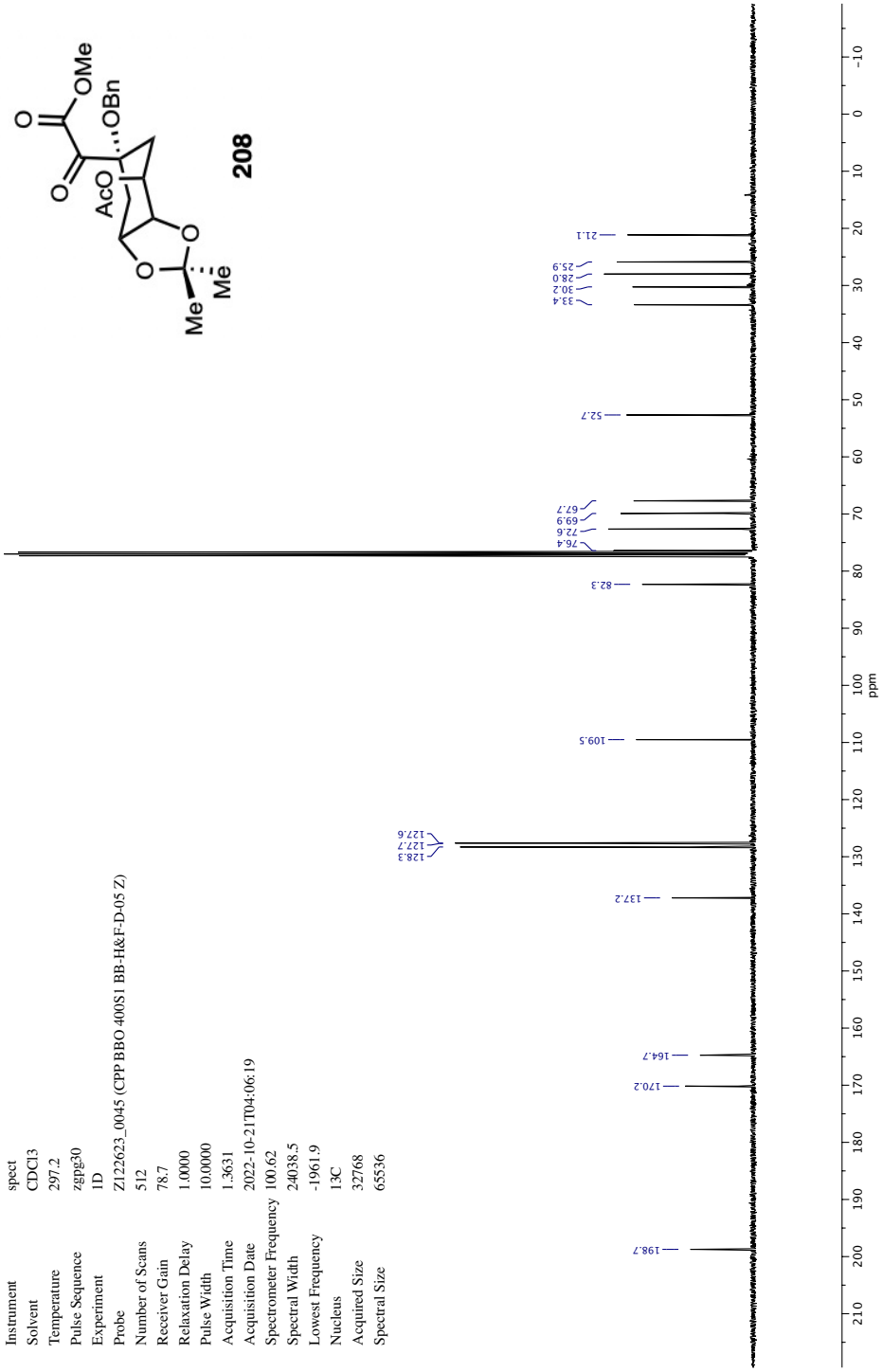

Parameter	Value
Title	CH-YT-14.2.fid
Origin	Bruker BioSpin GmbH
Instrument	spect
Solvent	CDCl3
Temperature	297.2
Pulse Sequence	zgpg30
Experiment	1D
Probe	Z122623_0045 (CPP BBO 400S1 BB-H&F-D-05 Z)
Number of Scans	512
Receiver Gain	78.7
Relaxation Delay	1.0000
Pulse Width	10.0000
Acquisition Time	1.3631
Acquisition Date	2022-10-21T04:06:19
Spectrometer Frequency	100.62
Spectral Width	24038.5
Lowest Frequency	-1961.9
Nucleus	13C
Acquired Size	32768
Spectral Size	65536

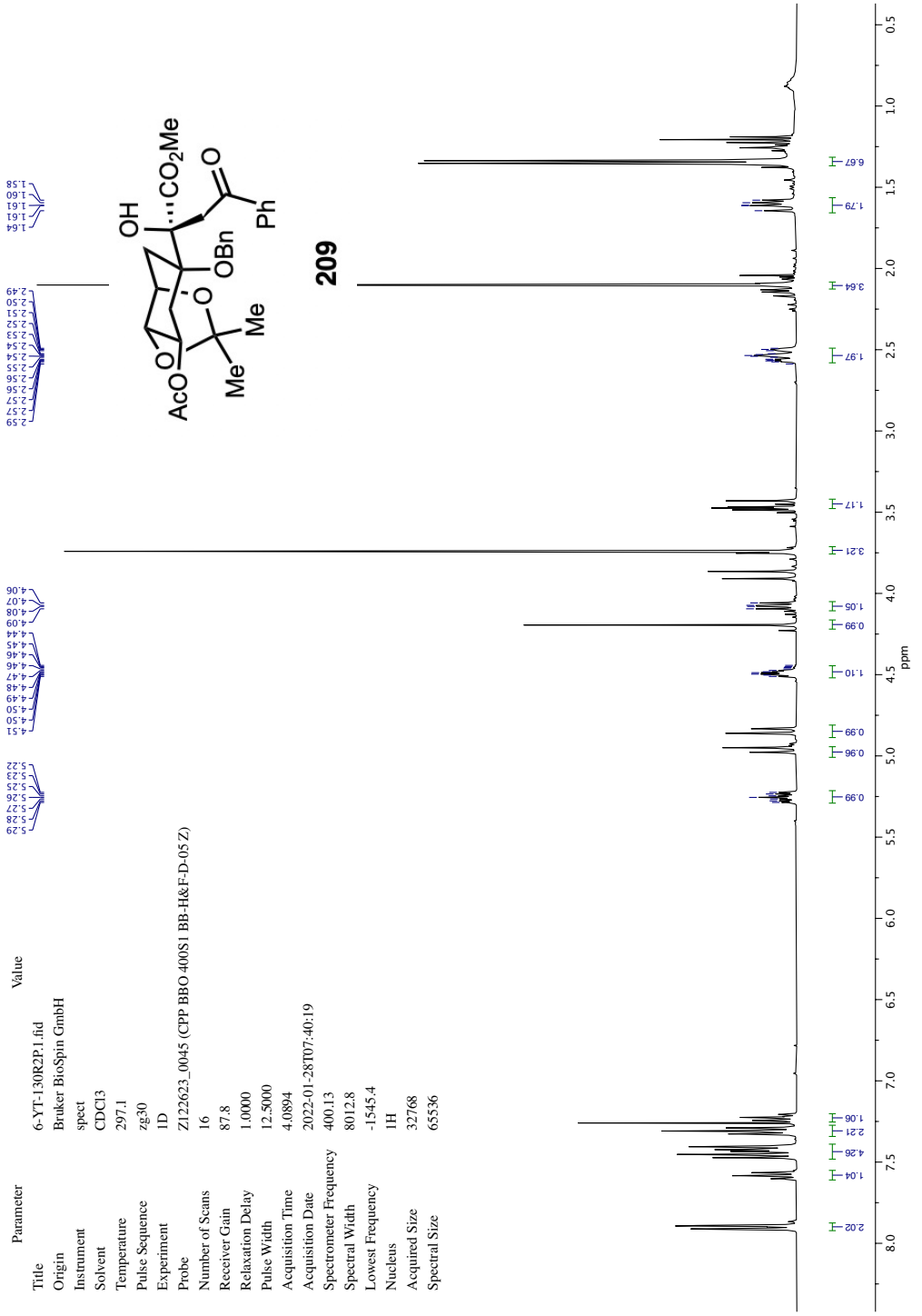

Parameter	Value
Title	6-YT-130R2P1.fid
Origin	Bruker BioSpin GmbH
Instrument	spect
Solvent	CDCl3
Temperature	297.1
Pulse Sequence	zg30
Experiment	1D
Probe	Z122623_0045 (CPP BBO 400S1 BB-H&F-D-05 Z)
Number of Scans	16
Receiver Gain	87.8
Relaxation Delay	1.0000
Pulse Width	12.5000
Acquisition Time	4.0894
Acquisition Date	2022-01-28T07:40:19
Spectrometer Frequency	400.13
Spectral Width	8012.8
Lowest Frequency	-1545.4
Nucleus	1H
Acquired Size	32768
Spectral Size	65536

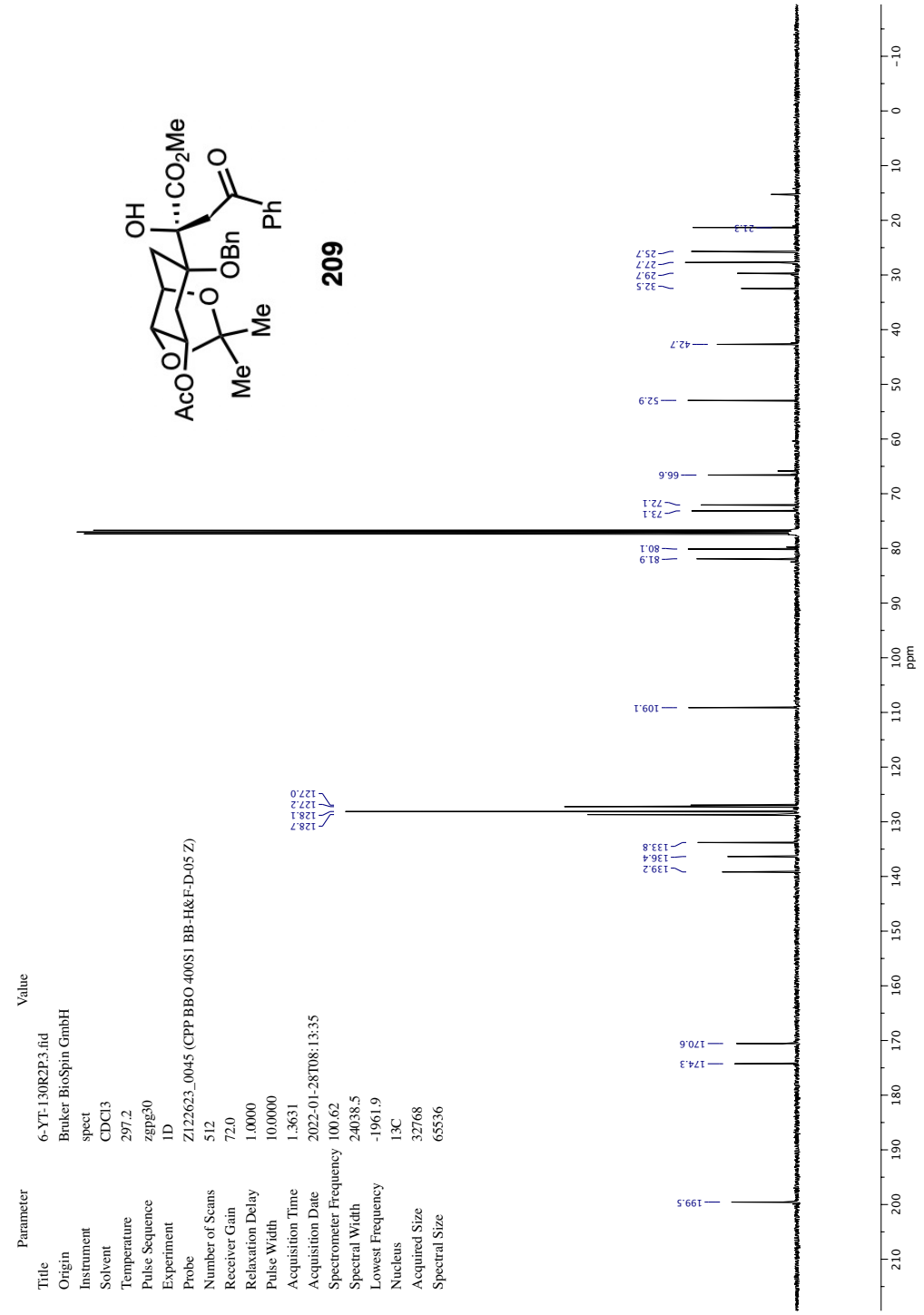

Parameter	Value
Title	6-YT-130R2P3.fid
Origin	Bruker BioSpin GmbH
Instrument	spect
Solvent	CDCl3
Temperature	297.2
Pulse Sequence	zgpg30
Experiment	1D
Probe	Z122623_0045 (CPP BBO 400S1 BB-H&F-D-05 Z)
Number of Scans	512
Receiver Gain	72.0
Relaxation Delay	1.0000
Pulse Width	10.0000
Acquisition Time	1.3631
Acquisition Date	2022-01-28T08:13:35
Spectrometer Frequency	100.62
Spectral Width	24038.5
Lowest Frequency	-1961.9
Nucleus	13C
Acquired Size	32768
Spectral Size	65536

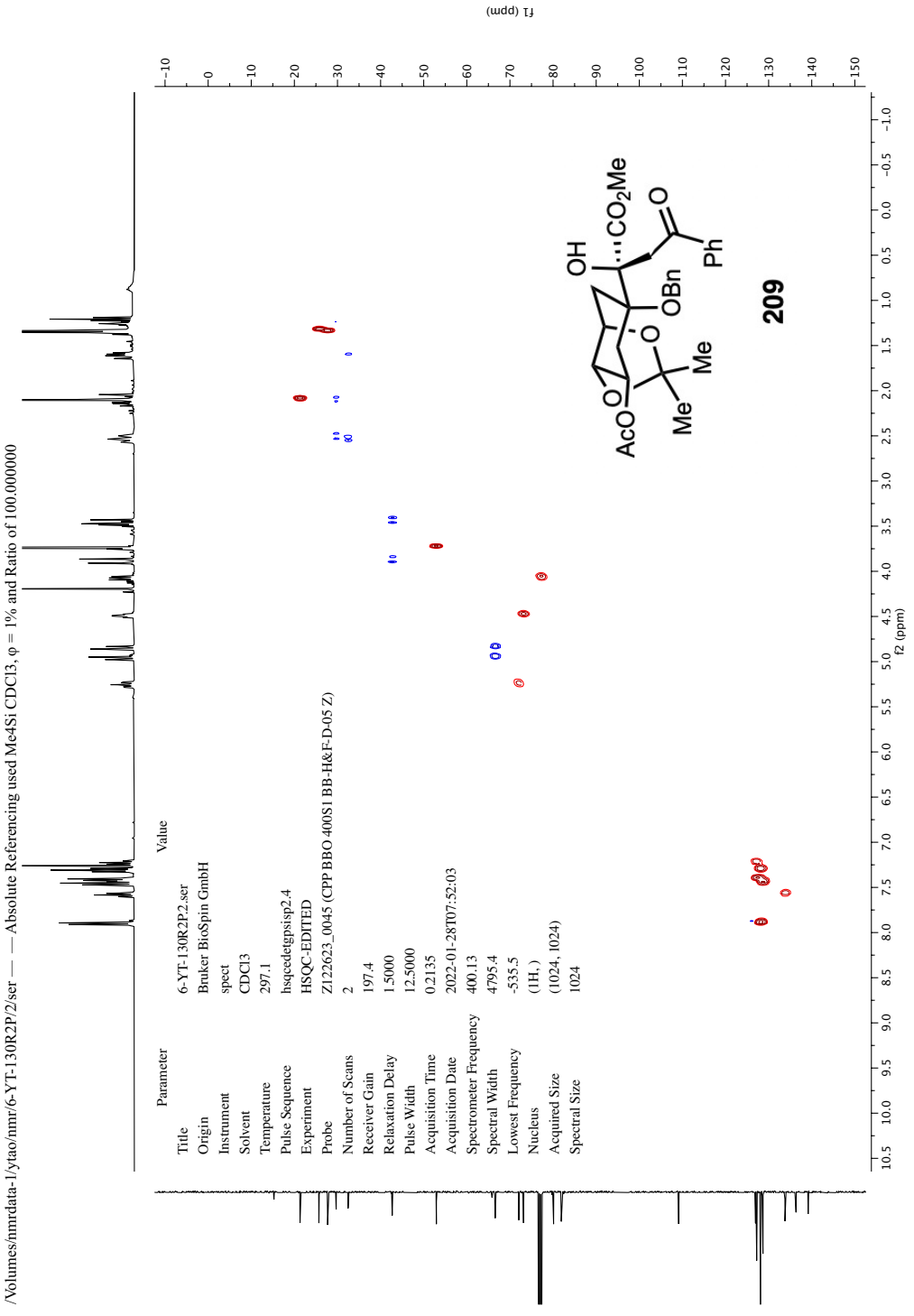
/Volumes/nmrdata-1/ytao/nmr/6-YT-130R2P/2/ser — — Absolute Referencing used Me4Si CDCl3, φ = 1% and Ratio of 100.000000
Parameter Value
Title 6-YT-130R2P2.ser
Origin Bruker BioSpin GmbH
Instrument spect
Solvent CDCl3
Temperature 297.1
Pulse Sequence hsqcedetgpsisp2.4
Experiment HSQC-EDITED
Probe Z122623_0045 (CPP BBO 400S1 BB-H&F-D-05 Z)
Number of Scans 2
Receiver Gain 197.4
Relaxation Delay 1.5000
Pulse Width 12.5000
Acquisition Time 0.2135
Acquisition Date 2022-01-28T07:52:03
Spectrometer Frequency 400.13
Spectral Width 4795.4
Lowest Frequency -535.5
Nucleus (1H,)
Acquired Size (1024, 1024)
Spectral Size 1024
f2 (ppm)
f1 (ppm)
OH
CO2Me
O
OBn
Ph
AcO
O
Me
Me
209

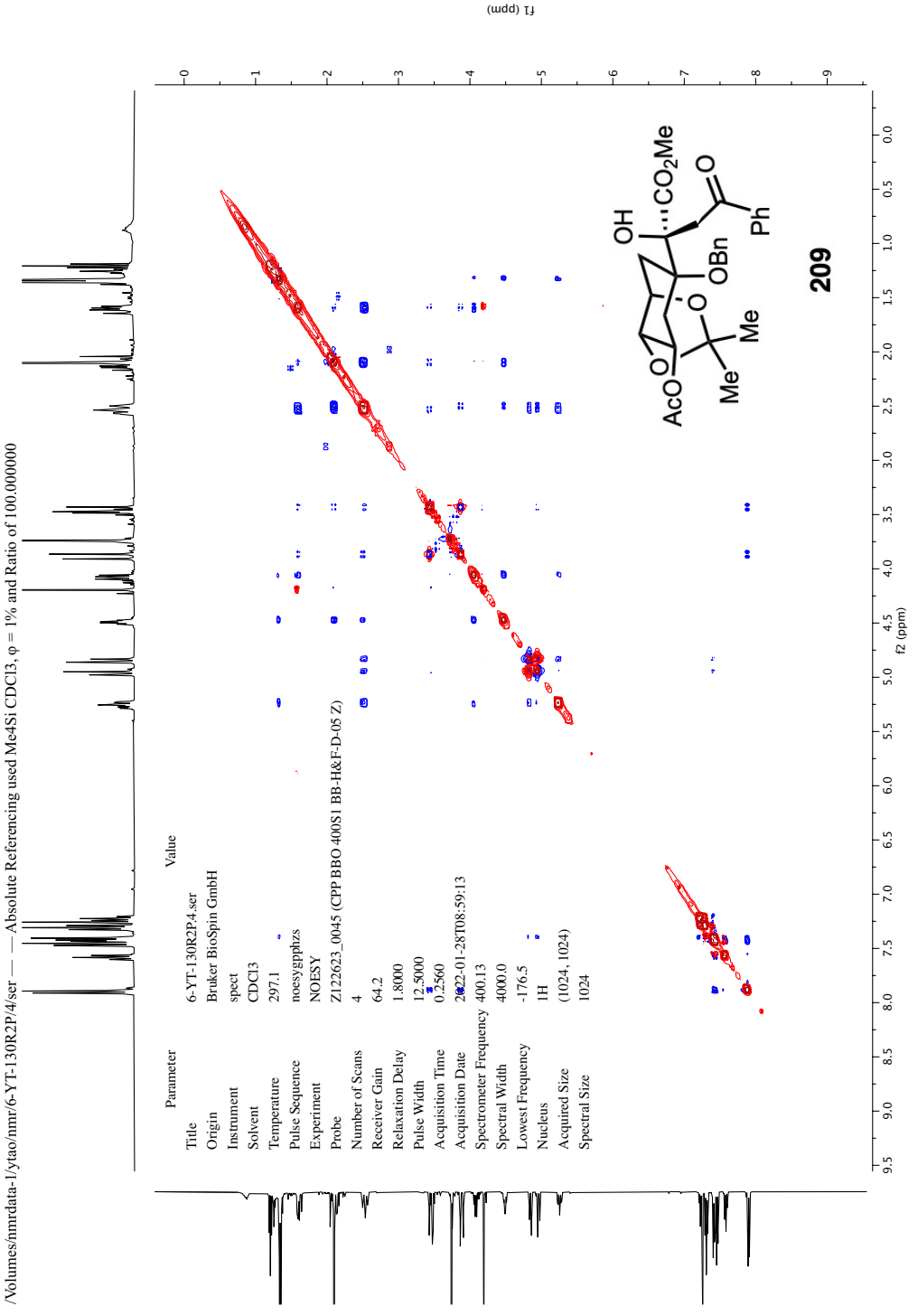
/Volumes/nmrdata-1/ytao/nmr/6-YT-130R2P/4/ser — — Absolute Referencing used Me4Si CDCl3, φ = 1% and Ratio of 100.000000
Parameter Value
Title 6-YT-130R2P4.ser
Origin Bruker BioSpin GmbH
Instrument spect
Solvent CDCl3
Temperature 297.1
Pulse Sequence noesygpphzs
Experiment NOESY
Probe Z122623_0045 (CPP BBO 400S1 BB-H&F-D-05 Z)
Number of Scans 4
Receiver Gain 64.2
Relaxation Delay 1.8000
Pulse Width 12.5000
Acquisition Time 0.2560
Acquisition Date 2022-01-28T08:59:13
Spectrometer Frequency 400.13
Spectral Width 4000.0
Lowest Frequency -176.5
Nucleus 1H
Acquired Size (1024, 1024)
Spectral Size 1024
f2 (ppm)
f1 (ppm)
OH
CO2Me
O
OBn
Ph
AcO
O
Me
Me
209

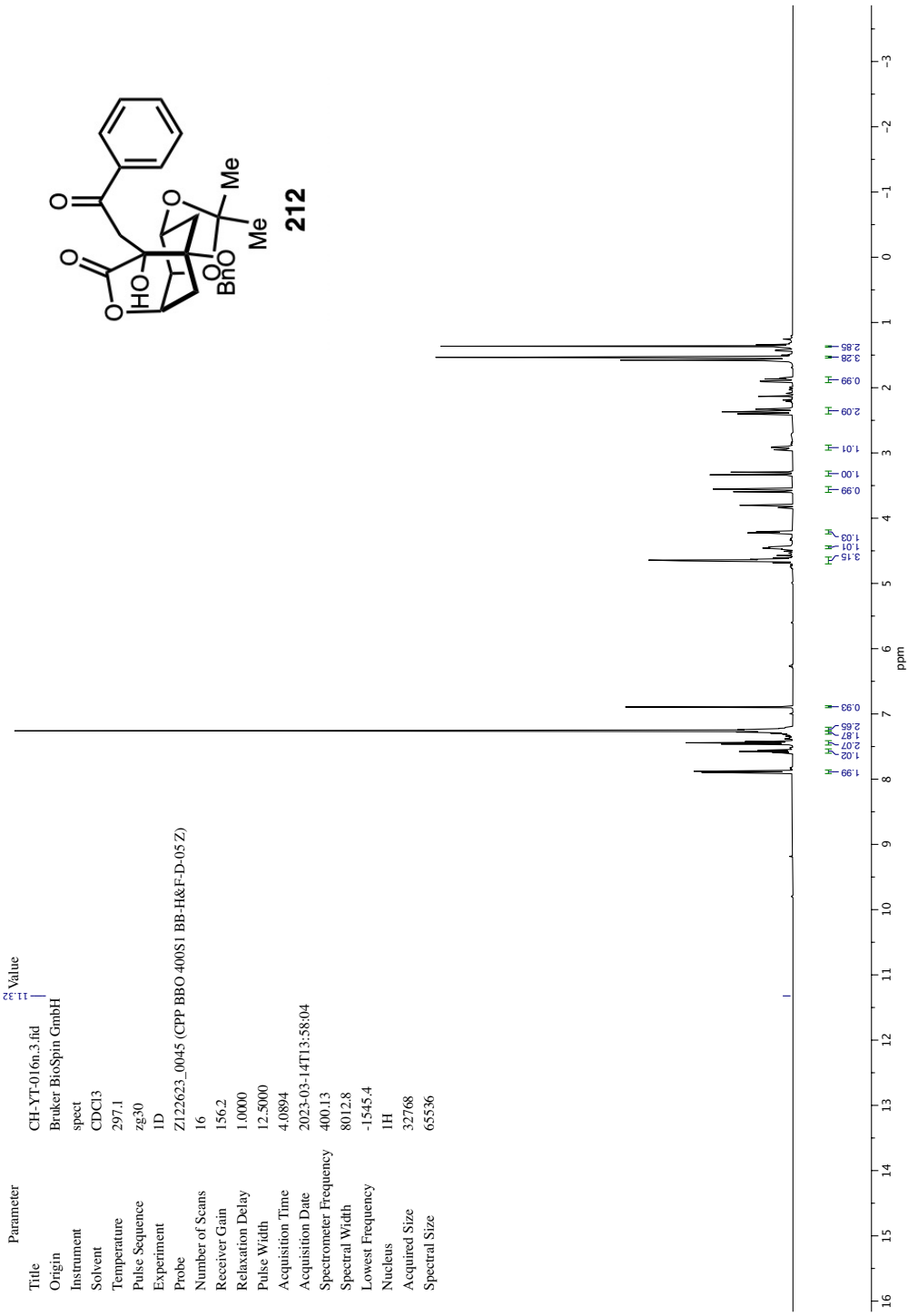
Value
11.32
Parameter
Title CH-YT-016n.3.fid
Origin Bruker BioSpin GmbH
Instrument spect
Solvent CDCl3
Temperature 297.1
Pulse Sequence zg30
Experiment 1D
Probe Z122623_0045 (CPP BBO 400S1 BB-H&F-D-05 Z)
Number of Scans 16
Receiver Gain 156.2
Relaxation Delay 1.0000
Pulse Width 12.5000
Acquisition Time 4.0894
Acquisition Date 2023-03-14T13:58:04
Spectrometer Frequency 400.13
Spectral Width 8012.8
Lowest Frequency -1545.4
Nucleus 1H
Acquired Size 32768
Spectral Size 65536
O
O
O
HO
O
O
BnO
Me
Me
212
1.99
1.02
2.07
1.87
2.65
0.93
3.15
1.01
1.03
0.99
1.00
1.01
2.09
0.99
3.28
2.85
ppm

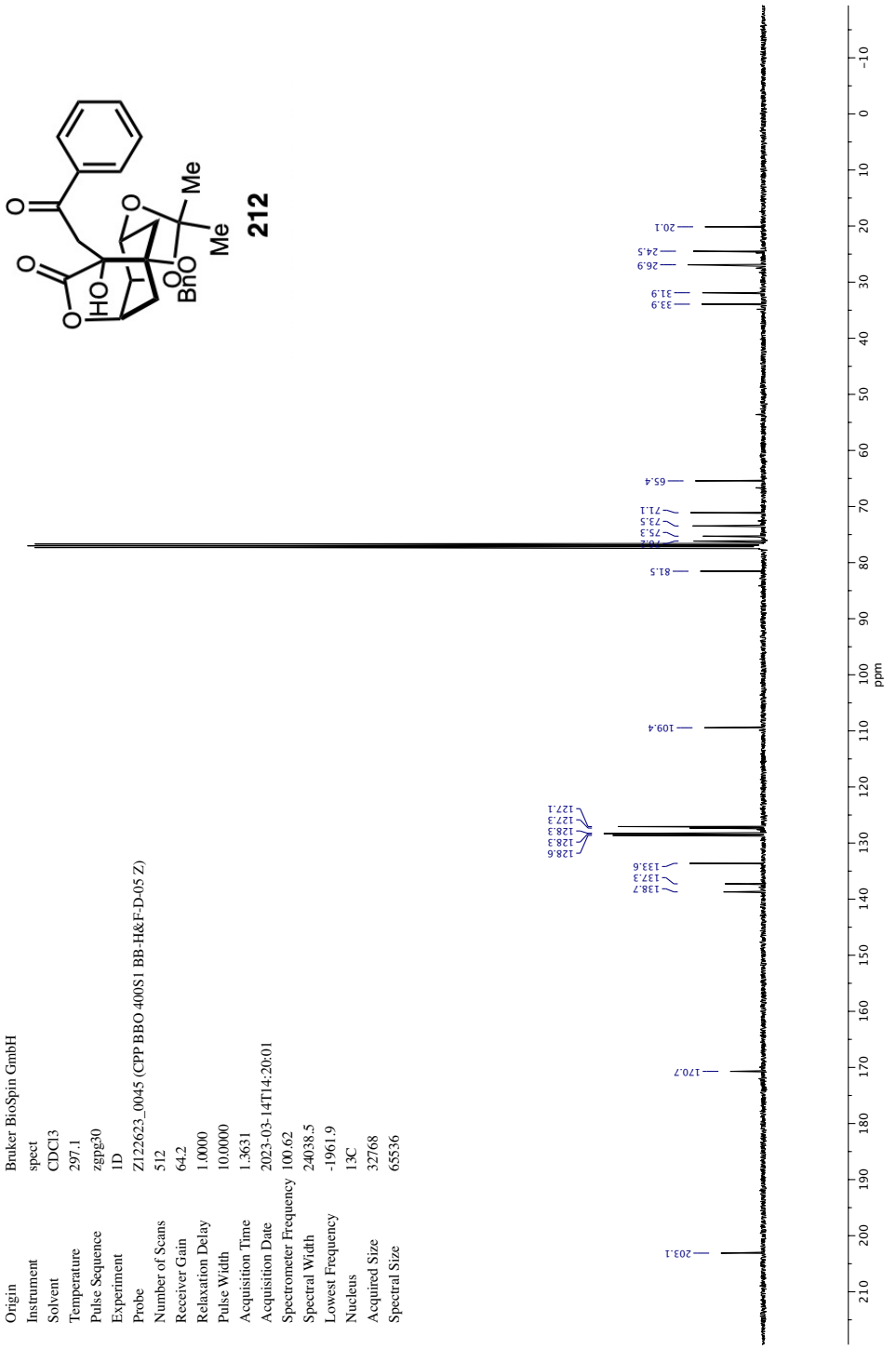

Parameter	Value
Title	CH-YT-016n.4.fid
Origin	Bruker BioSpin GmbH
Instrument	spect
Solvent	CDCl3
Temperature	297.1
Pulse Sequence	zgpg30
Experiment	1D
Probe	Z122623_0045 (CPP BBO 400S1 BB-H&F-D-05 Z)
Number of Scans	512
Receiver Gain	64.2
Relaxation Delay	1.0000
Pulse Width	10.0000
Acquisition Time	1.3631
Acquisition Date	2023-03-14T14:20:01
Spectrometer Frequency	100.62
Spectral Width	24038.5
Lowest Frequency	-1961.9
Nucleus	13C
Acquired Size	32768
Spectral Size	65536

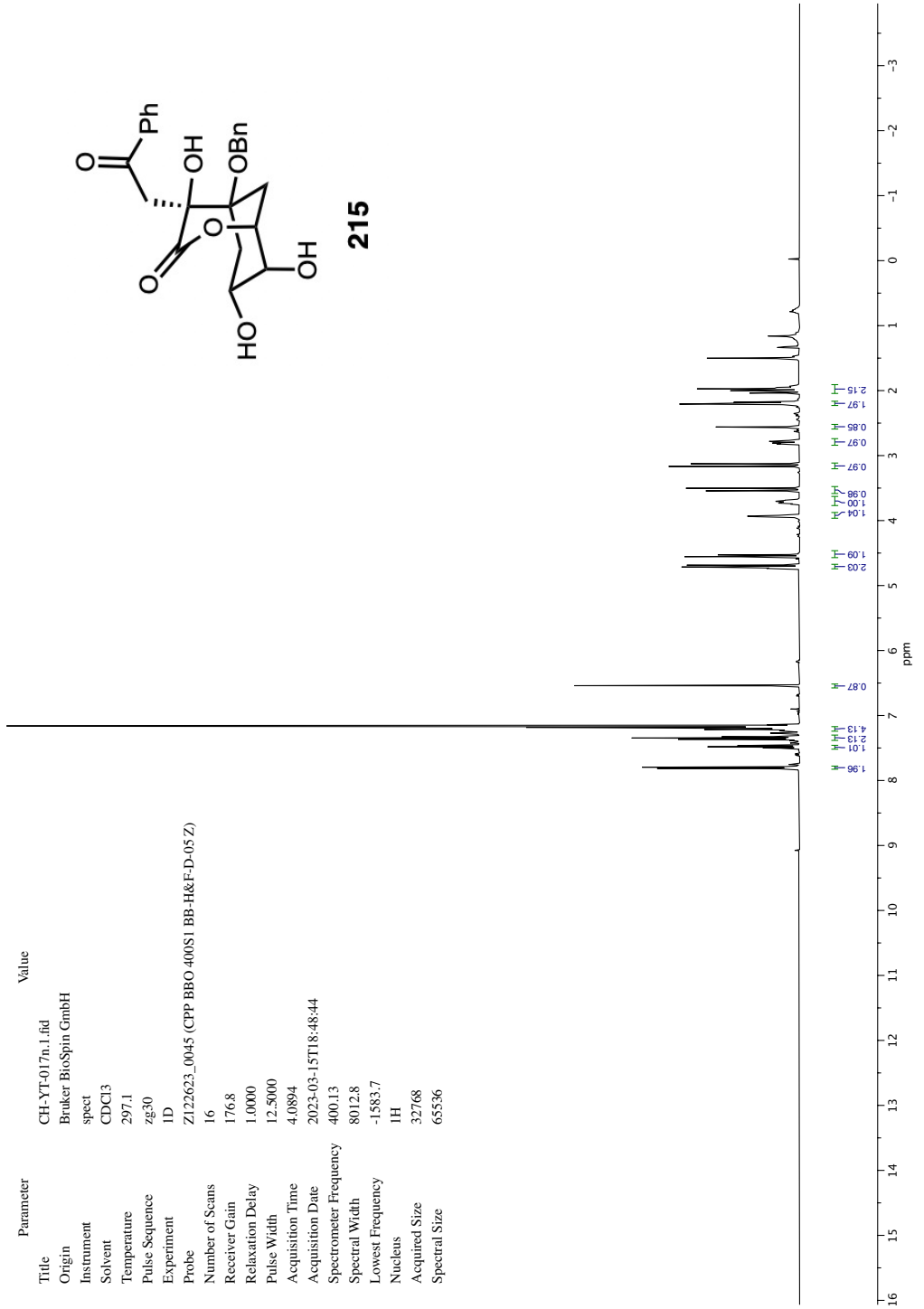

Parameter	Value
Title	CH-YT-017n.1.fid
Origin	Bruker BioSpin GmbH
Instrument	spect
Solvent	CDCl3
Temperature	297.1
Pulse Sequence	zg30
Experiment	1D
Probe	Z122623_0045 (CPP BBO 400S1 BB-H&F-D-05 Z)
Number of Scans	16
Receiver Gain	176.8
Relaxation Delay	1.0000
Pulse Width	12.5000
Acquisition Time	4.0894
Acquisition Date	2023-03-15T18:48:44
Spectrometer Frequency	400.13
Spectral Width	8012.8
Lowest Frequency	-1583.7
Nucleus	1H
Acquired Size	32768
Spectral Size	65536

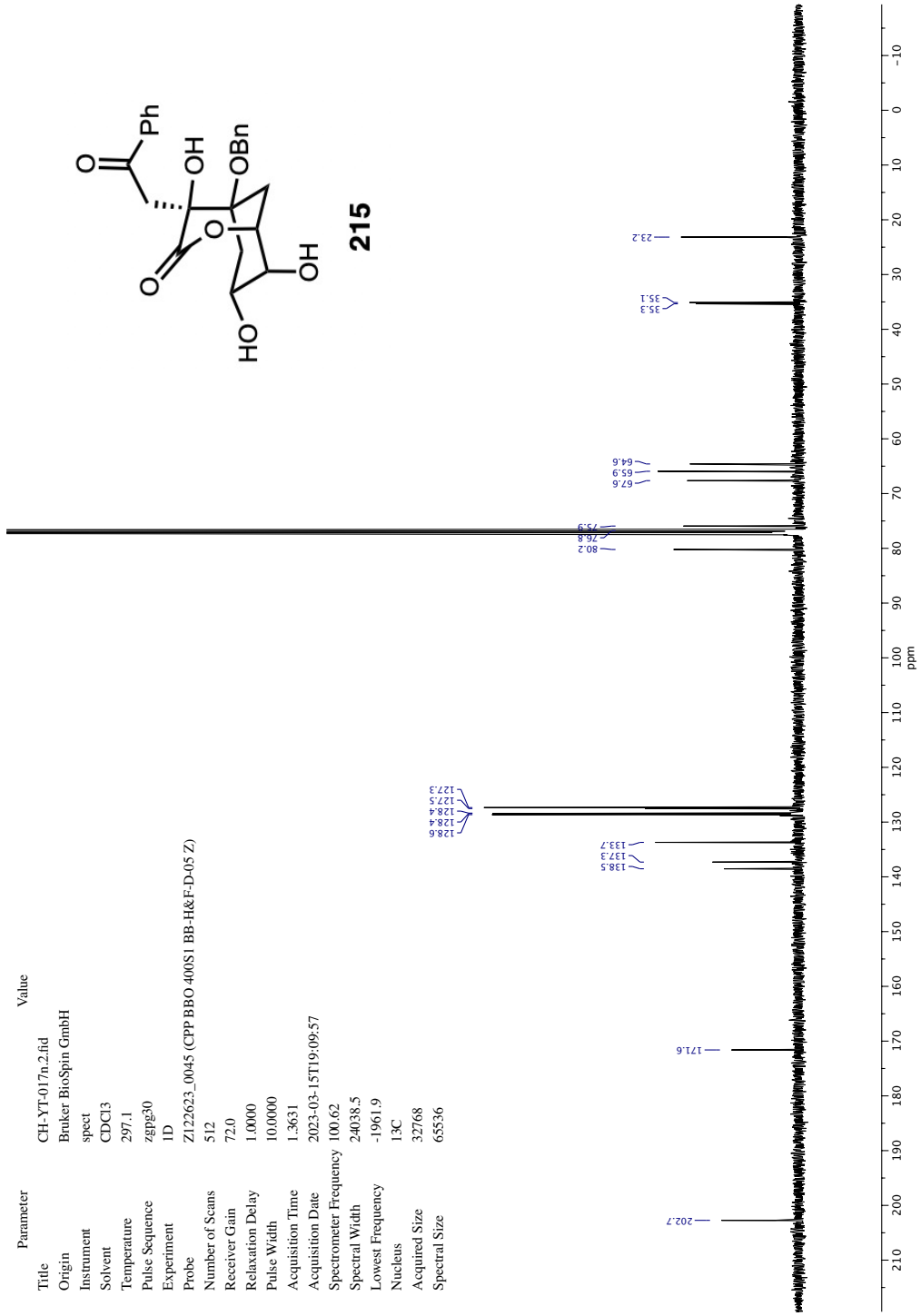
Ph
O
OH
OBn
O
O
OH
HO
215
Parameter Value
Title CH-YT-017n.2.fid
Origin Bruker BioSpin GmbH
Instrument spect
Solvent CDCl3
Temperature 297.1
Pulse Sequence zgpg30
Experiment 1D
Probe Z122623_0045 (CPP BBO 400S1 BB-H&F-D-05 Z)
Number of Scans 512
Receiver Gain 72.0
Relaxation Delay 1.0000
Pulse Width 10.0000
Acquisition Time 1.3631
Acquisition Date 2023-03-15T19:09:57
Spectrometer Frequency 100.62
Spectral Width 24038.5
Lowest Frequency -1961.9
Nucleus 13C
Acquired Size 32768
Spectral Size 65536
202.7
171.6
138.5
137.3
133.7
128.6
128.4
128.4
127.5
127.3
80.2
76.8
75.9
67.6
65.9
64.6
35.3
35.1
23.2
ppm

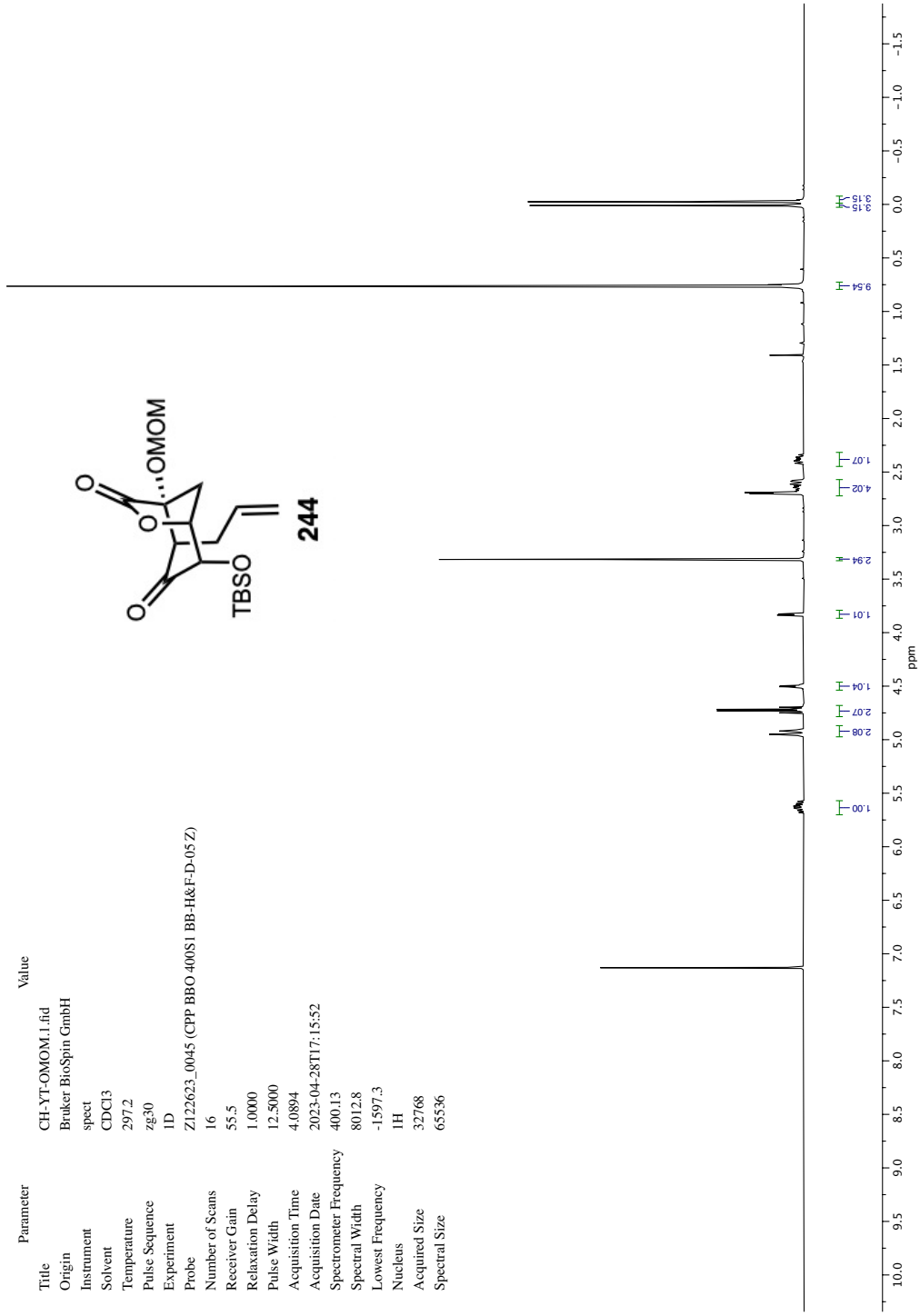

Parameter	Value
Title	CH-YT-OMOM.1.fid
Origin	Bruker BioSpin GmbH
Instrument	spect
Solvent	CDCl3
Temperature	297.2
Pulse Sequence	zg30
Experiment	1D
Probe	Z122623_0045 (CPP BBO 400S1 BB-H&F-D-05 Z)
Number of Scans	16
Receiver Gain	55.5
Relaxation Delay	1.0000
Pulse Width	12.5000
Acquisition Time	4.0894
Acquisition Date	2023-04-28T17:15:52
Spectrometer Frequency	400.13
Spectral Width	8012.8
Lowest Frequency	-1597.3
Nucleus	1H
Acquired Size	32768
Spectral Size	65536

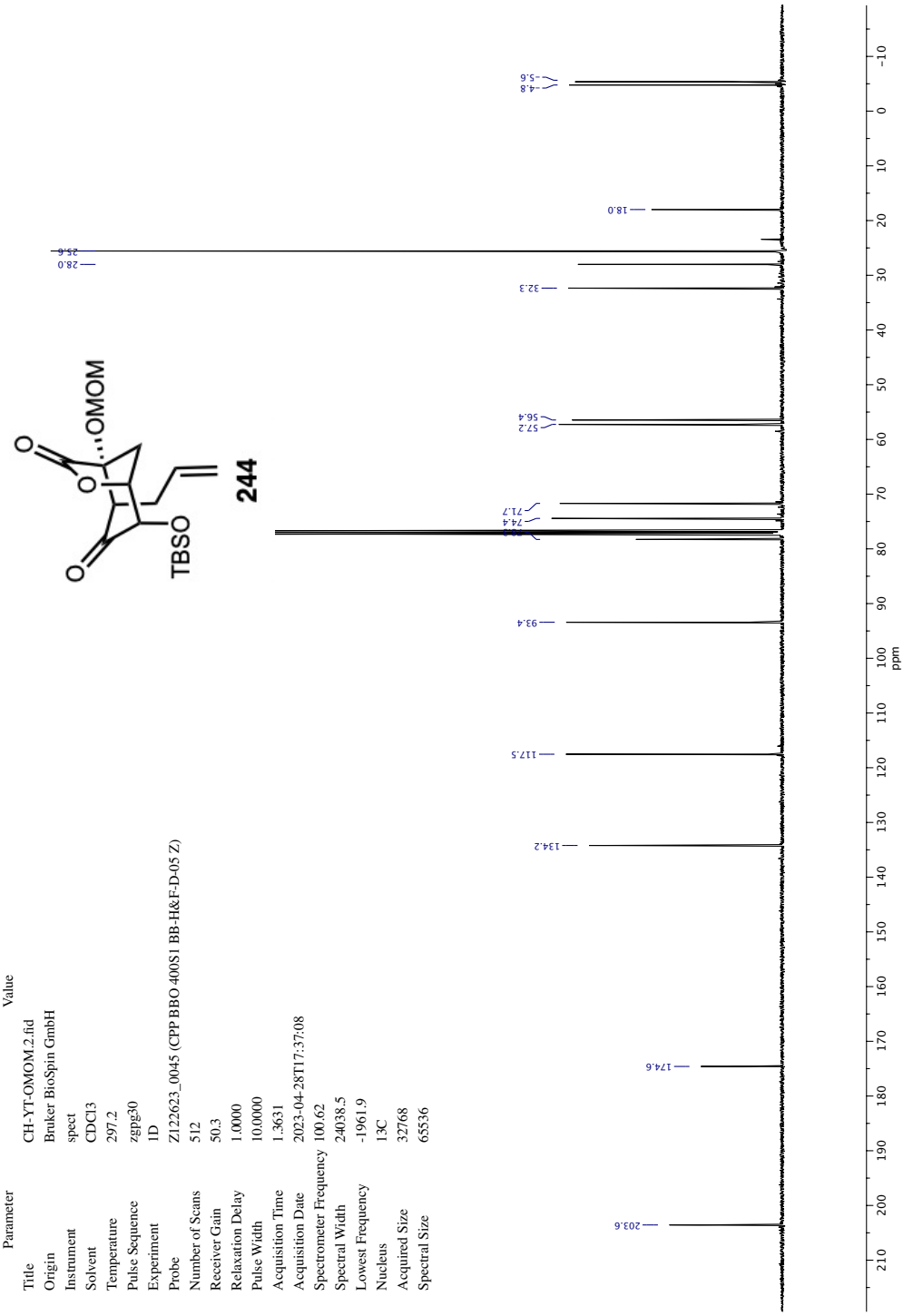
OMOM
TBSO
244
Parameter Value
Title CH-YT-OMOM 2.fid
Origin Bruker BioSpin GmbH
Instrument spect
Solvent CDCl3
Temperature 297.2
Pulse Sequence zgpg30
Experiment 1D
Probe Z122623_0045 (CPP BBO 400S1 BB-H&F-D-05 Z)
Number of Scans 512
Receiver Gain 50.3
Relaxation Delay 1.0000
Pulse Width 10.0000
Acquisition Time 1.3631
Acquisition Date 2023-04-28T17:37:08
Spectrometer Frequency 100.62
Spectral Width 24038.5
Lowest Frequency -1961.9
Nucleus 13C
Acquired Size 32768
Spectral Size 65536
203.6
174.6
134.2
117.5
93.4
74.4
71.7
57.2
56.4
32.3
28.0
25.6
18.0
-4.8
-5.6
ppm

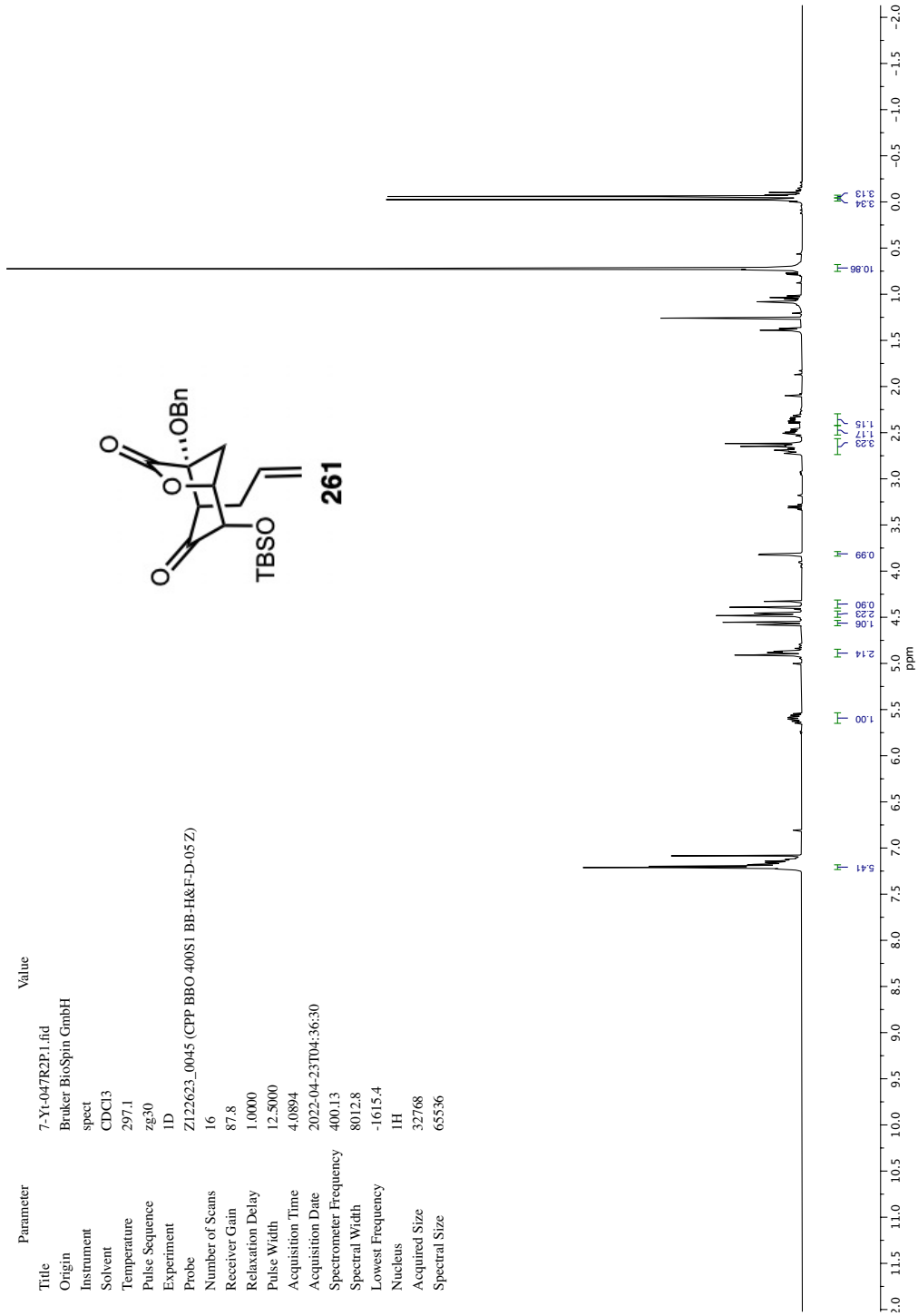

Parameter	Value
Title	7-Yt-047R2P1.fid
Origin	Bruker BioSpin GmbH
Instrument	spect
Solvent	CDCl3
Temperature	297.1
Pulse Sequence	zg30
Experiment	1D
Probe	Z122623_0045 (CPP BBO 400S1 BB-H&F-D-05 Z)
Number of Scans	16
Receiver Gain	87.8
Relaxation Delay	1.0000
Pulse Width	12.5000
Acquisition Time	4.0894
Acquisition Date	2022-04-23T04:36:30
Spectrometer Frequency	400.13
Spectral Width	8012.8
Lowest Frequency	-1615.4
Nucleus	1H
Acquired Size	32768
Spectral Size	65536

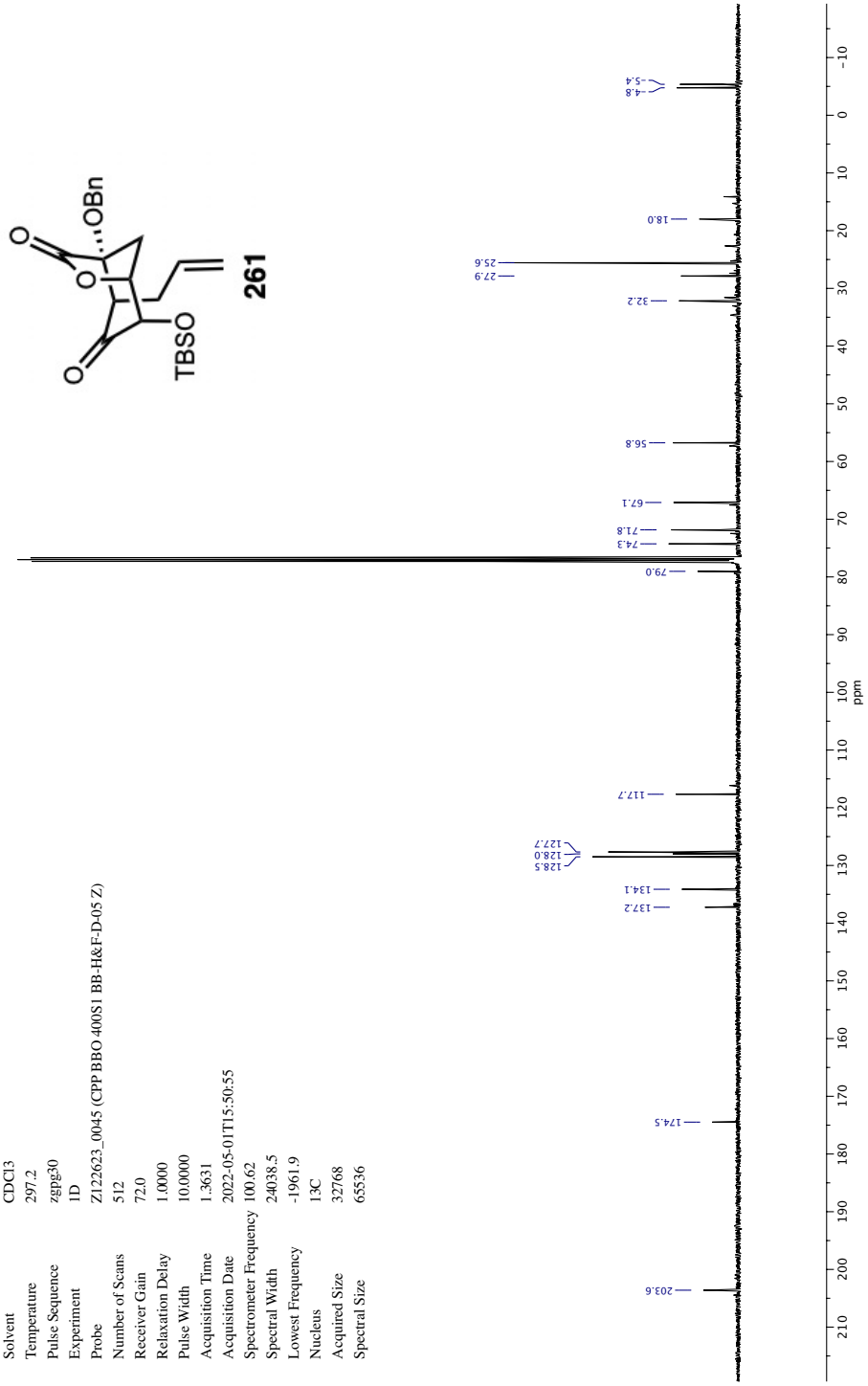

Parameter	Value
Title	7-Yt-055SM 2.fid
Origin	Bruker BioSpin GmbH
Instrument	spect
Solvent	CDCl3
Temperature	297.2
Pulse Sequence	zgpg30
Experiment	1D
Probe	Z122623_0045 (CPP BBO 400S1 BB-H&F-D-05 Z)
Number of Scans	512
Receiver Gain	72.0
Relaxation Delay	1.0000
Pulse Width	10.0000
Acquisition Time	1.3631
Acquisition Date	2022-05-01T15:50:55
Spectrometer Frequency	100.62
Spectral Width	24038.5
Lowest Frequency	-1961.9
Nucleus	13C
Acquired Size	32768
Spectral Size	65536

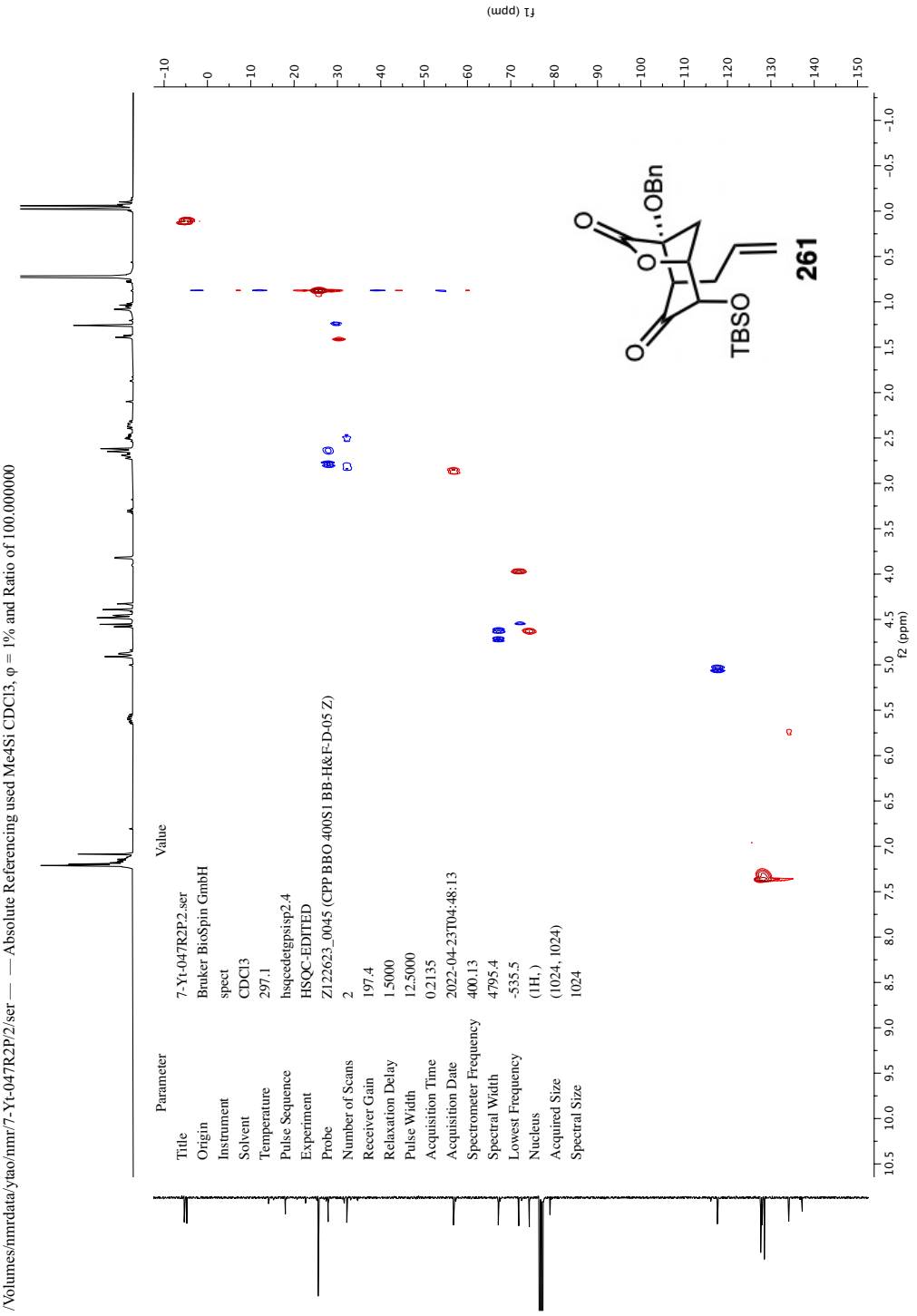
/Volumes/nmrdata/ytao/nmr/7-Yt-047R2P/2/ser — — Absolute Referencing used Me4Si CDCl3, φ = 1% and Ratio of 100.000000
Parameter Value
Title 7-Yt-047R2P2.ser
Origin Bruker BioSpin GmbH
Instrument spect
Solvent CDCl3
Temperature 297.1
Pulse Sequence hsqcedetgpsisp2.4
Experiment HSQC-EDITED
Probe Z122623_0045 (CPP BBO 400S1 BB-H&F-D-05 Z)
Number of Scans 2
Receiver Gain 197.4
Relaxation Delay 1.5000
Pulse Width 12.5000
Acquisition Time 0.2135
Acquisition Date 2022-04-23T04:48:13
Spectrometer Frequency 400.13
Spectral Width 4795.4
Lowest Frequency -535.5
Nucleus (1H,)
Acquired Size (1024, 1024)
Spectral Size 1024
f1 (ppm)
f2 (ppm)
OBn
TBSO
261

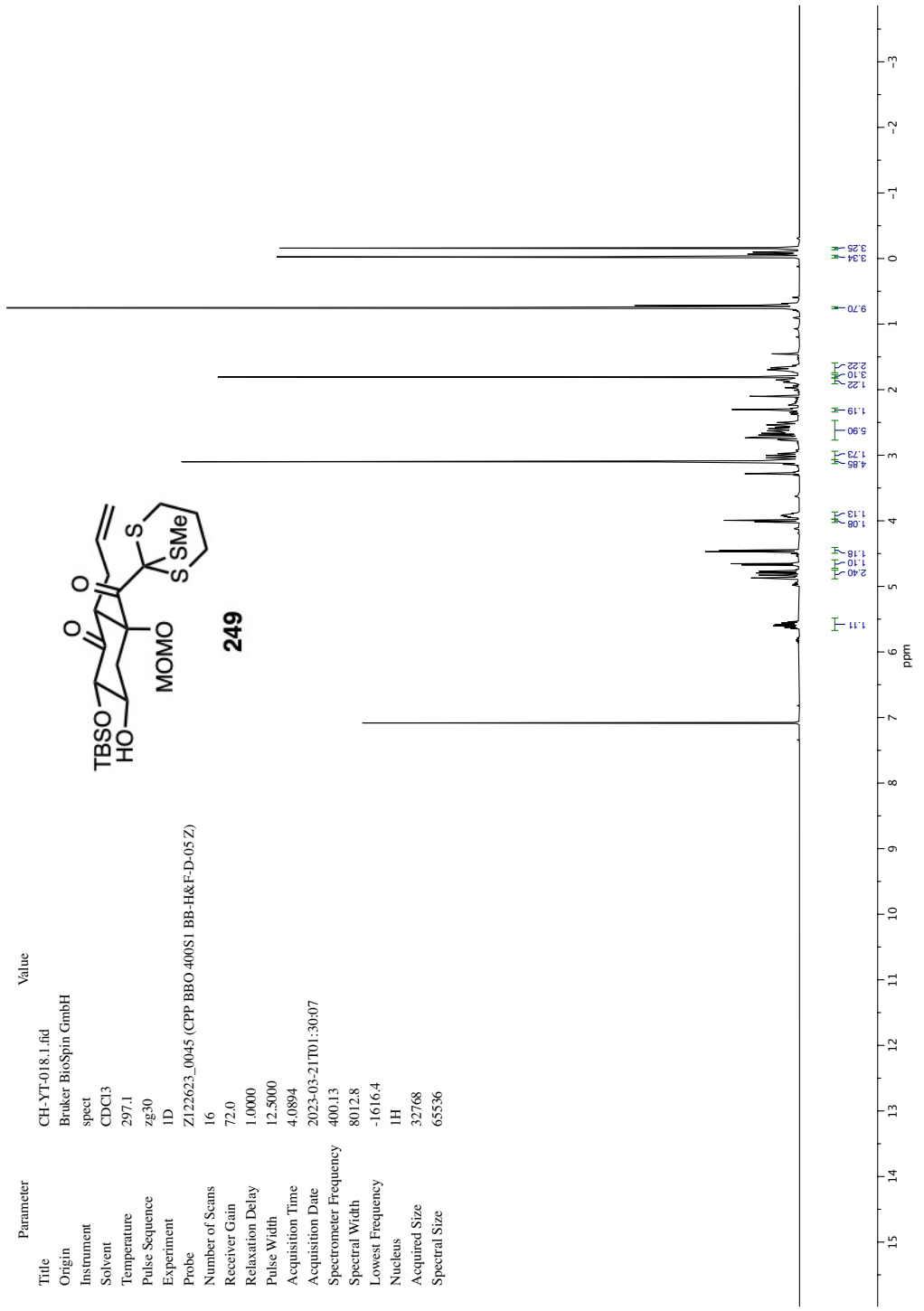

Parameter	Value
Title	CH-YT-018.1.fid
Origin	Bruker BioSpin GmbH
Instrument	spect
Solvent	CDCl3
Temperature	297.1
Pulse Sequence	zg30
Experiment	1D
Probe	Z122623_0045 (CPP BBO 400S1 BB-H&F-D-05 Z)
Number of Scans	16
Receiver Gain	72.0
Relaxation Delay	1.0000
Pulse Width	12.5000
Acquisition Time	4.0894
Acquisition Date	2023-03-21T01:30:07
Spectrometer Frequency	400.13
Spectral Width	8012.8
Lowest Frequency	-1616.4
Nucleus	1H
Acquired Size	32768
Spectral Size	65536

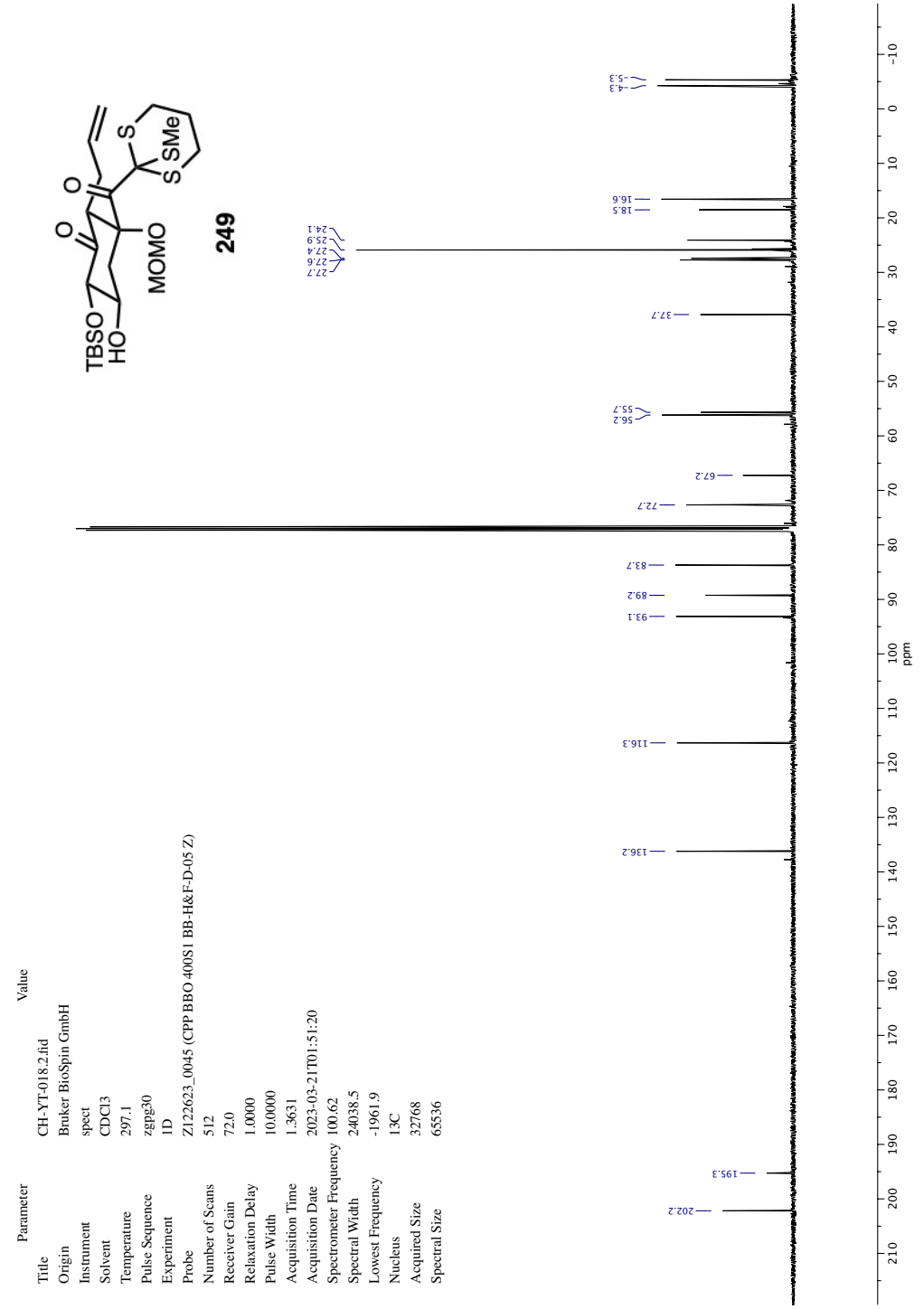

Parameter	Value
Title	CH-YT-018.2.fid
Origin	Bruker BioSpin GmbH
Instrument	spect
Solvent	CDCl3
Temperature	297.1
Pulse Sequence	zgpg30
Experiment	1D
Probe	Z122623_0045 (CPP BBO 400S1 BB-H&F-D-05 Z)
Number of Scans	512
Receiver Gain	72.0
Relaxation Delay	1.0000
Pulse Width	10.0000
Acquisition Time	1.3631
Acquisition Date	2023-03-21T01:51:20
Spectrometer Frequency	100.62
Spectral Width	24038.5
Lowest Frequency	-1961.9
Nucleus	13C
Acquired Size	32768
Spectral Size	65536

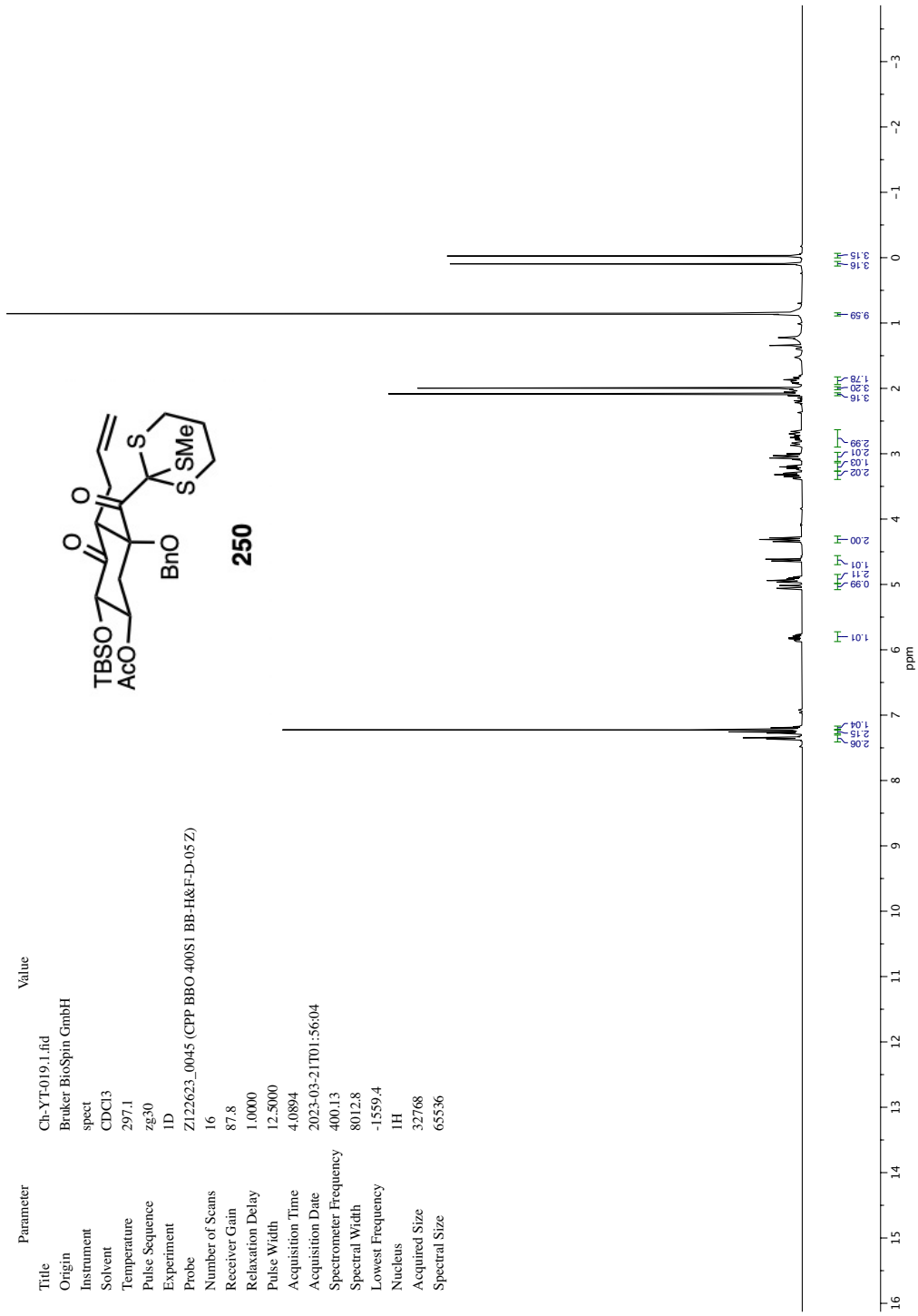

Parameter	Value
Title	Ch-YT-019.1.fid
Origin	Bruker BioSpin GmbH
Instrument	spect
Solvent	CDCl3
Temperature	297.1
Pulse Sequence	zg30
Experiment	1D
Probe	Z122623_0045 (CPP BBO 400S1 BB-H&F-D-05 Z)
Number of Scans	16
Receiver Gain	87.8
Relaxation Delay	1.0000
Pulse Width	12.5000
Acquisition Time	4.0894
Acquisition Date	2023-03-21T01:56:04
Spectrometer Frequency	400.13
Spectral Width	8012.8
Lowest Frequency	-1559.4
Nucleus	1H
Acquired Size	32768
Spectral Size	65536

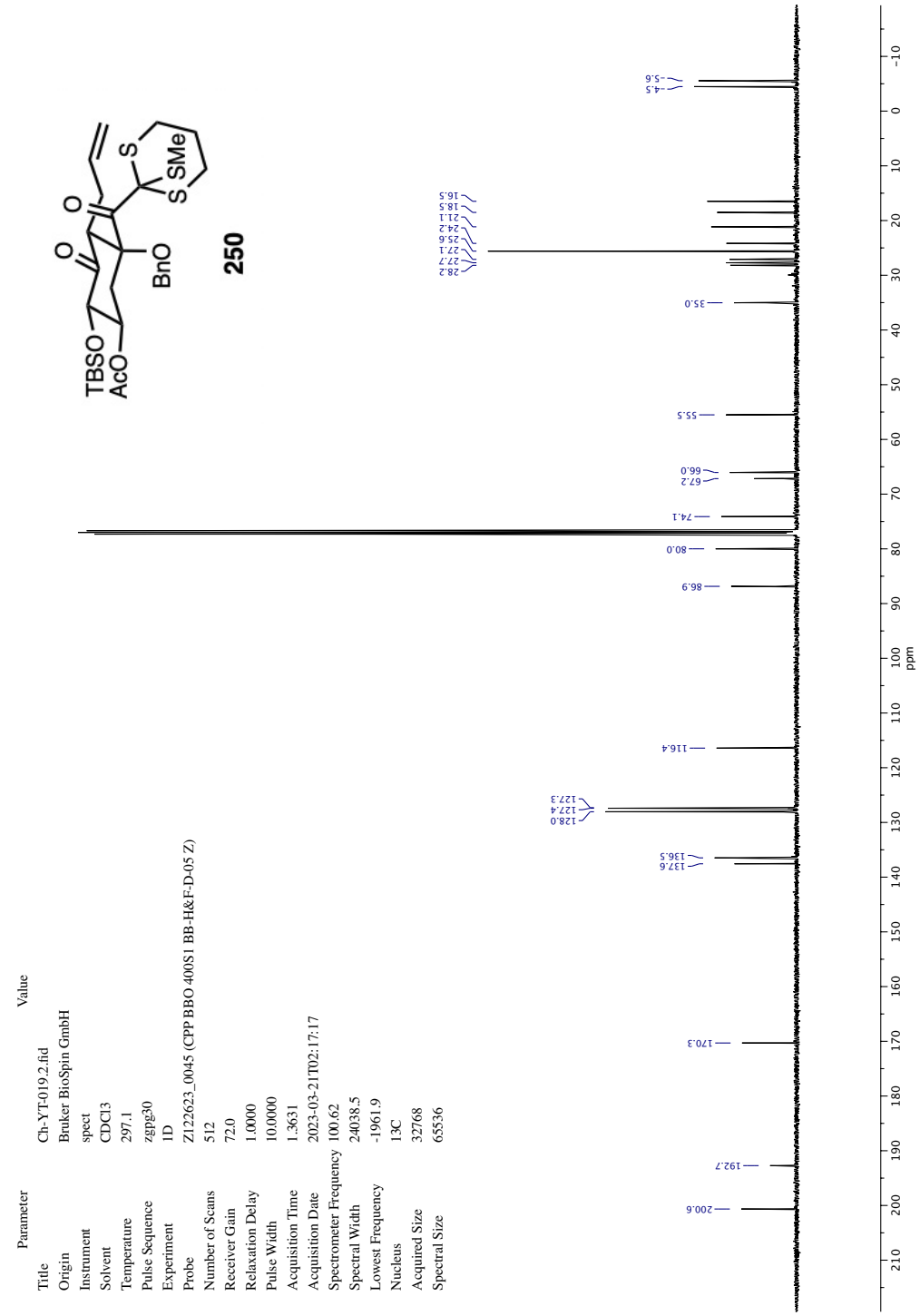
TBSO
AcO
O
O
BnO
S
S
SMe
250
Parameter Value
Title Ch-YT-019.2.fid
Origin Bruker BioSpin GmbH
Instrument spect
Solvent CDCl3
Temperature 297.1
Pulse Sequence zgpg30
Experiment 1D
Probe Z122623_0045 (CPP BBO 400S1 BB-H&F-D-05 Z)
Number of Scans 512
Receiver Gain 72.0
Relaxation Delay 1.0000
Pulse Width 10.0000
Acquisition Time 1.3631
Acquisition Date 2023-03-21T02:17:17
Spectrometer Frequency 100.62
Spectral Width 24038.5
Lowest Frequency -1961.9
Nucleus 13C
Acquired Size 32768
Spectral Size 65536
200.6
192.7
170.3
137.6
136.5
128.0
127.4
127.3
116.4
86.9
80.0
74.1
67.2
66.0
55.5
35.0
28.2
27.7
27.1
25.6
24.2
21.1
18.5
16.5
-4.5
-5.6
ppm

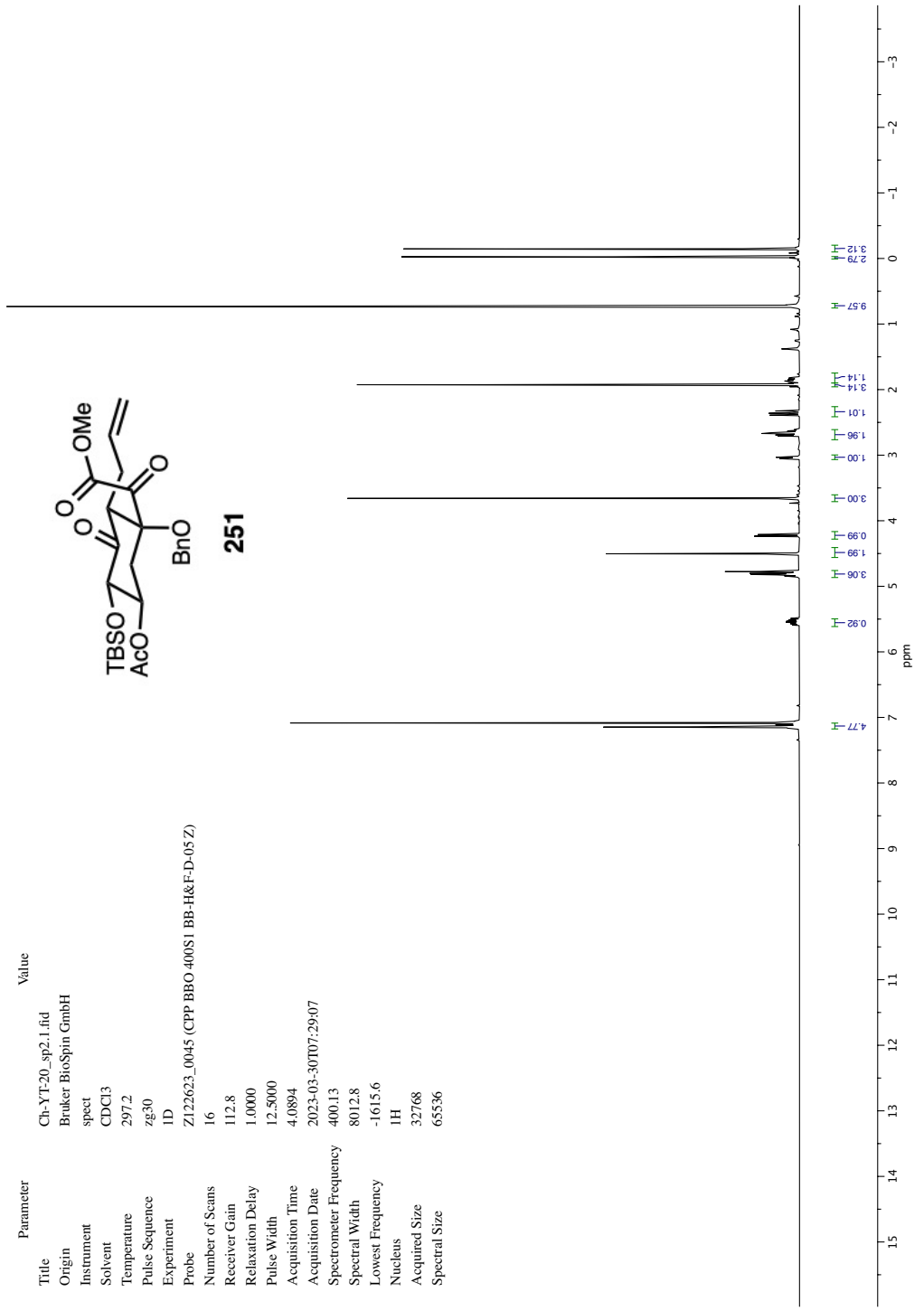

Parameter	Value
Title	Ch-YT-20_sp2.1.fid
Origin	Bruker BioSpin GmbH
Instrument	spect
Solvent	CDCl3
Temperature	297.2
Pulse Sequence	zg30
Experiment	1D
Probe	Z122623_0045 (CPP BBO 400S1 BB-H&F-D-05 Z)
Number of Scans	16
Receiver Gain	112.8
Relaxation Delay	1.0000
Pulse Width	12.5000
Acquisition Time	4.0894
Acquisition Date	2023-03-30T07:29:07
Spectrometer Frequency	400.13
Spectral Width	8012.8
Lowest Frequency	-1615.6
Nucleus	1H
Acquired Size	32768
Spectral Size	65536

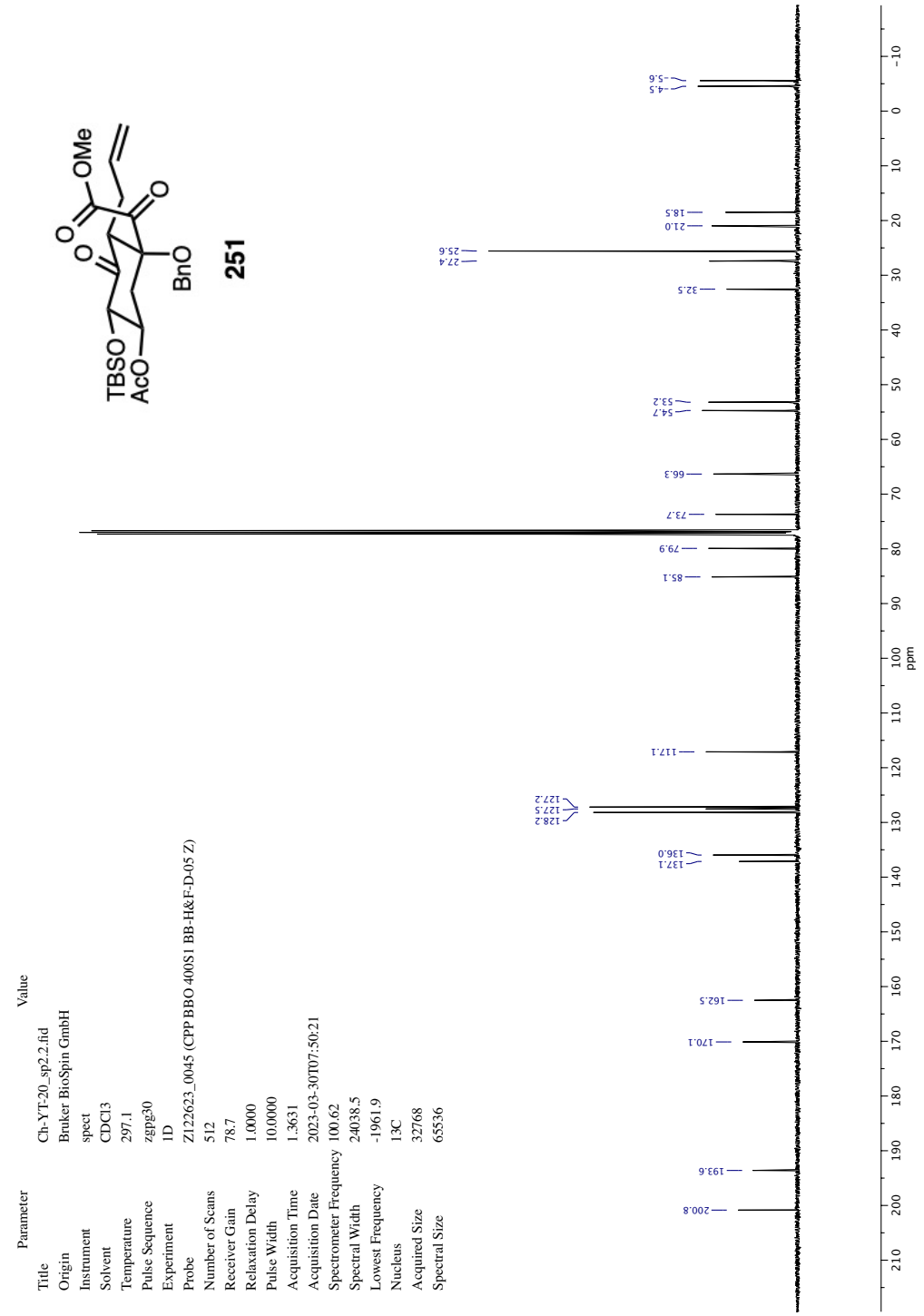

Parameter	Value
Title	Ch-YT-20_sp2.2.fid
Origin	Bruker BioSpin GmbH
Instrument	spect
Solvent	CDCl3
Temperature	297.1
Pulse Sequence	zgpg30
Experiment	1D
Probe	Z122623_0045 (CPP BBO 400S1 BB-H&F-D-05 Z)
Number of Scans	512
Receiver Gain	78.7
Relaxation Delay	1.0000
Pulse Width	10.0000
Acquisition Time	1.3631
Acquisition Date	2023-03-30T07:50:21
Spectrometer Frequency	100.62
Spectral Width	24038.5
Lowest Frequency	-1961.9
Nucleus	13C
Acquired Size	32768
Spectral Size	65536

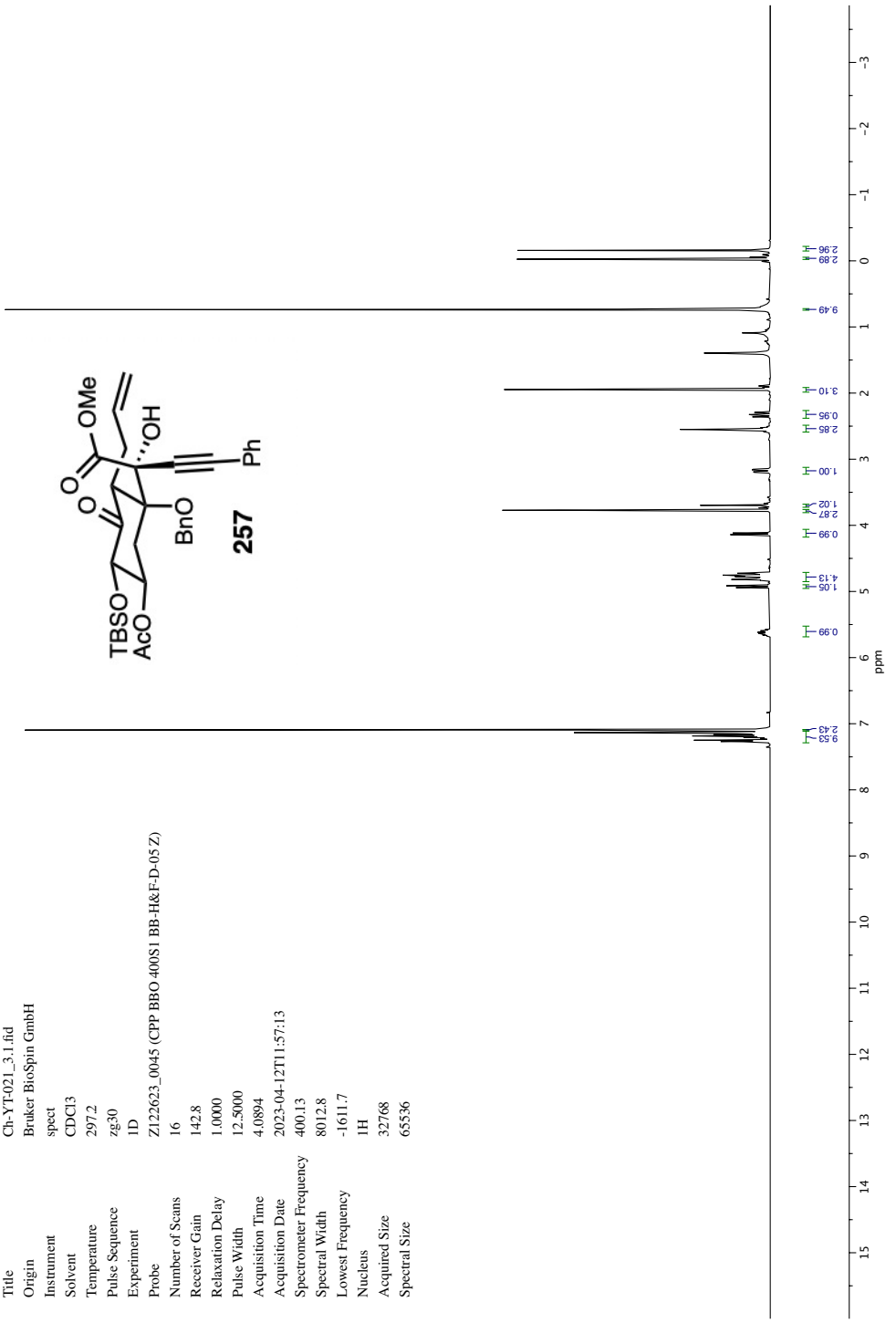

Parameter	Value
Title	Ch-YT-021_3.1.fid
Origin	Bruker BioSpin GmbH
Instrument	spect
Solvent	CDCl3
Temperature	297.2
Pulse Sequence	zg30
Experiment	1D
Probe	Z122623_0045 (CPP BBO 400S1 BB-H&F-D-05 Z)
Number of Scans	16
Receiver Gain	142.8
Relaxation Delay	1.0000
Pulse Width	12.5000
Acquisition Time	4.0894
Acquisition Date	2023-04-12T11:57:13
Spectrometer Frequency	400.13
Spectral Width	8012.8
Lowest Frequency	-1611.7
Nucleus	1H
Acquired Size	32768
Spectral Size	65536

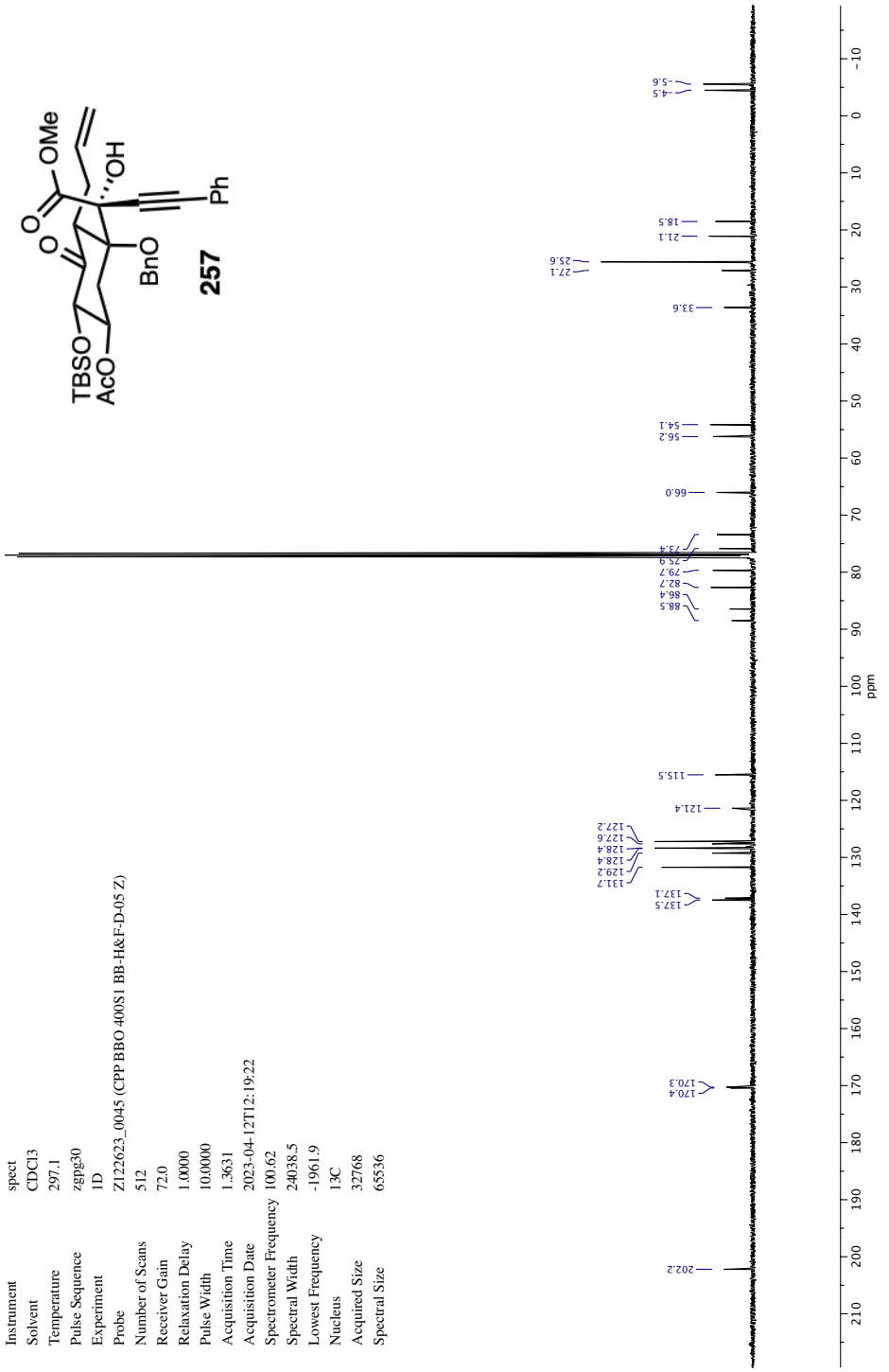

Parameter	Value
Title	Ch-YT-021_3.2.fid
Origin	Bruker BioSpin GmbH
Instrument	spect
Solvent	CDCl3
Temperature	297.1
Pulse Sequence	zgpg30
Experiment	1D
Probe	Z122623_0045 (CPP BBO 400S1 BB-H&F-D-05 Z)
Number of Scans	512
Receiver Gain	72.0
Relaxation Delay	1.0000
Pulse Width	10.0000
Acquisition Time	1.3631
Acquisition Date	2023-04-12T12:19:22
Spectrometer Frequency	100.62
Spectral Width	24038.5
Lowest Frequency	-1961.9
Nucleus	13C
Acquired Size	32768
Spectral Size	65536

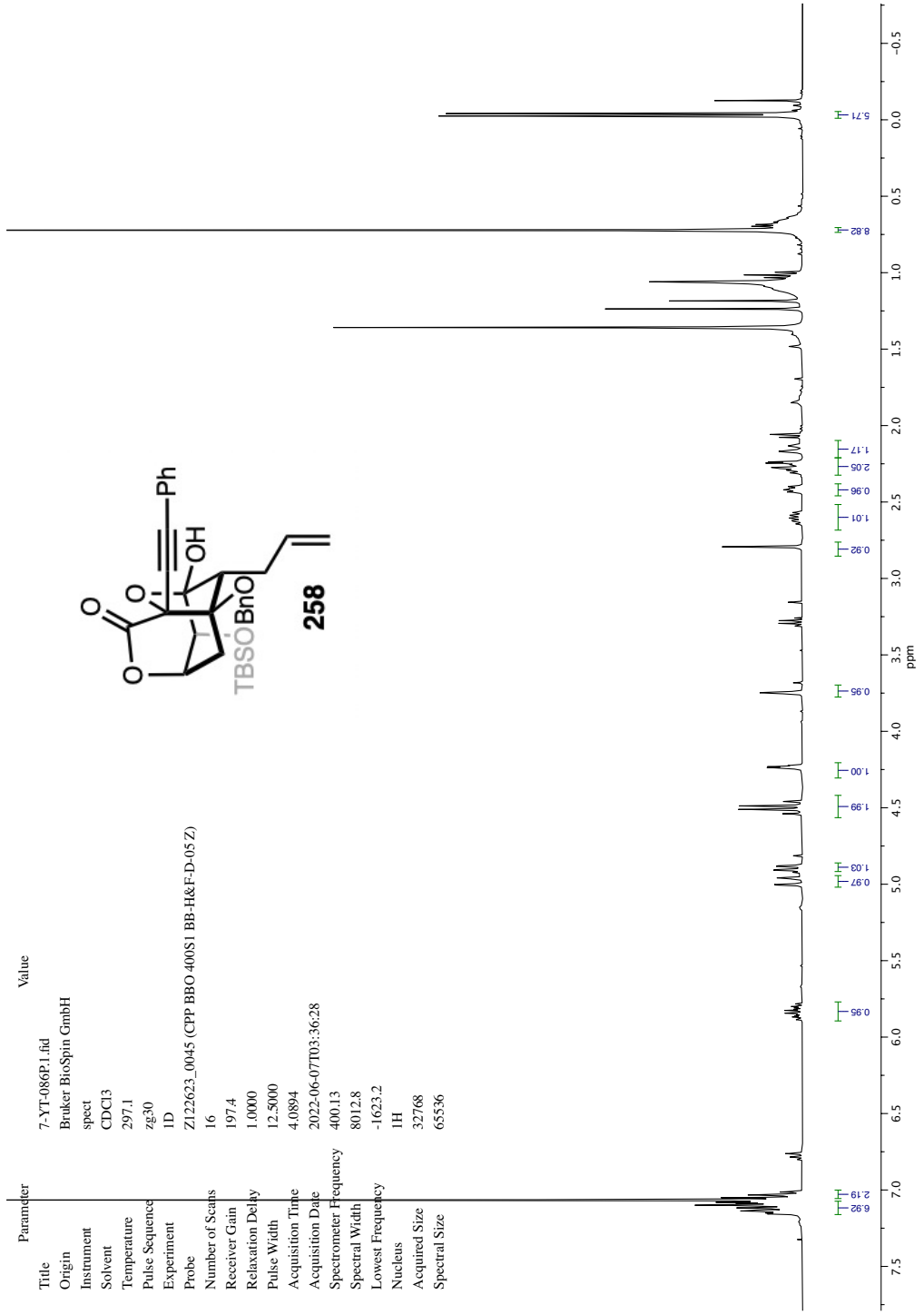
Parameter
Value
Title
7-YT-086P1.fid
Origin
Bruker BioSpin GmbH
Instrument
spect
Solvent
CDCl3
Temperature
297.1
Pulse Sequence
zg30
Experiment
1D
Probe
Z122623_0045 (CPP BBO 400S1 BB-H&F-D-05 Z)
Number of Scans
16
Receiver Gain
197.4
Relaxation Delay
1.0000
Pulse Width
12.5000
Acquisition Time
4.0894
Acquisition Date
2022-06-07T03:36:28
Spectrometer Frequency
400.13
Spectral Width
8012.8
Lowest Frequency
-1623.2
Nucleus
1H
Acquired Size
32768
Spectral Size
65536
Ph
OH
O
O
O
TBSO
BnO
258
6.92
2.19
0.95
0.97
1.03
1.99
1.00
0.95
0.92
1.01
0.96
2.05
1.17
8.82
5.71
7.5
7.0
6.5
6.0
5.5
5.0
4.5
4.0
3.5
3.0
2.5
2.0
1.5
1.0
0.5
0.0
-0.5
ppm

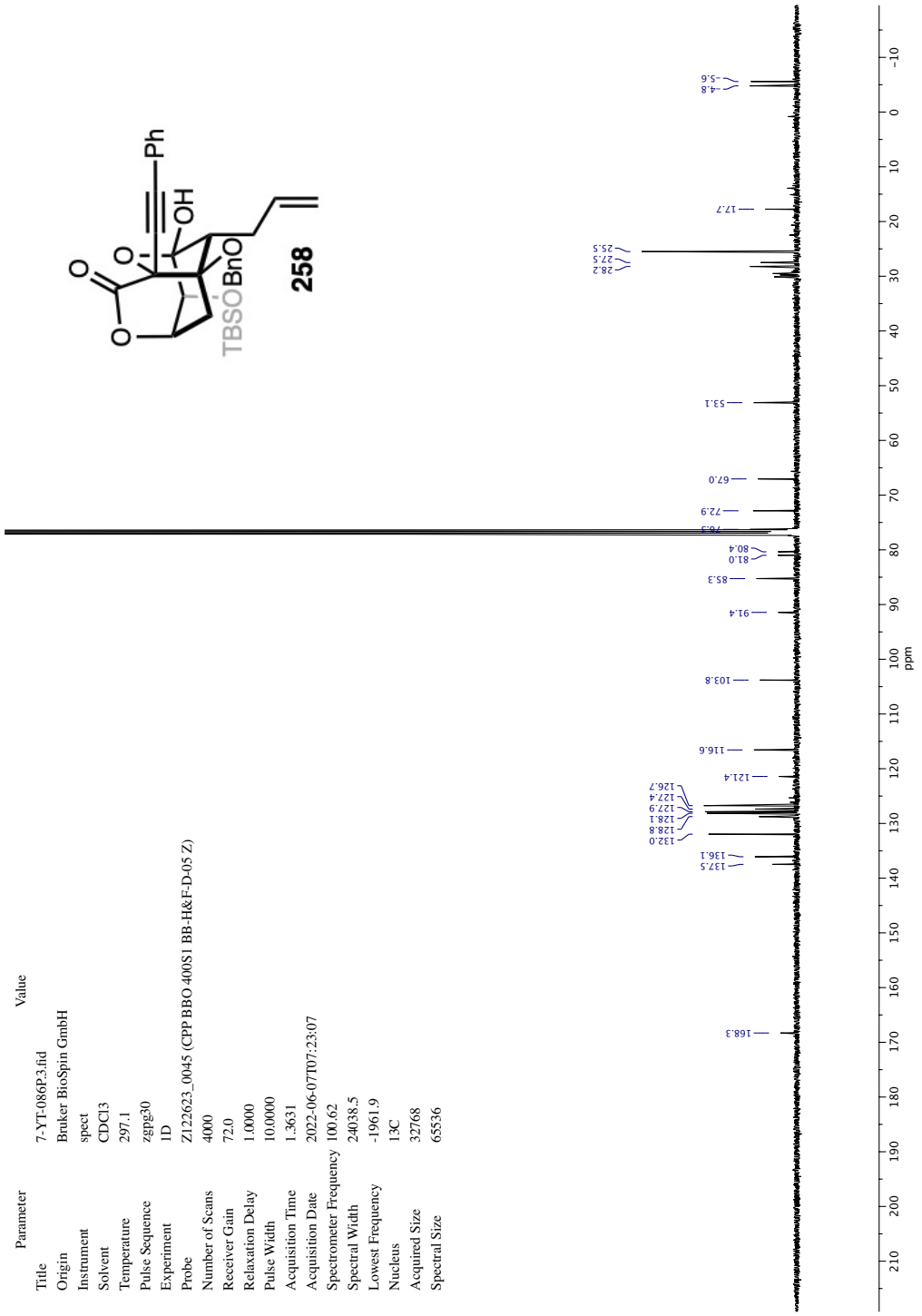

Parameter	Value
Title	7-YT-086P3.fid
Origin	Bruker BioSpin GmbH
Instrument	spect
Solvent	CDCl3
Temperature	297.1
Pulse Sequence	zgpg30
Experiment	1D
Probe	Z122623_0045 (CPP BBO 400S1 BB-H&F-D-05 Z)
Number of Scans	4000
Receiver Gain	72.0
Relaxation Delay	1.0000
Pulse Width	10.0000
Acquisition Time	1.3631
Acquisition Date	2022-06-07T07:23:07
Spectrometer Frequency	100.62
Spectral Width	24038.5
Lowest Frequency	-1961.9
Nucleus	13C
Acquired Size	32768
Spectral Size	65536

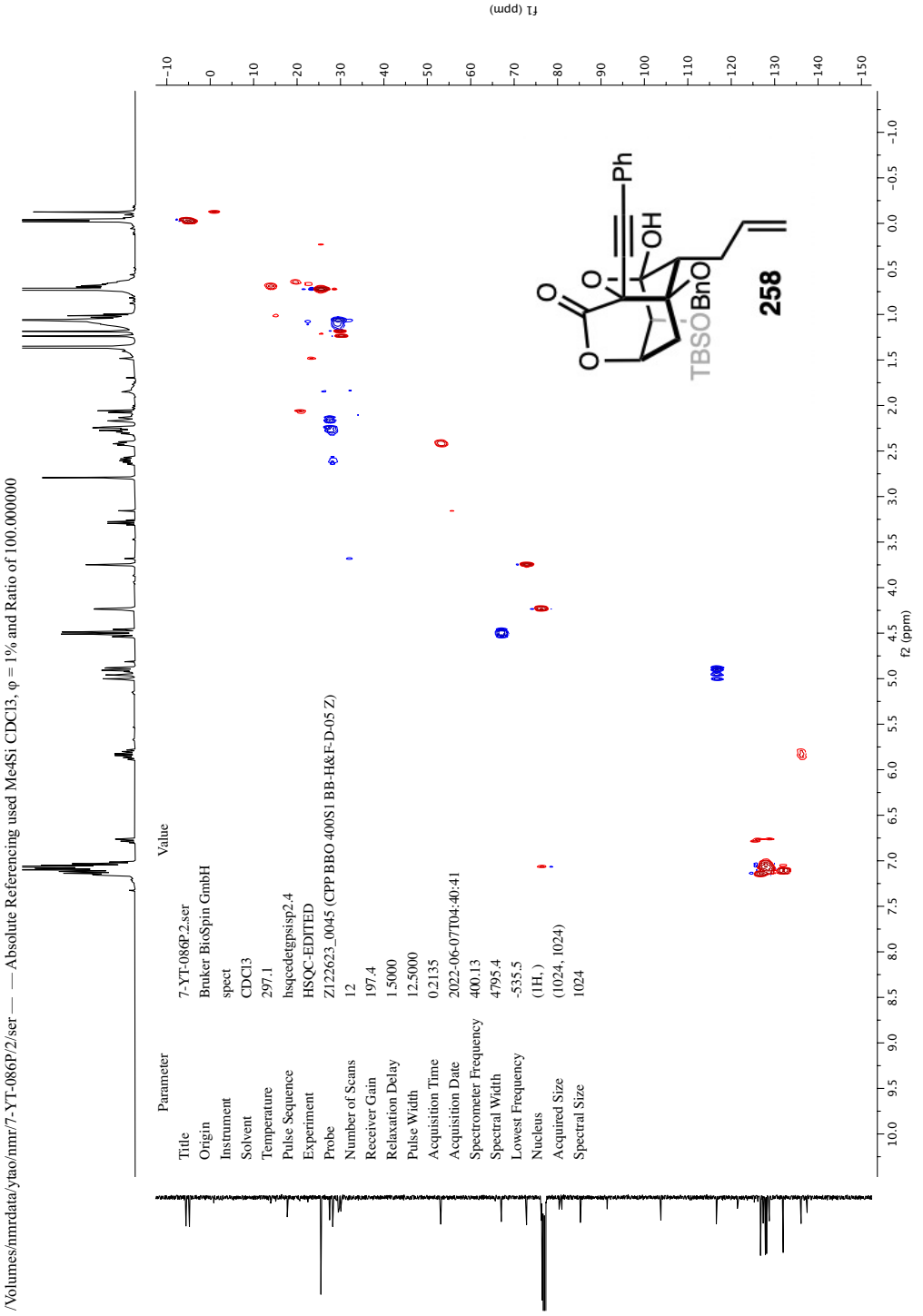
/Volumes/nmrdata/ytao/nmr/7-YT-086P/2/ser — — Absolute Referencing used Me4Si CDCl3, φ = 1% and Ratio of 100.000000
Parameter Value
Title 7-YT-086P.2.ser
Origin Bruker BioSpin GmbH
Instrument spect
Solvent CDCl3
Temperature 297.1
Pulse Sequence hsqcedetgpsisp2.4
Experiment HSQC-EDITED
Probe Z122623_0045 (CPP BBO 400S1 BB-H&F-D-05 Z)
Number of Scans 12
Receiver Gain 197.4
Relaxation Delay 1.5000
Pulse Width 12.5000
Acquisition Time 0.2135
Acquisition Date 2022-06-07T04:40:41
Spectrometer Frequency 400.13
Spectral Width 4795.4
Lowest Frequency -535.5
Nucleus (1H,)
Acquired Size (1024, 1024)
Spectral Size 1024
f1 (ppm)
f2 (ppm)
Ph
OH
O
O
O
TBSO
BnO
258

Appendix 5

X-Ray Crystallography Reports Relevant to Chapter 6:

An intermolecular aldol approach toward enterocin

A5.1 X-RAY CRYSTAL STRUCTURE ANALYSIS

Low-temperature diffraction data (φ- and ω-scans) were collected on a Bruker AXS D8 VENTURE KAPPA diffractometer coupled to a PHOTON 100 CMOS detector with Cu-K_α radiation (λ = 1.54178 Å) from a $I_\mu S$ HB micro-focus sealed X-ray tube. All diffractometer manipulations, including data collection, integration, and scaling were carried out using the Bruker APEXII software.[1] Absorption corrections were applied using SADABS.[2] The structure was solved by intrinsic phasing using SHELXT[3] and refined against F^2 on all data by full-matrix least squares with SHELXL-2014[3] using established refinement techniques.[4] All non-hydrogen atoms were refined anisotropically. All hydrogen atoms were included into the model at geometrically calculated positions and refined using a riding model. The isotropic displacement parameters of all hydrogen atoms were fixed to 1.2 times the *U* value of the atoms they are linked to (1.5 times for methyl groups and hydroxyl groups). Absolute configuration was determined by anomalous dispersion.[5] Crystallographic data for **212** and **258** can be obtained free of charge from The Cambridge Crystallographic Data Centre (CCDC) via www.ccdc.cam.ac.uk/data_request/cif under CCDC deposition numbers 2259507 and 2259508. Graphical representation of the structures with 50% probability thermal ellipsoids was generated using Mercury visualization software.

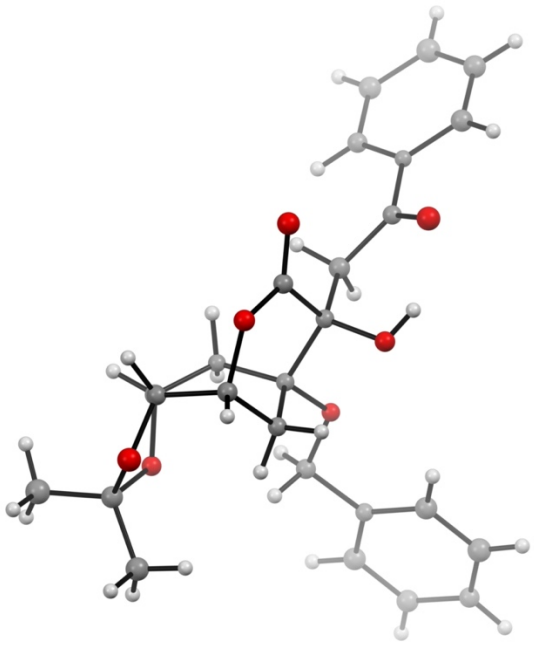

Figure A5.1. *Structure of* ***212*** *with 50% probability anisotropic displacement ellipsoids.*

Table A5.1. *Crystal data and structure refinement for V22075.*

Identification code	V22075
Empirical formula	$C_{26}H_{28}O_7$
Formula weight	452.508
Temperature/K	100.0
Crystal system	monoclinic
Space group	$P2_1$
a/Å	11.4655(11)
b/Å	6.1418(7)
c/Å	16.2482(16)
α/°	90
β/°	107.456(5)
γ/°	90

Volume/Å^3	1091.5(2)
Z	2
ρ_{calc}g/cm^3	1.377
μ/mm^{-1}	0.822
F(000)	481.7
Crystal size/mm^3	0.3 × 0.05 × 0.05
Radiation	Cu Kα (λ = 1.54178)
2Θ range for data collection/°	5.7 to 158.18
Index ranges	$-14 \leq h \leq 14$, $-7 \leq k \leq 7$, $-20 \leq l \leq 20$
Reflections collected	13705
Independent reflections	4433 [R_{int} = 0.0424, R_{sigma} = 0.0386]
Data/restraints/parameters	4433/1/301
Goodness-of-fit on F^2	1.078
Final R indexes [I>=2σ (I)]	R_1 = 0.0290, wR_2 = 0.0741
Final R indexes [all data]	R_1 = 0.0302, wR_2 = 0.0753
Largest diff. peak/hole / e Å^{-3}	0.22/-0.20
Flack parameter	0.01(9)

Special Refinement Details for 212

Compound **212** crystallizes in the monoclinic space group $P2_1$ with one molecule in the unit. Absolute configuration was determined by anomalous dispersion (Flack = 0.01(9)).[5] The coordinate for the hydrogen atom bound to O3 was located in the difference Fourier synthesis and refined semi-freely with the help of a restraint on the O-H distance (0.84(4) Å).

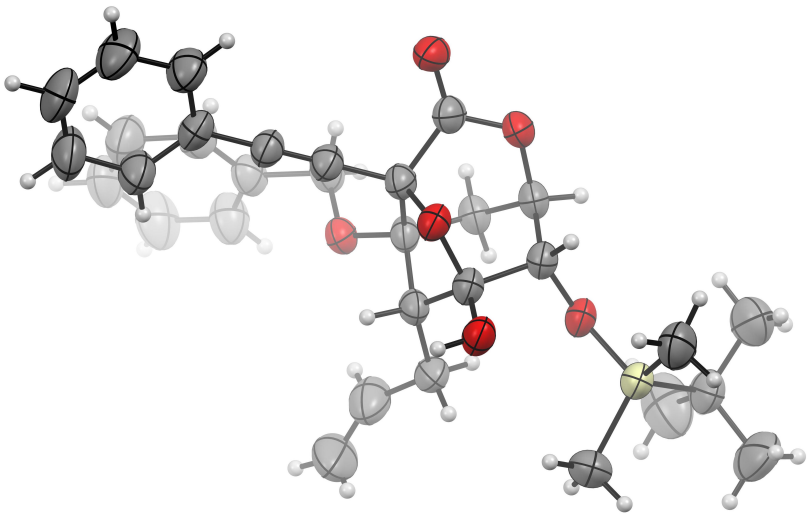

Figure A5.2. *Structure of* ***258*** *with 50% probability anisotropic displacement ellipsoids.*

Table A5.2. *Crystal data and structure refinement for V22200.*

Identification code	V22200	
Empirical formula	C32 H38 O6 Si	
Formula weight	546.71	
Temperature	200(2) K	
Wavelength	1.54178 Å	
Crystal system	Monoclinic	
Space group	$P2_1$	
Unit cell dimensions	a = 13.1719(18) Å	a= 90°.
	b = 10.4535(11) Å	b= 90.327(7)°.
	c = 22.311(3) Å	g = 90°.
Volume	3072.0(7) $Å^3$	
Z	4	
Density (calculated)	1.182 Mg/m^3	
Absorption coefficient	1.002 mm^{-1}	

F(000)	1168
Crystal size	0.400 x 0.200 x 0.100 mm^3
Theta range for data collection	1.980 to 75.090°.
Index ranges	-16<=h<=16, -13<=k<=13, -27<=l<=26
Reflections collected	74886
Independent reflections	12477 [R(int) = 0.1149]
Completeness to theta = 67.679°	100.0 %
Absorption correction	Semi-empirical from equivalents
Max. and min. transmission	0.7538 and 0.4096
Refinement method	Full-matrix least-squares on F^2
Data / restraints / parameters	12477 / 873 / 867
Goodness-of-fit on F^2	1.037
Final R indices [I>2sigma(I)]	R1 = 0.0844, wR2 = 0.2281
R indices (all data)	R1 = 0.0954, wR2 = 0.2431
Absolute structure parameter	-0.04(6)
Extinction coefficient	n/a
Largest diff. peak and hole	0.411 and -0.295 $e.Å^{-3}$

Special Refinement Details for 258

Compound V22200 crystallizes in the monoclinic space group $P2_1$ with two molecules in the asymmetric unit. The tert-butyldimethylsilyl and vinyl groups on both molecules were disordered over two positions. The coordinates for the hydrogen atoms bound to O2 and O202 were located in the difference Fourier synthesis and refined semi-freely with the help of a restraint on the O-H distance (0.84(4) Å).

A5.2 REFERENCES

1. APEX2, Version 2 User Manual, M86-E01078. Bruker Analytical X-ray Systems: Madison, WI.
2. Sheldrick, G. M. SADABS (version 2008/1): Program for Absorption Correction for Data from Area Detector Frames. University of Göttingen, 2008.
3. Sheldrick, G. M. *Acta Cryst.* **2008**, *64*, 112.
4. Müller, P. *Crystallogr. Rev.* **2009**, *15*, 57.
5. Parsons, S.; Flack, H. D.; Wagner, T. *Acta Cryst.* **2013**, *69*, 249.

ABOUT THE AUTHOR

Yujia Tao was born on August 15th, 1996 to Yong Tao and Qing Zhang in Hangzhou, China. She grew up and studied in Hangzhou before college. In 2014, Yujia moved across the Pacific Ocean to Berkeley, CA to study at UC Berkeley, where she earned B.S. in Chemistry and B.A. in Geology degrees. She originally wanted to become a mineralogist until she took Organic Chemistry as a sophomore with Professor Thomas Maimone. The beauty of the organic reactions captured her, and therefore Yujia joined Professor Thomas Maimone's research group to conduct undergraduate research in total synthesis, under the guidance of her mentor Dr. Xirui Hu.

Yujia thereafter moved to the California Institute of Technology to earn her doctoral degree under the direction of Professor Sarah Reisman. Her research has focused on the concise total synthesis of highly oxygenated natural products. Following the completion of her PhD in May of 2023, she will join the medicinal chemistry team at Amgen in Thousand Oaks.